GES 1657–1800

ISSN 0003–2654

THE ROYAL SOCIETY OF CHEMISTRY

Founded 1841

The Analyst

A monthly international journal dealing with all branches of the theory and practice of analytical chemistry, including instrumentation and sensors, and physical, biochemical, clinical, pharmaceutical, biological, environmental, automatic and computer-based methods

Vol.117 No.11 November 1992

The Analyst

The Analytical Journal of The Royal Society of Chemistry

Editorial Manager, Analytical Journals: Judith Egan

Editor, *The Analyst*
Harpal S. Minhas
The Royal Society of Chemistry,
Thomas Graham House, Science Park,
Milton Road, Cambridge CB4 4WF, UK
Telephone 0223 420066.
Fax 0223 423623. Telex No. 818293 ROYAL.

US Associate Editor, *The Analyst*
Dr J. F. Tyson
Department of Chemistry,
University of Massachusetts,
Amherst MA 01003, USA
Telephone 413 545 0195
Fax 413 545 4490

Senior Assistant Editor
Paul Delaney

Assistant Editors
Brenda Holliday, Sheryl Youens

Editorial Secretary: Navlette Dennis

Advertisements: Advertisement Department, The Royal Society of Chemistry, Burlington House, Piccadilly, London, W1V 0BN. Telephone 071-437 8656. Telex No. 268001. Fax 071-437 8883.

The Analyst (ISSN 0003–2654) is published monthly by The Royal Society of Chemistry, Thomas Graham House, Science Park, Milton Road, Cambridge CB4 4WF, UK. All orders, accompanied with payment by cheque in sterling, payable on a UK clearing bank or in US dollars payable on a US clearing bank, should be sent directly to The Royal Society of Chemistry, Turpin Distribution Services Ltd., Blackhorse Road, Letchworth, Herts SG6 1HN, United Kingdom. Turpin Distribution Services Ltd., is wholly owned by the Royal Society of Chemistry. 1992 Annual subscription rate EC £276.00, USA $589, Rest of World £310.00. Purchased with *Analytical Abstracts* EC £604.00, USA $1299.00, Rest of World £669.00. Purchased with *Analytical Abstracts* plus *Analytical Proceedings* EC £712.00, USA $1527.00, Rest of World £791.00. Purchased with *Analytical Proceedings* EC £351.00, USA $749.00, Rest of World £395.00. Air freight and mailing in the USA by Publications Expediting Inc., 200 Meacham Avenue, Elmont, NY 11003.

USA Postmaster: Send address changes to: *The Analyst,* Publications Expediting Inc., 200 Meacham Avenue, Elmont, NY 11003. Second class postage paid at Jamaica, NY 11431. All other despatches outside the UK by Bulk Airmail within Europe, Accelerated Surface Post outside Europe. PRINTED IN THE UK.

Information for Authors

Full details of how to submit material for publication in *The Analyst* are given in the Instructions to Authors in the January issue. Separate copies are available on request.

The Analyst publishes papers on all aspects of the theory and practice of analytical chemistry, fundamental and applied, inorganic and organic, including chemical, physical, biochemical, clinical, pharmaceutical, biological, environmental, automatic and computer-based methods. Papers on new approaches to existing methods, new techniques and instrumentation, detectors and sensors, and new areas of application with due attention to overcoming limitations and to underlying principles are all equally welcome. There is no page charge.

The following types of papers will be considered:

Full research papers.

Communications, which must be on an urgent matter and be of obvious scientific importance. Rapidity of publication is enhanced if diagrams are omitted, but tables and formulae can be included. Communications receive priority and are usually published within 5–8 weeks of receipt. They are intended for brief descriptions of work that has progressed to a stage at which it is likely to be valuable to workers faced with similar problems. A fuller paper may be offered subsequently, if justified by later work. Although publication is at the discretion of the Editor, communications will be examined by at least one referee.

Reviews, which must be a critical evaluation of the existing state of knowledge on a particular facet of analytical chemistry.

Every paper (except Communications) will be submitted to at least two referees, by whose advice the Editorial Board of *The Analyst* will be guided as to its acceptance or rejection. Papers that are accepted must not be published elsewhere except by permission. Submission of a manuscript will be regarded as an undertaking that the same material is not being considered for publication by another journal.

Regional Advisory Editors. For the benefit of potential contributors outside the United Kingdom and North America, a Group of Regional Advisory Editors exists. Requests for help or advice on any matter related to the preparation of papers and their submission for publication in *The Analyst* can be sent to the nearest member of the Group. Currently serving Regional Advisory Editors are listed in each issue of *The Analyst.*

Manuscripts (four copies typed in double spacing) should be addressed to:

Harpal S. Minhas, Editor, *The Analyst,*
Royal Society of Chemistry,
Thomas Graham House,
Science Park, Milton Road,
CAMBRIDGE CB4 4WF, UK *or:*

Dr. J. F. Tyson
US Associate Editor, *The Analyst*
Department of Chemistry
University of Massachusetts
Amherst MA 01003, USA

Particular attention should be paid to the use of standard methods of literature citation, including the journal abbreviations defined in Chemical Abstracts Service Source Index. Wherever possible, the nomenclature employed should follow IUPAC recommendations, and units and symbols should be those associated with SI.

All queries relating to the presentation and submission of papers, and any correspondence regarding accepted papers and proofs, should be directed either to the Editor, or Associate Editor, *The Analyst* (addresses as above). Members of the Analytical Editorial Board (who may be contacted directly or via the Editorial Office) would welcome comments, suggestions and advice on general policy matters concerning *The Analyst.*

Fifty reprints are supplied free of charge.

Biosensors: Recent Trends
A Review

Pankaj Vadgama and Paul W. Crump
Department of Medicine (Clinical Biochemistry), University of Manchester, Hope Hospital, Salford, UK M6 8HD

Summary of Contents

Keywords: *Biosensor; enzyme electrode; waveguide; piezoelectric crystal; review*

Introduction

A general, strategic aim in analytical chemistry is the simplification of analytical methodology to a level where practical, routine measurement becomes possible; preferably this should be with a minimal demand upon operator skills. For the applied scientist, certainly, any analytical system that allows a degree of de-skilling that significantly widens the horizons for practical exploitation must be regarded as an important advance. Achievement of such practical goals has motivated much of the current research into biosensors, and explains why they have captured the attention of basic and applied scientist alike.

A biosensor can be defined as any probe or transducer that incorporates a biological component as the key functional element in the over-all transduction sequence. After the first description of a biosensor, where the bio-component was an enzyme operating in combination with an electrochemical transducer,[1] interest in biosensors has grown substantially. Research efforts have become multi-disciplinary, witnessed endeavour from within both scientific and commercial sectors, and taken on an international dimension with co-ordinated efforts now in play to tackle common practical problems. There certainly remain practical difficulties to overcome; these stem partly from the stringent operational requirements placed upon what is an inherently metastable biolayer, and partly from the need for direct contact between the biosensor and a sample matrix, which can be colloidal, interfacially active and potentially detrimental to function.[2] There, nevertheless, remains a fundamental structural elegance to the bio-transducer combination, which is both unique in analytical chemistry, and which exploits the molecular resolving power of a biological reagent in a particularly direct way. The incorporation of a bioreagent with its high selectivity and sensitivity thus adds a special capability for direct analysis that builds upon what has been possible for chemical sensors.

Application areas where biosensors are set to make a significant impact reach well beyond the established needs of medicine and veterinary science, where efficient access to biochemical information has always been at a premium. These additional areas include environmental monitoring and control, food processing, bioprocessing, agriculture, pharmaceuticals, and even defence and the petrochemical industry.[3] A common requirement of all these is the need for on site chemical information on some dynamic or rapidly evolving process, preferably on a real-time basis. The resultant benefits of closer monitoring range from a more efficient industrial production process, through to ultimately better informed legislation on safety standards and population exposure to chemical hazards.

Increased research effort in biosensors is certainly matched by a burgeoning literature, with many excellent general reviews[4–6] and monographs[7,8] now available. This particular review will, therefore, only focus on developments of the last 1–2 years, to give an indication of the new directions that research is taking. The basic principles of biosensors will not be described in any detail, unless they highlight some novel approach, and the classification of various systems will be along entirely classical lines, illustrated in Fig. 1. Although practical issues of sampling and biological interfacing are important,[9] devices will be reviewed from the perspective of the basic analytical chemist wishing to advance new strategies, rather than from that of the applied researcher attempting to put such strategies into practical operation.

A broad, useful sub-division of biosensors is between affinity and affinity/catalytic devices. In the former, binding of analyte simply leads to its passive capture with some subtle charge effect or conformational change in the bioreagent adduct. Here, unless a specially labelled species is involved in the binding interaction, transduction of the binding event can prove difficult; modalities such as a change in biolayer charge, thickness, refractive index viscosity and mass are commonly used in this context. Where initial binding is followed by analyte degradation (affinity/catalytic device), the 're-coding' of the analyte into some alternative reactive species allows for simpler and more classical modes of transduction. These include electrochemical and optical, and if the reactive product generates a further reaction cascade, this also can be interrogated in a variety of ways.

A biosensor also constitutes a foremost example of an interfacial technique, and as such, the rate of approach (flux)

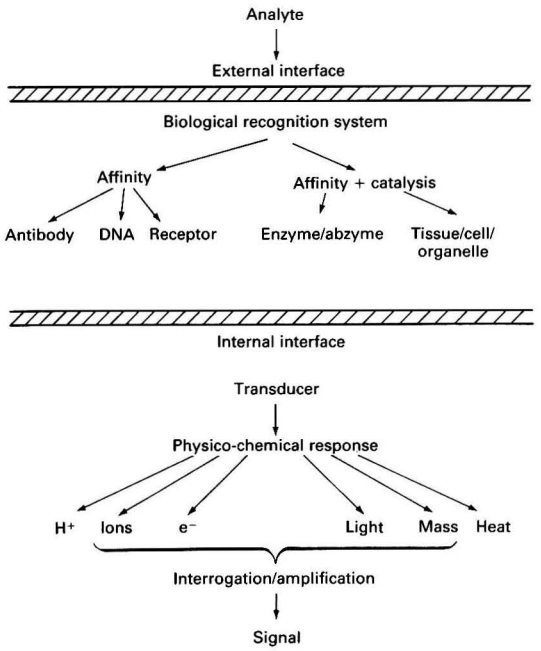

Fig. 1 Schematic diagram of possible biosensor analyte recognition cascade

of analyte to the analytical surface, degree of exposure of the biolayer and immobilization effects, can have a significant bearing upon both dynamic and steady biosensor response. Solute mass transport, along with diffusion gradients and partitioning both internal to and within any covering film are particularly relevant to function.[10] Theoretical treatments for these processes abound, and in the main, these are derivatives of the principles established in chemical engineering for immobilized catalysis and bioseparation. Thus, Varanasi *et al.*[11] developed a predictive model for pH based enzyme electrodes where a hydrolase (urease, penicillinase) is used to generate changes in pH in response to substrate. Coupled catalysis and diffusion are fundamental to operation here, but in addition, this model took into account the effects of accelerated proton transport through buffer shuttle mechanisms,[12] a commonly neglected process at pH based devices operating in buffer of variable composition.

Binding affinity is of underlying importance for any affinity biosensor, and usually for such devices, analyte binding is implicitly considered in terms of bulk solution affinity constants. However, with a biolayer at a surface, a heterogeneous equilibrium results; Weber[13] segregated the thermodynamic steps for binding and dissociation, and concluded that surface equilibria would have the same numerical values as bulk solution constants, but this was only provided that direct solute interactions with the basic surface were allowed for and that receptor layers were not either crowded or modified in some way through cross-linking. Also, if a membrane was used to cover the affinity layer, an internal 'assay' compartment was created where the internal volume would alter the relative binding efficiencies of analyte and some membrane-retained competing label.

Chemical Transduction Methods

Amperometry

Electroanalytical chemistry has established the theoretical and practical framework from which the development of amperometric biosensors can proceed. Biosensor systems receiving by

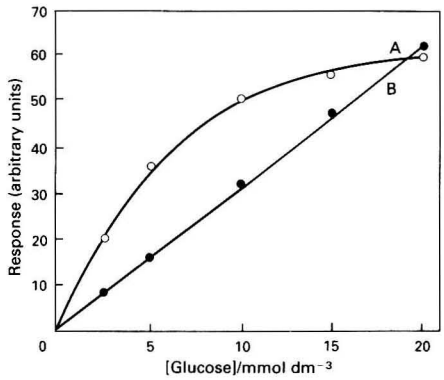

Fig. 2 Modifying effect of isopropyl myristate in a microporous polycarbonate membrane used as an outer covering layer at a glucose enzyme electrode; 1 μm pore size membrane: A, untreated; and B, isopropyl myristate treated (from ref. 19)

far the greatest attention to date have been enzyme electrodes. Of these, oxidase enzyme mounted sensors have proved the most popular for study:

$$\text{Substrate} + O_2 \xrightarrow{\text{Oxidase}} \text{product} + H_2O \qquad (1)$$

allowing, for example, reagentless monitoring of O_2 consumption at a (Clark) oxygen electrode, or of H_2O_2 production at a positively polarized electrode:

$$H_2O_2 \xrightarrow[\textit{versus}\ \text{Ag–AgCl}]{+650\ \text{mV}} O_2 + 2H^+ + 2e^- \qquad (2)$$

Substrates assayed include lactate,[14] ascorbate,[15] oxalate[16] and pyruvate,[17] but interest in glucose measurement remains unabated and is the consistent focus of current research efforts.

A near-universal drawback to the analysis of unmodified samples has been a restricted linear range owing to the saturation kinetics exhibited by the enzyme. This is particularly significant, as most normal levels of metabolites and substrates in biological samples are not only above the limits for a linear signal output, but can also be at levels where the response is zero order with respect to substrate. A generic solution to the problem has been the use of diffusion-limiting external covering membranes; these reduce the effective substrate concentrations within the enzyme layer to well below the saturation threshold. In one example, neutron track-etched polymeric membranes with low (<5%) porosity have been employed.[18] An advantage with such polymeric materials is their gas permeability, which has allowed control over substrate to O_2 permeability ratios, so leading to relatively enhanced O_2 levels within the enzyme layer. In this way, oxygen limitation upon the enzymic reaction is diminished, and the analytical range is even further extended, with reduced dependence upon background p_{O_2} fluctuations that are typical of biological samples. A composite membrane system bearing a specifically oxygen permeable organosilane layer has further extended this differential permeability approach,[19] and equivalent functional advantage (Fig. 2) accrued from the incorporation of oxygen permeable lipid (isopropyl myristate[20]) within structured microporous membranes. An advantage of the latter liquid barrier is the reduced tendency to surface protein deposition and, therefore, to signal deterioration in biological fluids. The requirement for continuous, stable substrate mass transport to the enzyme layer makes such devices much more vulnerable to surface fouling than would be the case where a thermodynamic detection principle is used, as with ion-selective electrodes, and specific, protective membrane strategies have proved vital for success.

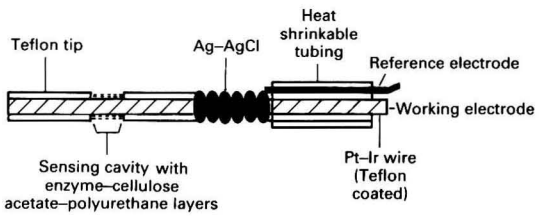

Fig. 3 Schematic diagram of implantable glucose enzyme electrode (from ref. 26)

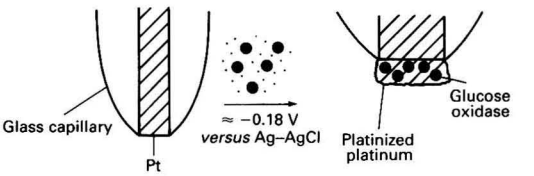

Fig. 4 Electrochemical fabrication of microenzyme sensor: glucose oxidase electrochemically incorporated with a porous platinum layer (from ref. 36)

Biomimetic membranes, in particular lipid bilayer films analogous to external cell membranes, confer an ideal biocompatibility advantage to biosensors used in media containing colloid or cell suspensions. An unsupported lipid layer has obvious mechanical deficiencies, but one stable form of the lipid bilayer is the liposome; this vesicular membrane system is structurally stable, capable of retaining reagent solution and has already been applied successfully to *in vivo* reagent and/or drug delivery. By immobilizing glucose oxidase loaded liposomes over H_2O_2 electrodes, it has proved possible to devise functional glucose sensors;[21] such liposome activated electrodes offer the future prospect of enhanced biocompatibility. In addition, through appropriate choice of the membrane lipid and any incorporated carrier, it might be possible to engineer parameters such as membrane fluidity and transport specificity whereby permeability to substrate and product can be adapted to a range of biological applications.

Cellulosic membranes are easily formed physically robust and chemically inert barriers that have been used to control substrate diffusion into the enzyme layer, and which readily reject macromolecules.[22] Cellulose acetate, in particular, furnishes thin stable layers, that can be either dip-coated onto a device or spin-coated as a separate, discrete layer. Recently, Gunasingham *et al.*[23] used acylated cellulose to create more hydrophobic, and therefore, apparently biocompatible, membranes that served to extend enzyme electrode linearity.

In recent years, particularly in relation to efforts in *in vivo* monitoring, one of the most commonly used external barrier membranes has been that based upon the polyurethanes.[24,25] This polymer class is particularly attractive for such use, as it has already been tried and evaluated *in vivo* for prosthetic devices, and has some claims to biocompatibility. Polyurethanes can be coated over planar microfabricated electrodes, or on needle-type enzyme electrodes. They probably present a tortuous microporous barrier to substrate diffusion while allowing freer passage for O_2. A recent design for an implantable oxidase based glucose sensor[26] has deployed the electrode sensor surface along the needle shaft rather than at the tip, as is usual, to facilitate membrane coating (Fig. 3).

Future membrane fabrication technologies will probably lead to further improvement in membrane bulk properties to optimize mass transport and bioreagent immobilization; also, differential control over surface interfacial properties through surface derivatization will be possible. Thus, in one study, by partial ozonolysis of an isoprene–propoxysilane copolymer layer, it has proved possible to create highly controlled pores that are tailored for enzyme attachment,[27] and recently, plasma deposition of diamond-like carbon on pre-formed membranes has led to improved surface properties for sensors interfaced with blood.[28] Thick-film technology, adapted from the microelectronics industry,[29] also provides an attractive route to the mass fabrication of enzyme electrodes that could be adapted for reproducible, *in situ* deposition of multilayer membranes; this is an ultimate route to the creation of multi-channel devices.[30] A price to pay for membrane-based control of enzyme electrode behaviour is slower dynamic response.[23] However, by reducing membrane thickness, and, therefore, over-all diffusion distances, using newer diffusionally resistant materials, response times of the order of <30 s are possible, presenting few problems to the monitoring of dynamic events in most biochemical systems.

In addition to controlling solute access, an external boundary membrane also serves to retain the catalytically active enzyme layer. Whereas the membrane polymer network might be deposited around the enzyme, as has been reported for enzyme entrapment with cellulose acetate,[31] enzyme retention usually involves some separate step to create a distinct membrane and biolayer. Early efforts at retention of simple, concentrated enzyme solution, or physical enzyme entrapment in a gel such as polyacrylamide or gelatin, have given way to specific covalent immobilization methods. Thus, attachment to a derivatized membrane surface, to a modified electrode or by creation of cross-links with an inert protein are now commonplace. Many of these covalent methods, particularly the frequently used cross-link of an enzyme with albumin with the bifunctional reagent glutaraldehyde,[19] are difficult to control, lead to high activity losses and result in enzyme layers with both an uncertain permeability and activity. This is unsatisfactory for both inter-electrode comparison in basic studies, and in commercial scale-up to create reproducible devices. Partly as a result of these drawbacks some substantial diversification of immobilization methodology is now in evidence. Thus, for example, reliable enzyme immobilization on nylon has been reported by the avoidance of a direct glutaraldehyde bridge,[32] with study of spacer arm effects[33] confirming the importance of coupling distances in immobilization strategies, as is known for immobilized enzyme reactor systems. An interesting variant on physical immobilization of enzyme has been entrapment (of tyrosinase) in a high-vacuum silicone grease filling the pores of a graphite electrode;[34] this allowed the enzyme to operate in a desired non-polar environment while permitting electrode deployment in polar aqueous solution.

The special constructional needs of microelectrodes has prompted a range of 'fine-tuned' enzyme deposition methods. Thus, enzymes have been covalently attached to a platinized platinum wire electrode,[35] and electrode platinization in enzyme (glucose oxidase) solution has allowed incorporation of the enzyme within a platinum matrix (Fig. 4), with the electrochemical process allowing control over matrix porosity.[36] The large functional surface area of the latter microelectrode enabled glucose detection down to 0.5 μmol dm^{-3}. Wang and Angnes[37] co-deposited rhodium and glucose oxidase over a carbon fibre electrode using a potentiometric approach; again, a highly porous structure was created, which, through the electrocatalysis effect of rhodium, enabled detection of H_2O_2 from the enzyme reaction at reduced overvoltage (+0.3 V *versus* Ag–AgCl). Patterned enzymic layers have been possible using photopolymers; a photo cross-linkable poly(vinylpyrrolidone) and 2,5-bis(4′-azido-2′-sulfobenzol)cyclopentanone mixture was used for enzyme co-entrapment.[38] More recently, a non-aqueous mixture of binder, initiator and monomer has been reported with an enzyme suspension,[39] and here, by varying surfactant amounts used for the enzyme dispersion, it proved possible to manipulate the degree of enzyme aggregation and, therefore, the kinetics and linear range. Light scattering by the enzyme

particles during photopolymerization, however, set a limit of 150 μm on pattern resolution. Undoubtedly in future, high resolution patterning will be possible with improvements in such sophisticated polymerization mixtures.

Gamma irradiation can also achieve a targeted immobilization of enzyme for microsensors. Although some radiation inactivation of the protein is inevitable, irradiation in a polymer can generate fairly rigid structures with an ultimately enhanced enzyme stability. Glucose oxidase[40] and lactate oxidase[41] have thus been immobilized in poly(*N*-vinylpyrrolidone) and poly(vinyl alcohol), respectively, to give rapid response electrodes.

Where miniature electrodes are used *in vivo*,[42] either for clinical or experimental purposes, an alternative to using a membrane to enhance relative O_2 access to an oxidase enzyme would be to supply oxygen directly, *e.g.*, down the electrode shaft. Cronenberg *et al.*[43] showed that far from this being a constructionally complex problem, O_2 could be supplied to microelectrodes with tip diameters of 5–25 μm and that such devices could be fairly simply fabricated. Also, agar gel within the recess of the electrode tip served as a barrier 'membrane' to oxygen loss, so maintaining a high p_{O_2} microenvironment.

Enzyme entrapment is possible within electrochemically polymerized films and allows controlled, selective deposition of enzyme over an electrode surface. Electrochemically polymerized pyrroles were reported in some earlier work, which demonstrated that it was possible to modify enzyme electrode performance through an effect on solute mass transport.[44,45] Recently, poly(*o*-phenylenediamine) has allowed deposition of thin (10 nm) films capable of giving 1 s electrode response times while at the same time rejecting ascorbate interference.[46] The very low solute permeability of such membranes, as compared with hydrophilic gels such as polyacrylamide,[47] will allow modulation of sensor behaviour while ensuring that over-all diffusion distances are minimal. Phenol and its derivatives have also been studied, and have resulted in glucose enzyme electrodes with variable controlled sensitivity to substrate.[48]

The poor selectivity of classical H_2O_2 based oxidase enzyme electrodes has been a drawback to their operation in biological fluids. Most such fluids have a cocktail of interferents that are electrochemically active at the high polarizing voltages needed for H_2O_2 detection [eqn. (2)]; in blood, thiols, ascorbate, urate and occasionally drugs, can cause interference during clinical measurement. Specialist membranes with permselectivity properties for H_2O_2 have, therefore, been extensively studied in recent years. These have included solvent cast cellulose acetate,[49] which, when fabricated as a dense membrane barrier, removes interference on the basis of charge and size (molecular mass cut-off ≈200 Da), and anionic membranes such as polyethersulfone,[24] Nafion (a perfluorinated, sulfonated exchanger)[50] and Eastman AQ-29D (a polyester sulfonic acid). There is some merit in using such discrete protective membranes over the working electrode, as they can be individually optimized, allowing versatility in the fabrication of the overlying enzyme and outer protective membrane layers. Recently, electropolymerized phenolic selective membranes over the working electrode have achieved the requisite interferent rejection, including the rejection of paracetamol,[51] which is a frequent problem in clinical metabolite analysis on patients taking this analgesic. *In situ* polymerized 1,2-diaminobenzene on reticulated vitreous carbon[52] (Fig. 5) has simultaneously eliminated ascorbate, urate and cysteine interference, while also incorporating the enzyme. Apparently, this polymer diminishes protein fouling and this over-all approach to polymer deposition is attractive for creating a protective barrier over surfaces that have a complex topography. A further characteristic of the deposition process with 1,2-diaminobenzene is that an insulating layer was formed leading to a self-limiting film and, therefore, a thin uniform membrane depth (<10 nm). More detailed structural and

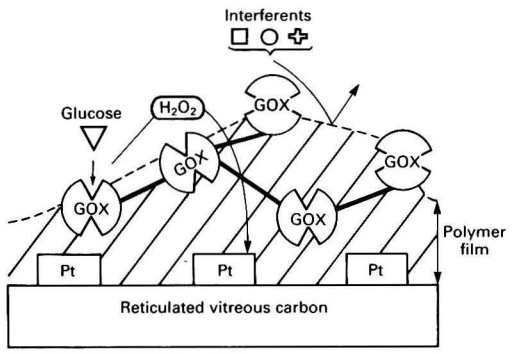

Fig. 5 Schematic diagram of possible enzyme/electrochemically polymerized 1,2-diaminobenzene layer (from ref. 52). Glucose unlike H_2O_2 does not penetrate the polymer, and only exposed enzyme sites are active

mechanistic information on specialist membrane materials is likely in the near future when ancillary techniques such as ellipsometry and microgravimetry are brought to bear on the film formation process.[53]

A particularly attractive approach to enzyme electrode fabrication, at least for the electrochemist, is the use of a retained electron mediator chain to effect electron transfer from an oxidoreductase enzyme active site to the working electrode material. The typical two-electron mediator (M) thus participates in two rapidly alternating reactions with an enzyme (E) that is first reduced by its substrate:

$$M_{oxidized} + E_{reduced} \rightarrow M_{reduced} + E_{oxidized} \quad (3)$$

$$M_{reduced} \xrightarrow[\text{electrode}]{\text{Polarized}} M_{oxidized} + 2H^+ + 2e^- \quad (4)$$

Provided there is efficient recycling without side reactions, continuous, mediated electron flow and, therefore, device operation is possible. For the oxidase catalysed reactions an obvious advantage is independence from any oxygen requirement and with mediators possessing low formal redox potentials[54] it is possible, at least in principle, to operate at polarizing voltages below those where most interferents can oxidize at the electrode. It must be recognized, however, that because the mediator has to compete with oxygen for reduction, some O_2 effect on signal amplitude cannot be ruled out. The organometallic electron mediator ferrocene, following its original description in a glucose biosensor,[55] has been studied in detail and this has led to a significant advance in biosensors research encompassing both basic bioelectrochemistry and practical analysis.[56] One practical outcome has been one of the few commercially available biosensor systems, notably a single use dip-stick for home blood glucose monitoring.[57] It is possible that leaching of mediator could be a problem during *in vivo* use or continuous operation and so derivatives allowing covalent linkage or a stronger physical adsorption to the underlying (carbon) electrode have been explored,[58] though with rather variable success.[54]

Substitution of the O_2 reduction step with an artificial mediator does, however, require adjustment to a new enzyme reaction chemistry and not all enzymes might be so amenable. For ferrocene, some oxidoreductases might either not react, or do so only with slow kinetics.[59] Redox potentials for the ferrocenes are in the range 100–400 mV (*versus* Ag–AgCl), and so some electrochemical interference is inevitable in biological solution. Wang *et al.*[60] fabricated a mediated carbon paste microelectrode for glucose where stearic acid incorporated into the enzyme containing paste helped to reduce interference from ascorbate, whereas Beh *et al.*[61] found that with a cellulose acetate barrier it was possible to reject interference while retaining a sufficiently porous barrier for the necessary intimate enzyme–mediator contact.

Covalent retention of mediator, but with sufficient mediator mobility, can provide an effective relay. Such 'hard wiring' has been demonstrated recently using ferrocene linked to flexible, insoluble siloxane polymers:[62]

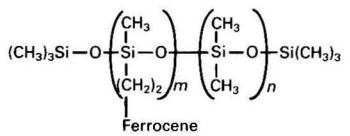

The need for polymer chain flexibility was subsequently confirmed,[63] and it was found that both mediator spacing along the polymer and bridging distances to the polymer were important determinants of electrode current and dynamic response.

An electron relay from the enzyme took on a new dimension when 'hard wiring' extended to the enzyme active centre itself. Thus, by binding ferrocene directly to the glucose oxidase glycoprotein, Heller was able to produce a functional system.[64] Interestingly, a reproducible, efficient relay was only obtained when approximately 12 ferrocene functions were introduced to buried sites near the flavin adenine dinucleotide (FAD) prosthetic group of the enzyme, in addition to attachments to the external enzyme surface. Without the 'internal' relay, the glycoprotein shell around the FAD apparently formed an insulating layer, so exaggerating the normal (exponential) fall in electron transport efficiency that results as the mutual separation distance between redox centres is increased. An electron relay based on benzoquinone attached to glucose oxidase, apparently is not subject to the same 'insulator' effects.[65] A complex between the redox centre $[Os(2,2'\text{-bipyridine})_2Cl]^{1+/2+}$ and poly(vinylpyridine) has also been used as an electron 'wire'.[66] The cationic polymer here could form electrostatic complexes with the negatively charged glucose oxidase molecule (Fig. 6) held over glassy carbon, graphite, gold or platinum working electrodes. Enzyme diffusion to and, therefore, direct contact with a denaturing working electrode surface can be avoided by cross-linking the bioactive layer. A microelectrode version of this system using a 7 μm diameter carbon fibre has been reported,[67] and has provided current densities an order of magnitude greater than with macroelectrodes, a probable result of the amplifying effects of radial, as opposed to planar, diffusion to the small electrode surface. Other mediators reported with flavoprotein enzymes include tetrathiofulvalene[68] and quinones.[69]

Organic conducting salts, such as tetrathiofulvalene–tetracyanoquinodimethane (TTF–TCNQ) can combine both working electrode and mediator functions. There is uncertainty as to whether electron transfer is mediated here by the active component of the electrode being solubilized from the electrode surface or whether this occurs through the agency of mobile surface components;[70,71] a possibility of direct, mediatorless electron transport to the electrode was also proposed in the past.[72] An electrode with TTF–TCNQ crystallized over carbon fibre[71] has shown the feasibility of making microenzyme electrodes using conducting salts, especially useful for biological studies in tissue. However, even with such elegant systems, oxygen competes with the electron cycling reaction, and at low substrate concentrations, oxygen attenuation of the response might be significant, with some ascorbate interference also possible.

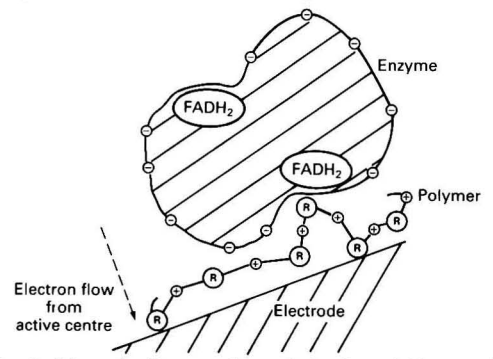

Fig. 6 Schematic diagram of negatively charged binary redox enzyme (*e.g.*, glucose oxidase) with electrostatically (and covalently) attached cationic polymer functionalized with a redox centre R {*e.g.*, $[Os(2,2'\text{-bypyridine})_2Cl]^{1+/2+}$}. From ref. 66

Established, direct electron transfer from enzyme to electrode without a mediator has been achieved through the use of a range of surface immobilized promoter molecules.[69,73] Alternatively, studies of reduction currents at unmodified carbon electrodes with adsorbed horseradish peroxidase, suggest that direct electron transport occurs to this enzyme when it has been pre-oxidized (*e.g.*, by H_2O_2).[74,75] Here, electron transfer commences at +600 mV *versus* a saturated calomel electrode (SCE) and reaches a maximum at 0 mV, and by co-immobilizing glucose oxidase and peroxidase, it is then possible to measure glucose *via* H_2O_2 generation. The lack of interference at the low applied voltage used in this method holds promise for direct metabolite measurement without recourse to a selective membrane barrier.[74]

A much wider analytical range would be possible with enzyme electrodes, if dehydrogenases could be utilized effectively. The general reaction catalysed is:

$$\text{Substrate} + \text{NAD}^+ \rightleftharpoons \text{product} + \text{NADH} + \text{H}^+ \quad (5)$$

where NADH = nicotinamide adenine dinucleotide (reduced).

Unfortunately, electrochemical recycling of cofactor at carbon or noble metal electrodes is inappropriate for most purposes, owing to side reactions and the high overvoltages necessary. While soluble mediators have helped to overcome such problems, immobilization of mediator is more practicable. Quinones and *p*-phenylenediimines are known to be suitable for mediating NADH electro-oxidation, and the latter as the active group of a phenoxazine or phenothiazine molecule, adsorbed onto graphite, has allowed NADH detection at 0 mV *versus* an SCE.[74] Used together with a covering anionic membrane to retain enzyme and cofactor, reagentless glucose and ethanol measurement has been possible for short periods. Other devices reported for dehydrogenase substrate assay have exploited conductive organic salts[76] and vitamin K_3 as mediator.[77]

Within the biolayer itself, sequential or parallel reactions can be catalysed by means of co-immobilized enzymes. In particular, this approach has been used for signal amplification; Scheller *et al.*[65] have developed enzyme pairs where one enzyme catalyses generation of substrate for the second enzyme, such recycling then resulting in enhanced sensitivity with substrate measurable down to ≈1 nmol dm^{-3}. More recently, the first enzyme in the biolayer was used to re-generate an excess local accumulation of co-substrate required for the second indicator reaction.[78]

Enzymes have also been used in increasingly novel, some would argue esoteric, combinations to effect sequential conversion of substrate to a detectable end product. Thus, nucleoside phosphorylase, which uses phosphate as co-substrate, has been combined with xanthine oxidase for inorganic phosphate determination[79] and a malate dehydrogenase–NADH oxidase combination has been utilized for estimation of L-malate.[80] Although commercial enzyme availability could be a 'bottle neck' to such enzyme innovations in future, less common microbial systems are being exploited directly by some researchers, and genetically engineered strains might yet be a source of enzymes with 'designer' kinetics.

Enzymes have long been known to be able to operate in organic solvents. Consequently, it has proved possible to

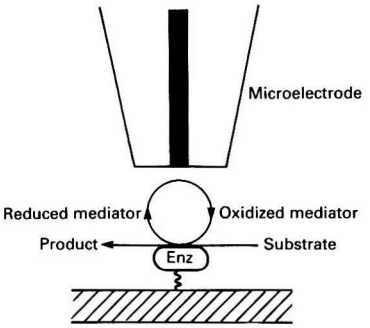

Fig. 7 Schematic diagram showing accumulation of mediator at surface immobilized enzyme; current measurement is at microelectrode of a scanning electron microscope. Locally resolved currents allow spatial, surface resolution of functional activity. (From ref. 83)

devise electrodes for biochemical analysis in a range of such solvents. The many possibilities have been reviewed,[81] and such devices would be suitable for analytes that are either insoluble or sparingly soluble in water, *e.g.*, oils, fats, cholesterol and bilirubin. Furthermore, a suitable choice of organic phase could allow optimization of enzyme–substrate affinities, reduce interference from polar molecules, and in some cases, enhance thermal stability.[81] Also, it is suggested that by combining immiscible solvent phases within the biolayer, improved catalysis rates for enzymes with high activity at the solvent interface might be achieved. Monoalkylated ferrocene used as surfactant stabilized aggregates in an enzyme layer can certainly function efficiently as electron mediators,[82] and this would support the notion of such a multiphase reagent/enzyme system.

As suggested above, future progress warrants wider use of surface and other stucture analysis techniques. In many cases, these techniques can be adapted from those already used in the study of biomaterials and polymers. One new uniquely applicable method, however, would be scanning electrochemical microscopy.[83] This recent technique has enabled surface images to be produced in a manner analagous to those by scanning tunnelling microscopy, although now with the image being based on localized surface electrochemical reactivity (functional imaging). To achieve this, a polarized microelectrode is moved with nanometre resolution over a surface and current flow measured. Local accumulation of a mediator, for example, resulting from high local enzyme activity, leads to positive feedback current (Fig. 7) which then allows localization and spatial resolution of activity, as well as a quantitative measurement of kinetic constants.

Potentiometry

Potentiometric enzyme electrodes have been investigated from the very earliest days of biosensor research.[1,84] Typically, an ion-selective or gas-sensing electrode is used to monitor changes in product or co-substrate concentrations within the enzyme layer, but because modulation of electron flow is not involved, there is probably less scope for innovation than is the case for amperometric systems. However, the advent of ion-selective field effect transistors (ISFETs) has stimulated further research and the rather limited range of substrate analysis may be extended in future. Hitherto, reports have been confined to substrates for deaminases, (NH_3/NH_4^+ detection), decarboxylases (CO_2 detection) and hydrolases, with the near-ubiquitous interconversion of H^+ in enzymic reactions a useful route to monitoring the enzyme layer. The pH-based enzyme electrodes could certainly provide a form of universal biosensor; however, the need for some control over sample pH and buffer capacity poses significant problems for practical substrate monitoring.

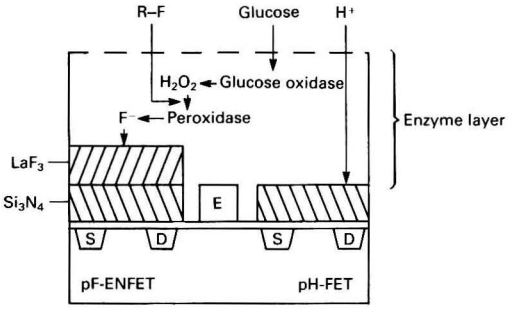

Fig. 8 Dual FET for glucose detection based on F^-/pH differential measurement. (From ref. 65)

Urea measurement remains a popular target for basic researches; urease immobilized over a pH ISFET[85] used to follow the consumption of hydrogen ions during enzymic hydrolysis, or over an ammonia gas electrode to follow NH_3 generation[86] are two recent examples. A gas-selective membrane, although highly selective, adds a further diffusion barrier that reduces sensitivity and extends response time, so in the latter study, a thin, high activity enzyme layer helped mitigate these problems and allowed a high throughput of serum samples. Simple physical entrapment of urease and creatinine deiminase, respectively, in cellulose triacetate, has allowed Campanella *et al.*[87] to fabricate stable electrodes for urea and creatinine. Cellulose triacetate membranes with surface chemical derivatization, can allow covalent attachment of enzyme; Chu and Meyerhoff[88] used this approach, with carbonate ion the potentiometrically detected enzyme product. In the fabrication of a penicillin electrode,[89] ultrathin (1–2 μm) penicillinase enzyme layers have been formed over glass pH electrodes by cross-linking surface-deposited enzyme with a spray coat of glutaraldehyde. Response times of ≈10 s were thereby achieved, though the magnitude of response to penicillin was inevitably dependent on buffering by a particular sample matrix (buffer, fermentation broth, milk).

Whereas the responses of gas sensors (CO_2, NH_3) are largely independent of sample matrix effects, any background variation in the detected gaseous species requires compensation. Alternatively, most ion-selective electrodes have problems of selectivity. It might, however, be possible to incorporate additional barrier membranes to improve the performance of some ion-selective electrodes. Thus, for an NH_4^+ electrode used for urea detection, a covering ion-exchange membrane bearing quaternary ammonium ions, rejected interferent K^+ in solution and also avoided errors from background NH_4^+ changes.[90]

Miniaturization of potentiometric enzyme electrodes has been achieved using coated wire electrodes and ISFETs. Taguchi *et al.*[91] have reported a tridodecylamine H^+ selective neutral carrier coated over a Pt wire for the fabrication of a penicillin microelectrode, and electrodes for glucose, urea and other substrates utilizing pH ISFETs have been described by many researchers.[84,85,92] Scheller *et al.*[65] have reported an interesting variant on the latter, which is a dual function FET responsive to pH and F^-. In this device, the electrode response to glucose, based upon the usual glucose oxidase catalysed reaction, is now mediated *via* a horseradish peroxidase indicator reaction that liberates F^- from an organofluoro substrate (Fig. 8). The lanthanum fluoride coated surface is the true enzyme FET (ENFET), but the key advantage of the system is that the second (pH) ISFET eliminates the need for a large external reference electrode, at least in a constant pH environment. More conventional differential mode operation

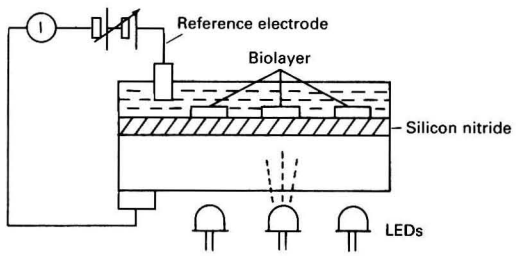

Fig. 9 Light addressable semiconductor sensor with pH-sensitive silicon nitride layer. (From ref. 98)

of ISFETs has been reported where a dual pH FET gate is mounted with active enzyme and inert (albumin) cross-linked layers;[93] this allows pH and temperature compensation, but again, this could not compensate for variation in sample buffer capacity. Apparently, diluted tissue fluid, under some circumstances, can have the requisite, stable ionic composition for uncompensated measurements. Thus, the removal under negative pressure of tissue fluid through (permeabilized) skin provided samples for Ito *et al.*[94] with sufficiently stable (and presumably low) buffer capacity after dilution to enable reliable pH FET based measurement of glucose. Also, enzyme inhibition has been exploited for analysis by the pH FET system;[95] inhibition of an acetylcholinesterase layer in the presence of organic phosphate pesticide allowed detection of this agent through attenuation of the acetic acid 'signal' from the enzymic reaction. By a similar inhibition principle, though with metal oxide (Pd–PdO, Ir–IrO_2) and pH electrodes, Tran-Minh *et al.*[96] detected nicotine and fluoride. Additionally, titanium and palladium electrodes can be used for H^+ detection and, recently, urease covalently linked to an oxidized tungsten surface allowed urea measurement in simple buffer.[97] Overall, there would now seem to be greater scope for innovation in potentiometric systems, but this is most likely to occur in regard to the transducer element.

The light addressable potentiometric sensor (LAPS) exploits the H^+ sensitivity of silicon nitride but, in contrast to the pH ISFET, without the obligatory stringent encapsulation required to protect the device in solution. The basis for the operation is that an appropriate bias potential is applied to a silicon plate, which has its surface nitride layer exposed to solution (Fig. 9). An alternating photocurrent subsequently created by means of a (modulated) light emitting diode then achieves an amplitude, which for any given bias potential is a function of solution pH.[98] The sensor has been used, for example, for immunoassay of human chorionic gonadotrophin (HCG) based upon a sandwich assay where the second (indicator) captured antibody is labelled with urease, and so produces a local pH change in the presence of urea.[99]

For reasons of functionality and availability, enzymes have been the predominant bioreagent used in potentiometric devices. In a novel departure from this, Blackburn *et al.*[100] succeeded in using a catalytic antibody (abzyme) for the pH based detection of phenyl acetate as a model substrate. Catalytic antibodies operate by providing a thermodynamically stabilizing binding surface for a transition state (TS) molecule, so lowering the transition state energy of a given reaction pathway. In this reported study, a monoclonal antibody was raised to a putative tetrahedral TS structure:

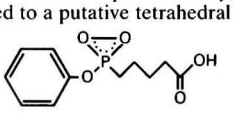

that served to catalyse the ester hydrolysis reaction:

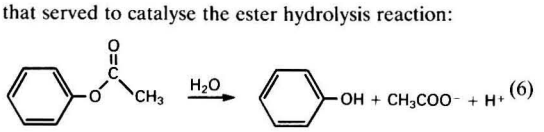

(6)

and gave a biosensor with a detection limit of 5 μmol dm^{-3}. Such reagents show particular promise as they combine the high affinity properties of an antibody with the signal generating capability of an enzyme. The possibility for reversible antigen attachment could also make continuous reversible operation possible, allowing unprecedented continuous monitoring of an antigen.

Rather less promising would seem to be attempts at direct potentiometric detection of analyte by its binding to an affinity surface. Thus, although any potentiometric detector surface can, in principle, be functionalized with antibody, binding of antigen cannot be followed readily using the resulting small alterations in interfacial potentials; the swamping effects of non-specific adsorption (mediated by electrostatic, hydrophobic and van der Waals interactions) generate a response that precludes analysis in all but the simplest of aqueous samples. Surface binding, however, also produces capacitance changes, and these were recently measured at a silicon–silica surface[101] and used to detect enterotoxin B from *Staphylococcus aureas*; whether such an approach can extend to complex media remains to be established.

Conductimetry

Where an enzyme reaction generates a net change in the concentrations of some ionized species, solution conductivity will change. The general principles underlying conductivity based measurement of enzymic reactions have been well established,[102] and the range of possible enzymic systems that can be followed is almost as broad as that for pH based measurement. Though conductimetry itself cannot select for a particular ion, substrate selectivity is attained *via* the specific nature of the enzymic reaction. Watson *et al.*[103] integrated an enzyme with a conductimetric detector by cross-linking urease over gold interdigitated electrodes that were microfabricated on a silicon wafer; in a subsequent report, enzyme was immobilized within an electrochemically synthesized poly-(pyrrole) layer giving a monolithic device that also included an amperometric enzyme electrode.[104] Because part of a conductimetric response is the result of change in H^+ concentration, with the formation of weakly acidic groups, both sensitivity and response times can be expected to be a function of sample pH and buffer capacity. This was indeed observed by Mikkelsen and Rechnitz,[105] who devised a conductimetric D-amino acid sensor using an oxidase. A further complication is that any ions that are generated might be partially retained by the enzyme molecule and this could have implications for the analytical reproducibility of conductimetric devices.

Optical Detection

Manual and automated spectrophotometric techniques have played a critical role in the development of a range of applied biological disciplines. Not only has spectrophotometry allowed a variety of different approaches to be brought to bear on a given analytical problem, but also the degree of speciation (selectivity) possible has been unrivalled by other readily accessible analytical techniques. It is, therefore, not surprising that once the technology for optical waveguides had been developed, that many waveguide structures would come into use as part of optical biosensors. As with other biosensors, the attractive features include miniaturization and the prospect of direct transduction. Optical properties that can be used in constructing a sensor include absorption, fluorescence/phosphorescence, bio/chemiluminescence, reflectance, scattering and refractive index. Such biosensors have been thoroughly reviewed recently,[106–109] and only a selected perspective on contemporary advances is provided here.

One of the most promising and straightforward of approaches is to utilize a change in the intensity of absorbed or emitted light from an indicator dye that can in turn interact

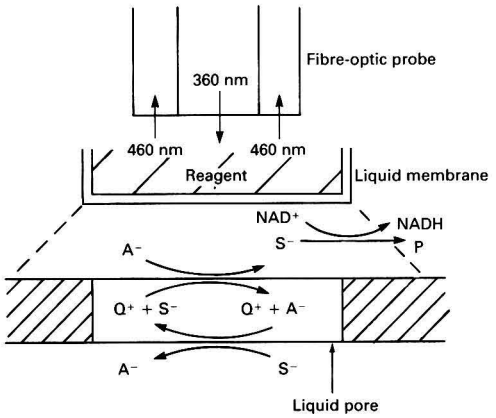

Fig. 10 Schematic diagram of liquid membrane containing ion exchanger (Q^+) for substrate ion (S^-) transport driven by anion (A^-) counter transport. (From ref. 112)

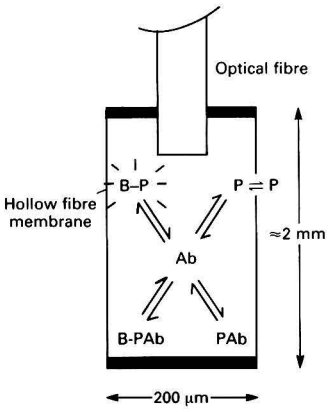

Fig. 11 Schematic diagram of fluoroimmunosensor showing sensor microchamber with phenytoin (P) and membrane retained labelled phenytoin (B-P) competing for antibody (Ab) binding. (From ref. 114)

with a biological reporter molecule. This is an onward development from pH, p_{O_2} and p_{CO_2} fibre-optic probes that achieve transduction *via* the indicator dye alone. One such device for glucose is based on a cellulose acetate membrane incorporating a benzidine derivative, where H_2O_2 generated by glucose oxidase can result in a detectable absorbance change.[110] Alternatively, an oxygen optical fibre has been used to follow O_2 consumption by the oxidase;[111] O_2 detection here is based on the luminescence quenching of tris(1,10-phenanthroline)ruthenium(II) retained in a high O_2 permeability silicone layer. Apparently, the high quenching efficiency of the indicator here enabled low glucose levels (<1 mmol dm^{-3}) to be detected.

A fibre-optic biosensor for measuring dehydrogenase substrates was reported by Schelp *et al.*[112] who were able to retain enzyme with a macromolecular poly(ethylene glycol) derivative of nicotinamide adenine dinucleotide phosphate [NAD(P)$^+$] behind an ultrafiltration membrane; proof of principle was indicated with substrates able to traverse the membrane (*e.g.*, ethanol, glucose and formate). Although the system was able to exploit the 360 nm fluorescence of reduced cofactor generated by the primary enzymic indicator reaction, a second enzyme was required to regenerate the NAD(P)$^+$. By means of a cellulose acetate supported liquid membrane to retain native (low molecular mass) cofactor instead, it was proposed that a dissolved anion exchanger in the liquid membrane phase could then be used to transport anionic substrate into the reaction phase (Fig. 10).

Bacterial luciferase catalyses the production of light in the presence of molecular oxygen, a long chain aldehyde, and reduced flavine mononucleotide (FMN). By coupling this reaction with an oxidoreductase:

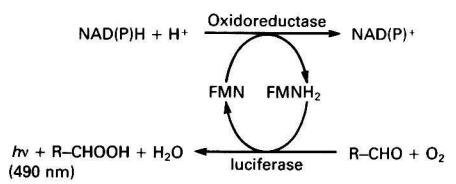

(7)

Gautier *et al.*[113] fabricated a highly selective bioluminescence fibre-optic probe for NADH that was capable of detecting 1×10^{9}–1×10^{-6} mol dm^{-3} cofactor solutions. In addition to the immobilization of enzyme, it proved possible to entrap FMN in a poly(vinyl alcohol) matrix, as a promising step towards a fully reagentless probe.

Antibody incorporated into a semipermeable microchamber held at the tip of a fibre-optic has enabled reagentless detection of phenytoin.[114] In this immunoprobe, the fluorescence of a high molecular mass fluorecent label (B-phycoerythrin) attached to phenytoin was quenched following binding to the antibody. Competition between labelled and unlabelled phenytoin provided a measure of free phenytoin in the assay solution (Fig. 11); dissociation of bound drug apparently proved sufficiently rapid for reversible phenytoin monitoring. Bright *et al.*[115] have described a fibre-optic immunosensor format that uses fluorescently labelled antibody fragments immobilized at the fibre tip; when binding of a large antigen (in this case, albumin) occurs, the label (dansyl chloride) appears to be shielded from solvent molecules, and the fluorescence output from the sensor is increased.

Controlled immobilization of reagent at the tip of optical fibres is likely to feature in the further development of these devices, irrespective of the specific underlying chemistry. Although not producing a biosensor, Barnard and Walt[116] established a useful general method of selective reagent deposition at fibre-optic probe tips, giving discrete loci suitable for multianalyte recognition (Fig. 12). Illuminating fibres multiplexed with a waveguide bundle were used to target transmission of light to specific fibre tips, so initiating highly localized polymerization of reagent, and reagent deposition without further manipulation.

Light transmitted along a waveguide undergoes total internal reflection and the electrical vector of the optical standing wave then created at the waveguide interface extends into the surrounding medium.[117] This evanescent wave penetrates only a sub-micrometre distance beyond the physical surface. As a typical decay distance ($\frac{1}{e}$) for the exponential drop in light intensity is 0.16 μm, the field provides an ideal opportunity for selective interrogation of surface immobilized biolayers with a low cross-contamination from the bulk solution. Exploitation of the evanescent wave is exemplified in many systems, but one recent enzymic sensor monitored the acetylcholinesterase catalysed reaction.[118] In this device, fluorescein isothiocyanate labelled enzyme was immobilized over a quartz waveguide and the effect of local pH change on dye fluorescence was used to follow acetylcholine hydrolysis.

By far the most common optical biosensor combination has been that of an evanescent wave detector with an antibody. For a competitive assay format, fluorophore-labelled antigen can be used to compete with an unlabelled molecule (analyte) for binding to a limited amount of antibody on the waveguide.

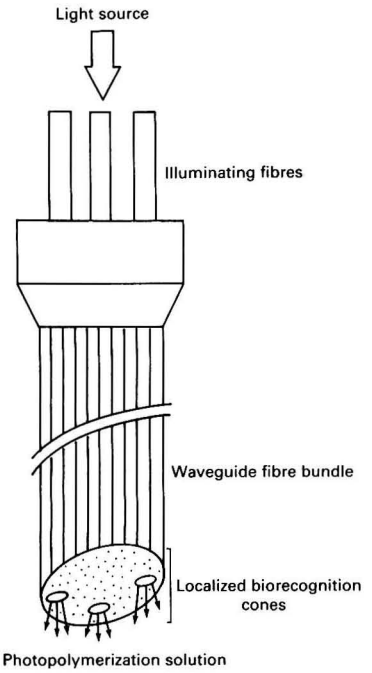

Fig. 12 Transmission of polymerization light source down fibre-optic bundle to form biorecognition cones at selected tip locations. (From ref. 116)

After equilibration, coupling of surface fluorescent light from the label back into the waveguide then allows estimation of the amount of surface captured label. The practical advantage of the surface optical approach is that separation of free from bound label is not necessary, so making a one-step immunoassay a distinct possibility. In one configuration, a planar waveguide formed as one side of a parallel plate 'capillary fill' device has proved an ideal combination sampling and assay system. Sample is taken up to a fixed volume by capillarity and all reagents can be pre-incorporated, so analysis is considerably de-skilled. This over-all construction has been used recently for devices measuring HCG[119] and rubella antibody,[120] respectively. Extension to whole blood analysis seems feasible, though there is some effect on rates of equilibration, possibly due to a restricted solute diffusion in such a suspended cell medium. With fluorophore excitation by internally reflected light, rather than an external source, it seems possible to resolve binding at different surface locations for multi-analysis.[121]

A surface grating can be used to couple a coherent laser light source into a waveguide and can operate as part of a biosensor. The efficiency of such light coupling can be measured, and is a direct function of the surface refractive index; even very small changes in refractive index can be resolved in this way,[117] so monitoring of immunocomplex formation between a surface antibody and protein, which causes a change in refractive index, becomes possible.[122] In an alternative strategy, optical diffraction by biomolecules at a surface has been proposed as an assay principle by Tsay *et al.*[123] Here, alternating areas of active and light inactivated antibody are first created on a silicon surface using a strong illuminating light source/photomask combination. Any binding of bulky antigen to the active areas then creates surface irregularities and, therefore, a surface grating, measurement of diffracted light intensity then allowing quantification of antigen levels (Fig. 13). This simple fabrication, with avoidance of a labelled compound or additional reagent, would be

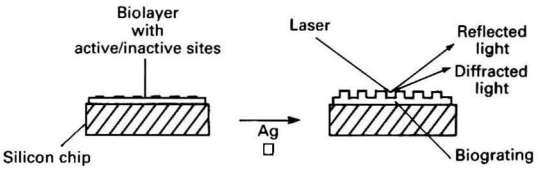

Fig. 13 Schematic diagram of optical biosensor assay based on creation of a biograting; binding of antigen to alternate areas of active antibody creates a surface grating that diffracts light. (From ref. 123)

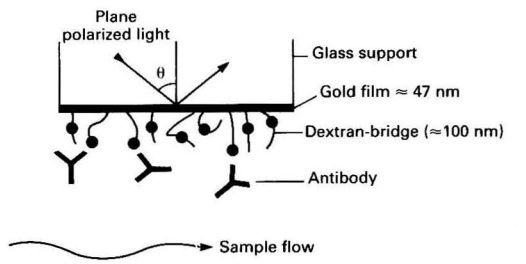

Fig. 14 Schematic diagram of sensor chip of Pharmacia Biosensor showing antibody immobilized on dextran hydrogel at terminal linkage sites. (From ref. 126)

highly advantageous for future commercialization. However, without label or some means of signal amplification, there might be a limit to the ultimate sensitivity attainable. For an immunoassay where a label is used, as an alternative to single label attachment, Choquette *et al.*[124] were able to exploit liposomes that contained carbofluorescein solution. The result was a large fluorescent label mass attached per antigen molecule and when immunoassay of theophylline was carried out, in this case using surface immobilized antibody, a 10-fold increase in sensitivity over a conventional fluorescent label could be demonstrated.

Surface plasma resonance (SPR) is a further important sensing technique that allows non-labelled immunoassay. The evanescent wave is again utilized, but now the electric field of (polarized) light couples into an electromagnetic surface wave, *i.e.*, the surface plasmon that exists at the interface of a coated metal film and the sample.[106] Maximum coupling occurs at some characteristic angle, which results in a minimum in the reflected light intensity. The determinants of this characteristic angle include wavelength, waveguide optics, the metal used, metal film thickness and the refractive index of the covering liquid film. Any specific analyte binding to a surface immobilized antibody or other bioreagent on the metal film allows direct, quantitative assay. Feasibility has been demonstrated using immobilized antibody and an oligonucleotide probe,[125] the latter being used to detect specific DNA (deoxyribonucleic acid) target sequences. A commercial laboratory analyser based on SPR is now also available (Pharmacia Biosensor AB).[126,127] A unique feature of the commercial system is the use of a dual-purpose surface-attached hydrophilic polymer (carboxymethyl dextran) that gives covalent linkage sites for antibody binding, and also serves to protect the vulnerable metal film from non-specific protein adsorption (Fig. 14). The polymer has the further effect of increasing the amount of bioreagent loading that is possible on a planar surface, and helps to set the micro-environment for optimum antigen binding to the solid-phase antibody. The system has thus far enabled dynamic monitoring of antigen–antibody binding and dissociation in experimental situations, and has variously allowed fundamental binding studies involving human immunodeficiency virus (HIV)-1 core protein, theophylline,[128] tobacco mosaic virus, cowpea mosaic virus[129] and protein A.[130] In addition to a development of direct immunoassay using SPR,

surface field enhancement by the SPR technique has allowed amplification of a fluorophore signal in a classical internal reflectance fluoroimmunoassay; data on the assay of HCG in serum indicate that this hybrid approach may extend the limit of sensitivity possible with either method alone.[131]

Physical Transduction Methods

Microgravimetric Detection

Piezoelectric materials have been used in a variety of configurations as microgravimetric detectors, and their general theory and use has been well reviewed.[5,132–135] They offer an attractive, near-universal mode of transducing the biorecognition event, but this is only provided that changes in detector mass following analyte binding can be made sufficiently large. Resolution of mass changes to $<1 \times 10^{-9}$ g cm^{-2} is possible in liquid media and, at least for high molecular mass substances, this provides for a viable transduction strategy.

Piezoelectric transducers also offer the advantages of a solid-state construction, chemical inertness, durability and ultimately the possibility of low cost mass production. Attention to date has mainly on AT-cut quartz crystals as the piezoelectric material that can function in a 'microbalance' mode. In order to carry out a measurement here, an external voltage is used to deform the quartz crystal plate so that there is relative motion between the two parallel crystal surfaces (thickness shear), crystal relaxation and oscillation at the resonant frequency then being maintained by means of an appropriate external circuit. Sauerbrey[136] showed that the change in frequency (Δf) resulting from any added mass (Δm) to the device could be described by:

$$\Delta f = \frac{-2f_0^2 \Delta m}{A\sqrt{\mu_q \rho_q}} \quad (8)$$

where f_0 is the resonant frequency of the unloaded crystal, μ_q is the shear modulus, ρ_q the density and A the surface area of the (active) crystal face. Thus, at least to a first approximation, the change in mass per unit area on the crystal is directly proportional to the change in frequency. A number of basic assumptions underlie this relation, however, and various modifying theories have been proposed for deviations in both gas- and liquid-phase operation.[132]

Mass detection with piezoelectric material can also be achieved using the principle of the surface acoustic wave (SAW). In such devices, an interdigitated array of electrodes in the material (usually ST cut quartz), generates local deformations that are transmitted as mechanical waves to a receiver electrode array. Interaction of the launched wave with any surface material alters SAW speed and amplitude, so enabling quantification of the deposited mass. In the liquid phase, sensitivity is reduced due to dampening of the measured wave component, normal to the surface.[135] If very thin piezoelectric material is used, vertical motion in the entire substrate can be produced and these Lamb wave devices can also be used for mass determination.[137] However, for liquids, shear horizonal acoustic plate mode (SH-APM) devices are preferred;[133] as the transmitted vibration here is horizontal to the surface, sensitivity with these systems is similar to the quartz microbalance. It needs to be emphasized that even here the movement of an entrained layer of liquid over any vibrating surface influences signal output.[133]

The mechanism of liquid phase operation of piezoelectric devices remains uncertain for some conditions,[138] and for the future, closer study of the liquid/solid interface is necessary. Rajakovic *et al.*[139] have drawn attention to interfacial viscosity effects, and changes in surface viscoelastic properties have been proposed as the mechanism for biotransduction using some quartz crystal systems.[140] Solutes so far measured on the basis of mass change have been mainly proteins through selective binding to surface immobilized antibody,[141] but antibodies have also been employed to bind micro-organisms, as was shown for a recent quartz microbalance detector for *Salmonella typhimurium*.[142]

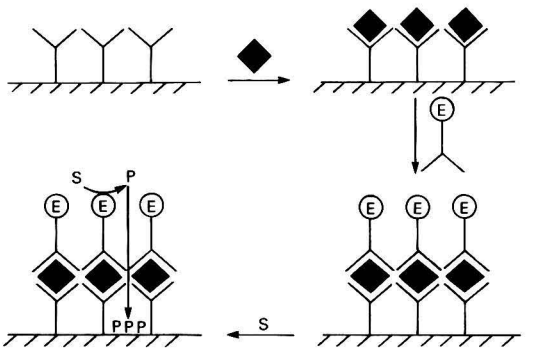

Fig. 15 Schematic diagram of sandwich immunoassay at a quartz microbalance surface where an antigen (◆) is assayed by binding of a second enzyme (E) labelled antibody used to generate insoluble product (P) from a soluble substrate (S). (From ref. 143)

Considerable enhancement of the measured signal is necessary if microgravimetric devices are to be used in biological fluids, with compensation of non-specific binding being obligatory either by some dynamic difference in the specific/non-specific binding process or by compensation with a second electrode. One approach to signal amplification is the use of a surface enzyme to generate a product that deposits on the crystal surface giving a cumulative microgravimetric signal. An alkaline phosphatase (AP) label in a sandwich-type immunoassay (Fig. 15) was used by Ebersole and Ward[143] to measure a protein (adenosine 5′-phosphosulfate reductase). Once the AP labelled second antibody had bound to the microbalance surface, exposure to 5-bromo-4-chloro-3-indolyl phosphate substrate solution led to the progressive generation and surface deposition of an insoluble, dephosphorylated dimer that adhered to the microbalance. This precipitation–amplification technique enabled $\approx$5 ng cm^{-3} of protein to be detected. A similar principle was used by this group in the piezoelectric biodetection of a DNA target strand of herpes simplex virus;[144] here, the enzyme adduct was first formed in bulk solution and then captured at an avidin sensitized piezoelectric sensor through a biotin conjugate.

Although low molecular mass solute detection might be less accessible by microgravimetry, viscoelastic changes in an enzyme layer, *e.g.*, through conformational change or altered molecular flexibility, could be used for low molecular mass substrate detection.[145] This might be a route to general substrate analysis provided a sufficiently high surface density of enzyme–substrate complexes can be generated over a detector surface.

Calorimetry

Most enzyme catalysed reactors are sufficiently exothermic to make calorimetric detection a practical proposition. However, even with the quantitative conversion of substrate to product that occurs using an enzyme reactor column, the temperatures generated are in the milli-degrees centigrade range. The development of enzyme thermistors has been pioneered at the University of Lund[146,147] for the assay of a wide range of substrates (*e.g.*, urea, glucose, ethanol, lactate, penicillin, oxalate, sucrose and urate) in this way, along with appropriate flow systems to enable continuous monitoring. By optimization of the enzyme support matrix, use of heat exchangers in the flow systems and appropriate construction of thermostating surrounds, sensitivities down to 0.01 mmol dm^{-3} substrate have been achieved. Enzyme sequences used to recycle substrate or coenzyme have enabled a sufficient excess of heat accumulation to extend assay into the nanomolar range,[148] and recently, an advance in design has been a miniaturized

enzyme thermistor system.[149,150] Also, modulation of immobilized metalloenzyme reactor activity by variable binding of the requisite metal ion has allowed calorimetric analysis of heavy metals. In one example, reactivation of galactose oxidase apoenzyme after binding with its copper(II) ion enabled copper in the range 1.0–15 mmol dm^{-3} to be assayed. Binding affinities determine analytical sensitivities and the sensitivity range shifted down to 1–5 μm when binding to ascorbate oxidase was used.[151]

The reduced heat capacity of organic solvents, together with the increased enthalpy for some enzymic reactions in organic solvent, has been used to advantage for analysis by enzyme thermistor. Thus, for triglyceride analysis, the enhanced temperature response translated into a 2.5-fold increment in signal using lipoprotein lipase in cyclohexane and a ≈50-fold increment in the temperature response to a peroxidase catalysed reaction in toluene.[152]

Although the enzyme column and thermistor combination of the enzyme thermistor is principally a reactor system, considered an 'honorary' biosensor by many, close apposition of an enzyme to the thermistor sensor surface in a thermal enzyme probe (TEP) more legitimately conforms to a biosensor concept. The TEP is structurally more compact,[153] but its disadvantage is its low temperature yield. Outward diffusion of heat from the enzyme layer is at least an order of magnitude greater than the inward diffusion of substrate, and most of the heat is dissipated into the surroundings. Compensation for background temperature variations and hydrothermal noise have been attempted with a second compensating thermistor, as with enzyme thermistors, but this strategy has proved inadequate for the rejection of the common mode thermal signal because of the very small initial analyte response. Recently, a thermoelectric glucose sensor[154] has been reported that employs a thin-film thermopile on Mylar with a glucose oxidase and catalase combination. The enzymes were immobilized on alternate junctions of the thermopile, and the temperature yield was now sufficient for substrate detection without external temperature compensation. There would, therefore, seem to be some scope for probe re-design and optimized heat collection[155] to allow for future TEP based measurements.

Special Bioreagent Systems

Whole Cells

The commercial availability of high activity enzyme preparations has removed one key specialist biochemical preparative step and so has facilitated the biosensor research efforts of many physical laboratories. Harnessing of the enzyme, fully intact in its bioenvironment, *i.e.*, in the whole cell or organelle, requires rather more in the way of biological manipulation and preparation, hence, rather less work has been reported along these lines. The advantage of an intact cellular system is that the enzyme is now retained in its natural immobilized state and is pre-supplied with any requisite cofactor or reagent. In addition, it becomes possible to exploit fairly complicated intrinsic metabolic pathways for analysis. The drawback is that a cell retains many active enzymes, even after *in vitro* storage, and response is sometimes not specific enough for analytical purposes;[6] in addition, cell viability is vulnerable to adverse solution conditions, and also the tortuous diffusion pathway provided by a concentrated cellular layer can prolong dynamic response.

Microbial cells are more readily harvested than eukaryotic cells, they are a large and, as yet, incompletely tapped source of enzymic pathways. Appropriate genetic engineering or even simple chemical metabolic pathway inhibition or induction[4] could make for specific and sensitive assay. In one report, a microbial layer consisting of *Alteromonas putrefaciens* was monitored using an O_2 electrode and, following exposure to solutes eluted from fish meat, altered cell respiration allowed an assessment of meat quality.[156] *Pseudomonas aminovorans* pre-grown on trimethylamine has similarly enabled monitoring of fish quality based on O_2 uptake by the organism;[157] here, response to trimethylamine was the basis of the test, and although interference from other amines did occur, this was compensated using a second electrode containing organisms not grown on trimethylamine, and which could not degrade this amine. A flow system built around an immobilized *Pseudomonas cepacia* reactor column has been used to determine the metabolic effects of various aromatics, including salicylate;[158] interestingly downstream monitoring by simultaneous O_2 electrode and calorimeter enabled different types of metabolic effect to be registered. To use lack of selectivity to advantage, Scheper *et al.*[159] have exploited a *Saccharomyces cerevisiae* thermistor column to determine general nutrient availability in a fed batch microbial fermenter.

Microbial biosensors have also been under development for environmental water monitoring. Tailoring of microbial species to have particular vulnerability to a toxin or toxin group would appear to be a requirement if meaningful specific data are to be obtained here. However, even with rather unselective organisms, provided there is system stability, it should be possible to achieve general toxic alarms. Many different modes of microbial monitoring are possible, but general progress has now been made, using electron mediators applied variously to monitor cell respiratory activity following environmental insult.[160]

Eukaryotic cells and tissues can have fairly high enzyme loadings, and their research use is now well established.[161] In recent developments, a carbon paste electrode incorporating banana tissue rich in polyphenol oxidase[162] has enabled detection of urine constituents following liquid chromatography, and a high sensitivity, rapid detection of dopamine and H_2O_2 has been achieved by packing potato (tyrosinase) and horseradish root (peroxidase), respectively, into the pores of reticulated vitreous carbon electrodes.[163] Instead of available plant material used directly, it might be preferable to generate high enzyme loaded cultured cells from explanted material; such callus tissue has been obtained for tobacco cells (peroxidase) to measure H_2O_2 with a sub-μmol detection limit.[164]

Though metabolically highly demanding, cultured mammalian cells can be maintained in flow microchambers, and have been monitored using light activated photoaddressable (LAPS) pH sensors (Fig. 9).[165] The sensor surface of the device here forms the base and walls of an array of micromachined wells, the generation of acidic metabolites during cessation of flow providing an estimate of cell metabolism under chosen environmental condition. Such a (microphysiometer) system is available in commercial form (Molecular Devices Corporation), and has been suggested as a general mode of monitoring the cellular action of cell activators, inhibitors, toxins, *etc.* In one example, the dynamics of cultured cell response to β-adrenergic receptor stimulation was studied.[166] For adherent cells, there will undoubtedly be some influence of surface deposited extracellular materials on response that need study, as has been suggested by an investigation of the surface activity of a laminin coating on Si_3N_4 substrate.[167] It should be added that tissue slices can be utilized as well as adherent single cells, but information on the relative merits for function, stability and ease of use is incomplete at present.

A more ambitious approach to biosensing is to use intact chemoreceptor organs present in some (lower level) animal species. Relevant studies have been conducted using crab chemoreceptor end organs. In one example, the isolated antennule of the Hawaiian crab[168] was used to measure a stimulant (trimethylene oxide) in solutions down to ≈10^{-15} mol dm^{-3}. Measurement exploited the frequency of neuronal firing with glass 'pick-up' electrodes. By switching to a

freshwater species (the freshwater crayfish[169]) periods of measurements were extended (8–10 h) and tap water could be used as the assay medium; the analyte measured here was the anti-tuberculosis drug pyrazinamide.[169] Intact cells have been part of a system used to follow serotonin, with intracellular electrodes implanted in isolated neurones,[170] and to follow catecholamines by the photometric monitoring of intracellular pigment granules in fish scales.[171] Provided such cell structures can be stabilized and constituted in a reproducible way, their practical sensing applications could become as mainstream as purified affinity molecules.

Receptors

The cell is bounded by a plasma membrane consisting of a lipid bilayer. Within this mobile layer reside proteins that traverse the full thickness of the membrane, and which also have molecular recognition properties, *i.e.*, receptors. These receptor molecules are difficult to isolate and tend to denature when removed from their natural lipid environment. The reversible binding of solute by receptors with an affinity and specificity matching that of antibodies makes them functionally attractive for biosensors; therefore, although receptors are difficult to work with, some effort is directed towards their exploitation.[172] Neuroreceptors and their recognition of neurotransmitters, neurotransmitter antagonists and neurotoxins has been a favoured line of investigation. A nicotinic acetylcholine receptor adsorbed directly onto a quartz optical fibre was used to bind to the toxin α-bungarotoxin with a remarkable retention of activity (half activity at 30 d),[173] and kinetic and equilibrium binding constants have become available based on measurements with fluorescent labelled neurotoxin.[174] In another study, the receptor itself was labelled with a fluorescent probe and, when retained in lipid vesicles, demonstrated fluorescence changes following binding to the effector molecule;[175] the mechanism is uncertain, but might provide a significant means of detecting general receptor binding.

Signal transduction and amplification following receptor binding will continue to pose problems with many receptors used in biosensors. Thus, some receptors operate in cells through the triggering of secondary messenger cascades, and these are likely to require additional transduction elements to generate a signal. However, others work by opening membrane ion channels and can be more readily envisaged as part of a biosensor; in a study of the isolated receptor lactose permease,[176] lactose dependent transport of H^+ was actually followed by means of a pH-sensitive dye, but voltage changes and current flow could also be followed in principle by a transducer system (Fig. 16). Lipid layer incorporation of such receptors could eventually enable their harnessing for biosensors, although more robust systems need to be developed in future and commercial systems remain far off at present.[177] An understanding of the biophysics of lipid films[178,179] at the type of basic solid surfaces that make up chemical transducers would seem to be a worthwhile area for future research.

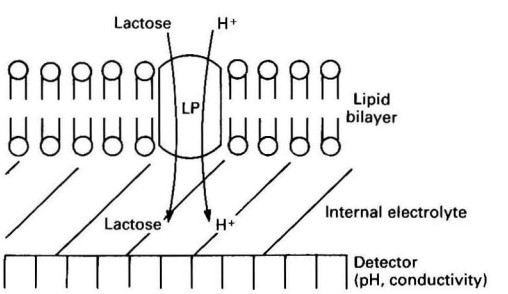

Fig. 16 Schematic diagram of receptor mediated response to lactose using the lactose permease (LP) co-transporter. (From ref. 176)

Conclusions

Ultimately, a biosensor has to be a device with a useful, practical analytical end function, irrespective of whether this is targeted to applied biology or to basic research. While there are grounds for studying biosensors as simply an expression of fundamental science, these alone cannot fully justify the level of current research efforts. This review has highlighted developments that recognize this important proviso and work which, increasingly, seeks to integrate fundamental advance with the practical utility of biosensors. Possibilities for innovative configurations have clearly not been exhausted, at least as revealed in recent publications. These should provide the necessary sound basis for applications that the applied scientist would consider relevant and the industrialist to be of commercial importance. Increased confidence in outcome might now be justified by the deeper understanding gained of the critical interface between a bioreagent and the transducer surface. This has allowed for improved selective interrogation and, therefore, more efficient signal transduction. This is especially notable in work on amperometric enzyme electrodes and in surface waveguide devices.

A further common theme running through many researches is the incorporation of polymeric membrane/surface modifying phases. This now allows stable operation of various internal biosensor components within the environment of an unstable sample matrix. In this regard, there has been success in the controlled penetration of diffusible interferent and passivating solutes and in the protection afforded against surface-active macromolecules liable to foul the recognition surface of biosensors. It is here that materials science and biosensor research might converge[180] and achieve a common strategy.

This review has highlighted fundamental advances, so biointerfacial reactions, well recognized with implantable and other biomaterials, have not been emphasized, but attention to these might be the next important stage of development. This will augment the requisite interdisciplinary contributions to biosensor research, and help establish biosensors as a mainstream analytical technique with success in practical analysis.

The North West Regional Health Authority is thanked for financial support.

References

1 Clark, L. C., and Lyons, C., *Ann. N.Y. Acad. Sci.*, 1962, **102**, 29.
2 Vadgama, P., *Sens. Actuators B*, 1990, **1**, 1.
3 *Biosensors: Today's Technology Tomorrow's Products*, ed. Jarvis, M. T., Technical Insights, SEAI Technical Publications, Madison, GA.
4 Scheller, F., Schubert, F., Pfeiffer, D., Hintsche, R., Dransfield, I., Rennenberg, R., Wollenberger, U., Riedel, K., Pantova, M., Kühn, M., Müller, H.-G., Tan, P. H., Hoffman, W., and Moritz, W., *Analyst*, 1989, **114**, 653.
5 Thompson, M., and Krull, U. J., *Anal. Chem.*, 1991, **63**, 393A.
6 Schultz, J. S., *Sci. Am.*, 1991, **265**, 48.
7 *Biosensors: Fundamentals and Applications*, eds., Turner, A. P. F., Karube, I., and Wilson, G. S., Oxford University Press, Oxford, 1989.
8 *Biosensor Principles and Applications*, eds., Blum, L. J., and Coulet, P. R., Marcel Dekker, New York, 1991.
9 Vadgama, P., Desai, M., Koochaki, Z., and Treloar, P., *Biochem. Soc. Trans.*, 1991, **19**, 11.
10 McDonnel, M. B., and Vadgama, P., *Sel. Electrode Rev.*, 1989, **11**, 17.
11 Varanasi, S., Stevens, R. L., and Rackenstein, E, *AIChE J.*, 1987, **33**, 558.
12 Nicholas, C. V., Vadgama, P., Desai M., McDonnell, M. B., and Lucas, S., *Analyst*, 1991, **116**, 463.
13 Weber, S. G., *Anal. Chem.*, 1992, **64**, 332.
14 Peterson, B. A., *Anal. Chim. Acta*, 1988, **209**, 213.
15 Daily, S., Armfield, S. J., Haggett, B. G. D., and Downs, M. E. A., *Analyst*, 1991, **116**, 569.

16 Assolant-Vinet, C. H., Bardeletti, G., and Coulet, P. R., *Anal. Lett.*, 1987, **20**, 513.
17 Peguin, S., Coulet, P. R., and Bardeletti, G., *Anal. Chim. Acta*, 1989, **222**, 83.
18 Vadgama, P., Mullen, W. H., and Churchouse, S. J., *UK Pat. Appl.*, 8522834, 1985.
19 Keedy, F. H., and Vadgama, P., *Biosens. Bioelectron.*, 1991, **6**, 491.
20 Tang, L. X., Koochaki, Z. B., and Vadgama, P., *Anal. Chim. Acta*, 1990, **232**, 357.
21 Rosenberg, M., Jones, M. N., and Vadgama, P., *Biochim. Biophys. Acta*, 1992, **1115**, 157.
22 Risinger, L., Buch-Rasmussen, T., and Johansson, G., *Anal. Chim. Acta*, 1990, **231**, 165.
23 Gunasingham, H., Teo, P. Y. T., Lai, Y. H., and Tan, S. G., *Biosensors*, 1989, **4**, 341.
24 Vadgama, P., Spoors, J., Tang, L. X., and Battersby, C., *Biomed. Biochim. Acta*, 1989, **48**, 935.
25 Sternberg, R., Barrau, M. B., Gangiotti, L., Thevenot, D. R., Bindra, D. S., Wilson, G. S., Velho, G., Froguel, P., and Reach, G., *Biosensors*, 1988, **4**, 27.
26 Bindra, D., Zhang, Y., Wilson, G. S., Sternberg, R., Thevenot, D., Maotti, D., and Reach, G., *Anal. Chem.*, 1991, **63**, 1692.
27 Lee, J. S., Nakahama, S., and Hirao, A., *Sens. Actuators B*, 1991, **3**, 215.
28 Higson, S. P. J., and Vadgama, P., *Anal. Chim. Acta*, in the press.
29 Bilitewski, U., Ruger, P., and Schmid, R. D., *Biosens. Bioelectron.*, 1991, **6**, 369.
30 Scholze, J., Hampp, N., and Branchle, C., *Sens. Actuators B*, 1991, **4**, 211.
31 Campanella, L., Sammartino, M. P., and Tomassetti, M., *Analyst*, 1990, **115**, 827.
32 Vrbova, E., and Marek, M., *Anal. Chim. Acta*, 1990, **239**, 263.
33 Beh, S. K., Moody, G. J., and Thomas, J. D. R., *Analyst*, 1989, **114**, 1421.
34 Connor, M. P., Sanchez, J., Wang, J., Smyth, M. R., and Mannino, S., *Analyst*, 1989, **114**, 1427.
35 Beh, S. K., Moody, G. J., and Thomas, J. D. R., *Analyst*, 1989, **114**, 29.
36 Ikariyama, Y., Yamauchi, S., Yukiashi, T., and Ushioda, H., *J. Electrochem. Soc.*, 1989, **136**, 702.
37 Wang, J., and Angnes, L., *Anal. Chem.*, 1992, **64**, 456.
38 Hanazato, T., Nakako, M., Maeda, M., and Shiono, S., *Anal. Chim. Acta*, 1987, **193**, 87.
39 Vopel, T., Ladde, A., and Muller, H., *Anal. Chim. Acta*, 1991, **251**, 117.
40 Saliatsatos, C., Ikariyama, Y., Mark, J. E., and Heineman, W. R., *Biosens. Bioelectron*, 1990, **47**, 5.
41 Hajizadeh, K., Halsall, H. B., and Heineman, W. R., *Anal. Chim. Acta*, 1991, **243**, 23.
42 Reach, G., and Wilson, G. S., *Anal. Chem.*, 1992, **64**, 381A.
43 Cronenberg, C., von Groen, B., de Beer, D., and van den Heuvel, H., *Anal. Chim. Acta*, 1991, **242**, 275.
44 Yabuki, S., Shinohara, H., and Aizawa, M., *J. Chem. Soc., Chem. Commun.*, 1989, 945.
45 Furtier, G., Brassard, E., and Belanger, D., *Biosens. Bioelectron.*, 1990, **5**, 473.
46 Malitesta, C., Padmisano, F., Torsi, L., and Zambonin, P. G., *Anal. Chem.*, 1990, **62**, 2735.
47 Gorton, L., *Anal. Chim. Acta*, 1983, **178**, 247.
48 Bartlett, P. N., Telbutt, P., and Tyrrell, C. M., *Anal. Chem.*, 1992, **64**, 138,
49 Koochaki, Z. B., Christie, I., and Vadgama, P., *J. Membr. Sci.*, 1991, **57**, 83.
50 Gorton, L., Karan, H. I., Hale, P. D., Inagaki, T., Okamoto, Y., and Skotheim, T. A., *Anal. Chim. Acta*, 1990, **228**, 23.
51 Vadgama, P., Christie, I. M., and Lloyd, S., *UK Pat. Appl.* 9112510, 1991.
52 Sasso, S. V., Pierce, R. J., Walla, R., and Yacynych, A. M., *Anal. Chem.*, 1990, **62**, 1111.
53 Rishpon, J., and Gottesfeld, S., *Biosens. Bioelectron.*, 1991, **6**, 143.
54 Gorton, L., Csoregi, E., Dominguez, E., Emneus, J., Jonsson-Petterson, G., Marko-Vargo, G., and Persson, B., *Anal. Chim. Acta*, 1991, **250**, 203.
55 Cass, A. E. G., Davis, G., Francis, G. D., Hill, H. A. O., Aston, W. J., Higgens, I. J., Plotkin, E. V., Scott, L. D. L., and Turner, A. P. F., *Anal. Chem.*, 1984, **56**, 667.
56 Hilditch, P. I., and Green, M. J., *Analyst*, 1991, **116**, 1217.
57 Ross, D., Heinemann, L., and Chantelan, E. A., *Diabetes Res. Clin. Pract.*, 1990, **10**, 281.
58 Jonsson, G., Gorton, L., and Pettersson, L., *Electroanalysis*, 1989, **1**, 49.
59 Kulys, J., and Schmid, R. D., *Bioelectrochem. Bioenerg.*, 1990, **24**, 305.
60 Wang, J., Wu, L. H., Lu, Z., Li, R., and Sanchez, J., *Anal. Chim. Acta*, 1990, **228**, 251.
61 Beh, S. K., Moody, G. J., and Thomas, J. D. R., *Analyst*, 1991, **116**, 459.
62 Gorton, L., Karan, H. I., Hale, P. D., Inagaki, T., Okamoto, Y., and Skotheim, T. A., *Anal. Chim. Acta*, 1990, **228**, 23.
63 Hale, P. D., Boguslavsky, L. I., Inagaki, T., Karan, H. I., Lee, H. S., and Skotheim, T. A., *Anal. Chem.*, 1991, **63**, 677.
64 Heller, A., *Acc. Chem. Res.*, 1990, **23**, 128.
65 Scheller, F., Pfeiffer, D., Hintsche, R., Dronsfield, I., Wollenberger, U., and Schubert, F., *Ann. N.Y. Acad. Sci.*, 1990, **613**, 68.
66 Gregg, B. A., and Heller, A., *Anal. Chem.*, 1990, **62**, 258.
67 Pishko, M. V., Michael, A. C., and Heller, A., *Anal. Chem.*, 1991, **63**, 2268.
68 Bartlett, P. N., and Bradford, J., *J. Chem. Soc., Chem. Commun.*, 1990, 1135.
69 Senda, M., *Ann. N.Y. Acad. Sci.*, 1990, **613**, 79.
70 Hale, P. D., and Skotheim, T. A., *Synth. Met.*, 1989, **28**, C853.
71 Kawagoe, J. L., Niehaus, D. E., and Wightman, R. M., *Anal. Chem.*, 1991, **63**, 2961.
72 Albery, W. J., Bartlett, P. N., and Cass, A. E. G., *Philos. Trans. R. Soc. London*, 1987, **316**, 107.
73 Albery, W. J., Cass, A. E. G., and Shu, Z. X., *Biosens. Bioelectron.*, 1990, **5**, 379.
74 Gorton, L., Bremle, G., Csoregi, E., Jonsson-Pettersson, G., and Persson, B., *Anal. Chim. Acta*, 1991, **249**, 43.
75 Kulys, J. J., and Schmid, R. D., *Bioelectrochem. Bioenerg.*, 1990, **24**, 305.
76 Kulys, J. J., *Enzyme Microb. Technol.*, 1981, **3**, 344.
77 Miki, K., Todoriki, J., Ikeda, T., and Senda, M., *Anal. Sci.*, 1989, **5**, 269.
78 Schubert, F., Lutter, J., and Scheller, F., *Anal. Chim. Acta*, 1991, **243**, 17.
79 Haemmerli, S. D., Suleiman, A. A., and Guilbault, G. G., *Anal. Biochem.*, 1990, **191**, 106.
80 Mitzutani, F., Yabuki, S., and Asai, M., *Anal. Chim. Acta*, 1991, **245**, 145.
81 Saini, S., Hall, G. F., Downs, M. A., and Turner, A. P. F., *Anal. Chim. Acta*, 1991, **249**, 1.
82 Loffler, U., Wiemhofer, H. D., and Gopel, W., *Biosens. Bioelectron.*, 1991, **6**, 343.
83 Bard, A. J., Fon, F. R., Pierce, D. T., Unwin, P. R., Wipf, D. O., and Zhon, F., *Science*, 1991, **254**, 68.
84 Monroe, D., *CRC Crit. Rev. Clin. Lab. Sci.*, 1989, **27**, 109.
85 Lehman, J., *Biotechnology*, 1990, **8**, 729.
86 Narinesingh, D., Mungal, R., and Ngo, T. T., *Anal. Chim. Acta*, 1991, **249**, 387.
87 Campanella, L., Sammartino, M. P., and Tomassetti, M., *Analyst*, 1990, **115**, 827.
88 Chu, G. S., and Meyerhoff, M. E., *Talanta*, 1989, **36**, 271.
89 Meir, H., Kumaran, S., Danna, A. M., and Tran-Minh, C., *Anal. Chim. Acta*, 1991, **249**, 405.
90 Rosario, S. A., Cha, G. S., Meyerhoff, M. E., and Trojanowicz, M., *Anal. Chem.*, 1990, **62**, 2418.
91 Taguchi, H., Ishihara, N., Okumura, K., and Shimabayashi, Y., *Anal. Chim. Acta*, 1990, **228**, 159.
92 Dransfield, I., Hintsche, R., Moritz, W., Pham, M. T., Hoffmann, W., and Hueller, J., *Anal. Lett.*, 1990, **23**, 437.
93 Wang, Z. X., Li, S. Y., Zhang, L. C., and Li, G. X., *Clin. J. Biotechnol.*, 1990, **6**, 149.
94 Ito, N., Saito, A., Miyamoto, S., Shinohara, S., Kuriyama, T., Kimura, J., Arai, T., Kichuchi, M., Kagashima, and Nagata, N., *Sens. Actuators B*, 1990, **1**, 488.
95 Dumschat, C., Muller, H., Stein, K., and Schwedt, G., *Anal. Chim. Acta*, 1991, **252**, 7.
96 Tran-Minh, C., Pandey, P. C., and Kumaran, S., *Biosens. Bioelectron.*, 1990, **5**, 461.
97 Przybyt, M., and Sugier, H., *Anal. Chim. Acta*, 1990, **239**, 269.
98 Hafeman, D. G., Parce, J. W., and McConnell, H. M., *Science*, 1988, **240**, 1182.
99 Olson, J. D., Panfili, P. R., Armenta, R., Femmel, M. B., Merrick, H., Gumperz, J., Goltz, M., and Zuk, R. F., *J. Immunol. Methods*, 1990, **134**, 71.

100 Blackburn, G. F., Talley, D. B., Booth, P. M., Durfor, C. N., Mertin, M. T., Napper, A. D., and Rees, A. R., *Anal. Chem.*, 1990, **62**, 2211.
101 Billard, V., Martelet, C., Binder, P., and Therasse, J., *Anal. Chim. Acta*, 1991, **249**, 367.
102 Lawrence, A. J., *Eur. J. Biochem.*, 1971, **18**, 221.
103 Watson, L. D., Maynard, P., Cullen, D. C., Sethi, R. S., Brettle, J., and Lowe, C. R., *Biosensors*, 1987, **3**, 101.
104 Yon Hin, B. F. Y., Sethi, R. S., and Lowe, C. R., *Sens. Actuators B*, 1990, **1**, 550.
105 Mikkelsen, S. R., and Rechnitz, G. A., *Anal. Chem.*, 1989, **61**, 1737.
106 Yellowlees, I. H., *Br. J. Anaesth.*, 1991, **67**, 100.
107 Robinson, G. A., *Biochem. Soc. Trans.*, 1991, **19**, 18.
108 Robinson, G. A., *Biosens. Bioelectron.*, 1991, **6**, 183.
109 Narayanaswamy, R., *Biosens. Bioelectron.*, 1991, **6**, 467.
110 Takai, N., Sakuma, I., Fukui, Y., Kaneko, A., Fujuie, T., Taguchi, K., and Nagaoka, S., *Artif. Organs*, 1991, **15**, 86.
111 Moreno-Bondi, M. L., Wolfbeis, O. S., Leiner, M. J. P., and Schaffer, B. P. H., *Anal. Chem.*, 1990, **62**, 2377.
112 Schelp, C., Scheper, T. H., Buckmann, F., and Reardon, K. F., *Anal. Chim. Acta*, 1991, **255**, 223.
113 Gautier, S. M., Blum, L. J., and Coulet, P., *Sens. Actuators B*, 1990, **1**, 580.
114 Anderson, F. P., and Miller, W. G., *Clin. Chem. (Winston-Salem, N.C.)*, 1988, **34**, 1417.
115 Bright, F. V., Betts, T. A., and Litwiler, K. S., *Anal. Chem.*, 1990, **62**, 1065.
116 Barnard, S. M., and Walt, D. R., *Nature (London)*, 1991, **353**, 338.
117 Norris, J. O. W., *Analyst*, 1989, **114**, 1359.
118 Rogers, K. R., Cao, C. J., Valdes, J. J., Eldefrawi, A. T., and Eldefrawi, M. E., *Fundam. Appl. Toxicol.*, 1991, **16**, 810.
119 Deacon, J. K., Thomson, A. M., Page, A. L., Stops, J. E., Roberts, P. R., Whiteley, S. C., *Biosens. Bioelectron.*, 1991, **6**, 193.
120 Parry, R. P., Love, C., and Robinson, C. A., *J. Virol. Methods*, 1990, **27**, 39.
121 Hlady, V., Lin, J. N., and Andrade, J. D., *Biosens. Bioelectron.*, 1990, **5**, 291.
122 Nellen, P. W., and Lukosz, W., *Biosens. Bioelectron.*, 1991, **6**, 517.
123 Tsay, Y. G., Lin, C. I., Lee, J., Gustafson, E. K., and Appelqvist, R., *Clin. Chem. (Winston-Salem, N.C.)*, 1991, **37**, 1502.
124 Choquette, S. J., Locascio-Brown, L., and Durst, R. A., *Anal. Chem.*, 1992, **64**, 55.
125 Pollard-Knight, D., Hawkins, E., Yeung, D., Pashby, D. P., Simpson, M., McDougall, A., Buckle, P., and Charles, S. A., *Anal. Biol. Clin.*, 1990, **48**, 642.
126 Jönsson, U., Fägerstam, L., Ivarsson, B., Johnsson, B., Karlson, R., Lundh, K., Lofas, S., Persson, B., Roos, H., and Ronnberg, I., *BioTechniques*, 1991, **11**, 620.
127 Stenberg, E., Persson, B., Roos, H., and Urbaniczky, C., *J. Colloid Polym. Sci.*, 1991, **143**, 513.
128 Karlsson, R., Michaelsson, A., and Mattson, L., *J. Immunol. Methods*, 1991, **145**, 229.
129 Dubs, M. C., Altschuh, D., and Van Rengenmortel, M. H., *Immunol. Lett.*, 1991, **31**, 59.
130 Johnsson, B., Löfas, S., and Lindquist, G., *Anal. Biochem.*, 1991, **198**, 268.
131 Attridge, J. W., Daniels, P. B., Deakon, J. K., Robinson, G. A., and Davidson, G. P., *Biosens. Bioelectron.*, 1991, **6**, 201.
132 Thompson, M., Kipling, A. L., Duncan-Hewitt, W. C., Rajaković, L. V., and Čavić-Vlasak, B. A., *Analyst*, 1991, **116**, 881.
133 Walton, P. W., Butler, M. E., and O'Flaherty, M. R., *Biochem. Soc. Trans.*, 1991, **19**, 44.
134 Fox, C. G., and Alder, J. F., *Analyst*, 1989, **114**, 997.
135 Ward, M. D., and Buttry, D. A., *Science*, 1990, **249**, 1000.
136 Sauerbrey, G., *J. Phys.*, 1959, **155**, 206.
137 Wenzel, S. W., and White, R. M., *IEEE Trans. Electron. Devices*, 1988, **35**, 735.
138 Calabrese, G. S., Wohltjen, H., and Roy, M. K., *Anal. Chem.*, 1987, **59**, 833.
139 Rajakovic, L. J., Čavić-Vlasak, B. A., Ghaemmaghami, V., Kallury, K. M. R., Kipling, A. L., and Thompson, M., *Anal. Chem.*, 1991, **63**, 615.
140 Barnes, C., D'Silva, C., Jones, J. P., and Lewis, T. J., *Sens. Actuators B*, 1991, **3**, 295.
141 Davis, K. A., and Leary, T. R., *Anal. Chem.*, 1989, **61**, 1227.
142 Luong, J. H. T., Prusak-Sochaczewski, E., and Guilbault, G. G., *Ann. N.Y. Acad. Sci.*, 1990, **613**, 439.
143 Ebersole, R. C., and Ward, M. D., *J. Am. Chem. Soc.*, 1988, **110**, 8623.
144 Ebersole, R. C., Miller, J. A., Moran, J. R., and Ward, M. D., *J. Am. Chem. Soc.*, 1990, **112**, 3239.
145 Lasky, S. J., and Buttry, D. A., *ACS Symp. Ser.*, 1989, **403**, 327.
146 Mosbach, K., and Danielsson, B., *Biochem. Biophys. Acta*, 1974, **364**, 140.
147 Danielsson, B., *Biochem. Soc. Trans.*, 1991, **19**, 27.
148 Danielsson, B., and Larsson, M. B., *TrAC, Trends. Anal. Chem. (Pers. Ed.)*, 1990, **9**, 223.
149 Urban, G., Kamper, H., Jachimowicz, A., and Koh, F., *Biosens. Bioelectron.*, 1991, **6**, 275.
150 Mosbach, K., *Biosens. Bioelectron*, 1991, **6**, 175.
151 Satoh, I., *Ann. N.Y. Acad. Sci.*, 1990, **613**, 401.
152 Danielsson, B., Flygate, F., and Velev, T., *Anal. Lett.*, 1989, **22**, 1417.
153 Weaver, J. C., Cooney, C. L., Fulton, S. P., Schuler, P., and Tannenbaum, S. R., *Biochim. Biophys. Acta*, 1976, **452**, 285.
154 Muehballer, M. J., Guilbeau, E. J., and Towe, B. C., *Anal. Chem.*, 1989, **61**, 77.
155 Urban, G., Jachimowicz, A., Kohl, F., Kuttner, H., Olcaytug, F., Kamper, H., Pittner, F., Mannbuscbaum, E., Schalkhammer, T., and Prohaska, O., *Sens. Actuators A*, 1990, **22**, 650.
156 Hoshi, M., Sasamoto, Y., Nonaka, M., Toyama, K., and Watanabe, E., *Biosens. Bioelectron.*, 1991, **6**, 15.
157 Gamati, S., Luang, S. H., and Mulchandani, A., *Biosens. Bioelectron.*, 1991, **6**, 125.
158 Thavarungkul, P., Hakanson, H., and Mattiasson, B., *Anal. Chim. Acta*, 1991, **249**, 17.
159 Scheper, T., Brandes, W., Grau, C., Hundeck, H. G., Reinhardt, B., Ruther, F., Plotz, F., Schelp, C., Schugerl, K., and Schneider, K. H., *Anal. Chim. Acta*, 1991, **249**, 25.
160 Gaisford, W., Richardson, N. J., Haggett, B. G. D., and Rawson, D. M., *Biochem. Soc. Trans.*, 1991, **19**, 15.
161 Rechnitz, G. A., *Science*, 1981, **214**, 287.
162 Connor, M. P., Wang, J., Kubiak, W., and Smyth, M. R., *Anal. Chim. Acta*, 1990, **229**, 139.
163 Wang, J., and Naser, N., *Anal. Chim. Acta*, 1991, **242**, 259.
164 Navaratne, A., and Rechnitz, G. A., *Anal. Chim. Acta*, 1992, **257**, 59.
165 Parce, J. W., Owicki, J. C., Kercso, K. M., Sigal, G. B., Wada, H. G., Muir, V. C., Bousse, L. J., Ross, K. L., Sikic, B. I., and McConnell, H. M., *Science*, 1989, **246**, 243.
166 Owicki, J. C., Parce, J. W., Kercso, K. M., Sigal, G. B., Muir, V. C., Venter, J. C., Fraser, C. M., and McConnell, H. M., *Proc. Natl. Acad. Sci.*, 1990, **87**, 4007.
167 Grattarola, M., Cambiaso, A., Cenderelli, S., and Tedesco, M., *Sens. Actuators*, 1989, **17**, 451.
168 Buch, R. M., Barker, T. Q., and Rechnitz, G. A., *Anal. Chim. Acta*, 1991, **243**, 157.
169 Wijesuriya, D., and Rechnitz, G. A., *Anal. Chim. Acta*, 1992, **256**, 39.
170 Skeen, R. S., Kisaalita, W. S., Van Wie, B. J., Fung, S. J., and Barnes, C. D., *Biosens. Bioelectron.*, 1990, **5**, 491.
171 Elwing, H., Karlsson, J. D., Grundstrom, N., Gustafsson, A. L., Von Schenck, H., and Sundgren, H., *Biosens. Bioelectron.*, 1990, **5**, 449.
172 Wingard, L. B., *Ann. N.Y. Acad. Sci.*, 1990, **613**, 44.
173 Rogers, K. R., Valdes, J. J., and Eldefrawi, M. E., *Biosens. Bioelectron.*, 1991, **6**, 1.
174 Rogers, K. R., Eldefrawi, M. E., Menking, D. E., Thompson, R. G., and Valdes, J. J., *Biosens. Bioelectron.*, 1991, **6**, 507.
175 Krull, V. J., Brown, R. S., Hougham, B. D., McGibbon, G., and Vandenberg, E. T., *Talanta*, 1990, **37**, 561.
176 Kiefer, H., Klee, B., John, E., Stierhof, Y. D., and Jahrig, F., *Biosens. Bioelectron.*, 1991, **6**, 233.
177 Taylor, R. F., Marenchic, I. G., and Spencer, R. H., *Anal. Chim. Acta*, 1991, **249**, 67.
178 Petty, M. C., *J. Biomed. Eng.*, 1991, **13**, 209.
179 Tien, H. T., and Salmon, Z., *Biotechnol. Appl. Biochem.*, 1990, **12**, 478.
180 Vadgama, P., *Chem. Br.*, 1992, **28**, 249.

Paper 2/02931F
Received June 3, 1992
Accepted July 2, 1992

Kinetic Model of pH-based Potentiometric Enzymic Sensors Part 2.* Method of Fitting

Stanisław Głąb, Robert Koncki and Izabela Holona
Department of Chemistry, University of Warsaw, Pasteura 1, 02-093 Warsaw, Poland

Methods of fitting theoretical calibration graphs, evaluated on the basis of a kinetic model of pH-based enzymic sensors, to experimental data obtained using glucose and acetylcholine sensors are presented. Bisection and simplex methods were used for this purpose. Good agreement between the theoretical predictions and the experimental results was achieved.

Keywords: *Potentiometric enzymic pH sensor; kinetic model; glucose sensor; acetylcholine sensor; simplex method*

A theoretical, kinetic model of pH-based enzymic sensors was described in Part 1[1] of this series and was presented without experimental verification. This model describes the response of sensors in which an enzymic reaction produces species with protolytic activity. To this group belongs the classical reaction of glucose to form glucolactone and hydrogen peroxide:

$$\beta\text{-D-Glucose} + O_2 \xrightarrow{\text{Glucose oxidase}} \text{glucolactone} + H_2O_2 \quad (1)$$

Glucolactone reacts very rapidly with water leading to the formation of gluconic acid

$$\text{Glucolactone} + H_2O \rightarrow \text{gluconic acid} \quad (2)$$

The enzymically catalysed hydrolysis of acetylcholine is of the same type of reaction:

$$\text{Acetylcholine} + H_2O \xrightarrow{\text{Acetylcholine esterase}} \text{acetic acid} + \text{choline} \quad (3)$$

In both instances a weak acid is formed as the protolytic product of the enzymic reaction. Several pH sensors can be employed to follow the course of these reactions; of these, hydrogen ion sensitive glass electrodes and hydrogen ion selective field effect transistors (ISFETs) have been used most often for construction of glucose[2–4] and acetylcholine[5–7] biosensors.

The reactions given above can be described by the general equation:

$$S + X \xrightarrow{\text{Enzyme}} n_A\,HA + Z \quad (4)$$

where S denotes the substrate of the enzymic reaction (the analyte), and X and Z are a non-protolytic substrate and the product, respectively. The species HA is a weak acid, *viz.*, gluconic acid ($pK_a = 3.77$) or acetic acid ($pK_a = 4.73$), for the reaction of glucose and acetylcholine, respectively. The weak acid formed in the enzymic reaction decreases the pH at the surface of the pH sensor, leading to a change in the analytical signal. Calibration graphs for these sensors can be described by the general equation of our model:[1]

$$\bar{k}_H([H]^B - [H]) + \bar{k}_W c_W^B\left(\frac{1}{1 + K_{aW}/[H]^B} - \frac{1}{1 + K_{aW}/[H]}\right) + \frac{1}{2}\left[[S]^B + \bar{k}_V + K_m - \sqrt{([S]^B - \bar{k}_V - K_m)^2 + 4K_m[S]^B}\right]\left(\frac{n_A}{1 + [H]/K_{aA}} - \frac{n_B}{1 + K_{aB}/[H]}\right) = 0 \quad (5)$$

where $[H]^B$, $[S]^B$ and c_W^B denote the concentration of hydrogen ion, substrate and buffer in the bulk solution, respectively, [H] is the concentration of hydrogen ion in the enzymic layer of the sensor, $\bar{k}_H = k_H/k_S$, $\bar{k}_W = k_W/k_S$ and $\bar{k}_V = V_{max}/k_S$ are normalized rate constants described by k_H, k_W, and k_S, which correspond to the transport rate constants of species from the bulk solution into the enzymic layer of the sensor for hydrogen ions (H), buffer (W) and substrate (S), respectively, V_{max} is the enzymic reaction-rate maximum, K_{aW}, K_{aH}, and are K_{aB} the acid dissociation constants of the buffer component, the acid formed in the course of the enzymic reaction and the conjugate acid of the base being the product of the reaction, respectively, K_m is the Michaelis–Menten constant, and n_A and n_B denote the stoichiometric coefficients for an acid and a base formed as products of the enzymic reaction.

The purpose of this paper is to present methods of fitting theoretical calibration graphs, evaluated on the basis of our model, to experimental points obtained during the calibration of glucose and acetylcholine sensors. The main reason for the choice of these sensors for the presentation of the fitting methods is the simplicity of their enzymic reactions. This is because, as was mentioned earlier, only one protolytic product is formed and the kinetic parameters of the enzymic reaction (V_{max}, K_m) are independent of pH in both instances. From a kinetic point of view the main difference between these reactions is due to the high value of the Michaelis–Menten constant for glucose oxidase in comparison with that for acetylcholine esterase. This is the reason for the different shapes of the calibration graphs for the glucose and acetylcholine sensors.

Experimental

Apparatus and Reagents

A digital pH meter (Radelkis Model OP-208/1) was used for measuring all electrode responses. A glass electrode with a spherical hydrogen ion sensitive surface (Radelkis Model OP-0718P) was used for the preparation of the glucose and acetylcholine sensors. A double-junction Ag–AgCl electrode (Radelkis Model OP-08209) was used as a reference electrode.

The enzymes glucose oxidase (EC 1.1.3.4) and catalase (EC 1.11.1.6) were obtained from Merck, and acetylcholine esterase (EC 3.1.1.7) was a product of Loba.

Analytical-reagent grade reagents were used to prepare buffers and standard glucose and acetylcholine solutions. Acetone was purified by distillation. Phosphate buffer solution (0.001 mol dm^{-3}) was prepared by dissolving the appropriate amount of NaH_2PO_4 in 0.1 mol dm^{-3} NaCl solution. Tris(hydroxymethyl)methylamine was used for pre-

* For Part 1 of this series see ref. 1.

paration of the Tris buffer (0.001 mol dm^{-3}). The pH of both buffers was adjusted to pH 7.00 with NaOH solution. Glucose solutions (0.005 and 2.5 mol dm^{-3}) were prepared by dissolving the appropriate amount of glucose in phosphate buffer solution, whereas for the preparation of acetylcholine solutions (0.005 and 2.5 mol dm^{-3}) Tris buffer was used as solvent.

Cellulose triacetate (BDH) was used for enzyme entrapment.

Preparation of Glucose and Acetylcholine Electrodes

For the preparation of glucose and acetylcholine sensors the procedure described previously for urea electrodes[8] was used. The hydrogen ion sensitive glass electrode was dipped for 5 min in a solution containing a mixture of cellulose triacetate and enzyme. During drying (5 min) the electrode with the gel layer was rotated horizontally around its axis in order to obtain a uniform layer on the glass surface. The electrode was dipped again briefly in the same solution and then dried in the same manner as before. Then, the dried electrode was immersed in a vigorously stirred 0.1 mol dm^{-3} NaCl solution for 30 min in order to eliminate any excess of enzyme from the electrode surface. The solution used for the preparation of glucose electrode membranes contained 200 mg of glucose oxidase, 100 mg of catalase and 20 mg of cellulose triacetate in 3 cm^3 of acetone. The solution used for the preparation of the acetylcholine esterase membranes contained 100 mg of acetylcholine esterase and 20 mg of cellulose triacetate in 3 cm^3 of acetone.

Measurements

The calibration of the glucose electrode in the range from 1×10^{-4} to 1×10^{-1} mol dm^{-3} glucose and of the acetylcholine electrode in the range from 2×10^{-5} to 1×10^{-1} mol dm^{-3} acetylcholine was carried out by stepwise addition of the appropriate standard solutions to the test solution. Phosphate buffer of concentration 0.001 mol dm^{-3} and pH 7.00 was used as the test solution during the course of the calibration of the glucose electrode. For the acetylcholine electrode, 0.001 mol dm^{-3} Tris buffer (pH 7.00) was used. After each addition, the steady-state potential of the electrode was measured.

The experimental results of the calibration of the electrodes are plotted in Fig. 1.

Results and Discussion

The kinetic model of pH-based potentiometric enzymic sensors discussed here refers to one of the simplest enzymic sensors. In both of the enzymic reactions discussed 1 mol of substrate (glucose or acetylcholine) forms 1 mol of weak acid. No other protolytic product is formed. According to the reaction given in eqn. (4), the stoichiometric coefficients are $n_A = 1$ and $n_B = 0$. It was assumed that the transport rate constants for all species are the same, and as a consequence $\bar{k}_W = \bar{k}_H = 1$. The next assumption was that the kinetic parameters of the enzymic reaction, K_m and $\bar{k}_V$, are independent of pH. Additionally, inhibition processes are not taken into account. With all the assumptions mentioned above the general equation describing our model [eqn. (5)] can be transformed into:

$$([H]^B - [H])\left[1 + \frac{K_{aW}c_W^B}{(K_{aW} + [H]^B)(K_{aW} + [H])}\right] + \frac{[S]^B + \bar{k}_V + K_m - \sqrt{([S]^B - \bar{k}_V - K_m)^2 + 4K_m[S]^B}}{2(1 + [H]/K_{aA})} = 0 \quad (6)$$

The dissociation constants, K_{aW}, of the acid component of the buffers used were taken as 6.2×10^{-8} and 8.0×10^{-9} for the phosphate and Tris buffer, respectively.

Equations (6) and (5) are given in the form of an implicit function with two variables, where:

$$F\left(\underbrace{[H], [S]^B}_{\text{variables}}, \underbrace{K_m, \bar{k}_V}_{\text{parameters}}, \underbrace{[H]^B, c_W^B, K_{aW}, K_{aA}, K_{aB}}_{\text{constants}}\right) = 0 \quad (7)$$

In order to obtain the best fits of the theoretical curves to the experimental data, in a similar way to the well-known least-squares method,[9] the following condition for the minimization of the function in eqn. (7) can be formulated:

$$\Phi = \sum_{i=1}^{n} [pH_{(i)} - pH([S]_{(i)}^B)]^2 = \text{minimum} \quad (8)$$

where n denotes the number of experimental points, $pH_{(i)}$ is an experimentally measured value of the analytical signal (pH) of the sensor at a substrate concentration in the bulk solution $[S]_{(i)}^B$. The parameter $pH([S]_{(i)}^B)$ denotes the calculated value of the analytical signal [eqn. (6)], *i.e.*, the pH in the enzymic layer of the sensor, at the same concentration of substrate $[S]_{(i)}^B$. The values of all the parameters and constants [eqn. (7)] have to be established. The parameter $pH([S]_{(i)}^B)$ is not given in an explicit way and its calculation gives rise to the same problems as the calculation of the pH of complex mixtures of weak acids and bases.[10]

The implicit function given by eqn. (6) is transformed into the polynomial, $f([H]) = 0$, when the values of all the constants, *i.e.*, $[H]^B$, c_W^B, K_{aA} and K_{aW}, and parameters, *i.e.*, K_m and $\bar{k}_V$, are known. A simple bisection method[9] is proposed here for the evaluation of [H] from this equation. Unfortunately, convergence of the classical bisection method

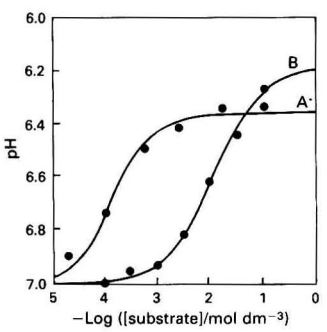

Fig. 1 Calibration graphs for A, acetylcholine and B, glucose enzymic sensors

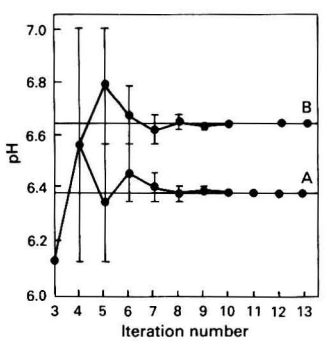

Fig. 2 Convergence of bisection procedure used for calculation of pH from eqn. (6). Curve A: acetylcholine, $c_S^B = 0.01$ mol dm^{-3}, $K_m = 5.97 \times 10^{-5}$ mol dm^{-3}, $\bar{k}_V = 5.95 \times 10^{-5}$. Curve B: glucose, $c_S^B = 0.01$ mol dm^{-3}, $K_m = 7.41 \times 10^{-3}$ mol dm^{-3}, $\bar{k}_V = 2.95 \times 10^{-4}$. Vertical bars correspond to the pH range in which the unknown pH value is included

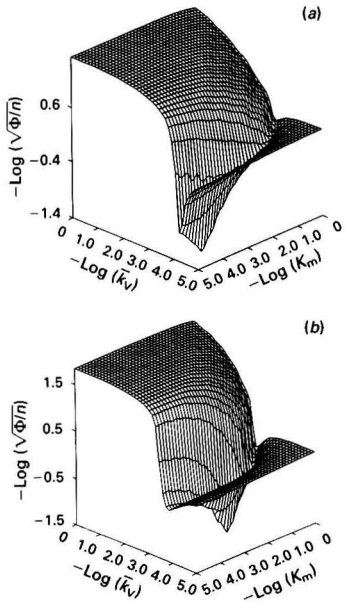

Fig. 3 Dependence of the function $\sqrt{\phi/n}$ on K_m and $\bar{k}_V$ for (*a*) acetylcholine and (*b*) glucose sensors

is slow. Only one accurate binary digit is obtained in each iteration step. It is possible to obtain one decimal digit, on average, every 3.3 iteration steps because $10^{-1} \approx 2^{-3.3}$. This is the reason why we propose to use the bisection method on the common logarithmic scale. This simple modification allows the pH value to be calculated with an accuracy of better than 1×10^{-4} of a pH unit after the use of only 10–20 iteration steps (Fig. 2). In our opinion the bisection method modified in this way might be useful for calculations connected with the investigation of complex protolytic equilibria.[10]

Minimization of the function ϕ [eqn. (8)] was carried out by using the simplex method.[11,12] The function ϕ was treated as the response function. The simplex was defined in two-dimensional space in terms of log K_m and log $\bar{k}_V$, and minimization of ϕ was carried out with respect to these two variables. The use of the common logarithmic scale ensured better convergence of the fitting procedure than for the parameters K_m and $\bar{k}_V$ using a linear scale. The dependence of the function ϕ on the parameters K_m and $\bar{k}_V$ for the response of the glucose and acetylcholine sensors under the experimental conditions given above is shown in Fig. 3. The simplex moves by reflection and changes its size by contraction.[11,12] Fig. 4 shows the progress of the simplex and Fig. 5 illustrates the convergence of the proposed procedure. The curves presented in Fig. 5 were plotted using data corresponding to the best vertex of the simplex for successive iteration steps.

For all the calculations involved in the proposed fitting procedure a computer program written in PASCAL was used. (A listing of the computer program is available from the authors). This program can be used for simultaneous curve fitting, *i.e.*, evaluation of the parameters K_m and $\bar{k}_V$, to the experimental data obtained under various experimental conditions, *e.g.*, for different values of pH and buffer concentration. This is possible because the minimization condition [eqn. (8)] was formulated in this program in a more general form, given by eqn. (9):

$$\Phi = \sum_{j=1}^{k} \sum_{i=1}^{n} [\mathrm{pH}_{(i,j)} - \mathrm{pH}\,([\mathrm{S}]^{\mathrm{B}}_{(i,j)}, K_{\mathrm{aW}(j)}, [\mathrm{H}]^{\mathrm{B}}_{(j)}, c^{\mathrm{B}}_{\mathrm{W}(j)})]^2 = 0 \quad (9)$$

where j denotes successive experiments.

The function ϕ is a good and useful criterion of the proposed

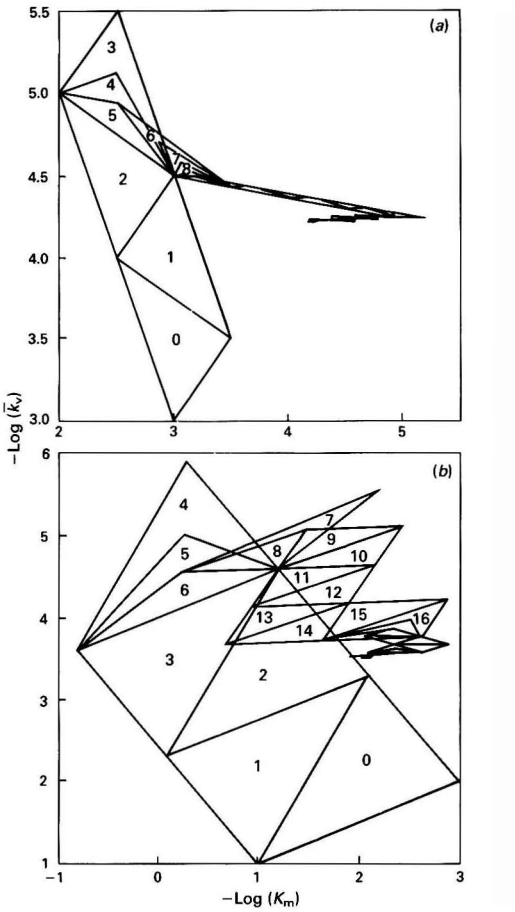

Fig. 4 Simplex moves in the course of the minimization procedure of the function ϕ for (*a*) acetylcholine and (*b*) glucose sensors. Numerals correspond to the iteration numbers

procedure because the expression $\sqrt{\phi/n}$ determines quantitatively the standard deviation of the fit. The standard deviation, calculated as $\sqrt{\phi/n}$, is given in pH units but after multiplying by the slope of the pH sensor (59 mV per pH unit for the theoretical case) has the dimension of potential (mV). In Figs. 1 and 6 (line E) the best fits of the calibration graphs, calculated on the basis of our model, to the experimental data obtained for the glucose and acetylcholine sensors are presented. Fig. 6 also shows the progress of the fitting procedures.

The evaluated kinetic parameters of the enzymic reaction for the glucose sensor are as follows: $K_m = 7.41 \times 10^{-3}$ mol dm^{-3}, $\bar{k}_V = 2.95 \times 10^{-4}$. The value of the function ϕ for these values of K_m and $\bar{k}_V$ is 5.6×10^{-4} with a standard deviation, $\sqrt{\phi/n}$, of 8.9×10^{-3} of a pH unit ($n = 7$). Similarly, for the acetylcholine sensor, $K_m = 5.97 \times 10^{-5}$ mol dm^{-3}, $\bar{k}_V = 5.95 \times 10^{-5}$ and $\phi = 3.2 \times 10^{-3}$, with a standard deviation, $\sqrt{\phi/n}$, of 0.023 of a pH unit ($n = 6$). The values of the standard deviation in both instances are virtually the same as the precision of measurements with glass electrodes. This confirms the good agreement between our theoretical model of the enzymic sensor response and the experimental data. An even better agreement between theory and practice could probably be achieved by taking into account the effect of pH on enzyme activity. In the glucose sensor an additional source of error is the consumption of oxygen in the enzymic reaction, which was not taken into account. The inhibition by the

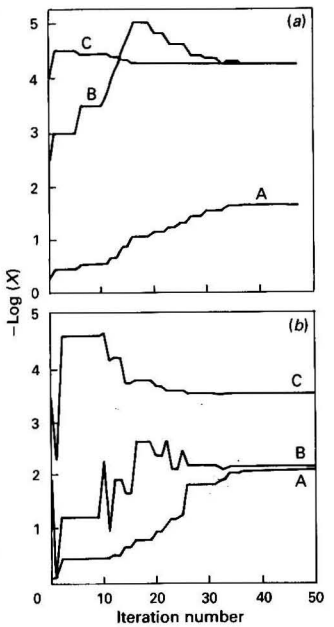

Fig. 5 Iteration progress of the fitting procedures for (*a*) acetylcholine and (*b*) glucose sensors. A, Log $\sqrt{\phi/n}$; B, log K_m; and C, log $\bar{k}_V$

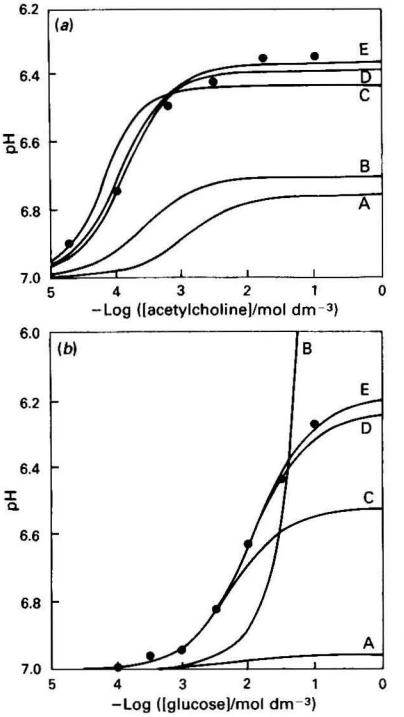

Fig. 6 Calibration graphs for (*a*) acetylcholine and (*b*) glucose sensors. Lines: theoretical curves calculated at various iteration numbers of the fitting procedure. Iteration numbers: A, 1; B, 10; C, 20; D, 30; and E, 40 (the last). The points show the experimental data

product of the reaction (H_2O_2) probably does not occur because the enzymic layer also contains catalase in addition to glucose oxidase. Acetylcholine at high concentration probably results in the inhibition of the enzymic reaction[13] and it might be a source of some deviation from the theoretical expectation.

The calibration graphs for the glucose and acetylcholine sensors have different shapes. This is caused by the difference in the value of the Michaelis–Menten constant, K_m, for the enzymic reactions. The rate, V, of the over-all enzymic reaction is given by the equation: $V = V_{max}[S]/(K_m + [S])$, where [S] denotes the substrate concentration in the enzymic layer. The low value of K_m for the acetylcholine enzymic reaction results in the appearance of the upper limit of determination at relatively low substrate concentrations and is the reason for the narrow response plot obtained for the acetylcholine sensor. A high value of the reaction rate at acetylcholine concentrations lower than the Michaelis—Menten constant ($[S] \ll K_m$) when the reaction is first order leads to high sensor sensitivity. The opposite situation exists with the glucose sensor. The high value of the Michaelis–Menten constant effectively results in the absence of an upper limit of determination. The enzymic reaction is first order over a wide range of glucose concentrations with a relatively low constant rate and this is the reason for the wide linear response range and the low electrode sensitivity.

The considerations presented here are based on very simple enzymic reactions. A more detailed experimental verification of the kinetic model of the response of pH-based sensors will be presented in Part 3 of this series.[14] The experimental results obtained under various experimental conditions with the use of a urea electrode will be discussed. In this instance, the product of the enzymic reaction is a complex mixture of a weak acid and a weak base. The kinetic parameters of the enzymically catalysed hydrolysis of urea depend on pH. The influence of pH on these parameters will be taken into account.

The authors are grateful to Professor Adam Hulanicki for valuable discussions, and to Maciej Wałcerz for his help in the preparation of the computer program. This study was supported by the Committee of Scientific Research (Grant No. 2-0587-9101).

References

1 Głąb, S., Koncki, R., and Hulanicki, A., *Analyst*, 1991, **116**, 453.
2 Nilsson, H., Akerlund, A. C., and Mosbach, K., *Biochim. Biophys. Acta*, 1975, **320**, 529.
3 Caras, S. D., Petelenz, D., and Janata, J., *Anal. Chem.*, 1985, **57**, 1920.
4 Eddowes, M. J., Pedley, D. G., and Webb, B. C., *Sens. Actuators*, 1985, **7**, 233.
5 Durand, P., David, A., and Thomas, D., *Biochim. Biophys. Acta*, 1978, **527**, 277.
6 Suaud-Chagny, M. F., and Pujol, J. F., *Analusis*, 1985, **13**, 25.
7 Tor, R., and Freeman, A., *Anal. Chem.*, 1986, **58**, 1042.
8 Koncki, R., Leszczyński, P., Hulanicki, A., and Głąb, S., *Anal. Chim. Acta*, 1992, **257**, 67.
9 Dahlquist, G., and Bjorck, A., *Numerical Methods*, Prentice-Hall, Englewood Cliffs, NJ, 1974.
10 Hulanicki, A., *Reactions of Acids and Bases in Analytical Chemistry*, Ellis Horwood, Chichester, 1989.
11 Deming, S. N., and Parker, L. R., *CRC Crit. Rev. Anal. Chem.*, 1978, **7**, 187.
12 Burton, K., *Anal. Proc.*, 1989, **26**, 285.
13 *The Enzymes*, ed. Boyer, P. D., Academic Press, New York, 1970, vol. 1.
14 Głąb, S., Koncki, R., and Hulanicki, A., *Analyst*, 1992, **117**, 1675.

NOTE—Refs. 1 and 14 are to Parts 1 and 3 of this series, respectively.

Paper 2/01220K
Received March 6, 1992
Accepted June 9, 1992

Kinetic Model of pH-based Potentiometric Enzymic Sensors Part 3.* Experimental Verification

Stanisław Głąb, Robert Koncki and Adam Hulanicki
Department of Chemistry, University of Warsaw, Pasteura 1, 02-093 Warsaw, Poland

An experimental verification of the kinetic model for a pH-based potentiometric enzymic sensor is presented. For this purpose the experimental results obtained using a urea sensor prepared by the immobilization of urease on the hydrogen ion sensitive surface of a glass electrode were employed. The effects of buffer capacity and pH and also the rate of solution stirring on the electrode response were examined and the results obtained were compared with those predicted theoretically. The influence of local changes in pH within the enzymic layer of the sensor on the enzyme kinetics is also discussed.

Keywords: *Potentiometric enzymic pH sensor; kinetic model; urea electrode*

A urea electrode prepared by the immobilization of urease on the measuring surface of a hydrogen ion sensitive glass electrode is an example of a pH-based enzymic sensor. It was used during experiments carried out for practical verification of a theoretical model.[1]

Urease (EC 3.5.1.5) catalyses the hydrolysis of urea specifically, presented formally as

$$(H_2N)_2CO + 2H_2O \rightarrow 2NH_3 + H_2CO_3 \quad (1)$$

which leads to the formation of carbonic acid and ammonia. The enzymically catalysed hydrolysis of urea results in an increase in the pH of the medium because the concentration of the ammonia formed is twice that of carbonic acid, which is a weaker acid than ammonia is a base $\{pK_{a(NH_4^+)} > pK_{a(H_2CO_3)}\}$

$$K_{a(H_2CO_3)} = \frac{[HCO_3^-][H^+]}{[H_2CO_3]} = 4.3 \times 10^{-7} \quad (2)$$

$$K_{a(NH_4^+)} = \frac{[NH_3][H^+]}{[NH_4^+]} = 5.6 \times 10^{-10} \quad (3)$$

The increase in pH within the urease layer is measured with a glass electrode. The response of such a sensor to urea concentration ($[H^+]$ or pH *versus* urea concentration) is described by the general algebraic equation of the kinetic model[1]

$$\bar{k}_H([H]^B - [H]) + \bar{k}_W c_W^B \left(\frac{1}{1 + K_{aW}/[H]^B} - \frac{1}{1 + K_{aW}/[H]}\right) + \frac{1}{2}\left[[S]^B + \bar{k}_V + K_m - \sqrt{([S]^B - \bar{k}_V - K_m)^2 + 4K_m[S]^B}\right] \times \left(\frac{n_B}{1 + [H]/K_{aA}} - \frac{n_B}{1 + K_{aB}/[H]}\right) = 0 \quad (4)$$

where [H] is the concentration of hydrogen ions inside the enzymic layer, $[S]^B$, c_W^B and $pH^B = \log[H]^B$ are the analyte concentration, buffer concentration and pH of the buffer, respectively, K_{aA}, K_{aB} and K_{aW} are the dissociation constants of carbonic acid [eqn. (2)], ammonium ion [eqn. (3)] and the acid component of the buffer, respectively, $\bar{k}_H = k_H/k_S$, $\bar{k}_W = k_W/k_S$, and $\bar{k}_V = V_{max}/k_S$ are the normalized rate constants described by k_H, k_W and k_S (the transport rate constants of hydrogen ions, buffer and substrate, respectively), and by the enzymic reaction rate maximum, V_{max}.

The equation given above and the experimental results obtained using a urea electrode are the basis of the experimental verification of the kinetic model of pH-based enzymic sensors. It was assumed that the rate constants of the transport of all the species are equal, and, as a consequence, the normalized rate constants, $\bar{k}_H$ and $\bar{k}_W$, are equal to unity. The stoichiometric coefficients of the hydrolysis of urea are: $n_A = 1$ and $n_B = 2$.

A simplex method[2] was used in this work to fit the theoretical response to the results obtained experimentally for the urea sensor. The standard deviation, given by the parameter $\sqrt{\Phi/n}$, was a criterion of fit. The method of fitting and the role of the parameter $\sqrt{\Phi/n}$ were described in detail in Part 2 of this series.[2] The fitting procedure allows the kinetic parameters of the enzymic reaction, K_m and $\bar{k}_V$, to be evaluated.

Urease is an enzyme that is sensitive to the pH of the medium; the influence of pH on the enzyme activity is well described by the model of Waley,[3] which was discussed in Part 1.[1]

In this paper, the experimental verification of our model for a case where two protolytic compounds are formed as the products of an enzymic reaction is presented. In addition, the influence of the protolytic side-reactions of the enzyme on the sensor response is discussed and explained theoretically on the basis of derived equations:[1]

$$\bar{k}'_V = \bar{k}_V \frac{pH_{opt}}{1 + K_{a1}/[H] + [H]/K_{b1}} \quad (5)$$

$$K_m = K_m\, pH_{opt} \frac{1 + K_{a2}/[H] + [H]/K_{b2}}{1 + K_{a1}/[H] + [H]/K_{b1}} \quad (6)$$

where $\bar{k}_V$ and K_m are the kinetic parameters of the enzymic hydrolysis of urea at a pH corresponding to the maximum activity of urease; $K_{a1} = 7 \times 10^{-9}$ mol dm^{-3}, $K_{a2} = 3.1 \times 10^{-8}$ mol dm^{-3}, $K_{b1} = 3.6 \times 10^{-5}$ mol dm^{-3} and $K_{b2} = 1.4 \times 10^{-6}$ mol dm^{-3}, which are the acid and base dissociation constants for urease and the urea–urease complex[4,5] (see Fig. 2 in ref. 1).

Experimental

Apparatus and Reagents

The apparatus and equipment used was the same as that described previously.[6] The enzyme urease (5 U mg^{-1}) (1 U = 16.67 nkat) was obtained from Merck. Phosphate buffer solutions were prepared by dissolving the appropriate amount of NaH_2PO_4 in 0.1 mol dm^{-3} NaCl solution. The pH was adjusted with NaOH solution. Urea solutions were prepared by dissolving urea in 0.1 mol dm^{-3} NaCl solution.

* For Part 2 of this series see ref. 2.

Preparation of the Urea-sensitive Glass Electrode

A hydrogen ion sensitive glass electrode was rinsed in water and then in acetone. After drying, the electrode was immersed in a solution containing 20 mg of cellulose triacetate and 200 mg of urease in 3 cm^3 of acetone and was then dried in air for 5 min. During the drying period, the electrode was rotated in a horizontal plane in order to obtain a uniform enzymic membrane on the measuring surface of the glass electrode. The immersing and drying procedures were repeated twice.

The preparation of the urea-sensitive glass electrodes and their properties have been described in detail elsewhere.[6]

Measurements

Measurements of the e.m.f. of the urea–silver–silver chloride electrode system as a function of the urea concentration were performed in solutions containing 0.1 mol dm^{-3} NaCl and phosphate buffer at different pH values and buffer concentration. Portions of the urea standard solution were added successively to the measured solution when the urea electrode had reached a steady-state potential.

Results

Influence of Buffer Concentration on the Shape of the Sensor Calibration Graph

The effect of the buffer concentration (c_W^B) on the sensor response was examined by calibrating the sensor in stirred solutions containing phosphate buffer (pH 7.00) at different concentrations (0.001, 0.005 and 0.02 mol dm^{-3}). The results are represented as points in Fig. 1. The lines are the predicted calibration graphs obtained by the fitting procedure. The results of fitting (for two cases, *viz.*, when the effect of pH on the enzymic reaction kinetics is both taken into account and ignored) are presented in Table 1.

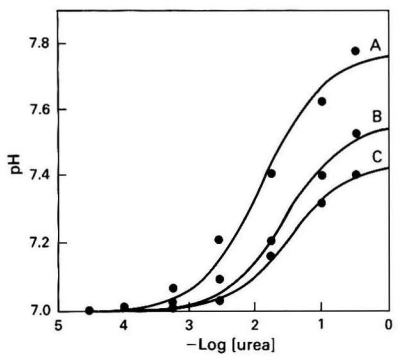

Fig. 1 Influence of buffer concentration, c_W^B, on the response of the pH-based urea sensor. Phosphate buffer, pH = 7.00. A, c_W^B = 1 mmol dm^{-3}; B, c_W^B = 5 mmol dm^{-3}; and C, c_W^B = 20 mmol dm^{-3}. The lines show the theoretical response which takes into account the effect of pH on the enzyme kinetics; the points represent the experimental data

Effect of Buffer pH on the Shape of the Sensor Calibration Graph

The influence of the acidity of the analysed solutions on the sensor response was examined by carrying out the calibration of the sensor in stirred solutions with a constant buffer concentration (0.005 mol dm^{-3}). The pH values of the solutions were 6.00, 7.00 and 8.00. The results of fitting the general equation [eqn. (4)] to the experimental data, when the influence of pH on the enzymic reaction kinetics is both taken into account and ignored, are summarized in Table 2. The experimental results (points) and calculated calibration graphs (lines) are presented in Fig. 2.

Effect of Solution Stirring Rate on the Shape of the Sensor Calibration Graph

The results of sensor calibration in solutions containing 0.005 mol dm^{-3} phosphate buffer (pH 7.00) were used to study the influence of stirring rate on the sensor response. The solutions were stirred at relative rates equal to 0, 20, 50 and 100% of the

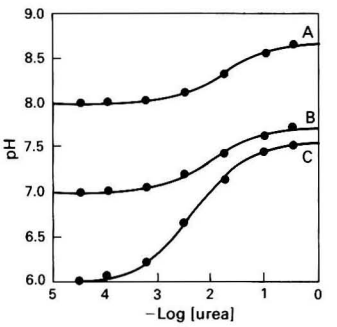

Fig. 2 Influence of buffer pH, pH^B, on the response of the pH-based urea sensor. Phosphate buffer, c_W^B = 5 mmol dm^{-3}. A, pH^B = 8.00; B, pH^B = 7.00; and C, pH^B = 6.00. The lines show the theoretical response (as in Fig. 1); the points represent the experimental data

Table 1 Results of fitting the theoretical to the experimentally observed response of the urea sensor at various concentrations of phosphate buffer, c_W^B, in the bulk solution. pH^B = 7.00. Constant rate of solution stirring. The kinetic parameters of the enzymic reaction, *viz.*, K_m and $\bar{k}_V = V_{max}/k_S$, were evaluated, ignoring the influence of pH on the enzyme kinetics and taking this effect into account (indicated by primes). $\sqrt{\Phi/n}$ is the standard deviation of fitting

c_W^B/ mmol dm^{-3}	K_m/ mmol dm^{-3}	$\bar{k}_V \times 10^{-3}$	$\sqrt{\Phi/n}$ (ΔpH)	K'_m/ mmol dm^{-3}	$\bar{k}'_V \times 10^{-3}$	$\sqrt{\Phi/n'}$ (ΔpH)
1.0	13.1	0.41	0.037	12.6	0.59	0.033
5.0	32.1	1.50	0.021	28.3	1.93	0.020
20.0	33.3	4.62	0.007	28.2	5.60	0.006
For all c_W^B	13.9	0.45	0.143	16.2	0.77	0.128

Table 2 Results of fitting the theoretical to the experimentally observed response of the urea sensor at various pH values of phosphate buffer with concentration, c_W^B = 5 mmol dm^{-3}. Constant rate of solution stirring. Abbreviations as in Table 1

pH^B	K_m/ mmol dm^{-3}	$\bar{k}_V \times 10^{-3}$	$\sqrt{\Phi/n}$ (ΔpH)	K'_m/ mmol dm^{-3}	$\bar{k}'_V \times 10^{-3}$	$\sqrt{\Phi/n'}$ (ΔpH)
6.0	11.2	3.05	0.012	10.9	3.83	0.011
7.0	10.7	1.90	0.019	9.8	2.63	0.016
8.0	16.5	0.86	0.010	14.6	3.88	0.003
For all pH^B	15.2	2.14	0.191	10.4	3.33	0.050

maximum rate. The results are presented in Fig. 3. The values of the parameters K_m and $\bar{k}_V$ are listed in Table 3. The fits were performed when the effect of pH on the enzymic reaction kinetics was both taken into account and ignored.

Discussion

The experimental data and fit results (Figs. 1–3 and Tables 1–3) indicate that there is good agreement between the theoretical model and the results obtained experimentally. The standard deviations of fitting, given by the expression $\sqrt{\Phi/n}$ (Tables 1–3), are the same as, or better than, the precision of the measurements obtained with the glass electrode used for the preparation of the enzymic sensor. Further improvement of the fitting procedures was achieved in all instances when the influence of pH on the kinetic parameters of the enzymic reaction was taken into account. The consideration of the effect of pH on the kinetics of the enzymic reaction is particularly important when local pH changes within the sensing layer are larger than 1 pH unit and hence the pH might lie outside the range of optimum enzyme activity (Table 2). The kinetic parameters of the enzymic reaction strongly depend on pH outside the pH range of optimum enzyme activity.[3–5] This is illustrated graphically in Fig. 4, where the curves are calculated using eqns. (5) and (6).

Effect of Buffer Concentration on Sensor Response

In agreement with theoretical predictions, the detection limit increases and the sensitivity of the sensor decreases with an increase in buffer concentration. This is because small changes in pH, caused by the mixture of ammonia and carbonic acid formed within the enzymic layer, are obtained when the buffer capacity increases. However, the decrease in sensitivity is not as high as would be expected when only protolytic equilibria[7] are considered. This fact can easily be explained if the increase in the enzyme activity caused by the increase in the buffer concentration is taken into account. The value of the parameter $\bar{k}_V$ ($\bar{k}'_V$) increases proportionally with the buffer concentration for a constant rate of solution stirring (Table 1), demonstrating that the increase in $\bar{k}_V = V_{max}/k_S$ is caused by an increase in the enzymic reaction rate maximum, V_{max}, because the transport rate constant of urea, k_S, does not change at a constant stirring rate. Phosphate, which was a component of the buffer used, influences the kinetic parameters of the enzymic reaction. The activation process is based on the formation of carbonyl phosphate as an intermediate reaction product.[8] The increase in urease activity caused by phosphate has also been reported by other workers.[9] The influence of phosphate as activator was not taken into account in our considerations, and this is probably the reason for the worse fit of our model to all the experimental points obtained at various buffer concentrations, c_W^B, than for one buffer concentration (Table 1). For the measurements discussed, only a small improvement in fit was achieved by taking into account the effect of pH on the kinetics of the enzymic reaction. This was caused by the very small changes in pH within the enzymic layer in the range of pH where the activity of urease is relatively constant (Fig. 4).

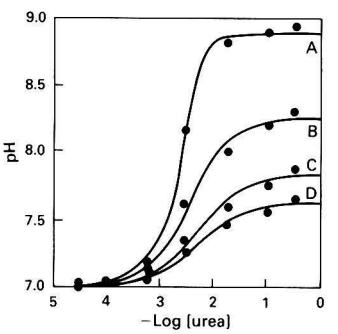

Fig. 3 Influence of the rate of solution stirring on the response of the pH-based urea sensor. Phosphate buffer with concentration 5 mmol dm^{-3} at pH 7.00 was used. 1, $\omega = 0$; 2, $\omega = 20$; 3, $\omega = 50$; and 4, $\omega = 100\%$ of ω_{max}. The lines show the theoretical response (as in Fig. 1); the points represent the experimental data

Effect of Buffer pH on the Sensor Response

An increase in pH in the bulk solution, pH^B, results in a decrease in the sensitivity of the enzyme sensor (Fig. 2). This effect is enhanced in the buffer of pH range 6.00–7.00. The calibration graph corresponding to pH 6.00 shows a low detection limit because of the low phosphate buffer capacity. The calibration graphs corresponding to pH 7.00 and 8.00 are similar. A slightly larger electrode slope was observed at pH 7.00 than at pH 8.00.[6] This was attributed to the theoretically possible changes in pH caused by the enzymic reaction, these being 2.3 and 1.3 pH units, respectively. These values were calculated under the assumption that the maximum obtainable pH value within the enzymic layer is 9.3.[6,7] Of course, this pH value is never reached in practice. When the effect of pH on the kinetic parameters is not taken into account it can be predicted, on the basis of the model discussed, that the detection limit at pH 8.00 should be slightly lower than at pH 7.00.[1] This conclusion is not consistent with the experimental results[6] because the activity of urease at pH 8.00 is lower than at pH 7.00 (Fig. 4). Therefore, the same concentration of urea in the analysed solution at pH 8.00 results in a smaller pH increase within the sensing layer than at pH 7.00. This causes

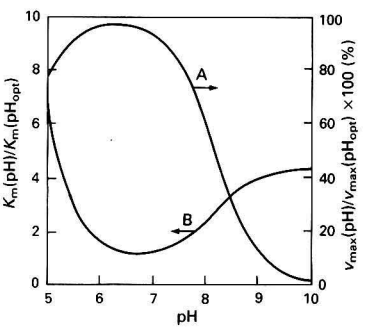

Fig. 4 Effect of pH on the kinetic parameters of the urea enzymic reaction (A, V_{max}; B, K_m) evaluated from eqns. (5) and (6)

Table 3 Results of fitting the theoretical to the experimentally observed response of the urea sensor at different stirring rates, ω. Phosphate buffer with concentration, $c_W^B = 5$ mmol dm^{-3} and pH = 7.00 was used. Abbreviations as in Table 1

ω (% of ω_{max})	K_m/ mmol dm^{-3}	$\bar{k}_V \times 10^{-3}$	$\sqrt{\Phi/n}$ (ΔpH)	K'_m/ mmol dm^{-3}	$\bar{k}'_V \times 10^{-3}$	$\sqrt{\Phi/n'}$ (ΔpH)
0	0.1	7.36	0.038	0.7	50.73	0.032
20	1.7	3.13	0.052	2.5	7.20	0.042
50	4.0	2.18	0.037	4.0	3.25	0.033
100	4.4	1.68	0.020	3.9	2.20	0.018

an increase in the detection limit and a decrease in the sensitivity for measurements carried out at pH 8.00 in spite of the high buffer capacity at pH 7.00, The contribution of pH and buffer capacity is similar, and, depending on the experimental conditions, one of these factors may predominate; consequently, the urea sensor may exhibit a higher sensitivity at pH 8.00.[6] Hence, it can be concluded that the determination of urea in phosphate buffer solution should be carried out at pH 6.00. Under these conditions the buffer capacity of the solution is relatively low, and the urease activity is virtually at a maximum. An increase in pH up to the pK_a of the buffer used ($pK_a = 7.2$ for phosphate) does not change the urease activity, but results in an increase in the buffer capacity, and in consequence leads to worse sensor characteristics. A further increase in pH influences the response of the urea sensor in two ways: the buffer capacity decreases, which is advantageous, but a simultaneous decrease in enzyme activity is observed at higher pH values (Fig. 4).

The fitting of our model to the experimental points obtained for phosphate buffers of various pH is presented in Fig. 2 and Table 2. The standard deviations ($\sqrt{\Phi/n}$) of the fit clearly show the strong influence of pH on the enzymic reaction kinetics. When this influence is not taken into account the values obtained for the parameter $\bar{k}_V = V_{max}/k_S$ (proportional to enzyme activity) decrease with increasing pH. Taking this effect into consideration [eqns. (5) and (6)] enables more correct values to be obtained. This also allows the theoretical curves and experimental results to be fitted better. This is shown particularly for the results obtained at pH 8.00 and for fitting all the experimental points (Table 2). In the above examples the standard deviation of fit decreases about four times.

Effect of Stirring Rate on Sensor Response

An increase in the stirring rate causes a decrease in the sensitivity of the sensor, a slight increase in the detection limit and an extension of the linear range of the sensor response (Fig. 3). The transport of the analyte from the bulk solution into the enzymic layer of the electrode strongly depends on the stirring rate. The stirring rate similarly influences the transport of the enzymic reaction substrate (urea) from the bulk solution into the enzymic layer of the sensor and the transport of the reaction product (ammonium carbonate) in the reverse direction. The enzymic reaction, the rate of which is independent of the transport rate, is the slowest step in the generation of the analytical signal. Hence an increase in the stirring rate results in a decrease in the electrode sensitivity, particularly for higher concentrations of urea. (When the enzymic reaction becomes zero order, its rate becomes independent of the urea concentration inside the enzymic layer.)

The stirring rate strongly influences the rate of transport of the enzymic reaction products from the enzymic layer and also the rate of transport of the buffer components. An increase in the stirring rate results in a steady state, leading to a decrease in ammonium carbonate within the enzymic layer, and consequently in a decrease in the analytical signal. On the other hand an increase in the stirring rate leads to a shorter response time.[6]

In the model discussed the effect of stirring rate on the sensor response is described by the parameter $\bar{k}_V = V_{max}/k_S$. For the experiments discussed, all the conditions except for the rate of solution stirring were the same. The stirring rate does not influence the reaction rate maximum, V_{max}. Hence, changes of the parameter $\bar{k}_V$ are caused only by changes in the transport rate constant of the substrate, k_S. An increase in the stirring rate results in an increase in the parameter k_S and consequently in a decrease in the parameters $\bar{k}_V$ and $\bar{k}'_V$ (Table 3). The difference between the evaluated parameters $\bar{k}_V$ and $\bar{k}'_V$ decreases when the stirring rate increases (Table 3). This is because, for a given urea concentration in the bulk solution, a high rate of solution stirring results in a small increase in pH within the enzymic layer, and hence urease acts within the pH range where there is no significant effect on the kinetic parameters. The best sensitivity and detection limit are obtained when the analysed solution is unstirred. However, measurements in unstirred solution are not recommended, because they are highly irreproducible, the response time is very long and the response plot is narrow.[6] A detailed examination of the influence of the solution stirring rate on the enzymic sensor response requires the study of a system where transport conditions are well defined, *e.g.*, in a continuous-flow system.

Conclusions

The model proposed previously[1] accurately describes the response of pH-based enzymic sensors. This model takes into account the transport conditions, all the protolytic equilibria and the enzyme kinetics. The present paper has shown that the experimental results for the urea electrode are in agreement with the predictions of the model. In particular, the model considers the effect of the buffer capacity and buffer pH of the analysed solution and also the rate of solution stirring on the sensor response. It also allows the influence of pH on the enzyme kinetics to be taken into account.

Optimum conditions for the use of pH-based enzymic sensors can be established on the basis of the proposed model. For urea measurements with a pH-based enzymic sensor, phosphate buffer of concentration 5 mmol dm^{-3} and pH 6.0–6.5 is recommended. The buffer capacity in this instance should be low in order to ensure a high electrode sensitivity. The buffer pH is close to the pH of the optimum urease activity. Stirring of the solution influences the sensor response. The analysed solution should be stirred at a rate that is a compromise between decreased sensitivity and increased time of response.

The kinetic model is mathematically simple and can be used successfully to explain and predict the response of pH-based enzymic sensors. The proposed model gives similar results to those obtained using the diffusion model,[10] which is mathematically very complicated.

This study was supported by the Committee of Scientific Research (grant No. 2-0587-9101).

References

1 Głąb, S., Koncki, R., and Hulanicki, A., *Analyst*, 1991, **116**, 453.
2 Głąb, S., Koncki, R., and Holona, I., *Analyst*, 1992, **117**, 1671.
3 Waley, S. G., *Biochim. Biophys. Acta*, 1953, **10**, 27.
4 Atkinson, B., and Rousseau, I., *Biotechnol. Bioeng.*, 1977, **19**, 1065.
5 Barth, A., and Michel, H.-J., *Biochem. Physiol. Pflanz.*, 1972, **163**, 103.
6 Koncki, R., Leszczyński, P., Hulanicki, A., and Głąb, S., *Anal. Chim. Acta*, 1992, **257**, 67.
7 Hulanicki, A., *Reaction of Acids and Bases in Analytical Chemistry*, Ellis Horwood, Chichester, 1989.
8 Fasman, G., and Niemann, C., *J. Am. Chem. Soc.*, 1951, **73**, 1646.
9 Katz, S. A., and Cowans, J. A., *Biochem. Biophys. Acta*, 1965, **107**, 605.
10 Moynihan, H. J., and Wang, N.-H. L., *Biotechnol. Prog.*, 1987, **3**, 90.

NOTE—Refs. 1 and 2 are to Parts 1 and 2 of this series, respectively.

Paper 2/01222G
Received March 6, 1992
Accepted June 9, 1992

Flow Injection Electrochemical Enzyme Immunoassay for Theophylline Using a Protein A Immunoreactor and *p*-Aminophenyl Phosphate–*p*-Aminophenol as the Detection System

Derek A. Palmer, Tony E. Edmonds and Nichola J. Seare
Department of Chemistry, Loughborough University of Technology, Loughborough, Leicestershire, UK LE11 3TU

A competitive electrochemical enzyme immunoassay has been developed for the antiasthmatic drug theophylline, utilizing a controlled-pore glass–protein A immunoreactor and flow injection techniques. *p*-Aminophenyl phosphate, a substrate for alkaline phosphatase, has been used in this assay, and its hydrolysis product *p*-aminophenol was determined at +0.2 V *versus* the saturated calomel electrode. For each sample the antibody–protein A reaction takes place at near-neutral pH, and the complexes are eluted at acid pH. Serum theophylline has been determined by this method, and good relative standard deviations and percentage recoveries have been achieved.

Keywords: *Electrochemical detection; enzyme immunoassay; flow injection; theophylline; protein A*

Theophylline is a member of the xanthine family of drugs, which are central nervous system stimulants. Theophylline is a bronchodilator and respiratory stimulant, its most important use being as a prophylactic agent for controlling the symptoms of chronic asthma. Adequate control of asthma is generally achieved with 8–20 μg cm^{-3}, but in cases of toxicity, levels as high as 60 μg cm^{-3} can be encountered.[1] Owing to the toxicity of theophylline and the variations in metabolism between individuals, the use of the drug as a therapeutic agent necessitates close monitoring.

Many methods have been used to determine theophylline and have been reviewed recently.[2] Gil *et al.*[3] have determined theophylline by an electrochemical enzyme immunoassay method involving flow injection, while other investigators have determined other analytes by flow injection immunoassays involving immunoreactors.[4–6] However, to date there have been no reports on the determination of theophylline or any other analyte by a flow injection electrochemical enzyme immunoassay involving use of a protein A immunoreactor.

Enzymes have been one of the most successful labels in immunoassays,[7] and both homogeneous and heterogeneous assays incorporating these labels are commercially available. Both of these assay formats are based on the inherent signal amplification capabilities of an enzyme label, with quantitative results being achieved by measuring the conversion of substrate into product. Alkaline phosphatase (E.C. 3.1.3.1; orthophosphoric monoester phosphohydrolase) is a commonly used enzyme label. This enzyme hydrolyses orthophosphoric monoesters, yielding inorganic phosphate and the corresponding alcohol, phenol, *etc.*

There are mainly four types of substrate available for alkaline phosphatase assays; the first group includes β-glycerophosphates and hexose phosphates,[8–10] the hydrolysis products of which can, for all practical purposes, be estimated only by the measurement of liberated phosphates. A second group of substrates is represented by phenyl phosphate[11,12] and β-naphthyl phosphate.[13] Phenol and β-naphthol, the hydrolysis products, resemble inorganic phosphates in requiring chromogens to make them determinable by spectrophotometric means; however, the blank values of the hydrolysis products liberated from these substrates are usually low. The third group of substrates is typified by *p*-nitrophenyl phosphate,[14–16] phenolphthalein diphosphate[17,18] and 4-methylumbelliferyl phosphate.[19] These substrates liberate 'self-indicating' products that are visible or fluorescent, although some may require the addition of alkali for full colour development. A fourth group is represented by phosphoenol pyruvate.[20] Alkaline phosphatase hydrolyses this compound with the release of free pyruvate. A second enzyme (lactic acid dehydrogenase) converts the pyruvate into lactate with the coupled disappearance of NADH (reduced nicotinamide adenine dinucleotide). This second reaction is monitored by spectrophotometry.

Enzyme products are commonly detected by spectrophotometric techniques;[21,22] however, absorbance measurements lack adequate sensitivity, while fluorescence detection often suffers from endogenous interference. The wide dynamic range and low detection limits of electroanalytical techniques offer an attractive alternative to spectrophotometric methods.

The use of electrochemical detection for a number of alkaline phosphatase substrates has been reported,[23–25] particularly for phenyl phosphate. Enzymic hydrolysis of this substrate produces phenol, which is determined by oxidative amperometry at +0.8 V *versus* Ag–AgCl.[26]

Recently, the substrate *p*-aminophenyl phosphate (PAPP) has been developed[25] for use with alkaline phosphatase in amperometric enzyme-linked immunoassays. Several immunoassays have been developed, using this substrate, involving detection of the hydrolysis product *p*-aminophenol (PAP) at approximately +0.1 V *versus* Ag–AgCl.[27–29] At this low potential there is no interference from protein oxidation.

Numerous flow injection immunoassays involving immunoreactors have been developed with either electrochemical or optical detection.[5,6] Sepharose,[30] non-porous silica,[6] Trisacryl GF 2000 (Pierce, Rockford, IL, USA),[4] Pall Immunodyne membranes (Pall Biosupport, East Hills, NY, USA)[31] and Biomag 4100 beads (Paesel, Frankfurt, Germany)[31] have all been used as solid phases in immunoreactors in flow injection immunoassays.

Antibodies are by far the most common ligand binders used in solid-phase assays that utilize flow injection techniques.[6,32] However, the antibodies are coupled with the support matrix in a random fashion, limiting the antigen binding capacity, although attempts have been made to overcome this problem.[4] In addition, the specificity of the immobilized antibody means that only a very limited range of antigens can be bound by each immunoaffinity column. These problems can be largely overcome by the use of protein A, most commonly immobilized on Sepharose[33] and controlled-pore glass.[34] Protein A, a protein component found in the cell wall of more than 90% of strains of *Staphylococcus aureus*, has a relative molecular mass of 42 000 and a structure consisting of five

different regions, four of which show strong, specific affinity for the F_c part of antibodies, leaving the antigen-binding sites free.[35] Immobilized protein A can bind at least two molecules of antibodies. As protein A binds the F_c region of antibodies, the antigen receptors are oriented away from the support material and into the mobile phase, maximizing potential binding sites. In addition, a whole range of antibodies with different specificities can be bound to and eluted from the affinity column,[35] ensuring that the matrix not only has high antibody-binding efficiency, but is also extremely flexible in its use.

A number of methods involving the use of immobilized protein A in a flowing system have been developed, the majority of which are used for isolating and purifying antibodies[33,36] and labelled antibody conjugates.[37] Surprisingly, the use of protein A in flow injection immunoassays appears limited.[30]

The extreme flexibility in the use of protein A has enabled this laboratory to develop a competitive immunoassay for theophylline based on the use of a controlled-pore glass–protein A immunoreactor and flow injection techniques, with polyclonal antiserum and electrochemical detection with enzymic amplification.

Experimental

Materials

p-Nitrophenyl phosphate, PAP and theophylline were obtained from Sigma (Poole, Dorset, UK). Theophylline-8-butyric acid lactam was purchased from Novabiochem (Nottingham, UK). *p*-Aminophenyl phosphate was synthesized from *p*-nitrophenyl phosphate as described previously.[38] Controlled-pore glass–protein A (CPG–ProA) was purchased from Oros Instruments (Slough, Berkshire, UK). Glass microcolumns (50 × 3 mm i.d.) were obtained from Omnifit (Cambridge, UK) and were packed with CPG–ProA by means of a peristaltic pump. Immunoassay-grade alkaline phosphatase [grade 1 from calf intestine; 10 mg cm^{-3} and >2500 U mg^{-1} (1 U = 16.67 nkat)] was obtained from Boehringer Mannheim (Lewes, UK). Sheep anti-theophylline antisera was purchased from International Laboratory Services (London, UK). The theophylline–alkaline phosphatase conjugate was prepared according to a published procedure.[39] All other reagents were of analytical-reagent grade, and all solutions were prepared in water purified by the Liquipure Modulab system (Liquipure Europe, Bicester, UK). The tris(hydroxymethyl)methylamine (Tris) equilibration and citric acid elution buffers were prepared according to the Oros data sheet, except that 0.5 mol dm^{-3} sodium chloride was added to the citric acid buffer.

Methods

Protein A/antibody binding study

The binding and elution profile of the theophylline antisera onto the CPG–ProA matrix was obtained by means of a Perkin-Elmer LS 50 fluorescence spectrometer (Norwalk, CT, USA) interfaced with an Epson AX3 personal computer (Epson UK, Wembley, Middlesex, UK). The excitation and emission monochromators were set at 280 and 335 nm, respectively.

Electrochemical methods

The cyclic sweep voltammetry apparatus consisted of a potentiostat, a Metrohm E611 VA detector and Metrohm E612 VA scanner (Herisau, Switzerland). a Gould HR2000 *x–y* recorder and an electrochemical cell. The electrochemical cell included a platinum working electrode, a stainless-steel counter electrode and a saturated calomel reference electrode (SCE).

The apparatus for flow injection was as follows. The flow of the eluent or carrier stream was produced with an LKB 2132 micro-Perspex peristaltic pump (Stockholm, Sweden). Injections of solutions were effected with a Rheodyne 5020 injection valve (Cotati, CA, USA). A pulse damper, constructed from glass with a platinum-wire ground connection, was fitted between the peristaltic pump and the injection valve to eliminate the static electricity pulses generated by the peristaltic pump. The injection valve was connected to the laboratory-built wall-jet detector cell by means of 0.8 mm bore size PTFE tubing. The wall-jet detector cell,[40] containing the platinum working electrode, the stainless-steel counter electrode and the SCE, was housed in a metal box. The potential of the platinum electrode was controlled by means of a Dionex Ionochrom pulsed amperometric detector (Sunnyvale, CA, USA). Current peaks were monitored on a Spectra-Physics 4290 integrator (San Jose, CA, USA).

General procedure for immunoassay

The electrochemical enzyme immunoassay was based on the on-line immobilization of the antibody–antigen complex on CPG–ProA. Fig. 1 shows a schematic diagram of the system used. The typical procedure used for the determination of theophylline was as follows. A known amount of enzyme-labelled theophylline (50 mm^3) and a given amount of standard theophylline (100 mm^3) were mixed with 50 mm^3 of theophylline antisera (1 + 999 dilution in 0.15 mol dm^{-3} phosphate buffered saline, pH 7.4). The mixture was incubated for 10 min, loaded into the 25 mm^3 sample loop of injection valve 1 (IV1) and injected into the CPG–ProA immunoreactor, using the Tris equilibration buffer at a flow rate of 0.4 cm^3 min^{-1}. The actual exposure time for this mixture within the immunoreactor was very short (approximately 20 s), after which the carrier buffer washed off the unbound species for 3 min. When injection valve 2 (IV2) was opened, 50 mm^3 of the substrate solution (1 mmol dm^{-3} PAPP in Tris buffer) passed through the immunoreactor at a flow rate of 0.6 cm^3 min^{-1}. The product of the enzymic reaction (*i.e.*, PAP) was detected downstream by the electrochemical cell operated in a wall-jet configuration. Results (*i.e.*, the oxidative peak areas of PAP) were recorded on a Spectra-Physics SP4290 integrator.

The immunoreactor was regenerated with 0.1 mol dm^{-3} citric acid buffer (pH 2.5) for 2 min to dissociate the complex between the theophylline antisera and the immobilized protein A. The immunoreactor was then re-equilibrated for 2

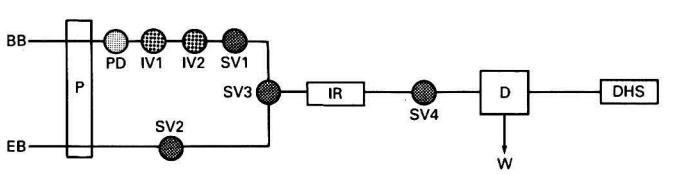

Fig. 1 Schematic diagram of the flow injection manifold used for the electrochemical enzyme immunoassay of theophylline. BB, Binding buffer; EB, elution buffer; P, peristaltic pump; PD, pulse damper; IV, injection valve; SV1–SV4, switching valves; IR, immunoreactor; D, detector; W, waste; and DHS, data handling system

min with the loading buffer (*i.e.*, Tris), after which the system was ready for another sample. The total time for the assay, including the regeneration and re-equilibration steps, was 18 min.

Results and Discussion

Electrochemical Characterization of PAPP and PAP

Cyclic voltammetry was used to examine the electrochemical properties of PAPP and its hydrolysis product PAP. The oxidation potentials for PAP and PAPP were +0.03 and +0.52 V *versus* the SCE, respectively. This is in agreement with previously published values.[25]

Hydrodynamic voltammetry was also used to determine the optimum detector potential of PAP because the PAPP/PAP system was to be used in a flow injection system. *p*-Aminophenol was electroactive from −0.1 V *versus* the SCE, while PAPP was electroactive from approximately +0.3 V *versus* the SCE. A potential of +0.2 V *versus* the SCE was used to detect PAP in all further experiments.

Protein A/Antibody Binding Study

The binding and elution profile for the reversible immobilization of theophylline sheep antisera on CPG–ProA is shown in Fig. 2. Albumin, transferrin and other non-immunoglobulin G (IgG) proteins constitute the non-binding peak, while the IgG-bound fraction is represented by the elution peak.

Enzyme Immunoassay

The theophylline–alkaline phosphatase conjugate used was prepared with the initial ratio of theophylline to enzyme in the reaction mixture of 25 : 1 by the procedure described previously.[39] The theophylline-to-enzyme ratio in the conjugates was determined by Erlanger's differential spectrophotometric method[41] and was found to be 4.2.

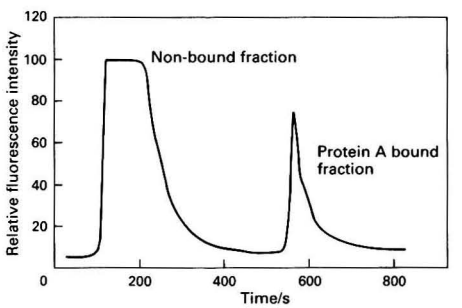

Fig. 2 Binding and elution profile of theophylline antisera on the CPG–protein A immunoreactor using fluorescence detection (excitation wavelength, 280 nm; emission wavelength, 335 nm)

In the competitive assay described, theophylline antibody, theophylline–alkaline phosphatase conjugate and the theophylline sample or standard were incubated for a brief, yet carefully controlled, period. The reaction mixture was then introduced into IV1 (Fig. 1) and injected into the protein A immunoreactor where the antibody-bound theophylline and antibody-bound theophylline–alkaline phosphatase complex were separated with use of Tris buffer as the carrier stream. The substrate solution (PAPP) was introduced into the protein A immunoreactor and hydrolysed by the enzyme portion of the conjugate to form the product (PAP), which was oxidized downstream in the electrochemical cell. The assay cycle was terminated by dissociating the theophylline antibody from the protein A immunoreactor with citric acid (pH 2.5). The column was then recharged with Tris buffer (pH 8.8) before another assay could take place. A general scheme of the assay cycle is depicted in Fig. 3.

Typical dose–response curves for theophylline (antisera dilution of 1 + 999 in 0.15 mol dm^{-3} phosphate buffered saline, pH 7.4) are depicted in Fig. 4. The calibration graphs were prepared by plotting (B/B_0) % *versus* theophylline concentration in the standards, where B is the peak oxidative area of PAP at the stated theophylline concentration, and B_0 is the peak oxidative area of PAP at zero theophylline concentration.

Serum samples were diluted 1 + 99 with 0.15 mol dm^{-3} phosphate buffered saline (pH 7.4) before study to minimize blockage of the frits in the protein A immunoreactor. The relative standard deviations (RSDs) for theophylline in serum at 60, 140 and 300 ng cm^{-3} were 7.4, 6.8 and 8.7%, respectively. Recoveries of theophylline from spiked serum at the same concentrations were 95.5, 108.3 and 104.7%, respectively. The limit of detection for this assay was less than 25 ng cm^{-3}. The total time of the assay was 18 min and the lifetime of each CPG–ProA immunoreactor was between 80 and 100 runs before needing replacement because of diminishing antibody activity.

Conclusions

The assay described in this paper permits the determination of serum theophylline levels in a simple manner by means of a flow injection electrochemical enzyme-immunoassay procedure involving use of a protein A immunoreactor.

The major advantage of this flow injection system is the improvement in the assay speed compared with that of micro-titre plate-based immunoassays. This was achieved by

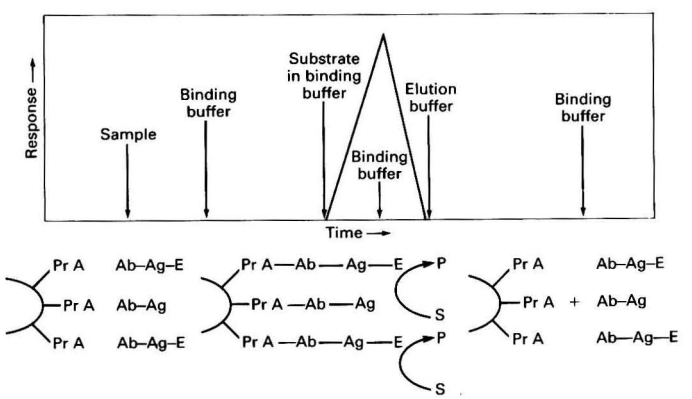

Fig. 3 Schematic diagram of the electrochemical enzyme immunoassay reaction cycle. Pr A, Protein A; Ab, antibody; Ag–E, enzyme labelled antigen; Ag, unlabelled antigen; S, enzyme substrate; and P, substrate hydrolysis product

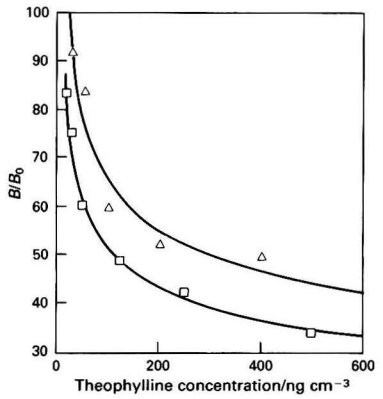

Fig. 4 Dose–response curve for theophylline in A, buffer and B, human serum

adopting non-equilibrium flow rates to deliver the sample and reagent solutions. In addition, the system did not require separate washing steps as all unbound and interfering species were washed out continuously by the stream of the flow injection carrier buffer.

The flexibility of protein A binding to various mammalian IgG and its use in an immunoreactor offers the potential for the development of flow injection immunoassays, based on different detection systems, for other drugs. The assay developed in this work made use of sheep antisera with electrochemical detection. Another flow injection immunoassay has been developed in this laboratory for the immunosuppressive drug cyclosporin A, which involves the use of mouse monoclonal antibodies with fluorescence detection.[42]

The work presented in this paper has been a preliminary investigation designed to demonstrate the feasibility of a flow injection electrochemical enzyme-immunoassay system involving use of a protein A immunoreactor. While the objective of this work has been successfully achieved, additional work is being carried out to optimize further the performance of this system, notably by a reduction in the assay time and also an improvement in the reproducibility.

The authors thank SERC (UK) for the studentship for D. A. P.

References

1 Kuhn, G., *Ann. Emergency Med.*, 1986, **15**, 344.
2 Rowe, D. J. F., Watson, I. D., Williams, J., and Berry, D. J., *Ann. Clin. Biochem.*, 1988, **25**, 4.
3 Gil, E. P., Tang, H. T., Halsall, H. B., Heineman, W. R., and Misiego, A. S., *Clin. Chem. (Winston-Salem, N.C.)*, 1990, **36**, 662.
4 De Alwis, U., and Wilson, G. S., *Anal. Chem.*, 1985, **57**, 2754.
5 De Alwis, U., and Wilson, G. S., *Anal. Chem.*, 1987, **59**, 2786.
6 Lee, I. H., and Meyerhoff, M. E., *Mikrochim. Acta, Part III*, 1988, 207.
7 *Electrochemical Sensors in Immunological Analysis*, ed. Ngo, T. T., Plenum Press, New York and London, 1987, p. 309.
8 Bodansky, A., *J. Biol. Chem.*, 1933, **101**, 93.
9 Shinowara, G. Y., Jones, L. M., and Reinhart, H., *J. Biol. Chem.*, 1942, **142**, 921.
10 Tietz, N. W., and Green, A., *Clin. Chim. Acta*, 1964, **9**, 392.
11 Kind, P. R. N., and King, E. J., *J. Clin. Pathol.*, 1954, **7**, 322.
12 King, E. J., and Armstrong, A. R., *Can. Med. Assoc. J.*, 1934, **31**, 376.
13 Seligman, A. M., Chauncery, H. H., Nachlas, M. M., Manheimer, L. H., and Ravin, H. A., *J. Biol. Chem.*, 1951, **190**, 7.
14 Ohmori, Y., *Enzymologia*, 1937, **4**, 217.
15 Bessey, O. A., Lowry, O. H., and Brock, M. J., *J. Biol. Chem.*, 1946, **164**, 321.
16 Fujita, H., *J. Biochem. (Tokyo)*, 1939, **30**, 69.
17 Huggins, C., and Talalay, P., *J. Biol. Chem.*, 1945, **159**, 399.
18 Fischl, J., Segal, S., and Rabiah, S., *Clin. Chem. (Winston-Salem, N.C.)*, 1967, **13**, 941.
19 Fernley, H. N., and Walker, P. G., *Biochem. J.*, 1965, **97**, 95.
20 Fischer, F., and Siebert, G., *Klin. Wochenschr.*, 1961, **39**, 202.
21 Blake, C., and Gould, B. J., *Analyst*, 1984, **109**, 533.
22 Gosling, J. P., *Clin. Chem. (Winston-Salem, N.C.)*, 1990, **36**, 1408.
23 McNeil, C. J., Higgins, I. J., and Bannister, J. V., *Biosensors*, 1988, **3**, 199.
24 Wehmeyer, K. R., Halsall, H. B., and Heineman, W. R., *Anal. Chem.*, 1986, **58**, 135.
25 Tang, H. T., Lunte, C. E., Halsall, H. B., and Heineman, W. R., *Anal. Chim. Acta*, 1988, **214**, 187.
26 Doyle, M. J., Halsall, H. B., and Heineman, W. R., *Anal. Chem.*, 1984, **56**, 2355.
27 Xu, Y., Halsall, H. B., and Heineman, W. R., *J. Pharm. Biomed. Anal.*, 1989, **7**, 1301.
28 Frew, J. E., Foulds, N. C., Wilshere, J. M., Forrow, N. J., and Green, M. J., *J. Electroanal. Chem. Interfacial Electrochem.*, 1989, **266**, 309.
29 Xu, Y., Halsall, H. B., and Heineman, W. R., *Clin. Chem. (Winston-Salem, N.C.)*, 1990, **36**, 1941.
30 *Enzyme Labelled Immunoassays of Hormones and Drugs*, ed. Pal, S. B., Walter de Gruyter, Berlin, 1987, pp. 91–105.
31 Stocklein, W., and Schmid, R. D., *Anal. Chim. Acta*, 1990, **234**, 83.
32 Locascio-Brown, L., Plant, A. L., Horvath, V., and Durst, R. A., *Anal. Chem.*, 1990, **62**, 2587.
33 Hjelm, H., and Hjelm, K., *FEBS Lett.*, 1972, **28**, 73.
34 Philips, T. M., Queen, W. D., More, N. S., and Thompson, A. M., *J. Chromatogr.*, 1985, **327**, 213.
35 Richman, D. D., *New Devel. Diagn. Virol.*, 1983, **104**, 159.
36 Goding, J. W., *J. Immunol. Methods*, 1976, **13**, 215.
37 Page, M., *Can. J. Biochem.*, 1979, **57**, 286.
38 DeRiemer, L. H., and Meares, C. F., *Biochemistry*, 1981, **20**, 1966.
39 Cook, C. E., Twine, M. E., Myers, M., Amerson, E., Kepler, J., and Taylor, G. F., *Res. Commun. Chem. Path. Pharm.*, 1976, **13**, 497.
40 Taylor, M. G., Ph.D. Thesis, Loughborough University of Technology, 1988.
41 Erlanger, B. F., Borek, F., Beiser, S. M., and Lieberman, S., *J. Biol. Chem.*, 1957, **222**, 713.
42 Miller, J. N., Palmer, D. A., and French, M. T., *J. Pharm. Biomed. Anal.*, 1991, **9**, 1115.

Paper 2/01168I
Received March 4, 1992
Accepted June 1, 1992

Poly(vinyl chloride) Matrix Membrane Electrodes for Manual and Flow Injection Determination of Metal Azides

Saad S. M. Hassan, Fatma M. El Zawawy and Sayed A. M. Marzouk
Department of Chemistry, Faculty of Science, Ain Shams University, Cairo, Egypt
Eman M. Elnemma
Department of Chemistry, Faculty of Science, Qatar University, Doha, Qatar

Novel poly(vinyl chloride) matrix membrane electrodes for the azide ion are developed, electrochemically evaluated and used for manual and flow injection determinations of soluble and insoluble metal azides. These electrodes incorporate iron(II) and nickel(II) bathophenanthroline–azide ion-pair complexes as ion exchangers and 2-nitrophenyl phenyl ether as a plasticizing solvent mediator. The electrodes exhibit (*i*) near-Nernstian response for 1×10^{-1}–3.5×10^{-5} mol dm^{-3} N_3^- with an anionic slope of 56–57 mV decade^{-1} of concentration; (*ii*) a wide working range of pH (6–12); (*iii*) a fast response time (<40 s); (*iv*) long-term stability (>1 month); and (*v*) reasonable selectivity for N_3^- over many common anions. Interference caused by ClO_4^-, ClO_3^- and NO_3^- can be easily tolerated by appropriate ion-exchange separation. Determination of as little as 0.8 μg cm^{-3} of soluble azides shows an average recovery of 99.4% and a mean standard deviation of 0.4%. Insoluble metal azides can be similarly determined after prior solubilization with alkaline ethylenediaminetetraacetic acid solution. Methods for measuring the solubility products of some sparingly soluble metal azides and for monitoring the concentration level of azide in primer mixtures are described. Significant advantages in terms of simplicity, sensitivity, selectivity and accuracy are offered by these electrodes.

Keywords: *Azide–poly(vinyl chloride) membrane electrode; iron(II) and nickel(II) bathophenanthroline azide complexes; potentiometric determination of metal azides; primer mixture; flow injection*

Instrumental methods in current use for the determination of azides include spectrophotometry,[1–7] cyclic voltammetry,[8] polarography,[9] amperometry,[10] potentiotitrimetry[11] and chromatography.[12–14] Many of these methods, however, suffer from severe interference by many common anions,[1–3,8] cations,[3,4] amines,[2] hydrazines and hydroxylamines,[2,10,13] require prior controlled derivatization reactions,[5,14] yield low or high results[1,4,13] and are influenced by variation of the pH of the reaction medium.[2] Determination of insoluble metal azides requires prior acidification and distillation of hydrogen azides.[15]

Ion-selective membrane electrodes are finding considerable use for monitoring various anions. Solid-state membrane electrodes for almost all anions known to form sparingly soluble silver salts [*e.g.*, I^-, Cl^-, Br^-, S^{2-}, CN^-, SCN^-, PO_4^{3-}, $Fe(CN)_6^{3-}$ and $Fe(CN)_6^{4-}$] have been developed,[16–19] except for the azide ion (N_3^-). This stems from the highly explosive nature of heavy metal azides when compressed. Polymeric and liquid membrane electrodes responsive to N_3^- have not, so far, been reported owing to the unavailability of suitable azide ion-pair complexes. Recently, we have described a Severinghaus-type gas sensor for the sensitive and selective determination of azides.[20] Inherent limitations of this arrangement, however, are the use of an expensive electrode barrel, interference from some salts of volatile weak acids and application over a narrow acidic range (pH 1.1–1.7).

The present investigation was undertaken to prepare some water-insoluble ion-association complexes of azide for use as electroactive materials in poly(vinyl chloride) (PVC) membranes responsive to N_3^-. It has been reported that azide quantitatively reacts with the iron(II)–phenanthroline cation to form a coloured, water-soluble ion-association complex.[6] The reaction has been used for the spectrophotometric determination of microgram amounts of azide and involves extracting the complex into organic solvents and measuring the absorbance of the solution.[6] In this work, bathophenanthroline (4,7-diphenyl-1,10-phenanthroline; bphen) was examined, in view of its higher lipophilicity, instead of 1,10-phenanthroline, to prepare iron(II) and nickel(II) tris(bathophenanthroline) azides. The complexes are water insoluble, extractable into organic solvents, and prove to be suitable exchangers for N_3^-. The PVC membrane electrodes incorporating these complexes exhibit fast, near-Nernstian response for 1×10^{-1}–3.5×10^{-5} mol dm^{-3} N_3^- over a wide pH range, they display reasonable selectivity of N_3^- and can be satisfactorily used for manual and flow injection (FI) determination of soluble and insoluble metal azides.

Experimental

Apparatus

Potentiometric measurements were performed at 25 ± 1 °C using an Orion Model SA 720 digital pH/millivoltmeter and the azide–PVC matrix membrane electrodes operated in conjunction with a single-junction Ag–AgCl reference electrode (Orion Model 90-91) filled with 10% m/v KCl. A solid-state Ag–S^{2-} membrane electrode (Orion 94-16) *versus* a double-junction Ag–AgCl reference electrode (Orion 90-02), containing 10% m/v KNO_3 in the outer compartment, was used for the standardization of azide solutions. A combination Ross glass pH electrode (Orion 81-02) was used for all pH measurements.

A laboratory-made FI sandwich cell was fabricated and incorporated into the manifold system (Fig. 1) with an Omnifit injection valve (Omnifit) and a peristaltic pump (Manostat cassette junior model). The potential output was measured with an Orion SA 720 digital pH/millivoltmeter and recorded with a strip-chart recorder (Linear 1200).

The infrared absorption spectra were measured with a Shimadzu spectrometer (IR 470).

Reagents and Materials

All chemicals were of analytical-reagent grade unless otherwise stated, and doubly distilled water was used throughout. 4,7-Diphenyl-1,10-phenanthroline, tetrahydrofuran (THF) and PVC powder were obtained from Aldrich. Sodium azide, Amberlite (IR-120; H^+ form) cation exchanger and Amberlite (IR-4B; OH^- form) anion exchanger were obtained from

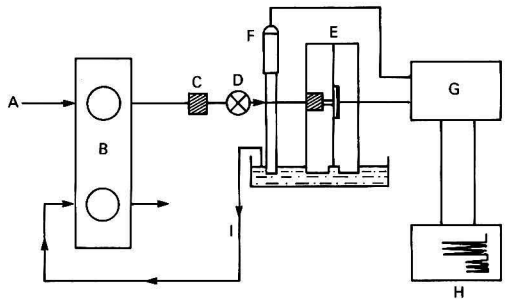

Fig. 1 Manifold for the single line FI apparatus used for the determination of azides: A, carrier KF solution; B, peristaltic pump; C, pulse damper; D, sample valve; E, potentiometric cell; F, reference electrode; G, Orion Microprocessor Ionalyzer; H, recorder; and I, waste

BDH (Merck). 2-Nitrophenyl phenyl ether (NPPE) was purchased from Kodak.

A 1.0 mol dm^{-3} stock solution of azide was prepared and standardized by potentiometric titration with 0.2 mol dm^{-3} $AgNO_3$, using the solid-state $Ag–S^{2-}$ membrane electrode in conjunction with a double-junction Ag–AgCl reference electrode for end-point detection. Standard azide solutions (1×10^{-1}–1×10^{-6} mol dm^{-3}) were prepared by accurate dilutions of the stock azide solution. Aqueous solutions of 3 mol dm^{-3} ammonia, 0.1 mol dm^{-3} ethylenediaminetetraacetic acid (EDTA) of pH 9, 6% m/v hydrogen peroxide, 0.1 mol dm^{-3} silver acetate and 0.05 mol dm^{-3} potassium fluoride were freshly prepared.

Nickel(II)– and Iron(II)–Tris(bathophenanthroline azide) Complexes

A 100 mg portion of bphen was dissolved in 20 cm^3 of 60% v/v ethanol–water, and the solution was mixed with 5 cm^3 of 0.02 mol dm^{-3} nickel(II) chloride or iron(II) ammonium sulfate solution. A few drops of ethanol or water were added to the reaction mixture to maintain a clear solution. After stirring for 5 min, 5 cm^3 of 1.0 mol dm^{-3} aqueous sodium azide was added. A yellowish-green precipitate of $Ni(bphen)_3(N_3)_2$ and a deep-red precipitate of $Fe(bphen)_3(N_3)_2$ ion-pair complexes were formed. The precipitates were filtered off on Whatman filter-paper No. 42, washed with cold water, dried at room temperature for 24 h and ground to a fine powder. Elemental analysis and infrared data confirmed the formation of 1 + 2 metal bathophenanthroline–azide complexes.

Azide–PVC Membranes

A 10 mg portion of the $Ni(bphen)_3(N_3)_2$ or $Fe(bphen)_3(N_3)_2$ ion-pair complex was thoroughly mixed in a glass Petri dish (5 cm diameter) with 0.45 g of NPPE, 0.19 g of PVC and 5 cm^3 of THF. The Petri-dish was covered with filter-paper and left to stand overnight to allow slow evaporation of the solvent at room temperature. A master PVC membrane (approximately 0.1 mm thick) was obtained.

Azide–PVC Membrane Electrodes

The PVC master membranes were sectioned with a cork borer (10 mm diameter) and glued to a polyethylene tube (3 cm × 8 mm i.d.) using THF. A laboratory-made electrode body was used, which consisted of a glass tube, to which the polyethylene tube was attached at one end and filled with the internal reference solution (1×10^{-2} mol dm^{-3} aqueous NaN_3–KCl). An Ag–AgCl internal reference wire electrode (1.0 mm diameter) was immersed in the internal solution. The electrode was conditioned by soaking in 1×10^{-1} mol dm^{-3} aqueous sodium azide for 1 h and was stored in the same solution when not in use.

Azide–PVC Coated Disc Membrane Electrode

A laboratory-made electrode body was used, which consisted of a silver disc (0.1 cm thick and 1.0 cm diameter) fixed to one end of a Perspex tube using Araldite glue. A shielded cable was connected to the silver disc with silver epoxy-resin. The other end of the tube was closed with a polyethylene cap. About 1 cm^3 of the membrane 'cocktail' consisting of 0.19 g of PVC, 10 mg of $Ni(bphen)_3(N_3)_2$ and 0.45 g of NPPE in 6 cm^3 of THF was deposited dropwise on the silver disc. After each addition, the solvent was allowed to evaporate slowly at room temperature to yield a thin film. This operation was repeated six times until a membrane with a suitable thickness (approximately 0.1 mm) was formed. The membrane was left to dry in air for 24 h. The electrode was conditioned by soaking in 0.1 mol dm^{-3} aqueous sodium azide for 1 h and was stored in the same solution when not in use.

Electrode Calibration and Azide Determination

Aliquots (10 cm^3) of 1×10^{-1}–1×10^{-6} mol dm^{-3} aqueous sodium azide were transferred into 50 cm^3 beakers. The azide–PVC membrane electrode, in conjunction with the single-junction Ag–AgCl reference electrode, was immersed in the solution. The solution was stirred, the potential was recorded after stabilization to ±0.2 mV, and the e.m.f. was plotted on semi-logarithmic paper as a function of azide concentration. Alternatively, the azide–PVC membrane electrode, in conjunction with the single-junction Ag–AgCl reference electrode, was immersed in a 50 cm^3 beaker containing 10 cm^3 of water. Aliquots (1.0 cm^3) of from 1×10^{-5} to 1×10^{-1} mol dm^{-3} sodium azide were successively added and the potential readings were recorded after stabilization to ±0.2 mV after each addition. The e.m.f. was plotted as a function of logarithmic azide concentration.

This calibration graph was used for the subsequent determination of unknown concentrations of azide. Alternatively, the standard-additions method was used, which involved measuring the potential displayed by the azide test solution before and after the addition of a 1.0 cm^3 aliquot of 1×10^{-2} or 1×10^{-1} mol dm^{-3} sodium azide. The change in the potential readings was recorded and used to calculate the unknown azide concentration in the test solution. Soluble metal azides could be similarly determined after prior treatment with 2 cm^3 of 0.1 mol dm^{-3} EDTA (pH 9).

Separation of Azides from Perchlorates, Chlorates and Nitrates for Determination

An aliquot (10 cm^3) of the test solution (containing 1–10 mg of N_3^- and 10–100 mg each of ClO_4^-, ClO_3^- and NO_3^-) was treated with 1 cm^3 of 0.1 mol dm^{-3} $FeCl_3$ and was passed, at a flow rate of 1 cm^3 min^{-1}, through a glass column (1 cm diameter) packed with approximately 2 g of Amberlite resin (IR-4B; Cl^- form). Elution was effected with approximately 60 cm^3 of water and the eluate collected in a 100 cm^3 calibrated flask. A 2 cm^3 aliquot of 0.1 mol dm^{-3} EDTA (pH 9) was added and the solution diluted to the mark with doubly distilled water. The potential of this solution was recorded with the azide–PVC electrode, as previously described, and the readings were referred to the calibration graph.

Potentiometric Titration of Azide

A 2–6 cm^3 aliquot of 1×10^{-2} mol dm^{-3} azide was transferred into a 50 cm^3 beaker and diluted to approximately 10 cm^3 with doubly distilled water. The solution was stirred, and titrated with 1×10^{-2} mol dm^{-3} aqueous silver acetate, using an

azide–PVC electrode operated in conjunction with a single-junction Ag–AgCl reference electrode. The electrode potential (E) was recorded as a function of the volume of the titrant added (V) and plotted as E *versus* V curves. The end-point was calculated from the maximum slope $\Delta E/\Delta V$ *versus* V.

Determination of Azide in Synthetic Primer Mixtures

A synthetic primer mixture, prepared by mixing 10 mg of $KClO_3$, 10 mg of Sb_2S_3 (stibnite) and various amounts of sodium azide (1–10 mg), was dissolved in approximately 10 cm^3 of doubly distilled water, the solution was filtered through Whatman filter-paper No. 7 to isolate the Sb_2S_3 precipitate, and the filter was washed several times with water. A 3 cm^3 aliquot of 0.1 mol dm^{-3} $FeCl_3$ was added to the azide–chlorate mixture in the filtrate and the solution was passed through a column packed with Amberlite (IR-4B; Cl^- form). Elution was effected with 60 cm^3 of water. The eluate was collected in a 100 cm^3 calibrated flask, treated with 2 cm^3 of 0.1 mol dm^{-3} EDTA (pH 9) and diluted to the mark with water. The azide content was potentiometrically determined, using the azide–PVC membrane electrode, by both the calibration-graph and standard-additions methods.

Determination of Insoluble Metal Azides

A portion of AgN_3 (3–15 mg) was dissolved in a few drops of 3 mol dm^{-3} aqueous ammonia solution, $Cu(N_3)_2$ (3–15 mg) was dissolved in 3 cm^3 of 0.1 mol dm^{-3} EDTA (pH 9), and thallium azide (30–120 mg) was treated with 1.0 cm^3 of 6% m/v H_2O_2 followed by 3 cm^3 of 0.1 mol dm^{-3} EDTA (pH 9). These solutions were transferred into a 50 cm^3 calibrated flask and diluted to the mark with doubly distilled water. The concentration of the azide ion was measured potentiometrically, using the azide–PVC membrane electrode, by the calibration-graph and standard-additions methods.

Determination of Solubility Products of Sparingly Soluble Metal Azides

Aliquots (5 cm^3) of 1×10^{-1} mol dm^{-3} sodium azide were added to equivalent volumes of 1×10^{-1} mol dm^{-3} Pb^{II}, Hg^{I}, Cu^{II} and Tl^{I} acetate solutions. The precipitates were washed thoroughly with doubly distilled water several times. A portion of each precipitate was suspended in 20 cm^3 of doubly distilled, de-ionized water and stored in an air-tight 100 cm^3 Erlenmeyer flask. The mixture was shaken for 3 h in a thermostatically controlled bath, adjusted to 20 ± 1 °C, and allowed to stand for 30 min to settle the precipitate. A 10 cm^3 aliquot of the supernatant or the filtrate was transferred to a 50 cm^3 beaker. The concentration of the azide was measured by the calibration-graph or the standard-additions method.

FI of Azides

A laboratory-made flow-through sandwich potentiometric cell, equipped with an azide–PVC membrane, was fabricated and used in a single-stream FI system. The azide sensor was prepared and conditioned as described previously for a coated-disc electrode. The cell was assembled and connected to the flow-injection system, as shown in Fig. 1. The cell and a single-junction Ag–AgCl reference electrode were placed in a Petri-dish filled with the electrolyte carrier solution. A carrier solution consisting of 0.05 mol dm^{-3} KF was propelled through the cell, by means of a peristaltic pump and PTFE tubing (0.8 mm i.d.), at a flow rate of 0.42 cm^3 min^{-1}. An Omnifit injection valve was used for successive injections of 20 mm^3 aliquots of azide sample solutions into the flowing stream. The tubing distance between the injection valve and the detector was about 10 cm. Both the azide sensor and reference electrode were connected to an Orion 720 pH/mV meter, which was attached to a strip-chart recorder to record the FI signals. The waste from the Petri-dish was continuously removed by the peristaltic pump. Soluble and insoluble metal azides, after suitable solubilization, were similarly determined. At least three signals for each sample were recorded and their average height was measured. A comparison was made with a calibration graph that was obtained under the same conditions with 20 mm^3 aliquots of 5×10^{-5} to 1×10^{-2} mol dm^{-3} standard solutions of sodium azide.

Results and Discussion

Nature and Composition of the Azide Membranes

Nickel(II) and iron(II) tris(bathophenanthroline) cations react with N_3^- to form water-insoluble 2 + 1 azide–ion-pair complexes of the type $M(bphen_3)(N_3)_2$. Membranes prepared using casting solutions of the composition: PVC–azide complex–NPPE plasticizer (28 + 2 + 70 m/m) were used for constructing three-electrode systems. Electrodes 1 and 2 were made as previously described for the conventional PVC type[21,22] with $Ni(bphen)_3(N_3)_2$ and $Fe(bphen)_3(N_3)_2$ as respective electroactive materials. Electrode 3 was a silver disc (1 cm diameter) coated with a PVC sensor 'cocktail' membrane containing $Ni(bphen)_3(N_3)_2$ and was structurally similar in principle to that previously described.[23] The electrochemical performance characteristics of the three-electrode systems were systematically evaluated according to IUPAC recommendations.[24]

The calibration graphs obtained with the three azide–PVC membrane electrodes (Fig. 2) are almost equivalent in terms of slope and detection limit. Near-Nernstian response holds for at least three orders of magnitude of azide concentration. Linear response in the range 3.5×10^{-5}–2×10^{-2} mol dm^{-3} N_3^- with an anionic slope of 56–57 mV $decade^{-1}$ change in concentration is obtained. The lower limit of detection is approximately 0.8 μg cm^{-3}. Table 1 summarizes the response characteristics of these electrode systems from data collected over a period of 3 months for four different electrode assemblies for each system.

Response Time of the Azide-determining Cell

The dynamic response times of the electrode systems were tested for 1×10^{-1}–1×10^{-4} mol dm^{-3} sodium azide. The

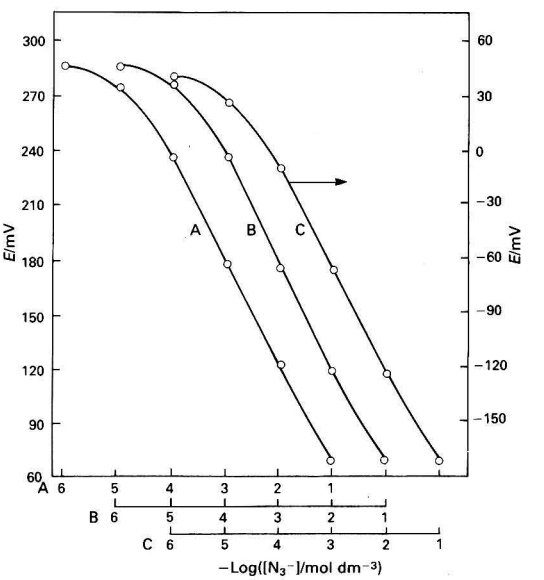

Fig. 2 Typical calibration graphs for: A, type 1; B, type 2; C, type 3 azide PVC matrix membrane electrodes

Table 1 Response characteristics of azide–PVC membrane electrodes

Parameter	Electrode 1	Electrode 2	Electrode 3
Slope/mV decade^{-1}	−57	−56	−56.5
Standard deviation/mV	0.5	0.7	0.6
Intercept/mV	8.0	5.0	238.0
Correlation coefficient/r	0.997	0.996	0.996
Lower limit of linear range/ mol dm^{-3}	3.5×10^{-5}	4×10^{-5}	4.8×10^{-5}
Lower limit of detection/ mol dm^{-3}	1.9×10^{-5}	1.95×10^{-5}	2.9×10^{-5}
Response time for 1×10^{-3} mol dm^{-3}/s	20	20	40
Recovery time/min	0.7	0.7	0.7
Working pH range	6–12	6–9	6–12

sequence of measurements was from low to high concentrations. The time required for the electrodes to reach values within ±0.2 mV from the final equilibrium potential, after increasing the azide concentration level 10-fold, was measured. The response time of electrodes 1 and 2 is fairly short; it reaches 97% of its final steady potential after 20 s for $[N_3^-] \geqslant 1 \times 10^{-3}$ mol dm^{-3} and 40 s for $[N_3^-] \leqslant 1 \times 10^{-3}$ mol dm^{-3}. Electrode 3 needs a slightly longer time for steady-state response, *i.e.*, 40 s, for $[N_3^-] \geqslant 1 \times 10^{-3}$ mol dm^{-3} and 60 s for $[N_3^-] \leqslant 1 \times 10^{-4}$ mol dm^{-3}.

Potential Stability of the Azide Electrodes

The potential displayed by the three azide–PVC membrane electrodes for consecutive analyses of 1×10^{-2}–1×10^{-5} mol dm^{-3} standard N_3^- solutions on the same day did not vary by more than ±1 mV ($n = 10$). Changes in the calibration slopes did not exceed ±0.4 mV decade^{-1} change of concentration. The long-term reproducibility and stability of the potential were evaluated by establishing replicate calibration graphs ($n = 20$) for each electrode over a period of 4 weeks. During this period, the electrodes were stored and conditioned in 1×10^{-1} mol dm^{-3} sodium azide and thoroughly washed with water between measurements. Although a positive shift in the absolute potentials (approximately 5 mV) was noticed, the slopes of the calibration graphs remained practically constant within ±1–2 mV decade^{-1} over the period. The detection limit, linear range, response time and selectivity coefficient values were almost constant for the three electrodes during this period.

Effect of pH

The effect of pH of the sodium azide test solutions (1×10^{-1}–1×10^{-4} mol dm^{-3}) on the electrode potential was investigated by monitoring the variation of potential with the change in pH over the range 3.5–12. Small volumes of dilute sodium hydroxide solution and small portions of a cation exchanger (H^+ form) were used for pH adjustment in the basic and acidic media, respectively. The cation-exchange resin was used instead of acids to avoid the possible interfering effect introduced by the acid anions.

The potential *versus* pH plots of electrodes 1 and 3 (Fig. 3), based on use of the $Ni(bphen)_3(N_3)_2$ complex, revealed that, within the working pH range 6–12, the potential did not vary by more than ±2 mV. There is a substantial effect of the OH^- concentration on the response of electrode 2 based on the use of $Fe(bphen)_3(N_3)_2$ complex, especially for low azide concentrations ($<1 \times 10^{-2}$ mol dm^{-3}). For 1×10^{-1}, 1×10^{-2}, 1×10^{-3} and 1×10^{-4} mol dm^{-3} azide solutions, the working pH ranges are 6.5–11, 6.5–11, 6–9 and 5.5–6.5, respectively. This behaviour can be attributed to the larger affinity of iron(II) compounds to form hydrated and/or hydroxo species compared with nickel(II) compounds. The potentials of the three electrodes are significantly changed below pH 6 owing to the progressive liberation of hydrazoic acid. Formation of the weakly dissociated and easily volatile HN_3 is associated with a decrease in the activity of N_3^-.

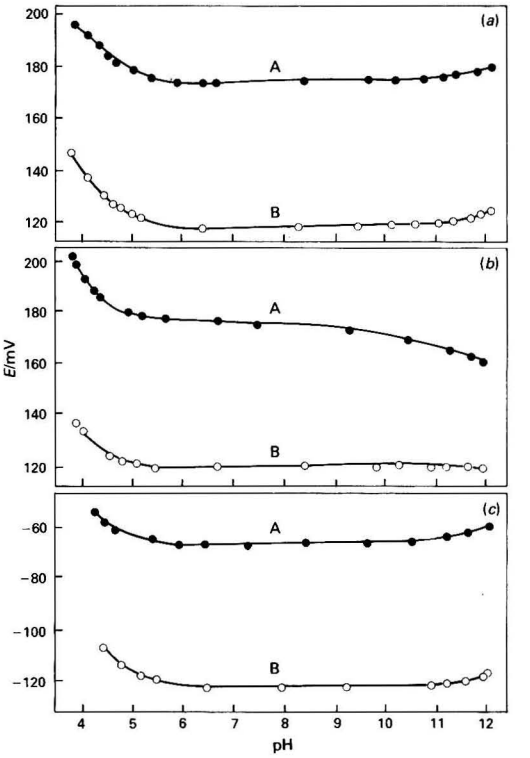

Fig. 3 Effect of pH on the response of: (*a*) type 1; (*b*) type 2; (*c*) type 3 azide PVC matrix membrane electrodes; A, 1×10^{-3} mol dm^{-3} and B, 1×10^{-2} mol dm^{-3} NaN_3 solutions

Effect of Foreign Ions

The performance of the three-electrode systems in the presence of 26 different inorganic and organic anions was assessed by measuring the selectivity coefficient values ($K^{pot}_{N_3^-,B}$ using the separate-solutions method,[22,24] with a fixed concentration of the interferent (1×10^{-3} mol dm^{-3}). The results obtained (Table 2) show reasonable selectivity for N_3^- in the presence of many common anions. Aliphatic amines, hydrazine and hydroxylamine have no significant effect on the electrode response. However, ClO_4^-, SCN^- and to a lesser extent I^-, CN^-, NO_3^-, ClO_3^- and S^{2-} interfere. The selectivity pattern for these anions is: $ClO_4^- > SCN^- > I^- > CN^- > NO_3^- > S^{2-} > ClO_3^-$. This order closely resembles the Hofmeister sequence most often observed for anion-responsive membrane electrodes and is in accordance with the relative lipophilicity of the anions and with their partition coefficients into the organic membranes.[25–27] The high stability and reasonable selectivity of iron(II) and nickel(II) bathophenanthroline–azide complexes as azide exchangers arise from the delocalization of the positive charge on the aromatic ring system, which creates low-charge density sites with high affinity for the polarizable N_3^- relative to non-polarizable anions.[28]

Interference from high concentrations of SO_3^{2-} and S^{2-} (>100-fold excess over N_3^-), is largely circumvented by a simple pre-treatment reaction with alkaline hydrogen peroxide to convert SO_3^{2-} and S^{2-} into the less-interfering SO_4^{2-}. On the other hand, the interfering effect of ClO_4^-, ClO_3^- and NO_3^- was completely eliminated by addition of

Table 2 Potentiometric selectivity coefficients for azide–PVC membrane electrodes

	Log $K^{pot}_{N_3^-,B}$		
Interferent (B)	Electrode 1	Electrode 2	Electrode 3
N_3^-	0	0	0
F^-	−1.89	−1.89	−1.79
Cl^-	−1.34	−1.18	−1.40
Br^-	−0.38	−0.24	−0.34
I^-	+1.78	+1.94	+1.80
ClO_3^-	+0.7	+0.9	+0.72
ClO_4^-	+3.6	+3.96	+3.64
NO_3^-	+0.68	+0.79	+0.62
SO_4^{2-}	−1.63	−1.80	−1.70
PO_4^{3-}	−1.58	−1.67	−1.60
$H_2PO_4^-$	−1.50	−1.64	−1.55
SCN^-	+2.38	+2.34	+2.45
CN^-	+1.05	+0.34	+1.10
OCN^-	−0.29	−0.25	−0.31
$S_2O_3^{2-}$	−0.96	−1.15	−1.00
SO_3^{2-}	−0.65	−1.30	−0.68
S^{2-}	−0.05	+0.75	−0.10
CO_3^{2-}	−0.95	−1.48	−1.00
HCO_3^-	−1.48	−1.62	−1.50
$B_4O_7^{2-}$	−1.38	−1.50	−1.32
WO_4^{2-}	−1.13	−1.58	−1.20
$Fe(CN)_6^{3-}$	+0.71	+0.67	+0.68
$Fe(CN)_6^{4-}$	−0.01	−0.41	−0.02
$HCOO^-$	−1.66	−1.66	−1.70
CH_3COO^-	−1.61	−1.77	−1.60
Citrate^{3-}	−0.74	−1.30	−0.78
$EDTA^{2-}$	−1.65	−1.80	−1.68

Fe^{III} to convert N_3^- into the cationic complex FeN_3^{2+},[1] followed by passage through an anion-exchange resin (Cl^- form) to retain the interfering ClO_4^-, ClO_3^- and NO_3^-. The iron(III)–azide complex in the eluate, on treatment with EDTA solution of pH 9, instantaneously and quantitatively releases N_3^-, which can be directly determined with the azide electrode. Following this procedure, ClO_4^-, ClO_3^- and NO_3^-, present with the azide in the test solution, are exchanged with the much less-interfering Cl^-. No significant interference is caused by the presence of up to 100-fold excesses of ClO_4^-, ClO_3^- and NO_3^- over N_3^-. The average azide recovery is 100.1% and the mean standard deviation is 0.4% (n = 15).

Direct Potentiometry and Potentiometric Titration of Azides

The results obtained for the direct potentiometric determination of from 2 μg cm^{-3} to 1.8 mg cm^{-3} (4.8×10^{-5}–4.2×10^{-2} mol dm^{-3}) of sodium azide in aqueous solutions, each in a triplicate, using the proposed electrode system and the standard-additions method, show average recoveries of 99.4% (mean standard deviation 0.4%), 99.3% (mean standard deviation 0.8%) and 99.3% (mean standard deviation 0.4%) for electrodes 1, 2 and 3, respectively (n = 24).

Electrode 1 was also tested as an indicator electrode for the potentiometric titration of sodium azide with Ag^+. Silver acetate was used instead of silver nitrate as a titrant to avoid the interfering effect of NO_3^- on the electrode response. The average recovery of the azide was 99.2% and the mean standard deviation was 0.9% (n = 15). The inflection break (40–60 mV) consistently and reproducibly appeared at points corresponding to a 1 + 1 (Ag^+–N_3^-) reaction.

Determination of Azide in Primer Mixtures

The azide contents of synthetic primer mixtures, prepared by mixing 10 mg of $KClO_3$, 10 mg of Sb_2S_3 (stibnite) and different accurately measured amounts of sodium azide (1.0–10 mg), were determined after a simple pre-treatment reaction to remove the interfering effect of ClO_3^- (see above). The average recoveries of the azide obtained by the calibration-graph and standard-additions methods with electrode 1 are 99.6% (mean standard deviation 0.8%) and 99.4% (mean standard deviation = 0.7%), respectively (n = 15).

Table 3 Determination of solubility products (K_{sp}) of some insoluble metal azides by using the azide–PVC membrane electrode (electrode type 1)

	K_{sp}	
Metal azide	Azide–PVC electrode*	Literature values[20,29]
$Pb(N_3)_2$	$1.99 (\pm 0.01) \times 10^{-9}$	2.01×10^{-9}
		2.05×10^{-9}
$Hg_2(N_3)_2$	$1.11 (\pm 0.02) \times 10^{-12}$	1.13×10^{-12}
		1.16×10^{-12}
$Cu(N_3)_2$	$6.47 (\pm 0.02) \times 10^{-10}$	6.50×10^{-10}
		6.66×10^{-10}
TlN_3†	$4.78 (\pm 0.03) \times 10^{-5}$	4.80×10^{-5}
		4.90×10^{-5}

* Average of three measurements.
† Measurements carried out at 0 °C.

Determination of Soluble Metal Azides

Azide–PVC matrix membrane electrode 1 was also assessed for the determination of 0.06–0.24 mg cm^{-3} of iron(III), cobalt(II) and nickel(II) azides by using both the calibration-graph and standard-additions methods. The results obtained for cobalt(II) and nickel(II) azides show average azide recoveries of 99.4% (mean standard deviation = 0.7%) and 99.5% (mean standard deviation = 0.8%), respectively (n = 12). With iron(III) azide, addition of EDTA solution (pH 9) was found to be a necessary pre-treatment step to release N_3^- from the cationic FeN_3^{2+} complex. Under these conditions, the azide recovery is 99% and the mean standard deviation is 0.3% (n = 6).

Determination of Insoluble Metal Azides

Azide–PVC matrix membrane electrode 1 was used for the direct potentiometric determination of insoluble metal azides. The method relies on a prior solubilization of the azides based on alkaline complexing reagents. Determination of 3–15 mg of silver azide by direct potentiometry after solubilization in 0.4% aqueous ammonia shows average recoveries of 99.1% (mean standard deviation = 0.8%) and 99.3% (mean standard deviation = 0.7%) by the standard-additions and calibration-graph methods, respectively (n = 6). The results obtained for direct potentiometric determination of 3–15 mg of lead and copper azides after prior treatment with EDTA (pH 9) show average recoveries of 99.7% (mean standard deviation = 0.8%) and 99.1% (mean standard deviation = 0.8%) by the standard-additions and calibration-graph methods, respectively (n = 12). Thallium(I) azide, however, neither dissolves in ammonia solution nor in alkaline EDTA. Prior treatment with H_2O_2 converts thallium(I) into thallium(III), which is readily complexed and dissolved in EDTA. The results obtained for the determination of 30–120 mg of thallium(I) azide each in triplicate, show an average recovery of 99.2%, and the mean standard deviation is 0.4%.

Determination of Solubility Products of Metal Azides

The solubilities of some sparingly soluble metal azides were determined at 20 ± 1 °C by direct measurements of the equilibrium potentials of their saturated solutions. The solubility product (K_{sp}) of thallium(I) azide was measured at 0 °C as previously recommended in the literature,[29] because of its appreciable solubility at ambient temperature. The K_{sp}

Table 4 Comparison of some instrumental methods for the determination of azides

Method	Lower limit of detection/ μg cm^{-3}	Mean relative error (%)	Interferent	Reference
Spectrophotometry—				
Fe^{II}–1,10-phenanthroline	8.4	1	S^{2-}	6
Arsenazo III	0.05	4	Th^{4+}, Zr^{4+}, U^{2+}, Fe^{2+}, Pb^{2+}, Fe^{3+}, Bi^{3+}, Cu^{2+}, reducing substances	4
Fe^{3+}	10.0	3–6	SCN^-, NO_2^-, SO_3^{2-}, S^{2-}, OCN^-, $S_2O_3^{2-}$	1,15
Cu^{2+}	1.2	1	CN^-, SO_3^{2-}, $S_2O_3^{2-}$, $S_4O_6^{2-}$, S^{2-}, I^-, NO_2^-, MnO_4^-, CrO_4^{2-}, Hg^{2+}, Pt^{2+}, Pb^{2+}	3
Pentacyanoamminoferrate(II)	0.42	2	Br^-, I^-, SCN^-, $S_2O_3^{2-}$, CrO_4^{2-}, NO_2^-, N_2H_4, NH_2OH, amines	2
CS_2	8.0	0.1	Amines	5
Electrochemistry—				
Polarography	4.2	1	NR*	9
Cyclic voltammetry	8.4		NO_2^-, I^-, Br^-, ClO_2^-, SCN^-, CN^-, SO_3^{2-}	8
Amperometry	8400	0.3	N_2H_4, NH_2OH, reducing substances	10
Azide–PVC electrode 1	0.8	0.4	ClO_4^-, ClO_3^-, NO_3^-, SCN^-,	Present work
Azide gas sensor	0.8	0.4	NO_2^-, SO_3^{2-}, S^{2-}	20
Chromatography—				
Gas–liquid	5	5	N_2H_4, NH_2OH	13
Ion	2	2	NR*	12
Liquid	0.01	2	NR*	14

* NR = not reported.

values obtained for lead(II), copper(II), mercury(I) and thallium(I) azides, presented in Table 3, compare favourably with values previously reported and obtained by other measurement techniques.[20,29]

FI of Azides

The fast response, high sensitivity, reasonable selectivity and good stability offered by the coated silver disc azide–PVC membrane electrode (electrode 3) suggested its use as a detector in a laboratory-made sandwich FI cell. Potassium fluoride solution (0.05 mol dm^{-3}) was used as a carrier stream, because F^- has the lowest interfering effect among all the anions investigated; Cl^- can also be used.

Standard sodium azide solutions containing 3–2000 μg cm^{-3} N_3^- were analysed in triplicate by the FI method. The results obtained show an average recovery of 99.3% and a mean standard deviation of 1.1% (n = 36). Insoluble lead(II), silver(I) and thallium(I) azides were also determined by FI after solubilization. The results obtained show an average recovery of 101.0% and a mean standard deviation of 0.8% (n = 36).

Comparison with other Methods

Table 4 shows a comparison of the results obtained for the proposed electrode methods with the reported analytical features of the earlier instrumental methods. It can be seen that the use of azide–PVC membrane electrodes offers a particularly favourable combination of simplicity, selectivity, sensitivity and measurement convenience.

References

1 Anton, A., Dodd, J. G., and Harvey, A. E., *Anal. Chem.*, 1960, **32**, 1209.
2 Mehra, M. C., and Garvie, R., *Microchem. J.*, 1980, **25**, 223.
3 Neves, E. A., Deoliveria, E., and Sant'agostino, L., *Anal. Chim. Acta*, 1976, **87**, 243.
4 Kubaszewski, E., and Kurzawa, Z., *Chem. Anal. (Warsaw)*, 1985, **30**, 609.
5 Franco, D. W., Neves, E. A., and De Andrade, J. F., *Anal. Lett.*, 1977, **10**, 243.
6 Ilcheva, L., and Todorova, G., *Acta Chim. Acad. Sci. Hung.*, 1979, **102**, 113.
7 Mehra, M. C., and Rioux, J., *Microchem. J.*, 1982, **27**, 112.
8 Ward, G. A., and Wright, C. M., *J. Electroanal. Chem.*, 1964, **8**, 302.
9 Bryant, J. I., and Kemp, M. D., *Anal. Chem.*, 1960, **32**, 758.
10 Dziegiec, J., and Ignaczak, M., *Acta Chim. Soc. Sci., Lodz*, 1971, **16**, 69.
11 Selig, W., *Mikrochim. Acta*, 1971, **II**, 46.
12 Mackie, H., Speciale, S. J., Throop, L. J., and Young, T., *J. Chromatogr.*, 1982, **242**, 177.
13 Kubaszewski, E., Kurzawa, Z., and Lozynski, M., *Anal. Chim. Acta*, 1987, **196**, 267.
14 Swarin, S. J., and Waldo, R. A., *J. Liq. Chromatogr.*, 1982, **5**, 597.
15 Roberson, C. E., and Austin, C. M., *Anal. Chem.*, 1957, **29**, 854.
16 Cammann, K., *Working with Ion Selective Electrodes*, Springer, Berlin, 1977, pp. 58–74.
17 Evans, A., *Potentiometry and Ion Selective Electrodes*, Wiley, Chichester, 1987, pp. 121–209.
18 Masakatsu, I., Motohiro, T., Isao, H., Keiji, H., and Tadashi, H., *Sci. Eng. Rev. Doshisha Univ.*, 1980, **21**, 18.
19 Ihn, G. S., Sohn, M. J., and Buck, R. P., *Anal. Chim. Acta*, 1988, **209**, 345.
20 Hassan, S. S. M., Ahmed, M. A., Marzouk, S. A. M., and Elnemma, E. M., *Anal. Chem.*, 1991, **63**, 1547.
21 Ma, T. S., and Hassan, S. S. M., *Organic Analysis Using Ion Selective Electrodes*, 1982, vols. 1 and 2, Academic Press, London, pp. 210–212.
22 Craggs, A., Moody, G. J., and Thomas, J. D. R., *J. Chem. Educ.*, 1974, **51**, 541.
23 Hassan, S. S. M. and Ahmed, M. A., *J. Assoc. Off. Anal. Chem.*, 1991, **74**, 900.

24 IUPAC, Analytical Chemistry Division, Commission on Analytical Nomenclature, *Pure Appl. Chem.*, 1976, **48**, 129.
25 Gibson, N. A., and Weatherburn, D. C., *Anal. Chim. Acta*, 1972, **58**, 159.
26 Reinsfelder, R. E., and Shultz, F. A., *Anal. Chim. Acta*, 1973, **65**, 425.
27 Rais, J., *Collect. Czech. Chem. Commun.*, 1971, **36**, 3253.
28 Ross, J. W., in *Ion Selective Electrodes*, ed. Durst, R. A., National Bureau of Standards Special Publication 314, Washington, DC, 1973, pp. 57–88.
29 Jones, K., in *Comprehensive Inorganic Chemistry*, ed. Bailer, J. C., Jr., Emeleus, H. J., Nyholm, R., and Trotman-Dickenson, A. F., Pergamon Press, Oxford, 1975, pp. 276–293.

Paper 2/02063G
Received April 22, 1992
Accepted June 23, 1992

Lead(II) Ion-selective Electrodes Based on Crown Ethers

Seng-Rong Sheen and Jeng-Shong Shih*
Department of Chemistry, National Taiwan Normal University, Taipei, 11718, Taiwan

Lead(II) ion-selective poly(vinyl chloride) membrane electrodes based on monobenzo-15-crown-5 (MB15C5), MB15C5–phosphotungstic acid (PW) and MB15C5–phosphomolybdic acid (PMo) as neutral carriers were prepared. All these crown ether electrodes gave linear responses with near-Nernstian slopes of 30 mV per decade within the concentration range 1×10^{-1}–1×10^{-5} mol dm^{-3} Pb^{2+}. The Pb^{2+} electrodes based on MB15C5–PW and MB15C5–PMo showed better sensitivities, with detection limits of 1×10^{-6} mol dm^{-3}, than the electrode based on MB15C5 with a detection limit of 1×10^{-5} mol dm^{-3}. Selectivity coefficients of various interfering ions for these electrodes were determined and were sufficiently small for most of them. Among these electrodes, the electrode based on pure MB15C5 exhibited the best selectivity. Effects of the pH of test solutions, the concentrations of internal solutions in the electrodes and the composition of the membranes were investigated.

Keywords: *Lead ion-selective electrode; crown ether*

Crown ethers have been demonstrated to be highly selective complexing agents for many metal ions[1–5] and can potentially be applied in their separation[6–9] and determination. In addition, taking advantage of their ion-discriminating ability, crown ethers are expected to be suitable as neutral carriers of ion-selective electrodes. Recently, some crown ethers have been successfully applied in some alkali metal ion electrodes.[10–14] Owing to the water-soluble properties of most mono(crown ethers), such as 18-crown-6 and 15-crown-5, poly(crown ethers) have been used in most instances. However, poly(crown ethers) are time consuming to prepare and, in addition, electrodes using them have the disadvantage that the response time is long (*e.g.*, 10 min).[15] We have prepared some precipitates of crown ethers with phosphotungstic acid (PW) which exhibit the characteristics of the crown ethers[16,17] and also low solubilities in water. In this study, lead(II) ion-selective electrodes based on monobenzo-15-crown-5 (MB15C5), MB15C5–PW and MB15C5–phosphomolybdic acid (PMo) precipitates were developed.

In most instances in the literature, crown ethers have been reported to be used as neutral carriers in alkali metal ion-selective electrode membranes, and only a very few other metal ion-selective electrodes based on crown ethers[18,19] have been reported. However, not only alkali metal ions but also some other metal ions such as Pb^{2+} and Cu^{2+} can form stable complexes with some crown ethers.[2,4,5] There is no doubt that crown ethers can also be used as neutral carriers for a wider range of metal ion electrodes. Only one lead(II) ion-selective electrode based on a mono(crown ether) (dicyclohexano-18-crown-6) has been reported.[20] As mentioned above, the mono(crown ethers) suffer from water soluble problems. Some lead(II) ion-selective electrodes based on other neutral carriers such as methylene bis(diisobutyldithiocarbamate),[21] polyalkoxylates,[22] acyclic amides[23] and dioxadicarboxylic amides[24] have been reported. In most instances, not only are these non-crown ether neutral carriers time consuming to prepare but also these lead(II) ion-selective electrodes are subject to interferences from some common transition metal ions such as Cu^{2+}, Fe^{3+}, Ni^{2+}, Co^{2+} and Zn^{2+}, with selectivity coefficients in the range 0.1–0.01. These ions exhibit relatively small interferences (selectivity coefficients 1×10^{-3}–1×10^{-6}) to lead(II) ion-selective electrodes based on MB15C5–PW and MB15C5.

Some heterogeneous lead(II) ion-selective electrodes based on PbS, PbS–PbSe, PbS–Ag_2S and PbS–Ag_2S–Cu_2S and single-crystal electrodes based on PbS and PbSe[25–28] have been reported, but most of them suffer strong interferences from some transition metal ions such as Cu^{2+}, Cd^{2+}, Ag^+ and Hg^{2+}. However, by using the crown ether–lead(II) ion-selective electrodes prepared in this study, virtually no interference from Cu^{2+} and Cd^{2+} and only slight interferences from Ag^+ and Hg^{2+} ions are observed.

Experimental

Reagents

Monobenzo-15-crown-5 was synthesized as described by Pedersen.[1] The MB15C5–PW and MB15C5–PMo precipitates were prepared by mixing 50 cm^3 of an aqueous solution containing 0.02 mol dm^{-3} PW or PMo with 50 cm^3 of dichloromethane solution containing about 1 g of MB15C5. The precipitates were dried under vacuum. The molecular formulae of these precipitates from elemental analysis seem to be 3.0(MB15C5)–PW and 2.9(MB15C5)–PMo.

Electrode Preparation

A mixture of 100 mg of poly(vinyl chloride) (PVC) and 50 mg of dibutyl phthalate as plasticizer was dissolved in 15 cm^3 of tetrahydrofuran (THF). The PVC–THF solution was mixed well with 100 mg of MB15C5 or 120 mg of MB15C5–PW or MB15C5–PMo. The resulting mixture was poured into a glass dish with a diameter of 3.0 cm and THF was evaporated at room temperature. A non-transparent membrane about 0.5 mm thick was obtained. A piece about 12 mm in diameter was cut out from the PVC membrane and attached to a polyethylene cap by wetting the membrane with the above PVC–THF solution. The diameter of the exposed membrane was about 7 mm. The polyethylene cap with the membrane was then incorporated into a silver–silver chloride wire electrode. After filling with a solution of 1×10^{-3} mol dm^{-3} $Pb(NO_3)_2$ as internal solution, the electrode was conditioned for 24 h by soaking in 1×10^{-3} mol dm^{-3} $Pb(NO_3)_2$ solution. The electrochemical system for this study is

Ag|AgCl|internal solution (1×10^{-3} mol dm^{-3} $Pb(NO_3)_2$|
PVC membrane|test solution|sat. KCl|AgCl|Ag

* To whom correspondence should be addressed.

Evaluation of Electrode Performance

The selectivity coefficients (k_{Pb}^{pot}) were evaluated graphically by the mixed solution method[29] from potential measurements on solutions containing a fixed amount of Pb^{2+} ions ($a_{Pb} = 1 \times 10^{-3}$ mol dm^{-3}) and various amounts of the interfering ion (M^{z+}) according to the equation

$$k_{Pb}^{pot}\, a^{2/z} = a_{Pb}\{\exp[(E_2 - E_1)F/RT]\} - a_{Pb}$$

where E_1 and E_2 are the electrode potentials for the solution of the Pb^{2+} ions alone (activity a_{Pb}) and for the mixed solution containing the interfering ions (activity a_m) and the Pb^{2+} ions (activity a_{Pb}). The selectivity coefficient k_{Pb}^{pot} can be obtained as the slope of the graph of $a_{Pb}\{\exp[(E_2 - E_1)F/RT]\}$ against $a^{2/z}$. The activities a_{Pb} and a_m are calculated using the Debye–Hückel equation. E.m.f. measurements were made with a Basic Model 321 digital pH/mV meter.

Results and Discussion

The potential responses of various ion-selective electrodes based on MB15C5 are shown in Fig. 1. Among these ions, Pb^{2+} and Ag^{+} with more sensitive responses seem to be suitably determined with the electrodes based on MB15C5. It is well known that crown ethers are very sensitive to the sizes of ions. Both Pb^{2+} and Ag^{+} ions, with sizes of 1.21 and 1.26 Å, respectively,[30] can be fitted into the cavity (about 1.1 Å[31]) of MB15C5 better than other ions such as Fe^{3+} (0.65 Å), Co^{2+} (0.74 Å), Ni^{2+} (0.70 Å), La^{3+} (0.85 Å) and Cu^{2+} (0.72 Å), and MB15C5 is expected to form stronger complexes with Pb^{2+} and Ag^{+}. Therefore, the Pb^{2+} and Ag^{+} ions in the test solutions are more easily attracted to the PVC–crown ether membranes, which results in more sensitive potential responses. As shown in Fig. 1, the lead(II) ion-selective electrode exhibits a linear response to the activity of Pb^{2+} ions within the concentration range 1×10^{-1}–1×10^{-5} mol dm^{-3} $Pb(NO_3)_2$ with a Nernstian slope of 30 ± 1 mV per decade. The silver ion-selective electrode also exhibits a linear response to the activity of Ag^{+} ions, but the silver electrode gives non-Nernstian responses with a slope of 27 ± 1 mV per decade and a linear response within only a very narrow concentration range of 1×10^{-1}–1×10^{-3} mol dm^{-3} $AgNO_3$. Therefore, the crown ether is suitable for use as a neutral carrier in the Pb^{II}–PVC membrane electrode for Pb^{2+} ions, but is not suitable for the Ag^{+} ions.

The effect of the composition of the electrode with the MB15C5–PVC membrane on the potential response of the lead(II) ion-selective electrode was investigated. As shown in Fig. 2, the 3.0 cm diameter membrane with 100 mg of PVC and 100 mg of MB15C5 exhibits the best response with a Nernstian slope of 30 ± 1 mV per decade. The concentration of the internal solution [$Pb(NO_3)_2$] in the electrode has only a very slight effect on the potential response of the electrode. As shown in Fig. 3, this seems to indicate that variation of the concentration of this internal solution (1×10^{-3}–1×10^{-5} mol dm^{-3}) does not cause any significant difference in the potential response.

As mentioned above, the lead(II) ion-selective electrode based on MB15C5 exhibits good sensitivity. However, although the solubility of MB15C5–PVC in water is much lower than that of other monocrown ethers such as 18-crown-6 (18C6), 15-crown-5 (15C5) and 12-crown-4 (12C4), the effect of the slight solubility of MB15C5 on the lifetime of the electrode membrane must still be considered. Therefore, we prepared some crown ether–PW precipitates that had been successfully applied as sorbents for rare earth ions[16] and transition metal ions.[17] These crown ether–PW precipitates are easily prepared and have lower solubilities than mono-(crown ethers). In addition, they also have the characteristics of crown ethers. In this study, precipitates of MB15C5 with

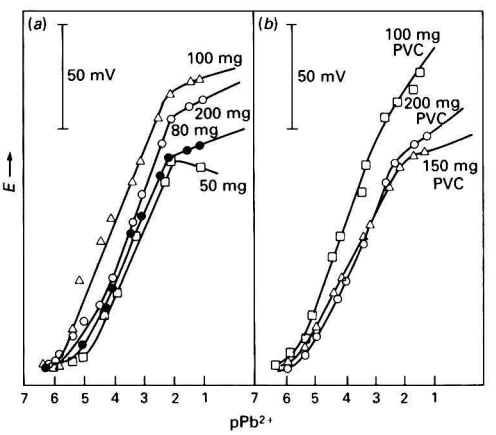

Fig. 2 Effects of the contents of (*a*) MB15C5 and (*b*) PVC in 3 cm diameter Pb^{II}–PVC electrode membranes

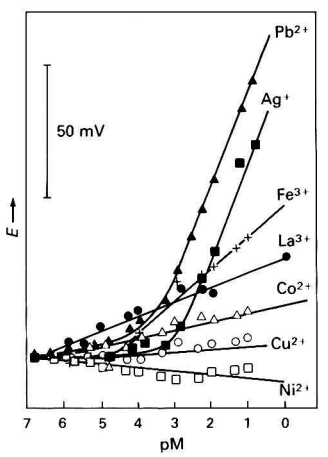

Fig. 1 Potential responses of various transition metal ion electrodes based on MB15C5

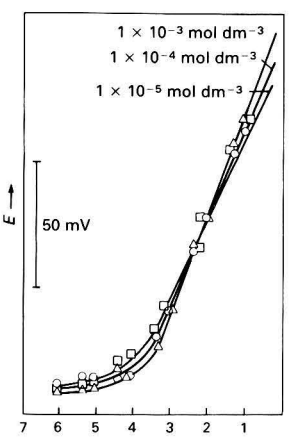

Fig. 3 Effect of internal solution concentration in Pb^{II}–PVC electrodes based on MB15C5

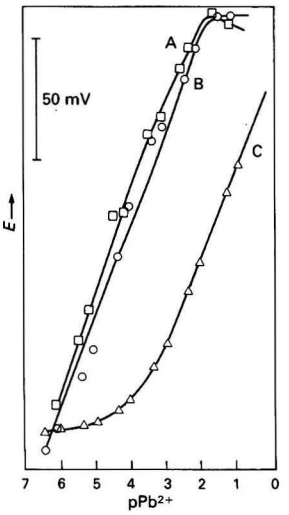

Fig. 4 Potential responses of Pb^{II} electrodes based on: A, MB15C5–PW; B, MB15C5–PMo; and C, MB15C5

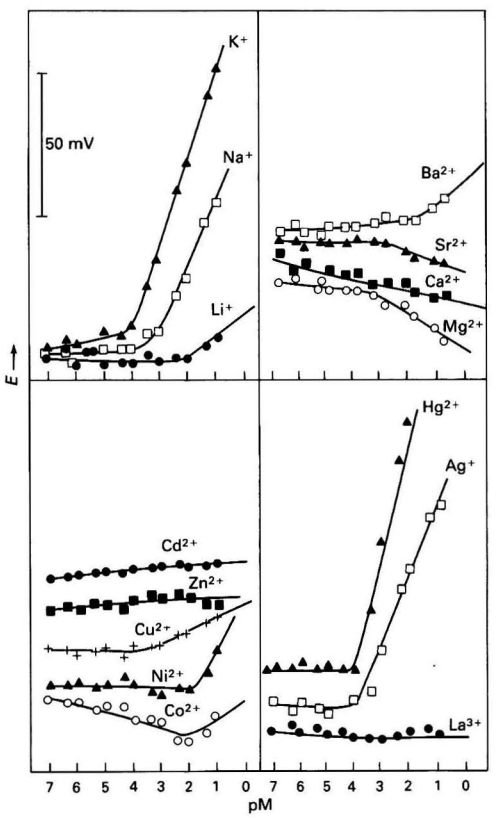

Fig. 5 Selectivity measurements for various ions with a Pb^{II} ion-selective electrode based on MB15C5. $[Pb^{2+}] = 10 \times 10^{-5}$ mol dm^{-3}

PW and PMo were prepared and applied as electrical carriers for the lead(II) ion-selective electrodes. As shown in Fig. 4, lead(II) ion-selective electrodes based on MB15C5–PW and MB15C5–PMo also exhibit linear responses with Nernstian

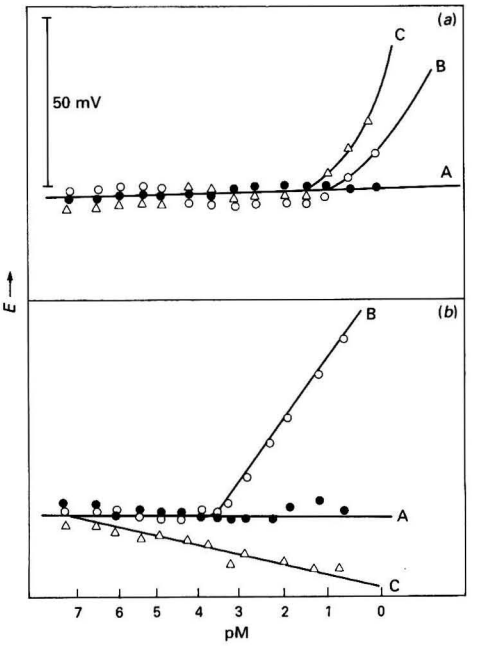

Fig. 6 Comparison of selectivities of Pb^{II} electrodes based on: A, MB15C5; B, MB15C5–PW; and C, MB15C5–PMo for (*a*) Cd^{2+} and (*b*) La^{3+} ions

slopes of 30 ± 1 mV per decade within the concentration range 1×10^{-1}–1×10^{-6} mol dm^{-3}. This obviously indicates that lead(II) ion-selective electrodes based on both MB15C5–PW and MB15C5–PMo show better sensitivities with lower detection limits (1×10^{-6} mol dm^{-3}) and a wider linear detection concentration range (1×10^{-1}–1×10^{-6} mol dm^{-3}) than the electrode based on MB15C5.

In addition to the detection limit and linear detection concentration range, the selectivity of the ion-selective electrode is also very important. The selectivity of the lead(II) ion-selective electrode was investigated from potential measurements in solutions containing a fixed amount of Pb^{2+} (1×10^{-3} mol dm^{-3}) and different amounts of the interfering ion (M^{z+}). As shown in Fig. 5, most transition metal ions such as Cd^{2+}, Cu^{2+}, Zn^{2+}, Ni^{2+}, Co^{2+} and La^{3+} show negligible interference at concentrations <0.1 mol dm^{-3} with the lead(II) ion-selective electrode based on MB15C5; alkaline earth metal ions such as Mg^{2+}, Ca^{2+}, Sr^{2+} and Ba^{2+} exhibit slight interference at concentrations >1×10^{-2} mol dm^{-3}; however, alkali metal ions such as K^+ and Na^+ and the heavy metal ions Hg^{2+} and Ag^+ show some interference. The electrodes based on both MB15C5–PW and MB15C5–PMo show similar effects with respect to the selectivity of the ions, but the electrodes based on MB15C5 seem to exhibit slightly better selectivity for Pb^{2+} ions with respect to other ions than the electrodes based on MB15C5–PW and MB15C5–PMo. For example, as shown in Fig. 6, the lead(II) ion-selective electrode based on MB15C5 shows better selectivity for Pb^{2+} ions in the presence of La^{3+} or Cd^{2+} than the electrodes based on MB15C5–PW or MB15C5–PMo.

The selectivity coefficients (k_{Pb}^{pot}) for various ions were evaluated as the slope of the graph of a_{Pb} $\{\exp[(E_2 - E_1)F/RT]\} - a_{Pb}$ against $a^{2/z}$. The results for the various electrodes are shown in Table 1. The selectivity coefficients for most transition metal and alkaline earth metal ions are small (1×10^{-4}–1×10^{-5}), which seems to indicate that these metal ions show negligible interference with these crown ether

Table 1 Selectivity coefficients (k_{Pb}^{pot}) of various interfering ions (M^{z+}) for lead(II) ion-selective electrodes based on various crown ethers at a lead(II) concentration of 1.0×10^{-5} mol dm^{-3}

M^{z+}	MB15C5	MB15C5–PMo	MB15C5–PW
Li^+	1.08×10^{-5}	4.85×10^{-3}	2.78×10^{-2}
Na^+	1.54×10^{-2}	2.45×10^{-1}	4.37×10^{-2}
K^+	2.44×10^{-1}	2.31×10^{-1}	5.28×10^{-2}
Mg^{2+}	3.10×10^{-5}	4.41×10^{-5}	1.58×10^{-5}
Ca^{2+}	1.28×10^{-5}	3.74×10^{-5}	7.74×10^{-6}
Sr^{2+}	2.74×10^{-5}	5.03×10^{-4}	3.91×10^{-4}
Ba^{2+}	7.40×10^{-5}	3.43×10^{-4}	1.77×10^{-4}
La^{3+}	1.45×10^{-5}	8.32×10^{-4}	2.65×10^{-3}
Fe^{3+}	5.66×10^{-5}	3.09×10^{-1}	6.40×10^{-3}
Co^{2+}	2.00×10^{-5}	2.08×10^{-4}	1.66×10^{-4}
Ni^{2+}	1.18×10^{-4}	2.37×10^{-4}	7.79×10^{-5}
Cu^{2+}	8.13×10^{-5}	2.08×10^{-4}	3.60×10^{-5}
Zn^{2+}	1.29×10^{-5}	1.74×10^{-5}	1.24×10^{-6}
Cd^{2+}	7.77×10^{-6}	9.97×10^{-5}	2.93×10^{-5}
Hg^{2+}	1.47×10^{-1}	5.69×10^{-5}	3.63×10^{-2}
Ag^+	4.89×10^{-2}	8.71×10^{-1}	2.43×10^{-1}

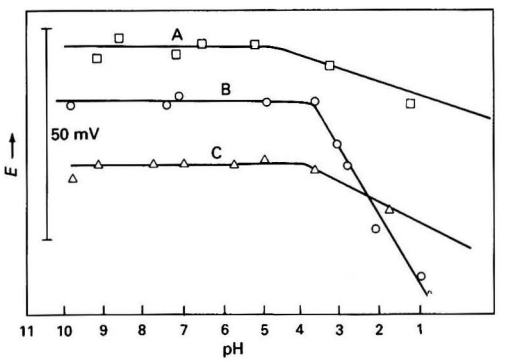

Fig. 7 Effect of pH on potential responses of Pb^{II} electrodes based on: A, MB15C5–PMo; B, MB15C5; and C, MB15C5–PW

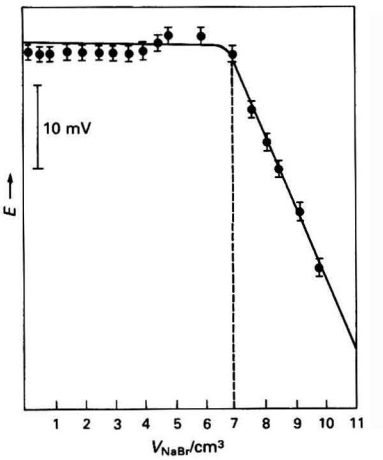

Fig. 8 Application of Pb^{II} electrode based on MB15C5 to the titration of 20.0 cm^3 of 1.75×10^{-4} mol dm^{-3} $Pb(NO_3)_2$ solution with 1.0×10^{-3} mol dm^{-3} NaBr. (The deviation of the data is about ±1.0 mV)

electrodes. Although the selectivity coefficients of alkali metal ions and Hg^{2+} and Ag^+ are about 0.1–0.01 and are larger than those for any other ions, the electrodes exhibit the highest selectivity for the Pb^{2+} ion, with $k_{Pb}^{pot} < 1$. The interference from Hg^{2+} and Ag^+ can be masked with thiosemicarbazide.[32,33] In addition, in a comparison of these crown ether electrodes, the electrode based on MB15C5 suffers a smaller interference from these interfering ions than the electrodes based on MB15C5–PW and MB15C5–PMo.

The effect of the pH of the test solution on the potential response of the electrodes was also investigated. As illustrated in Fig. 7, in the pH range 3–9 the potential responses of these electrodes hardly change, but at pH <2 the potential responses decrease considerably for all these electrodes. This could be due to the protonation of the crown ethers in the membrane, which results in their losing their ability to complex with Pb^{2+} ions.

The laboratory-built lead(II) ion-selective electrode was successfully applied to the precipitation titration of Pb^{2+} ions in aqueous solution with NaBr solution. As shown in Fig. 8, the amount of Pb^{2+} ions in solutions can be determined with the electrode based on MB15C5.

In conclusion, all the lead(II) ion-selective electrodes based on MB15C5, MB15C5–PW and MB15C5–PMo exhibit good sensitivity (1×10^{-5}–1×10^{-6} mol dm^{-3} of Pb^{2+} can be measured) with Nernstian slopes (30 mV per decade), a short response time (<1 min), good reproducibility and good selectivity. The MB15C5 electrode membrane shows the best selectivity with smaller selectivity coefficients for most common ions, but both the MB15C5–PW and MB15C5–PMo membranes have the advantages of lower solubility of the crown ether in water and better sensitivity with lower detection limits (1×10^{-6} mol dm^{-3}). In addition, in comparison with commercial PbS-based lead(II) electrodes, the crown ether–lead(II) ion-selective electrode demonstrates the advantage of virtually no interference from some common transition metal ions such as Fe^{3+}, Co^{2+}, Ni^{2+}, Cu^{2+}, Cd^{2+} and Zn^{2+}.

The authors express their appreciation to the National Science Council of the Republic of China for financial support of this study.

References

1 Pedersen, C. J., *J. Am. Chem. Soc.*, 1967, **89**, 7017.
2 Christensen, J. J., Batough, D. J., and Izatt, R. M., *Chem. Rev.*, 1974, **74**, 351.
3 Izatt, R. M., and Christensen, J. J., *Synthetic Multidentate Macrocyclic Compounds*, Academic Press, New York, 1978.
4 Kolthoff, I. M., *Anal. Chem.*, 1979, **51**, 1R.
5 Izatt, R. M., and Christensen, J. J., *Progress in Macrocyclic Chemistry*, Wiley-Interscience, New York, 1979.
6 Frensdroff, H. K., *J. Am. Chem. Soc.*, 1971, **93**, 4684.
7 Blasius, E., Janzen, K. P., Luxenburger, H., Nguyen, V. B., Klotz, H., and Stockenmer, J., *J. Chromatogr.*, 1978, **167**, 307.
8 Kopolow, I., and Smid, J., *Macromolecules*, 1973, **6**, 135.
9 Fernando, L. A., Miles, M. L., and Bowen, L. H., *Anal. Chem.*, 1980, **52**, 1115.
10 Jeng, J., and Shih, J. S., *Analyst*, 1984, **109**, 641.
11 Ryba, O., and Petranek, J., *Electrochemistry*, 1976, **67**, 321.
12 Petranek, J., and Ryba, O., *Anal. Chim. Acta*, 1974, **72**, 375.
13 Ryba, O., and Petranek, J., *J. Electroanal. Chem. Interfacial Electrochem.*, 1973, **44**, 425.
14 Shono, T., Okahara, M., Ikeda, I., Kimura, K., and Tamura, H., *J. Electroanal. Chem.*, 1982, **132**, 99.
15 Kimura, J., Maeda, J., and Shono, T., *J. Electroanal. Chem.*, 1979, **95**, 91.
16 Shih, J.-S., Tsay, L.-M., and Wu, S.-C., *Analyst*, 1985, **110**, 1387.
17 Tzeng, D.-L., Shih, J.-S., and Yeh, Y.-C., *Analyst*, 1987, **112**, 1413.

18 Czaban, J. D., and Rechnitz, G. A., *Anal. Chem.*, 1973, **45**, 471.
19 Lai, M.-T., and Shih, J.-S., *Analyst*, 1986, **111**, 891.
20 Evlanova, T. V., Timofeeva, S. K., and Popov, A. N., *Latv. PSR Zinat. Akad. Vestis, Kim. Ser.*, 1989, **2**, 165; *Chem. Abstr.*, 1990, **112**, 15677f.
21 Kamata, S., and Onoyama, K., *Anal. Chem.*, 1991, **63**, 1295.
22 Jaber, A. M. Y., Moody, G. J., and Thomas, J. D. R., *Analyst*, 1988, **113**, 1409.
23 Malinowska, E., *Analyst*, 1990, **115**, 1085.
24 Lindner, E., Toth, K., and Pungor, E., *Anal. Chem.*, 1984, **56**, 1127.
25 Hirata, H., and Higashiyama, K., *Anal. Chim. Acta*, 1971, **54**, 365.
26 Hirata, H., and Higashiyama, K., *Bull. Chem. Soc. Jpn.*, 1971, **44**, 2420.
27 Hirata, H., and Higashiyama, K., *Anal. Chim. Acta*, 1971, **57**, 476.
28 Mascini, M., and Liberti, A., *Anal. Chim. Acta*, 1972, **60**, 405.
29 Srinivasan, K., and Rechnitz, G. A., *Anal. Chem.*, 1969, **41**, 1203.
30 Cotton, F. A., and Wilkinson, F. R., *Advanced Inorganic Chemistry*, Wiley, New York, 4th edn., 1980, p. 14.
31 Pedersen, C. J., and Frensdroff, H. K., *Angew. Chem., Int. Ed. Engl.*, 1972, **11**, 16.
32 Rechnitz, G. A., and Kenny, N. C., *Anal. Lett.*, 1970, **3**, 259.
33 Iizuka, A. Y., Yasaki, T., Ohashi, K., Yokota, Y., Matsuzawa, A., and Kato, M., *J. Dent. Health*, 1973, **23**, 182.

Paper 2/00940D
Received February 24, 1992
Accepted May 18, 1992

Prediction of the Conditions for Supercritical Fluid Extraction of Atrazine from Soil

Sameena Ashraf, Keith D. Bartle,* Anthony A. Clifford, Robert Moulder,† Mark W. Raynor‡ and Gavin F. Shilstone
School of Chemistry, University of Leeds, Leeds, UK LS2 9JT

Samples of soil were spiked with known concentrations of atrazine and extracted with supercritical carbon dioxide. Quantitative analysis of the extracts was carried out by capillary gas chromatography and the kinetics of extraction were fitted to the 'hot-ball' model. The conditions for extraction were predicted from calculated solubilities using the Peng–Robinson equation of state, and were in satisfactory agreement with experiment.

Keywords: *Supercritical fluid extraction; atrazine; soil; capillary gas chromatography; Peng–Robinson equation*

The potential advantages of supercritical fluid extraction (SFE),[1–5] compared with conventional extraction methods such as Soxhlet or ultrasonic liquid extraction, include: more rapid extraction rates; the possibility of more efficient extractions; increased selectivity; and possible analyte fractionation during extraction. A further very important advantage is the compatibility of SFE with on-line analysis methods such as continuous spectroscopic monitoring or chromatographic analysis. Several recent studies have shown that analytical SFE provides comparable or better extraction efficiencies than the Soxhlet method.[1,2,5,6] Also, increased extraction rates have been achieved, which offer significant time-savings. The application of SFE to the isolation of herbicides from soil and sediment has been demonstrated.[7,8] Only recently has a model for analytical extraction in a flow system by a supercritical fluid been proposed that reproduces the important features of the behaviour of such systems.[9] This, the 'hot-ball' model, assumes no limitation of solubility of the extracted material in the supercritical fluid.

The choice of extraction conditions has largely been determined empirically, *i.e.* the conditions are varied until an apparently acceptable extraction efficiency is obtained; such a method is time consuming. This problem can be partially addressed through calculations of solubility of the analyte in the supercritical fluid, although the influence of the adsorptive properties of the matrix can also be significant. The purpose of this work was to ascertain whether there is a correlation between the predicted solubility of selected agrochemicals in a two component system and the observed variation of extent of extraction from a matrix, so that optimum extraction pressures and temperatures can be predicted.

Experimental

Samples of sandy loam soil containing 1.1% organic matter were air dried at 105 °C and were spiked with atrazine to 100 μg g^{-1} (Fig. 1) by dissolving the agrochemical in dichloromethane, adding to the soil and evaporating to dryness with stirring. Aliquots of 2 g were introduced into a 2 cm^3 glass tube. The tube was placed (Fig. 2) in a stainless-steel (SS) extraction vessel of approximately 7 cm^3 volume in a thermostated oven. The extraction vessel was pressurized with carbon dioxide supplied by a Varian 8500 syringe pump; pressure measurements were made with the pump transducer. All transfer tubing was $\frac{1}{16}$ in o.d. SS; the inlet tubing to the extraction vessel extended to the bottom of the glass tube so that the supercritical fluid passed through the soil matrix. The flow rate was controlled by a 20 cm length of 50 μm i.d. fused silica capillary restrictor, which was connected to the transfer tubing by a standard $\frac{1}{16}$ in o.d. SS Swagelok union by graphitized Vespel ferrules (Scientific Glass Engineering). The solute trap contained dichloromethane in which the end of the restrictor was immersed.

Extractions were performed within 24 h of spiking for a number of set pressures for a fixed time and at extraction temperatures of 50 and 80 °C. Flow rates were kept constant at an approximate average of 300 cm^3 min^{-1}, measured at atmospheric pressure and room temperature. These procedures were repeated for the extraction of atrazine for different periods of time at constant extraction pressure.

The extracts were analysed quantitatively by capillary gas chromatography (GC) on a 12 m × 320 μm i.d. SE-54 column in a Carlo Erba Vega 4160 chromatograph with on-column injection and flame ionization detection. The temperature

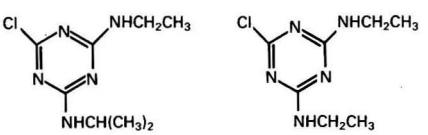

Fig. 1 Chemical structures of atrazine and simazine

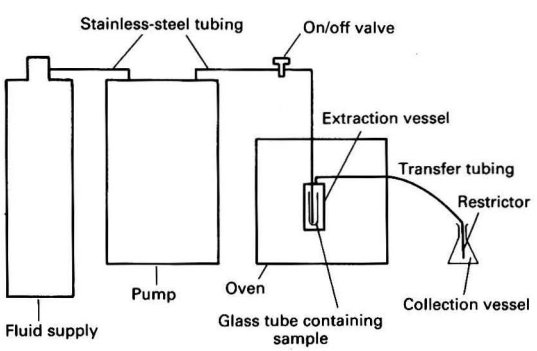

Fig. 2 Schematic diagram of extraction apparatus

* To whom correspondence should be addressed.
† Present address: Uppsala University, Department of Analytical Chemistry, Box 531, S-75121 Uppsala, Sweden.
‡ Present address: Department of Chemistry and Applied Chemistry, University of Natal, King George V Avenue, Durban 4001, South Africa.

programme for atrazine analysis was 50 °C for 3 min then taken to 180 °C at 40 °C min^{-1}, and from 180 to 250 °C at 5 °C min^{-1}.

Solubility Calculations

Solubilities, S, of atrazine in supercritical carbon dioxide were calculated at different pressures, P, and temperatures, T, by means of the equation:

$$\ln S = \ln (P_v/P) - \ln\phi - \ln V + PV_s/RT \quad (1)$$

Where P_v is the vapour pressure of the solute, ϕ is the fugacity coefficient of the solute in the supercritical phase, V is the molar volume of the CO_2, V_s is the molar volume of the solute and R is the gas constant. Eqn. (1) is derived by equating the chemical potential of the solute in the solid or liquid and supercritical phases, and assumes that the solutes are pure and incompressible, and that the solutions are dilute. The last term arises from the effect of pressure on the chemical potential of the solid, and the penultimate term allows conversion of the mole fraction to solubility. The use of eqn. (1) requires a suitable equation of state (EOS) for predicting ϕ; here the Peng–Robinson EOS was used,[10] which requires knowledge of a binary interaction parameter, δ, for each pair of components and an acentric factor, ω, for both solute and CO_2. Therefore:

$$\ln\phi = (b_1/b_2)(Z-1) - \ln(Z - b_2P/RT) - (a_{22}/2\sqrt{2}\,b_2RT)\,2a_{12}/a_{22} - (b_1/b_2)\ln\{[Z + (1+\sqrt{2})b_2P/RT]/[Z + (1-\sqrt{2})b_2P/RT]\} \quad (2)$$

where,

$$Z = PV/RT \quad (3)$$

$$b_1 = 0.07780RT_{c,1}/P_{c,1} \quad (4)$$

$$b_2 = 0.07780RT_{c,2}/P_{c,2} \quad (5)$$

$$a_{12} = [0.45724(1-\delta)R^2T_{c,1}T_{c,2}k_1k_2]/P_{c,1}P_{c,2})^{\frac{1}{2}} \quad (6)$$

$$a_{22} = (0.45724R^2T^2_{c,2}k^2_2)/P_{c,2} \quad (7)$$

$$k_1 = 1 + [1 - (T/T_{c,1})^{\frac{1}{2}}](0.37464 + 1.54226\omega_1 - 0.26992\omega^2_1) \quad (8)$$

$$k_2 = 1 + [1 - (T/T_{c,2})^{\frac{1}{2}}](0.37464 + 1.54226\omega_2 - 0.26992\omega^2_2) \quad (9)$$

Eqns. (2)–(9) assume that the solutions are dilute and that the solutes are incompressible, and do not dissolve in CO_2 under pressure (SI units are assumed in these equations). The subscript c denotes a critical parameter, and subscripts 1 and 2 refer to solute and CO_2, respectively.

The value of V was calculated from the IUPAC formulation,[11] $T_{c,1}$ and $P_{c,1}$ were calculated by Lyderson's method[12] from group contributions, the boiling point (T_b) and the relative molecular mass of the solute. Values of ω for the solutes were obtained from:

$$\omega = \frac{-\ln P_c - 5.92714 + 6.09648\,\Theta^{-1} + 1.28862\ln\Theta - 0.169347\,\Theta^6}{15.2518 - 15.6875\,\Theta^{-1} - 13.4721\ln\Theta + 0.43577\,\Theta^6} \quad (10)$$

Where $\Theta = T_b/T_c$, and P_c is measured in atmospheres (1 atm = 101 × 10^3 Pa), and P_v (in mmHg; 1 mmHg ≈ 133 Pa) was obtained from the equation:

$$\log_{10}(P_v) = A/T_{(k)} - B \quad (11)$$

Values of A and B were obtained from known values of P_v at 20 °C, and the atmospheric pressure at the measured T_b, and were adjusted for the heat of fusion.

The values of δ for each solute–CO_2 pair were estimated from compounds with similar critical properties and chemical structures.[13] The effect of changes in δ on the predicted value of S has been considered elsewhere;[14] essentially the shapes of graphs of S against P are unchanged. Values of the physical properties used in the solubility calculations are listed in Table 1.

Table 1 Physical properties of agrochemicals employed in solubility calculations

	Atrazine	Simazine
Relative molecular mass	215.7	201.7
$P_c/10^5$ Pa	26.0*	28.2*
T_c/K	665.2*	739.2*
ω	0.756*	0.734*
A/K	7534.3	7610.0
B	19.17	17.74
10^6 V/m^3 mol^{-1}	181.7†	168.0†
δ‡	0.1	0.1
Melting point/°C	176.0†	226.0†
Boiling point/°C	220.0	(270.0)

* See ref. 10.
† See ref. 15.
‡ See ref. 11.

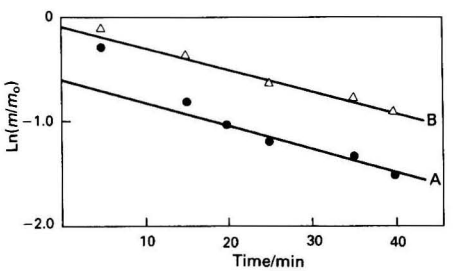

Fig. 3 Graphs of $\ln(m/m_0)$ *versus* time ('hot-ball' model) for extraction of atrazine from soil with supercritical CO_2 at 220 bar and A, 80 and B, 50 °C

Results and Discussion

Results of experiments in which percentage recovery was measured as a function of time at constant pressure were fitted to the hot-ball model[9] by plotting $\ln(m/m_0)$ *versus* time, t; m is the mass remaining at time t, and m_0 is the initial mass of extractable material. In this model the ratio m/m_0 is approximated by

$$m/m_0 = (6/\pi^2)\sum_{n=1}^{\infty}\frac{1}{n^2}\exp(-n^2\pi^2 Dt/r^2) \quad (12)$$

where n is an integer, and D is the diffusion coefficient of the material within the (assumed) spherical particle, radius r. Making the substitution

$$\pi^2D/r^2 = a \quad (13)$$

$$m/m_0 = 6/\pi^2\,[\exp(-at) + \tfrac{1}{4}\exp(-4at) + \tfrac{1}{9}\exp(-9at) + \ldots] \quad (14)$$

This represents a sum of exponential decays. At long times the later, more rapidly decaying, terms decrease in importance compared with the first term, which then dominates; the graph of $\ln(m/m_0)$ *versus* t becomes linear.

The $\ln(m/m_0)$ *versus* t curves for the extractions reported here (*e.g.*, Fig. 3) show the characteristic[9] behaviour corresponding to the hot-ball model in which a process akin to diffusion through the particle dominates (a steep fall followed by a linear region). This behaviour is surprising in that the samples were spiked, but indicates that the analytes have permeated the soil particles. For the extraction of atrazine from soil at 80 °C, extrapolation of the linear portion of the curve to the $t = 0$ axis gives (Fig. 3A) an intercept close to the theoretical $0.5 \approx \ln(6/\pi^2)$; this corresponds to extrapolation with no solubility limitation. Extraction of atrazine at 50 °C produces (Fig. 3B) a curve in which the slope of the linear portion is similar to that at 80 °C, as is expected for extraction

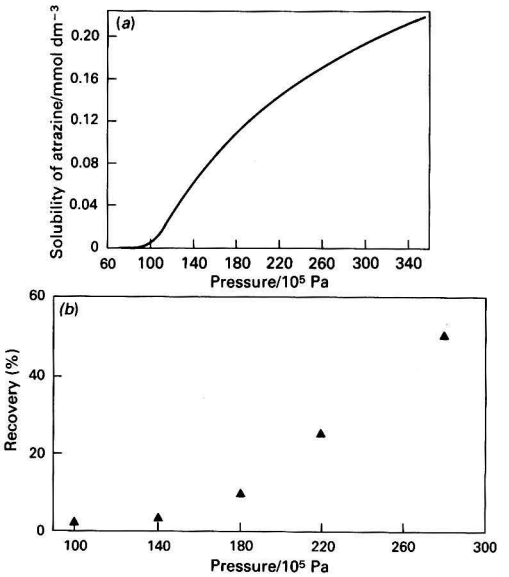

Fig. 4 Variation of (*a*) predicted solubility, and (*b*) experimental percentage recovery in unit time (15 min) with CO_2 pressure for extraction of atrazine from soil at 50 °C

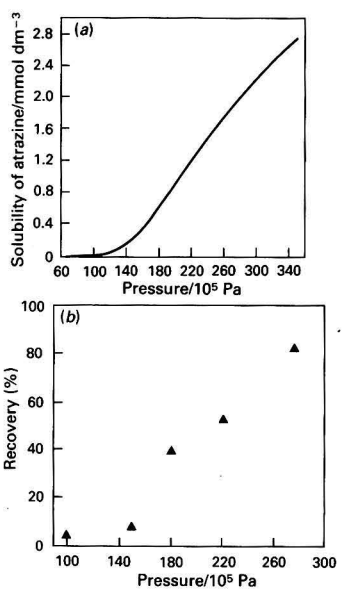

Fig. 5 Variation of (*a*) predicted solubility, and (*b*) experimental percentage recovery in unit time (15 min) with CO_2 pressure for extraction of atrazine from soil at 80 °C

from the same matrix, for which r and D are unchanged; however, the initial portion is less steep and the intercept is shifted to a less negative value, both corresponding[9] to reduced solubility. These observations are in keeping with the higher predicted and experimental solubilities of atrazine at 80 °C than at 50 °C (Figs. 4 and 5).

For atrazine the predicted solubilities [Figs. 4(*a*) and 5(*a*)] begin to rise at approximately 100×10^5 Pa, in agreement with the experimentally observed 'threshold' solubilities in the graphs of percentage recovery in unit time *versus* pressure

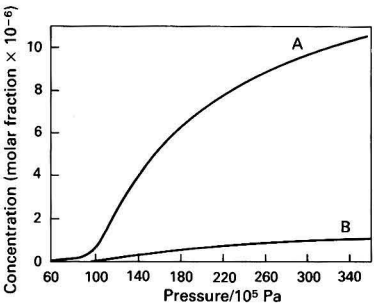

Fig. 6 Variation of predicted solubility with CO_2 pressure at 50 °C for: A, atrazine; and B, simazine

[Figs. 4(*b*) and 5(*b*)]. The calculated solubility curves [Fig. 4(*a*) and 5(*a*)] rise consistently with pressure at both 50 and 80 °C without reaching a maximum. These trends are also in agreement with experimental extraction efficiencies [Figs. 4(*b*) and 5(*b*)], with the curves still rising steeply at 300×10^5 Pa.

Janda *et al.*[8] observed that simazine was extracted with a much lower efficiency from sediment than atrazine by supercritical CO_2 at 42 °C. The calculated solubility curves for these compounds (Fig. 6) are in qualitative agreement with these results; on the basis of our calculations simazine is predicted to be much less soluble in supercritical CO_2 than atrazine, at 50 °C.

These results indicate the importance of solubility and diffusion in SFE, but effects arising from the adsorption of analyte on the sample matrix should also be addressed. The organic matter composition of the soil is likely to have an important bearing on the partition of organic compounds between the soil and the extracting fluids.[16] Active sites in (or on) the matrix can strongly influence the concentration of the analyte in the supercritical fluid solution at the surface; indeed, the greater rate of extraction at 80 °C as compared with 50 °C might also be, at least partially, a consequence of matrix effects, as has been noted in the extraction of polychlorobiphenyls from soils and sediments.[17]

Conclusions

The solubilities of complex agrochemicals in supercritical CO_2 at different pressures can be calculated by an approach incorporating the Peng–Robinson EOS; the necessary physical data can be estimated from that normally available.

The kinetics of extraction are fitted by the hot-ball model;[9] but the solubility in supercritical CO_2 is a major factor governing the extraction of agrochemicals from soil. Observed extraction efficiencies from different compounds are in the same sequence as calculated solubilities and the 'threshold' pressure beyond which extraction rapidly increases can be predicted, as can the qualitative effect of increasing the pressure or temperature of extraction.

Support of this work by the Science and Engineering Research Council through a grant and research studentships (to R. M. and G. F. S.) is gratefully acknowledged. We are also grateful to B. Frere for assistance with the GC measurements.

References

1 Wright, B. W., Wright, C. W., Gale, R. W., and Smith, R. D., *Anal. Chem.*, 1987, **59**, 38.
2 Hawthorne, S. B., and Miller, D. J., *Anal. Chem.*, 1987, **59**, 1705.

3 Davies, I. L., Raynor, M. W., Kithinji, J. P., Bartle, K. D., Williams, P. T., and Andrews, G. E., *Anal. Chem.*, 1988, **60**, 683A.
4 Wright, B. W., Fulton, J. L., Kopriva, A. J., and Smith, R. D., in *Supercritical Fluid Extractions and Chromatography*, eds. Charpentier, B. A., and Sevenants, M. R., Americal Chemical Society, Washington D.C., ACS Symposium Series No. 366, 1988, pp. 44–62.
5 Hawthorne, S. B., Krieger, M. S., and Miller, D. J., *J. Chromatogr. Sci.*, 1989, **27**, 347.
6 Hawthorne, S. B., *Anal. Chem.*, 1990, **62**, 633A.
7 Engelhardt, H., and Gross, A., *HRC CC J. High Resolut. Chromatogr. Chromatogr. Commun.*, 1988, **11**, 726.
8 Janda, V., Steenbeke, G., and Sandra, P. in *Proceedings 10th International Symposium on Capillary Chromatography*, eds. Sandra P., and Redant, G., Hüthig, Heidelberg, 1989, pp. 457, vol. 11.
9 Bartle, K. D., Clifford, A. A., Hawthorne, S. B., Langenfeld, J. L., Miller, D. J., and Robinson, R. E., *J. Supercrit. Fluids*, 1990, **3**, 143.
10 Peng, D. Y., and Robinson, D. B., *Ind. Eng. Chem. Fundam.*, 1976, **15**, 59.
11 Angus, S., Armstrong, B., and De Reuck, K. M., *International Tables of the Fluid State, Carbon Dioxide*, Pergamon, Oxford, 1976, vol. 3.
12 Reid, R. C., Prausnitz, J. M., and Sherwood, T. K., *The Properties of Gases and Liquids*, McGraw-Hill, New York, 1977.
13 Bartle, K. D., Clifford, A. A., and Shilstone, G. F., *J. Supercrit. Fluids*, in the press.
14 Bartle, K. D., Clifford, A. A., and Shilstone, G. F., *J. Supercrit. Fluids*, 1989, **2**, 30.
15 Worthing, C. R., *Pesticides Manual*, The Lavenham Press, Lavenham, Suffolk, 8th edn., 1987.
16 Rutherford, D. W., Chiou, C. T., and Kile, D. E., *Environ. Sci. Technol.*, 1992, **26**, 336.
17 Hawthorne, S. B., Miller, D. J., Langenfeld, J. J., Burford, M. D., Eckert-Tilotta, S., and Louie, P. K. K., *Abstracts 4th International Symposium on Supercritical Chromatography and Extraction, Cincinnati, Ohio, USA*, 1992, pp. 103.

Paper 1/06085F
Received December 2, 1991
Accepted June 23, 1992

On-line Preconcentration of Aqueous Samples for Gas Chromatographic–Mass Spectrometric Analysis

Jolan J. Vreuls, Albert-Jan Bulterman, Rudy T. Ghijsen and Udo A. Th. Brinkman
Department of Analytical Chemistry, Free University, De Boelelaan 1083, 1081 HV Amsterdam, The Netherlands

On-line trace enrichment as a treatment for the analysis of water samples by gas chromatography (GC) with subsequent detection by mass spectrometry (MS) is demonstrated. A 1 cm^3 sample is concentrated on a short polymer-packed liquid chromatography (LC) pre-column. After rinsing with high-performance LC-grade water, the pre-column is dried with nitrogen and desorbed with ethyl acetate. A fraction of 60 mm^3 is introduced on-line into a diphenyltetramethyldisilazane-deactivated retention gap. After evaporation of the solvent *via* an early solvent-vapour exit, the analytes are separated by means of GC and introduced into the ion source of the mass spectrometer *via* a restriction capillary. With the mass spectrometer as a sensitive and selective detector for on-line LC–GC, atrazine and other triazines can be determined in water at the low parts per trillion level.

Keywords: *Coupled liquid chromatography–gas chromatography—mass spectrometry; aqueous sample; triazine*

Sample preparation of water samples for gas chromatographic (GC) analysis normally involves a change of solvent in combination with an enrichment step. The change of solvent is carried out either by liquid–liquid extraction[1] or by solid-phase extraction.[2] A large enrichment factor can be obtained by concentrating the analytes from a 100 to 1000 cm^3 sample into, finally, 0.1–1.0 cm^3 of organic solvent. Analyte losses by poor extraction or due to breakthrough on the solid-phase extraction cartridge and contamination from the organic solvents used are two major problems.

Recently, we described a system for on-line and fully automated liquid chromatography (LC)-type trace enrichment, desorption and GC separation.[3] Only 1 cm^3 of water had to be preconcentrated to obtain detection limits of about 100 pg cm^{-3} for a series of analytes with flame-ionization detection. A drawback of the system, when analysing authentic samples, is that identification of compounds is based only on a comparison of retention times. Selective trace enrichment on a short LC pre-column containing antibodies raised against one analyte or a group of analytes[4] can be performed to eliminate interferences. Selectivity can also be obtained by using selective GC detectors, *e.g.*, a nitrogen–phosphorus detector (NPD)[5] or an electron-capture detector (ECD).

In this paper we report on the use of mass spectrometry (MS) as a detection system after on-line LC trace enrichment of aqueous samples and GC analysis. The optimum design of the valve-switching system is discussed. A rapid optimization of the LC–GC procedure and the potential of LC–GC–MS are demonstrated.

Experimental

Chemicals and Reagents

High-performance LC-grade water and ethyl acetate (J. T. Baker, Deventer, The Netherlands) were used to load the sample onto the LC trace enrichment cartridge and to desorb the analytes, respectively. Ethyl acetate was distilled before use. A stock solution containing *s*-triazine herbicides at a concentration of 10 ng mm^{-3} was used to prepare aqueous standards and spiked samples. 4,4′-Difluorobiphenyl in ethyl acetate was used as the internal standard (IS).

Equipment

The on-line coupled analytical system consisted of the commercially available Dualchrom 3000 (LC trace-enrichment module and gas chromatograph) equipped with a QMD 1000 mass spectrometer (Carlo Erba, Milan, Italy), as shown in Fig. 1. The on-line coupling of LC, GC and MS is a rather complex problem. Therefore, each unit will be discussed in a separate section.

LC Trace-enrichment System

The LC trace-enrichment system consists of a Phoenix 30 syringe pump (Gardiner, NY, USA) and a slave pump, a pneumatic six-port valve with a 1 cm^3 loop (V1), a pneumatic ten-port valve (V2) with a 10 mm^3 loop and a laboratory-made LC trace-enrichment column (pre-column: 10 × 2 mm i.d.) packed with 10 μm PLRP-S (Polymer Laboratories, Church Stretton, UK) styrene–divinylbenzene copolymer. The pre-column was mounted between two ten-port valves (V2 and V3; VICI, Houston, TX, USA). Transfer of the 60 mm^3 fraction containing the analytes was carried out *via* a 40 cm × 75 μm i.d. fused-silica capillary, which was permanently mounted in the on-column injector.

GC System

A 5 m × 0.53 mm i.d. diphenyltetramethyldisilazane (DPTMDS)-deactivated retention gap (Schilling, Zürich, Switzerland) was connected to the on-column injector. A 3 m section of the GC column, which served as a retaining pre-column,[6] was connected with a press-fit connector to the retention gap. Between the retaining pre-column and the 19 m × 0.32 mm i.d. GC column (CP-Sil 19, 0.2 μm film thickness; Chrompack, Middelburg, The Netherlands) a solvent-vapour exit was installed *via* a Graphpack-3D T-piece (Gerstel, Mülheim, Germany). A 10 cm × 0.9 mm i.d. stainless-steel capillary connected this T-piece to flexible silicone rubber tubing *via* a Valco T-piece (Houston, TX, USA). When the vapour exit is closed, a pinch solenoid valve (Type S104; Sirai, Piotello, Milan, Italy) blocks the rubber tubing, and a small helium purge flow is obtained through a 1 m × 50 μm i.d. fused-silica capillary, also connected to the Valco T-piece. The GC oven temperature during transfer was 70 °C. After closing of the solvent-vapour exit, the temperature was programmed at 10 °C min^{-1} to 295 °C.

MS Detection

The GC column was coupled *via* a Graphpack-3D connector to a 2 m × 0.15 mm i.d. deactivated fused-silica capillary. This

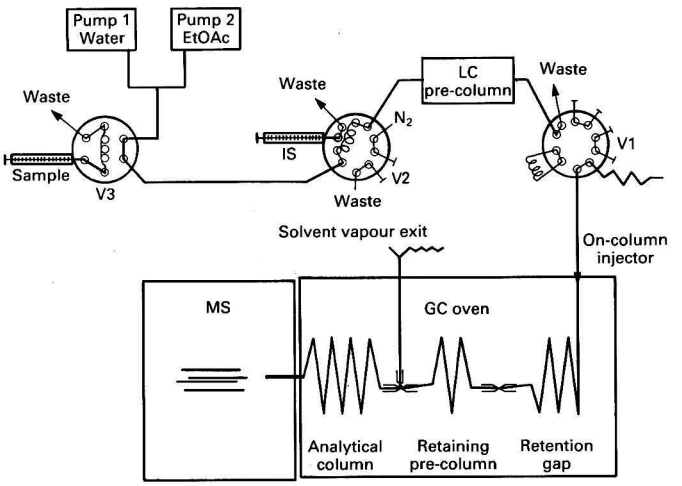

Fig. 1 Schematic diagram of the LC–GC–MS system for on-line trace enrichment of 1 cm³ of water, drying with nitrogen, desorption with ethyl acetate and GC–MS analysis

Table 1 Time schedule for automated preconcentration at 1 cm³ min⁻¹, drying with a nitrogen purge at 40 cm³ min⁻¹, desorption with ethyl acetate at 180 mm³ min⁻¹ and GC–MS analysis

Time/ min	F1*	F2*	V1†	V2†	V3†	Comment
0	1	0	A	A	A	Conditioning of PLRP-S column with water
1.00			B			Transport 1.0 cm³ sample to PLRP-S column
2.50			A			Further clean-up with water (about 0.5 cm³)
2.90	0					Decompression of PLRP-S column
3.00				B		Drying with nitrogen (30 min)
28.00		180				Switch on ethyl acetate pump; inject internal standard in loop of V2
33.00				A	B	Start transfer
33.33		25			A	End transfer; reduce ethyl acetate flow rate
34.67						Close solvent vapour exit; start GC programme
65.00	1	0				Ready for next run

* F1 is the flow rate of the water pump (cm³ min⁻¹), and F2 that of the ethyl acetate pump (mm³ min⁻¹).

† V1–V3 are the positions of the six-port valve (V1), the ten-port valve (V2) and the interface valve (V3); position A refers to the position in Fig. 1.

capillary was permanently mounted in the transfer interface to the mass spectrometer and ended in the ion source. The transfer line and the electron-impact ion source were kept at temperatures of 300 and 225 °C, respectively. For identification, chromatograms were recorded in the full-scan mode in the range *m/z* 45–400. For the determination of atrazine and simazine at the low parts per trillion (ppt) level, nine selected ions were recorded simultaneously during the whole GC run, *viz.*, *m/z* 190 for the internal standard, *m/z* 200, 202, 215 and 217 for atrazine, and *m/z* 186, 188, 201 and 203 for simazine.

Procedure

All parameters for the LC–GC system were loaded into the memories of the various units by the Dualchrom program (Carlo Erba) *via* a communication interface. Analysis was started by manual injection of the sample into the 1 cm³ loop. Trace enrichment by LC at a flow rate of 1 cm³ min⁻¹, drying of the PLRP-S column with nitrogen at 40 cm³ min⁻¹ by applying a pressure of 3 bar (300 kPa) to the column, analyte transfer from the LC to the GC system with ethyl acetate at a flow rate of 180 mm³ min⁻¹ and GC separation were initiated by pushing the start button of the gas chromatograph. The time schedule for the automated procedure is presented in Table 1. Data acquisition by MS was started by means of a closure contact given at the start of the LC–GC transfer. The filament current was switched on either manually or automatically after an appropriate solvent delay.

Results

Optimum Design of LC–GC Coupling

The optimization of the LC trace-enrichment step and the analyte desorption is carried out in such a way that this part of the procedure is compatible with the final analysis by GC–MS. During trace enrichment and clean-up with water, breakthrough of the analytes on the PLRP-S column has to be prevented. As regards retention of *s*-triazine herbicides on 10 × 2 mm i.d. polymer-packed pre-columns, it is known that breakthrough volumes are at least some 10–30 cm³,[7,8] *i.e.*, the loading of 1 cm³ of sample and subsequent clean-up with 1 cm³ of water will not present any problems. Further, it is essential that the ethyl acetate used to transfer the analytes to the retention gap does not contain water. A recent study has shown that purging the trace-enrichment column with nitrogen for 30 min is an efficient means to achieve this end.[9]

Once the desorption and the introduction of the solvent into the retention gap have started, the flow rate of the ethyl acetate should immediately reach the accurate value, which lies above the evaporation rate, to achieve the solvent effect for volatile compounds. As the rather long transfer line acts as a restriction capillary, there will be a pressure build-up in the syringe pump when the introduction is started, causing a flow rate that is too low during the first 10–15 s of solvent introduction. Therefore, the first solvent introduced will not create a solvent film on the wall of the retention gap, and volatile analytes in the first part of the fraction will be lost. In order to avoid this loss, it is necessary to use a similar restriction when the ethyl acetate pump is switched on. This restriction capillary cannot be installed on V3 in Fig. 1, because the pressure during trace enrichment will become too high. Installing it on V2 yields the desired results.

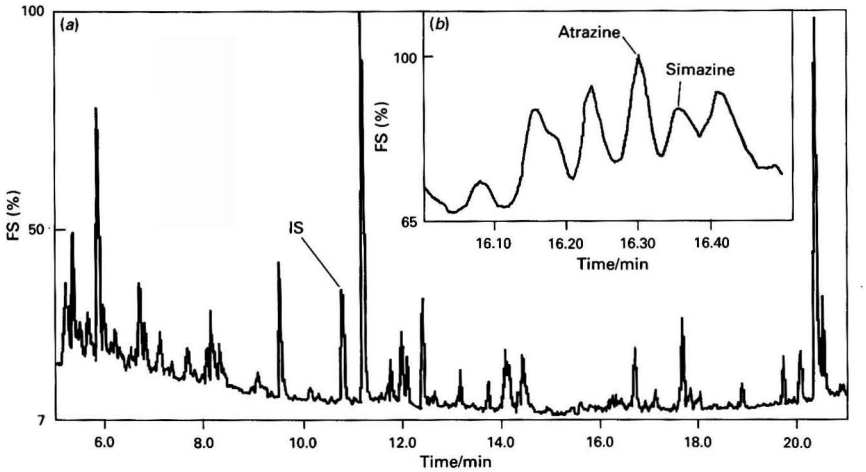

Fig. 2 Full-scan chromatogram after on-line LC–GC–MS analysis of 1 cm³ of River Rhine water spiked with 200 ppt of *s*-triazine herbicides. For conditions, see under Experimental. FS (= full scale) is given by the software

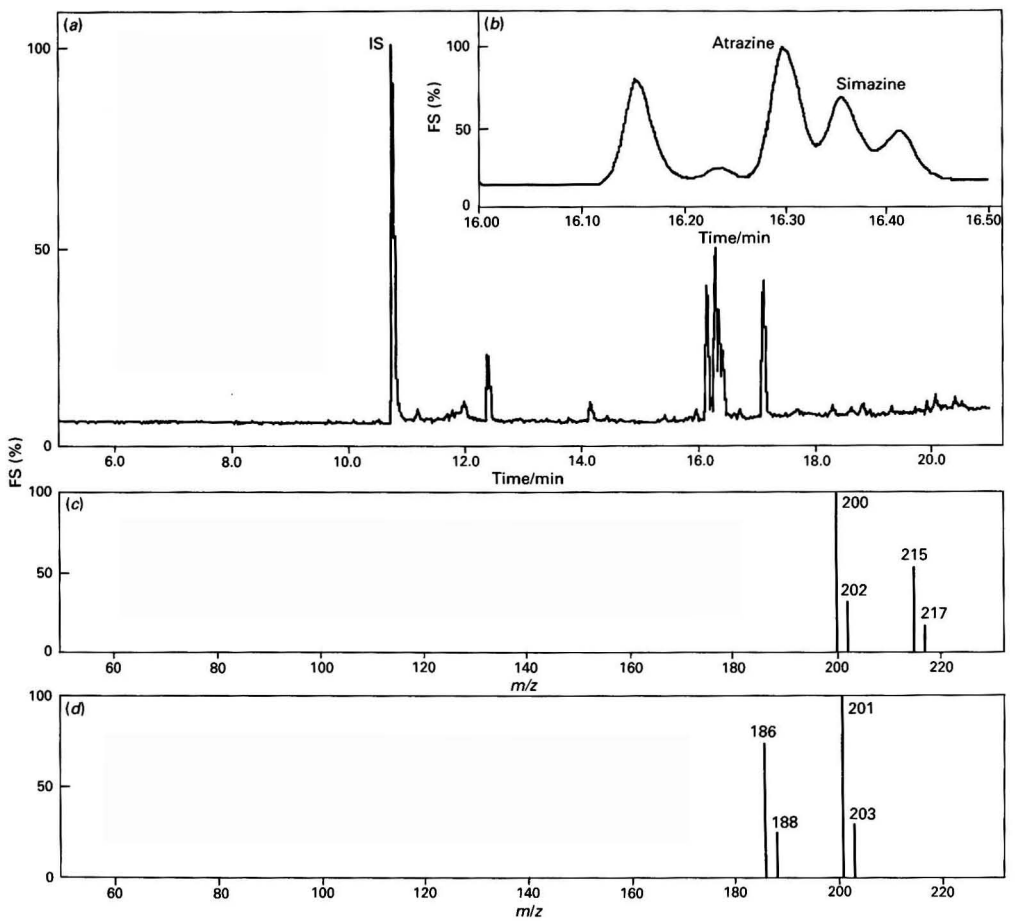

Fig. 3 (*a*) and (*b*) Chromatogram obtained, in the selected-ion recording mode, of the same sample as in Fig. 2 and (*c*) and (*d*) the mass spectra obtained at 16.30 and 16.36 min for atrazine and simazine, respectively. FS (= full scale) is given by the software

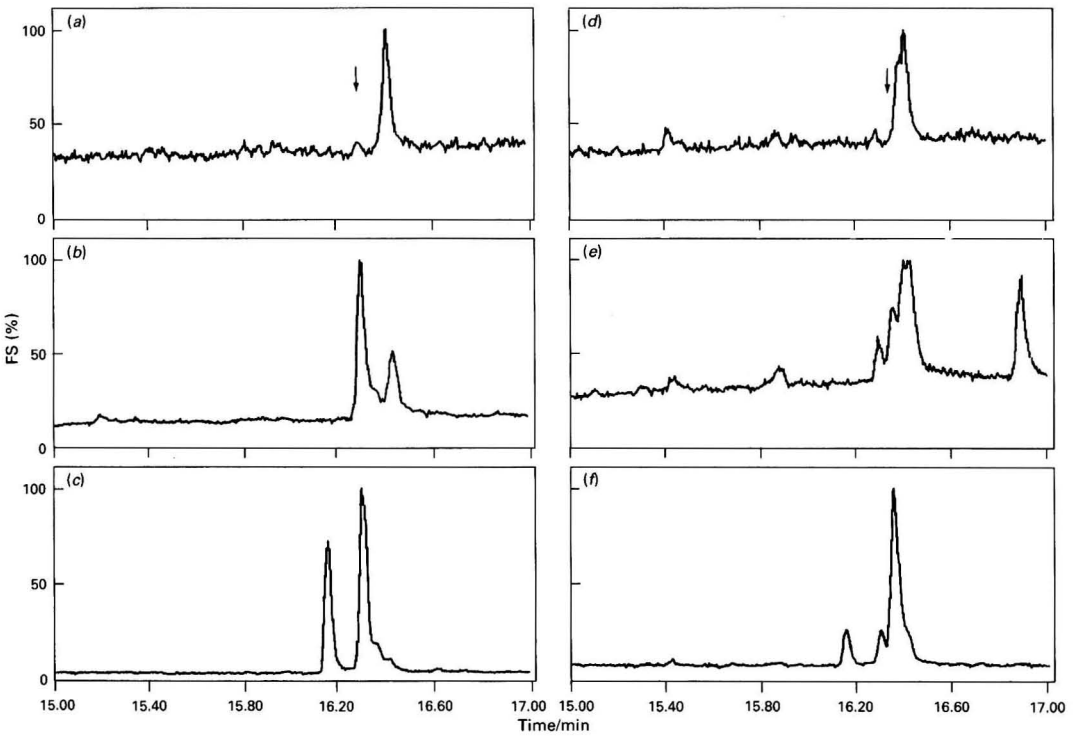

Fig. 4 Parts of chromatograms obtained, in the selected-ion recording mode, of (*a*) and (*d*) HPLC-grade water, (*b*) and (*e*) River Rhine water blank and (*c*) and (*f*) River Rhine water spiked with 200 ppt each of atrazine and simazine. (*a*)–(*c*) *m/z* = 200 (atrazine); (*d*)–(*f*) *m/z* = 201 (simazine). The position of the peak for each compound is indicated by a vertical arrow. FS (= full scale) is given by the software

Further, the solvent film should be prevented from reaching the stationary phase of the retaining pre-column. The length of the retention gap that is required can be calculated as the product of the volume of ethyl acetate introduced into the liquid state, and the length per unit volume of solvent, the so-called flooded zone. The volume of solvent that is introduced into the retention gap as liquid is calculated by subtracting the evaporation rate (see below) of the ethyl acetate from its flow rate and multiplying this value by the transfer time (20 s). In our example this yields: (180 − 64) $mm^3\ min^{-1} \times 0.33$ min = 38.3 mm^3. The flooded zone for ethyl acetate in a DPTMDS-deactivated retention gap is 10 $cm\ mm^{-3}$; *i.e.*, the retention gap should have a length of at least about 4 m.

The evaporation rate can be determined by methods published by Grob.[10] In this study, 30 mm^3 were injected at 180 $mm^3\ min^{-1}$ with the solvent exit open. In the transparent rubber silicone tubing, condensation of the solvent vapour indicates the start of the evaporation process, while the end is indicated by evaporation of the droplets. The evaporation of 30 mm^3 lasted 28 s, which yielded an evaporation rate of 64 $mm^3\ min^{-1}$.

LC–GC–MS of *s*-Triazine Herbicides

By using the procedure described in Table 1, on-line LC preconcentration of 1 cm^3 of Rhine water (sampled at Lobith, The Netherlands), spiked with 200 ppt of atrazine and simazine, and with three other *s*-triazines (see below), and subsequent GC–MS were performed. Detection and identification of the analytes was possible even at this low level. This is demonstrated in Fig. 2, where the chromatogram shows the full-scan trace obtained between 5 and 21 min. The inset represents the region between 16 and 16.5 min in which atrazine and simazine elute. The presence of atrazine and simazine was confirmed by subjecting the mass spectra obtained to a library search, which afforded a confidence level of 85%.

Target analysis for compounds at the low ppt level is preferably carried out by use of the selected-ion recording mode. The chromatogram so obtained for the same sample as analysed above, with use of four target ions each for atrazine and simazine, is shown in Fig. 3. There is a marked improvement in sensitivity compared with that shown by the chromatogram in Fig. 2, and it now appears possible to achieve a detection limit of 10–20 ppt. Selecting two significant ions certainly allows identification at this level, as becomes manifest from the mass spectra included in Fig. 3. For both atrazine and simazine, the molecular-ion peak and also a major fragment ion (loss of $\cdot CH_3$), with their characteristic chlorine isotope pattern, appear.

In Figs. 2 and 3, next to the peaks due to atrazine and simazine, several other peaks of interest appear. These can be assigned to the internal standard at 10.77 min and to the three other *s*-triazines, which were added during spiking. Trietazine (16.16 min), propazine (16.24 min) and subuthylazine (17.15 min) could be identified by their full-scan mass spectra at the 200 ppt level as readily as could atrazine and simazine.

Finally, Fig. 4 shows ion-extraction chromatograms for two *m/z* values, *viz.*, 200 for atrazine and 201 for simazine. The position of the peak for each compound is indicated by a vertical arrow. Results are presented for HPLC-grade water (top chromatogram), blank River Rhine water (middle chromatogram) and River Rhine water fortified with 200 ppt

each of atrazine and simazine (bottom chromatogram). The identification and quantification of other peaks in the chromatogram are subjects for future projects. Determination of the two compounds, carried out several times for Rhine water with use of these compound ions and other diagnostic ions, with 4,4′-difluorobiphenyl as internal standard, yielded values of 70–80 pg cm^{-3} for atrazine and 20–30 pg cm^{-3} for simazine. These results agree satisfactorily with data for the same sample recently published in another paper,[11] which dealt with the off-line combination of LC-type trace enrichment and GC–MS (45–50 and 25–30 pg cm^{-3}, respectively).

Conclusions

The present study illustrates the good selectivity and sensitivity of on-line LC–GC–MS for the analysis of aqueous environmental samples. The procedure,which is fully automated, requires sample volumes of only a few cubic centimetres to obtain detection and provisional identification limits at or below the 100 ppt level. It is especially gratifying that the example presented pertains to surface water, with which type of sample, pollutant levels of up to 1–3 ppb are still considered acceptable.

If one realizes that 10 × 2 mm i.d. pre-columns as used in this study are generally utilized for the trace enrichment of analytes from 10 to 30 cm^3 rather than 1 cm^3 sample volumes (without breakthrough creating a problem) and that selected-ion recording with 2–4 target ions is often sufficient for identification purposes, it is evident that the present system is capable of trace-level monitoring of environmental pollutants down to the 1–10 ppt level. On-going research is dealing with the collection of the proper analytical data and the further analysis of authentic samples in order to demonstrate the potential of the present approach.

The authors thank DSM (Geleen, The Netherlands) for their financial support.

References

1 Poole, C. F., and Schuette, S. A., in *Contemporary Practice of Chromatography*, Elsevier, Amsterdam, 1st edn., 1984, pp. 438–448.
2 Nielen, M. W. F., Frei, R. W., and Brinkman, U. A. Th., in *Selective Sample Handling and Detection in High-Performance Liquid Chromatography, Part A*, eds. Zech, K., and Frei, R. W., Elsevier, Amsterdam, 1988, pp. 8–34.
3 Vreuls, J. J., Cuppen, W. J. G. M., de Jong, G. J., and Brinkman, U. A. Th., *J. High Resolut. Chromatogr. Chromatogr. Commun.*, 1990, **13**, 157.
4 Farjam, A., Vreuls, J. J., Cuppen, W. J. G. M., Brinkman, U. A. Th., and de Jong, G. J., *Anal. Chem.*, 1991, **63**, 2481.
5 Kwakman, P. J. M., Vreuls, J. J., Ghijsen, R. T., and Brinkman U. A. Th., *Chromatographia*, 1992, **34**, 41.
6 Grob, K., Schmarr, H.-G., and Mosandl, A., *J. High Resolut. Chromatogr. Chromatogr. Commun.*, 1989, **12**, 375.
7 Liska, I., Brouwer, E. R., Ostheimer, A. G. L., Lingeman, H., and Brinkman, U. A. Th., *Int. J. Environ. Anal. Chem.*, 1992, **47**, 267.
8 Slobodnik, J., Brouwer, E. R., Geerdink, R. B., Mulder, W. H., Lingeman, H., and Brinkman, U. A. Th., *Anal. Chim. Acta*, 1992, **268**, 55.
9 Vreuls, J. J., Ghijsen, R. T., de Jong, G. J., and Brinkman, U. A. Th., *J. Chromatogr.*, in the press.
10 Grob, K., in *On-line Coupled LC–GC*, eds. Bertsch, W., Jennings, W. G., and Sandra, P., Hüthig Buch Verlag, Heidelberg, 1st edn., 1991, pp. 247–262.
11 Bagheri, H., Vreuls, J. J., Ghijsen, R. T., and Brinkman, U. A. Th., *Chromatographia*, 1992, **34**, 5.

Paper 2/02331H
Received May 6, 1992
Accepted July 1, 1992

Determination of Dietary Fibre as Non-starch Polysaccharides by Gas–Liquid Chromatography

Hans N. Englyst, Michael E. Quigley, G. J. Hudson and J. H. Cummings
Medical Research Council Dunn Clinical Nutrition Centre, 100 Tennis Court Road, Cambridge, UK CB2 1QL

An improved method is described for the measurement of total, soluble and insoluble dietary fibre as non-starch polysaccharides (NSP). An established procedure is modified to allow more rapid removal of starch and hydrolysis of NSP. In its present form the procedure is simpler and more robust than those previously published. In the modified method starch is removed enzymically within 50 min and NSP is precipitated with ethanol and then hydrolysed by treatment with sulfuric acid for 2 h. The constituent sugars can in turn be measured by gas–liquid chromatography, high-performance liquid chromatography or more rapidly by colorimetry. The improved procedure described here for the removal of starch and hydrolysis of NSP applies to all three techniques, but only the method for measurement of sugars by gas–liquid chromatography is described here in full.

Keywords: *Gas–liquid chromatography; non-starch polysaccharides; dietary fibre*

The original 'dietary fibre hypothesis' was that the absence of some Western diseases in rural Africans was the result of a diet rich in unrefined plant foods, and was specifically related to plant cell-wall material.[1] An accurate measurement of all the constituents of the plant cell wall is neither feasible nor necessary provided a measurement can be made that gives an index of this material. Plant cell-walls contain small amounts of protein, phenolic compounds and lignin, but the major components are polysaccharides. The cell-wall polysaccharides are not a single species but they share a common feature; unlike the storage polysaccharide starch, they do not contain α-glucosidic linkages and can be referred to collectively as non-starch polysaccharides (NSP). The NSP can be enzymically separated from starch, including retrograded starch, and are therefore independent of food processing, and they represent a good index of plant cell-wall material.

A procedure for the measurement of NSP in plant products has previously been reported.[2,3] This method has been used successfully for the analysis of more than 400 foods[4,5] and the NSP values obtained are now included in the UK food tables.[6–8] In the method, starch is hydrolysed by pancreatic amylase and pullulanase, and NSP are measured by gas–liquid chromatography (GLC) as their constituent sugars released upon acid hydrolysis. The modified procedure described here and summarized in Fig. 1 includes faster hydrolysis of starch and NSP, thus reducing the overall analysis time for the measurement of total, soluble and insoluble NSP.

Experimental

Reagents and Apparatus

High-purity reagents were used for all analyses. Sand, low in iron (about 40–100 mesh) was purchased from BDH (now Merck, Poole, Dorset).

Internal standard solution, 1 mg cm^{-3}. Weigh 500 mg of allose (dried to constant mass under reduced pressure in the presence of phosphorus pentoxide) to the nearest 0.1 mg. Make up to 500 cm^3 with 50% saturated benzoic acid to give a 1 mg cm^{-3} solution. The mixture is stable at room temperature for at least 6 months.

Enzyme solution 1. Take 2.5 cm^3 of Termamyl (Novo Industri, Copenhagen, Denmark) and make up to 200 cm^3 with pre-equilibrated acetate buffer (see below), mix, and keep it in a 50 °C water-bath. Prepare immediately before use.

Enzyme solution 2. Place 1.20 g of pancreatin (Paines and Byrne, Greenford, Middlesex) into a 50 cm^3 tube, add 12 cm^3 of water, vortex mix initially and then mix for 10 min with a magnetic stirrer. Vortex mix again, then centrifuge for 10 min at 1500*g*. Take 10 cm^3 of the (cloudy) supernatant, add 2.5 cm^3 of pullulanase (Novo Nordisk, Farnham, Surrey, UK) and vortex mix. Prepare immediately before use. [When using the option of overnight incubation then 2.5 cm^3 of pullulanase from Boehringer Mannheim, Lewes, East Sussex, UK (Cat. No. 108944) diluted 1:100 or 2.5 cm^3 of pullulanase diluted 1:25 is used.]

Sodium acetate buffer, 0.1 mol cm^{-3}, *pH* 5.2. Dissolve 13.6 g of sodium acetate trihydrate, $CH_3COONa{\cdot}3H_2O$, and make to 1 dm^3 with water. Adjust to pH 5.2 with 0.1 mol dm^{-3} acetic acid. In order to stabilize and activate the enzymes, add 4 cm^3 of 1 mol dm^{-3} calcium chloride to 1 dm^3 of buffer. (For the overnight incubation replace water with 50% saturated benzoic acid.)

Sodium chloride–boric acid solution. Dissolve 2 g of NaCl and 3 g of boric acid (H_3BO_3) in 100 cm^{-3} of water.

Sodium phosphate buffer, 0.2 mol dm^{-3}, *pH* 7. Adjust 0.2 mol dm^{-3} Na_2HPO_4 to pH 7 with 0.2 mol dm^{-3} NaH_2PO_4.

Ammonia solution, 12.5 mol dm^{-3}. This reagent must be kept in a well-stoppered bottle and should be replaced when more than 1.2 cm^{-3} is required to neutralize 3 cm^{-3} of hydrolysate (see later).

Ammonia solution–sodium tetrahydroborate solution. Accurately weigh 1.2 g of sodium tetrahydroborate ($NaBH_4$) into a 20 cm^3 vial, add 6 cm^3 of 12.5 mol dm^{-3} ammonia solution, and mix thoroughly.

Stock sugar mixture. Accurately weigh, to the nearest 0.1 mg, 520 mg of rhamnose, 480 mg of fucose, 4750 mg of arabinose, 4450 mg of xylose, 2300 mg of mannose, 2820 mg of galactose, 9400 mg of glucose and 2790 mg of galacturonic acid into a 1 dm^3 calibrated flask and make to the mark with 50% saturated benzoic acid.

Bromophenol blue solution, 0.4 g dm^{-3} (*BDH*).

Dimethylphenol solution 1.0 g dm^{-3}. Dissolve 0.1 g of 3,5-dimethylphenol [$(CH_3)_2C_6H_3OH$] in 100 cm^3 of glacial acetic acid.

Sulfuric acid, 12 mol dm^{-3}. Accurately measure 280 cm^3 of water into a strong 2 dm^3 beaker. Place the beaker in a bowl of ice-water in a fume cupboard and slowly add 390 cm^3 of concentrated sulfuric acid with stirring.

Chromatography

Gas–liquid chromatography is performed using a Supelco SP-2330 wide-bore capillary column (30 m × 0.75 mm:

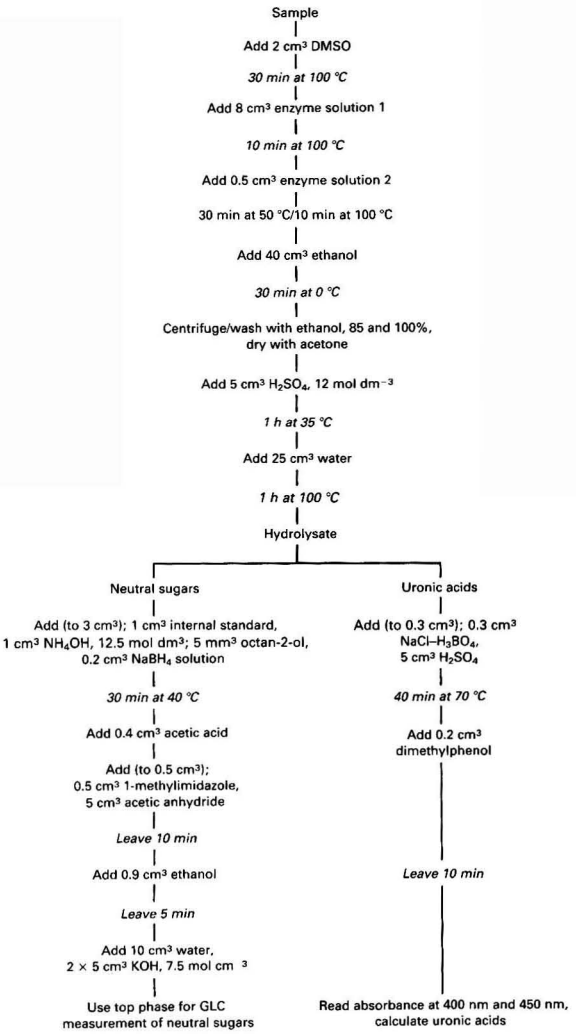

Fig. 1 Procedure for the analysis of non-starch polysaccharides (NSP) by gas–liquid chromatography. Total DF = neutral sugars + uronic acids. Soluble DF = total DF − insoluble DF. For measurement of insoluble DF, replace the 40 cm³ ethanol with 40 cm³ pH 7 buffer and extract for 30 min at 100 °C

Supelco Lot no. 2-3751) and a flame ionization detector. The column is maintained at 220 °C, and the injector and detector are kept at 275 °C. Carrier gas (helium) flow rate is 8 cm³ min⁻¹. Fig. 2 shows that separation of alditol acetates is obtained within 8 min using the GLC conditions described here.

Samples

Two portions, A and B, of each sample are required to obtain separate values for total, insoluble and soluble NSP. Portion A is used to measure total NSP; portion B is used to measure insoluble NSP. Soluble NSP is determined as the difference. The two portions are treated identically throughout the procedure, except where stated otherwise.

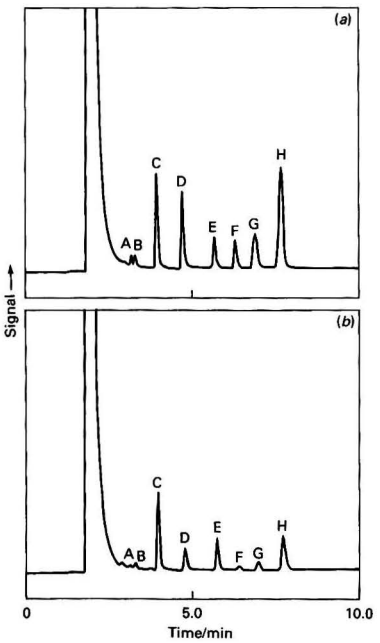

Fig. 2 Gas–liquid chromatogram for the alditol acetates of (*a*) a sugar mixture and (*b*) a haricot bean hydrolysate: A, rhamnose; B, fucose; C, arabinose; D, xylose; E, allose (internal standard); F, mannose; G, galactose; and H, glucose

Pre-treatment of the Sample

All samples should be finely divided so that representative sub-samples (dry or wet) can be taken. Foods with a low water content (<10 g per 100 g of sample) can be milled, and foods with a higher water content can be homogenized wet or milled after freeze-drying.

Sample Mass

Weigh sample portions, to the nearest 0.1 mg, of between 50 and 1000 mg depending on the water and NSP content of the sample, to give not more than 300 mg of dry matter (300 mg is adequate for most dried foods but smaller amounts should be used for bran and purified fibre preparation), into 50–60 cm³ screw-top glass tubes, add approximately 300 mg of sand (BDH) and add a magnetic stirrer bar to each. If the sample is dry (85–100 g of dry matter per 100 g of sample) and contains less than approximately 5 g of fat per 100 g of sample, proceed to the section on Dispersion and Enzymic Hydrolysis; otherwise proceed to Fat Extraction and Drying of Wet Samples.

Fat Extraction and Drying of Wet Samples

Add 40 cm³ of acetone, cap the tubes and mix for 30 min using the magnetic stirrer. Centrifuge at 1000*g* to obtain a clear supernatant and remove as much of the supernatant liquid as possible without disturbing the residue. Place the tubes in a beaker of water at 80 °C on a hot-plate stirrer and mix the residue until dry. Either use a fume-cupboard or cover the beaker and remove the acetone vapour with a water pump.

Dispersion and Enzymic Hydrolysis of Starch

Treatment with dimethyl sulfoxide

Pre-equilibrate sufficient sodium acetate buffer at 50 °C (8 cm³ required per sample). Add 2 cm³ of dimethyl sulfoxide to the

dry sample, cap the tube and immediately vortex mix. It is essential that all the sample is wetted and that no material is encapsulated or adhering to the tube wall before proceeding. Vortex mix two or three times during a 5 min period. Vortex mix and immediately place two tubes in a boiling water-bath. Remove after 20 s, vortex mix and immediately return the tubes to the bath. Repeat this procedure for subsequent pairs of tubes until all the tubes are in the bath and leave them for 30 min from that time. During this period, prepare enzyme solutions 1 and 2 if you wish to proceed with the 50 min incubation, or enzyme solution 2 only if you prefer the overnight incubation (see below). Proceed to either the 50 min incubation or the overnight incubation.

Treatment with enzyme solutions (50 min incubation)

After 30 min, remove one tube at a time, vortex mix, uncap and immediately add 8 cm^3 of enzyme solution 1 (kept at 50 °C), cap the tube and vortex mix thoroughly, ensuring that no material adheres to the tube wall, and replace it in the boiling water-bath. Leave the tubes for 10 min, timed from the last addition of enzyme. Transfer the rack of tubes to a 50 °C water-bath. After 3 min, remove the rack, add 0.5 cm^3 of enzyme solution 2 to each tube and mix the contents thoroughly to aid distribution of the enzyme throughout the sample. Replace the tubes in the 50 °C water-bath and leave for 30 min. Mix the contents of each tube continuously or after 10, 20 and 30 min. Transfer the rack of tubes to the boiling water-bath and leave for 10 min. Cool the samples by placing in water at room temperature.

Treatment with enzymes (overnight incubation)

Remove one tube at a time from the boiling water-bath, vortex mix, uncap and immediately add 8 dm^3 of sodium acetate buffer (pre-equilibrated at 50 °C). Cap the tube and vortex mix thoroughly, ensuring that no material adheres to the tube wall. Place the tubes in a water-bath at 42 ± 2 °C for 3 min, then add 0.5 cm^3 of enzyme solution 2 and vortex mix. Incubate at 42 ± 2 °C (water-bath or oven) for 16–18 h, mixing the contents of each tube continously or after 15 and 30 min as a minimum.

Precipitation and Washing of the Residue for Measurement of Total NSP

For sample portion A only, add 40 cm^3 of absolute ethanol, mix well by inversion, then leave in ice-water for 30 min. Centrifuge at 1500*g* for 10 min to obtain a clear supernatant liquid. Remove by aspiration as much of the supernatant as possible, without disturbing the residue, and discard it. Add approximately 10 cm^3 of 85% v/v ethanol and vortex mix. Make to 50 cm^3 with 85% v/v ethanol, mix by inversion then use the magnetic stirrer to form a suspension of the residue. Centrifuge and remove the supernatant liquid as above. Repeat this stage using 50 cm^3 of absolute ethanol. Add 20 cm^3 of acetone to the residue, vortex mix and then use the magnetic stirrer to form a suspension. Centrifuge at 1500*g* for 10 min and remove the supernatant as above. Place the uncapped tube in a beaker of water at 80 °C on a hot-plate stirrer and mix the residue until dry. (It is essential that the residue and tube are completely free of acetone.) Either use a fume-cupboard or cover the beaker and remove the acetone vapour with a water-pump. (If aggregation occurs during drying, disperse the sample using the vortex mixer. This is best done before the sample is completely dry).

Extraction and Washing of the Residue for Measurement of Insoluble NSP

For sample B only, after the treatment with enzymes, add 40 cm^3 of sodium phosphate buffer. Place the capped tubes in the boiling water-bath for 30 min. Mix continuously or, as a minimum, three times during this period. Place the tubes in water at room temperature and leave for 10 min. Centrifuge at 1500*g* for 10 min and remove the supernatant liquid as described above. Add approximately 10 cm^3 of water and vortex mix. Make up to approximately 50 cm^3 with water, mix by inversion, then use the magnetic stirrer to form a suspension of the residue. Centrifuge and remove the supernatant liquid as above. Repeat this stage using 50 cm^3 of absolute ethanol. Add 20 cm^3 of acetone to the residue, vortex mix and then use the magnetic stirrer to form a suspension. Centrifuge and remove the supernatant as above. Place the tube in a beaker of water at 80 °C on the hot-plate stirrer and mix the residue until it is dry. (It is essential that the residue and tube are completely free of acetone.) Either use a fume-cupboard or cover the beaker and remove the acetone vapour with a water-pump. (If aggregation occurs during drying, disperse the sample using the vortex mixer. This is best done before the sample is completely dry).

Acid Hydrolysis of the Residue from Enzymic Digestion

Add 5 cm^3 of 12 mol dm^{-3} sulfuric acid to the dry residue and immediately vortex mix. It is essential that all the material is wetted. Leave the tubes at 35 °C for 1 h with occasional or continuous mixing to disperse the cellulose. Add 25 cm^3 of water rapidly and vortex mix. Place into a boiling water-bath and leave for 1 h, timed from when boiling recommences; stir continuously or once after 10 min. Cool the tubes in tap water at room temperature.

Treatment of Hydrolysates and Calibration Mixture

Preparation of standard sugar solution

Mix 2000 mm^3 of the stock sugar mixture with 10 cm^3 of 2.4 mol dm^{-3} sulfuric acid. Treat 3 cm^3 of this mixture in parallel with the test samples.

Preparation of alditol acetate derivatives

Add 1000 mm^3 of the 1 mg cm^{-3} allose internal standard in 50% saturated benzoic acid, to 3000 mm^3 of the cooled hydrolysates and to 3000 mm^3 of the standard sugar mixture, and vortex mix. Place the tubes in ice-water, add 1 cm^3 of 12.5 mol dm^{-3} ammonia solution and vortex mix. Test that the solution is alkaline (add a little ammonia solution if necessary), then add approximately 5 mm^3 of the antifoam agent octan-2-ol and 0.2 cm^3 of the ammonia solution–sodium tetrahydroborate solution, vortex mix. Place the uncapped tubes in a heating block or water-bath at 40 °C and leave them there for 30 min. Remove all of the tubes, add 0.4 cm^3 of glacial acetic acid and vortex mix. Take 0.5 cm^3 into a 30 cm^3 glass tube; add 0.5 cm^3 of 1-methyl imidazole, 5 cm^3 of acetic anhydride and immediately vortex mix. Leave for 10 min then add 0.9 cm^3 of absolute ethanol, vortex mix and leave for 5 min. Add 10 cm^3 of water, vortex mix and leave for 5 min. Add 0.5 cm^3 of bromophenol blue solution and mix. Place the tubes in ice-water and add 5 cm^3 of 7.5 mol dm^{-3} potassium hydroxide. About 2 min later add a further 5 cm^3 of 7.5 mol dm^{-3} potassium hydroxide, cap the tubes and mix by inversion. Leave until the separation into two phases is complete (10–15 min) or centrifuge for 2–3 min. Draw the upper phase into the tip of an automatic pipette; if any of the blue phase is included, allow it to separate then run it out of the tip before transferring the upper phase alone to an auto-injector vial. Inject 0.5–1.0 mm^3 of the solution of alditol acetate derivatives. Carry out conventional GLC measurement of the neutral sugars.

Calculation of Neutral Sugars

For calibration, use the ratio given in Table 1 for the combination of the standard sugar mixture and internal

Table 1 Causes of incomplete recovery of sugars subjected to the conditions used for acid hydrolysis of polymers

Cause	Constituent sugar (g per 100 g of dry sample)								
	Rhamnose	Fucose	Arabinose	Xylose	Mannose	Galactose	Glucose	Uronic acids	Internal standard
Loss during treatment with sulfuric acid, 12 mol dm^{-3}	4	1	2	4	3	<0.5	<0.5	<0.5	—
Loss during treatment with sulfuric acid, 2 mol dm^{-3}	3	3	3	7	3	3	3	7	—
Under-estimation due to incomplete desulfation	0	0	0	0	2	3	3	0	—
Under-estimation due to incomplete hydrolysis	41	0	0	0	0	0	0	0	—
Overall recovery* (%)	52	96	95	89	92	94	94	93	—
Calibration mixture/g dm^{-3}	0.52	0.48	4.75	4.45	2.30	2.82	9.40	2.79	—
Calibration ratio	1	0.5	5	5	2.5	3	10	—	2

* The composition of the calibration mixture takes into account these incomplete recoveries.

standard. By using these values, corrections are made for incomplete recovery of NSP constituents.

The amounts of individual sugars (in g per 100 g of sample) are calculated as:

$$\frac{A_T \times M_I \times R_F \times 100}{A_I \times M_T} \times 0.89$$

where A_T and A_I are the peak areas of the sample and the internal standard, respectively; M_T is the mass of the sample (in mg); M_I is the mass of the internal standard if added to the whole sample (in mg; here 10); R_F is the response factor for individual sugars obtained from the calibration run with the sugar mixture treated in parallel with the samples; and 0.89 is the factor for converting the experimentally determined monosaccharides to polysaccharides. All calculations are performed with a computing integrator.

Measurement of Uronic Acids

The standard sugar mixture in 2 mol dm^{-3} sulfuric acid, prepared as described above contains, for the purpose of calibration, 500 μg cm^{-3} galacturonic acid. To prepare the standard solutions, take 0.5, 1.0, 2.0 and 3.0 cm^3 of the sugar mixture into separate tubes and make up to 10.0 cm^3 with 2 mol dm^{-3} sulfuric acid to give standard solutions of 25, 50, 100 and 150 μg cm^{-3}. Only the 100 μg cm^{-3} standard is required for routine analysis, and it can be kept at 5 °C for up to 2 months. Place into separate tubes (40–50 cm^3 capacity) 0.3 cm^3 of blank solution (2 mol dm^{-3} sulfuric acid), 0.3 cm^3 of each of the standard solutions and 0.3 cm^3 of the test hydrolysates, diluted if necessary with 2 mol dm^{-3} sulfuric acid, to contain uronic acids at no more than 150 μg cm^{-3} (*e.g.*, no dilution for flour, 1 : 2 dilution for bran, and 1 : 5 for most fruits and vegetables). Add 0.3 cm^3 of sodium chloride–boric acid solution and mix. Add 5 cm^{-3} of concentrated sulfuric acid and vortex mix immediately. Place the tubes in a heating block at 70 °C and leave for 40 min. Remove the tubes and cool to room temperature in water. (The tubes can be kept at room temperature for 1 h, which is convenient for the colorimetic reaction with small batches of samples. This is important, because readings must be taken between 10 and 15 min after addition of the colorimetric reagent). Add 0.2 cm^3 of dimethyl phenol solution and vortex mix immediately. Between 10 and 15 min later, measure the absorbance at 400 and 450 nm against the blank solution. Subtract the reading at 400 nm from that at 450 nm, to correct for the interference from hexoses.

Calculation of Uronic acids

The amount of uronic acids (in g per 100 g of sample) is calculated as:

$$\frac{A_T \times V_T \times D \times C \times 100}{A_S \times M_T} \times 0.91$$

where A_T is the difference in absorbance of the sample solution; V_T is the total volume of sample solution (in cm^3; here 30); D is the dilution of the sample solution; C is the concentration of the standard used (in mg cm^{-3}; here 0.1); A_S is the difference in absorbance of the 100 μg cm^{-3} standard; M_T is the mass of the sample (in mg); and 0.91 is the factor for converting the experimentally determined monosaccharides to polysaccharides.

Calculation of Total, Soluble and Insoluble NSP

The amount of total, soluble and insoluble NSP (in g per 100 g of sample) is calculated as: total NSP = neutral sugars calculated for portion A + uronic acids calculated for portion A; insoluble NSP = neutral sugars calculated for portion B + uronic acids calculated for portion B; and soluble NSP = total NSP − insoluble NSP.

Breaks in the Procedure

The procedure can be halted at any of the following stages. (*i*) After precipitating, washing and drying the starch-free residue. The residue can be stored dry for at least 3 months. (*ii*) After hydrolysis with 2 mol dm^{-3} sulfuric acid. The hydrolysate can be kept at 5 °C for 24 h. (*iii*) After acidification of the reduced samples. The samples can be stored at room temperature for 2–3 d. (*iv*) After acetylation and transfer to auto-injector vials. The samples can be kept at room temperature for 2–3 d before analysis by GLC. (*v*) The acid hydrolysate can be kept for up to 2 months at 5 °C before the measurement of uronic acids.

Results and Discussion

In the previously described procedure[2,3] starch, including that retrograded as a result of food processing, is dispersed using dimethyl sulfoxide. For some foods, material can adhere to the tube wall making dispersion less effective. It was found that the addition of acid-washed sand and immediate vortex mixing after the treatment with dimethyl sulfoxide at 100 °C for 20 s (see Experimental) was successful in preventing all types of samples from adhering to the tube wall.

Table 2 Results for total NSP in haricot beans and long grain white rice in which starch has been removed either by an overnight incubation with pancreatin (with and without pullulanase) or by the rapid hydrolysis conditions described here using a combination of Termamyl and pancreatin (with and without pullulanase)

Food		Incubation enzymes		Rhamnose	Fucose	Arabinose	Xylose	Mannose	Galactose	Glucose	Uronic acids	Total
Haricot bean	Overnight	Pancreatin only	Mean	0.10	0.30	5.41	1.71	0.32	1.00	4.90	3.18	16.92
			σ	0.00	0.01	0.14	0.05	0.01	0.01	0.11	0.11	0.41
	Overnight	Pancreatin + pullulanase	Mean	0.10	0.30	5.31	1.67	0.32	0.98	4.08	3.26	16.02
			σ	0.01	0.01	0.06	0.02	0.01	0.02	0.05	0.08	0.15
	50 min	Pancreatin + Termamyl	Mean	0.10	0.32	5.44	1.78	0.36	1.00	5.06	3.11	17.17
			σ	0.00	0.01	0.13	0.05	0.01	0.01	0.05	0.10	0.08
	50 min	Pancreatin, Termamyl + pullulanase	Mean	0.10	0.31	5.28	1.69	0.38	1.03	4.22	3.10	16.11
			σ	0.00	0.01	0.10	0.06	0.02	0.02	0.12	0.15	0.27
White rice	Overnight	Pancreatin only	Mean	0.00	0.00	0.15	0.09	t*	0.04	1.48	t	1.76
			σ	—	—	0.00	0.00	—	0.00	0.11	—	0.11
	Overnight	Pancreatin + pullulanase	Mean	0.00	0.00	0.15	0.08	t	0.03	0.25	t	0.51
			σ	—	—	0.01	0.00	—	0.00	0.01	—	0.02
	50 min	Pancreatin + Termamyl	Mean	0.00	0.00	0.15	0.08	t	0.04	1.57	t	1.84
			σ	—	—	0.01	0.00	—	0.00	0.25	—	0.26
	50 min	Pancreatin, Termamyl + pullulanase	Mean	0.00	0.00	0.16	0.08	t	0.05	0.26	t	0.55
			σ	—	—	0.01	0.00	—	0.00	0.03	—	0.04

* t = trace.

In the procedure as it was described in 1988, starch was hydrolysed during a 16 h incubation with pancreatin and pullulanase. By introducing a pre-treatment with heat-stable amylase (Termamyl) and using the optimized conditions for dispersion and enzymic hydrolysis given here (see Experimental), we have demonstrated for a variety of foods, including cereals, legumes, fruit and vegetables, that complete removal of starch can be achieved after only 50 min incubation. Values are given in Table 2 for NSP glucose in rice and haricot beans. The 50 min incubation is as effective in the removal of starch as the previously validated overnight incubation.[3] The values obtained for rice and haricot beans following incubation with various combinations of enzymes (Table 2) demonstrate that pullulanase is essential for complete removal of starch and that the two pullulanase preparations and Termamyl when used as described here do not result in loss of NSP constituents.

The hydrolysis of cellulose requires dispersion with 12 mol dm^{-3} sulfuric acid. This treatment, however, causes extensive sulfation of monosaccharides. Desulfation requires hydrolysis with dilute acids at high temperature. This, in turn, causes some destruction of the monosaccharides released from NSP. The conditions chosen for hydrolysis therefore have to be a compromise with respect to adequate release, desulfation and destruction of monosaccharides. Accurate measurement of NSP can be achieved using various sets of hydrolysis conditions, but for routine investigation the aim must be rapid hydrolysis with minimal destruction, requiring only small correction factors.

The treatment with 12 mol dm^{-3} sulfuric acid for 1 h at 35 °C as previously used in the Englyst procedure[3] was re-tested as part of the procedure described here. The analysis of ten foods with a wide range of NSP content showed that the mean values obtained after incubation with 12 mol dm^{-3} sulfuric acid, for 1 h at 30 or 35 °C, followed in each case by 2 mol dm^{-3} sulfuric acid, for 1 h at 100 °C, were 31.8 and 32.7% for total neutral sugars, 19.3 and 19.7% for glucose, and 4.8 and 4.8% for xylose, the most labile sugar, respectively. Treatment with 12 mol dm^{-3} sulfuric acid at 45 °C resulted in slightly lower values for xylose. Only small differences were observed between recoveries obtained after 0.5 and 1 h treatment with 12 mol dm^{-3} sulfuric acid at 35 °C but treatment for 1 h is more robust and has therefore been incorporated into the procedure.

Following treatment with 12 mol dm^{-3} sulfuric acid, desulfation of the various sugars requires hydrolysis with dilute acid at 100 °C. Desulfation of sulfated glucose, as measured by the increase in glucose, requires treatment with 0.5 mol dm^{-3} sulfuric acid for 5 h or with 1 mol dm^{-3} for 3 h, but with 2 or 3 mol dm^{-3} for only 1 h (Fig. 3). Desulfation of xylose is complete within 0.5 h using sulfuric acid at either 2 or 3 mol dm^{-3} but treatment with sulfuric acid at 3 mol dm^{-3} causes greater destruction of xylose (Fig. 4). When using 2 mol dm^{-3} sulfuric acid galactose and mannose are desulfated at a rate similar to that observed for glucose, whereas the rate of desulfation for rhamnose and arabinose is similar to that for xylose. Both glucose and glucose 6-sulfate can be monitored by high-performance liquid chromatography (HPLC). For a solution of glucose subjected to 12 mol dm^{-3} sulfuric acid for 1 h at 35 °C we observed two major peaks corresponding to glucose and glucose 6-sulfate. On treatment with 2 mol dm^{-3} sulfuric acid for 1 h at 100 °C, 94.7% of the glucose in the sample was measured as glucose and only 1.6% as glucose 6-sulfate. Similar additional peaks were observed for all the monosaccharides after treatment with 12 mol dm^{-3} sulfuric acid. However, after treatment with 2 mol dm^{-3} sulfuric acid for 1 h at 100 °C, only glucose, galactose and mannose require correction for a small amount of residual sulfated sugars (see Table 1).

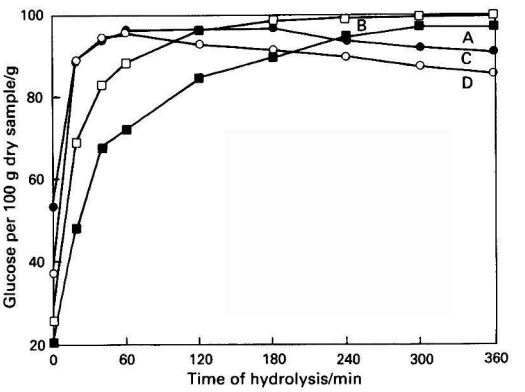

Fig. 3 Observed recovery of glucose subjected to treatment with sulfuric acid, 12 mol dm^{-3}, for 1 h at 35 °C followed by treatment with sulfuric acid at different concentrations: A, 0.5; B, 1.0; C, 2.0; and D, 3.0 mol dm^{-3}

Losses during the treatment with 12 mol dm^{-3} sulfuric acid were calculated, taking into account the incomplete desulfation of sulfated hexoses, as the difference between recoveries obtained after treatment with sulfuric acid both at 12 and 2 mol dm^{-3}, and with 2 mol dm^{-3} sulfuric acid at 100 °C alone. These losses were small, ranging from <0.5 to 4% h^{-1}. The losses resulting from treatment with 2 mol dm^{-3} sulfuric acid range from 3% h^{-1} for glucose to 7% h^{-1} for xylose (Table 1).

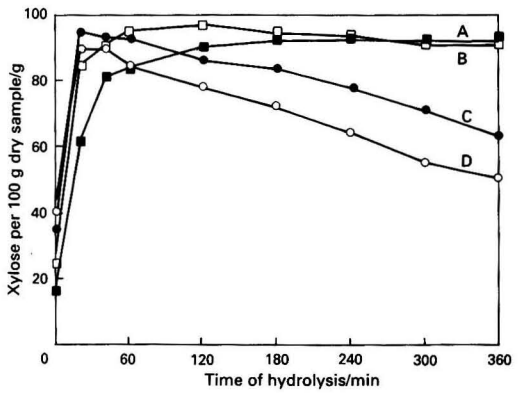

Fig. 4 Observed recovery of xylose subjected to treatment with sulfuric acid, 12 mol dm^{-3}, for 1 h at 35 °C followed by treatment with sulfuric acid at different concentrations: A, 0.5; B, 1.0; C, 2.0; and D, 3.0 mol dm^{-3}

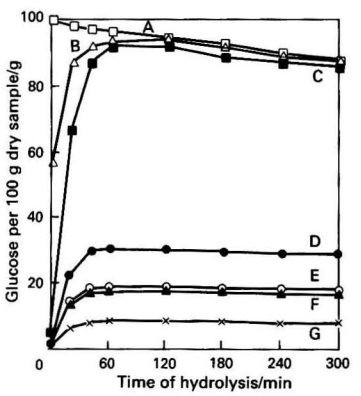

Fig. 5 Observed recovery of glucose from a sugar mixture after treatment with sulfuric acid, 2 mol dm^{-3}, at 100 °C (A). Recovery of glucose from samples treated with sulfuric acid, 12 mol dm^{-3}, for 1 at 35 °C followed by treatment with sulfuric acid, 2 mol dm^{-3} is shown: B, glucose; C, cellulose; D, sugar beet; E, soya bran; F, wheat bran; and G, cabbage

In order to optimize conditions for the release of constituent sugars using 2 mol dm^{-3} sulfuric acid samples of guar gum and cellulose, and the starch-free residue from haricot beans, oat bran, soya bran, wholemeal flour, carrots, cabbage, garden peas and sugar beet and a solution containing the constituent sugars of NSP were incubated with 12 mol dm^{-3} sulfuric acid at 35 °C for 1 h and then 2 mol dm^{-3} sulfuric acid at 100 °C for various times; the released sugars were measured by GLC as described here and by HPLC as described in an accompanying paper.[9] For the samples and the constituent sugar mixture, the times to maximum value for fucose, arabinose, xylose, mannose, glucose and galactose were very similar, indicating that NSP, including cellulose, are hydrolysed virtually completely during the treatment with 12 mol dm^{-3} sulfuric acid. Results for glucose are shown in Fig. 5. The time to maximum values for released rhamnose (4–5 h) was different from that required for the desulfation of sulfated rhamnose in the sugar mixture and a correction for incomplete release of rhamnose (a minor constituent of NSP) must be applied if 1 h hydrolysis with 2 mol dm^{-3} sulfuric acid is to be used. Analysis by HPLC[9] showed that, for cellulose and for guar gum, no oligomers were present in the hydrolysates treated for 1 h with 12 mol dm^{-3} sulfuric acid at 35 °C followed by 2 mol dm^{-3} sulfuric acid for 1 h at 100 °C. (Oligomers were observed for samples containing uronic acids, however, indicating incomplete hydrolysis. This is of no consequence if the Scott procedure[10] is used for the measurement of uronic acids but, if HPLC is to be used, then a further 2 h treatment with 2 mol dm^{-3} sulfuric acid at 100 °C is required for complete hydrolysis.)

It was shown that acetate ions are formed upon the destruction of arabinose and xylose but not from the destruction of mannose, fucose, galactose, glucose or hexosamines. Samples of wheat bran, xylan, ispaghula husk and soya bran, and test sugar solutions with monosaccharide compositions identical with that present in the samples were subjected to 12 mol dm^{-3} sulfuric acid for 1 h at 35 °C, followed by hydrolysis with 2 mol dm^{-3} sulfuric acid at 100 °C. The amount of acetate ions in the hydrolysates was found to be similar for the samples and the corresponding sugar mixtures: *e.g.*, 9.5 and 9.6 for wheat bran; 16.0 and 16.2 for xylan; 12.3 and 12.2 for ispaghula husk; and 5.0 and 5.3 for soya bran, respectively (all units are in g per 100 g of dry sample). These results indicate that the losses of sugars during the acid hydrolysis of polymers are identical with those from solutions of these constituent sugars subjected to the same treatment. Therefore, correction factors for neutral sugars, other than rhamnose, were determined on the basis of losses observed for monosaccharides. The correction factor for the incomplete hydrolysis of rhamnose-containing polymers was derived from measurement of hourly release (unpublished results). The data in Table 1 show that the overall recovery of monosaccharides subjected to 12 mol dm^{-3} sulfuric acid followed by 2 mol dm^{-3} sulfuric acid, (without corrections) range from 89% for xylose to 96% for fucose and that most losses occur during the treatment with 2 mol dm^{-3} sulfuric acid. A small correction is required for incomplete desulfation of the sulfated hexoses

Table 3 Comparison of values obtained for wheat bran subjected to (1) the conditions recommended by Selvendran;[12] (2) the conditions previously used in the Englyst procedure;[3] and (3) the conditions used in the Englyst procedure as described here

	Primary hydrolysis			Secondary hydrolysis			Recovery (g per 100 g sample)					
	Molarity	Time/h	Temperature/°C	Molarity	Time/h	Temperature/°C	Arabinose	Xylose	Mannose	Galactose	Glucose	Total
(1) Selvendran	12	3	20	1	2.5	100	14.4	24.7	0.4	1.1	16.9	57.5
(2) Englyst	12	1	35	1	2	100	13.9	23.6	0.4	1.1	16.1	55.1
(3) Englyst	12	1	35	2	1	100	14.6	25.0	0.5	1.2	17.9	59.2
(1) Selvendran	—	—	—	1	2.5	100	14.6	24.5	t*	1.1	1.2	41.4
(2) Englyst	—	—	—	1	2	100	14.6	24.4	t	1.1	1.2	41.3
(3) Englyst	—	—	—	2	1	100	14.9	24.8	0.2	1.3	1.4	42.6

* t = trace.

Table 4 Total, soluble and insoluble NSP in some plant foods

				Composition (g per 100 g of dry mass)									
					Non-cellulosic polysaccharides								
		Total g per 100 g of fresh mass	Total g per 100 g of dry mass	Cellulose	Rhamnose	Fucose	Arabinose	Xylose	Mannose	Galactose	Glucose	Uronic acids
Plain white flour												
	Soluble NSP	1.6	1.8	—	t*	t	0.6	0.7	t	0.2	0.3	t
	Insoluble NSP	1.6	1.8	0.1	t	t	0.6	0.8	0.1	t	0.2	t
	Total NSP	3.2	3.6	0.1	t	t	1.2	1.5	0.1	0.2	0.5	t
Wholewheat flour												
	Soluble NSP	2.5	2.8	—	t	t	0.8	1.3	0.1	0.2	0.3	0.1
	Insoluble NSP	7.2	8.1	1.6	t	t	2.3	3.3	t	0.1	0.6	0.2
	Total NSP	9.7	10.9	1.6	t	t	3.1	4.6	0.1	0.3	0.9	0.3
Rye flour, whole												
	Soluble NSP	3.9	4.5	—	t	t	1.4	2.1	0.1	0.1	0.7	0.1
	Insoluble NSP	7.8	9.0	1.4	t	t	2.2	3.6	0.2	0.2	1.3	0.1
	Total NSP	11.7	13.5	1.4	t	t	3.6	5.7	0.3	0.3	2.0	0.2
Porridge oats												
	Soluble NSP	3.6	4.0	—	t	t	0.2	0.2	t	0.1	3.4	0.1
	Insoluble NSP	2.8	3.1	0.3	t	t	0.7	1.0	0.1	0.1	0.8	0.1
	Total NSP	6.4	7.1	0.3	t	t	0.9	1.2	0.1	0.2	4.2	0.2
Cornflakes, Kelloggs												
	Soluble NSP	0.4	0.4	—	t	t	t	0.2	t	t	0.1	0.1
	Insoluble NSP	0.5	0.5	0.3	t	t	0.1	0.1	t	t	t	t
	Total NSP	0.9	0.9	0.3	t	t	0.1	0.3	t	t	0.1	0.1
Rice, white												
	Soluble NSP	—	t	—	t	t	t	t	t	t	t	t
	Insoluble NSP	0.4	0.5	0.2	t	t	0.1	0.1	t	t	0.1	t
	Total NSP	0.4	0.5	0.2	t	t	0.1	0.1	t	t	0.1	t
Apples, Cox												
	Soluble NSP	0.9	5.8	—	0.2	0.1	1.2	0.1	t	0.3	0.1	3.8
	Insoluble NSP	1.1	7.5	4.4	0.1	0.1	0.9	0.7	0.3	0.6	0.1	0.3
	Total NSP	2.0	13.3	4.4	0.3	0.2	2.1	0.8	0.3	0.9	0.2	4.1
Oranges												
	Soluble NSP	1.4	9.8	—	0.3	t	1.9	0.1	0.1	1.4	0.1	5.9
	Insoluble NSP	0.7	5.2	3.4	t	t	0.3	0.5	0.3	0.4	t	0.3
	Total NSP	2.1	15.0	3.4	0.3	t	2.2	0.6	0.4	1.8	0.1	6.2
Beans, french, cooked												
	Soluble NSP	1.3	12.7	—	0.2	t	1.1	0.2	0.2	2.6	0.1	8.3
	Insoluble NSP	1.8	17.7	11.1	0.1	t	1.2	1.5	1.2	1.5	0.5	0.6
	Total NSP	3.1	30.4	11.1	0.3	t	2.3	1.7	1.4	4.1	0.6	8.9
Beans, haricot, cooked												
	Soluble NSP	3.7	9.1	—	0.2	0.4	4.3	0.8	0.2	0.8	0.4	2.0
	Insoluble NSP	4.6	11.2	5.1	0.1	t	3.1	1.4	0.1	0.3	t	1.1
	Total NSP	8.3	20.3	5.1	0.3	0.4	7.4	2.2	0.3	1.1	0.4	3.1
Cabbage, winter												
	Soluble NSP	0.9	15.8	—	1.1	0.2	3.2	t	0.1	2.2	t	9.0
	Insoluble NSP	1.1	18.5	12.5	0.1	t	1.3	1.6	0.7	1.5	0.2	0.6
	Total NSP	2.0	34.3	12.5	1.2	0.2	4.5	1.6	0.8	3.7	0.2	9.6
Carrots, raw												
	Soluble NSP	1.4	11.4	—	0.7	t	1.7	t	0.1	3.0	t	5.9
	Insoluble NSP	1.0	8.1	6.4	t	t	0.3	0.3	0.3	0.4	0.1	0.3
	Total NSP	2.4	19.5	6.4	0.7	t	2.0	0.3	0.4	3.4	0.1	6.2

* t = trace.

but rhamnose is the only neutral sugar requiring correction for incomplete hydrolysis of polymers.

The Scott procedure used in conjunction with the GLC determination of neutral sugars measures free uronic acids and uronic acid-containing polymers in solution.[10] In contrast, the HPLC procedure measures only free uronic acids. The treatment with 12 mol dm^{-3} sulfuric acid, causes negligible losses of uronic acids, whereas the loss of free galacturonic acid is 15% h^{-1} during the treatment with 2 mol dm^{-3} sulfuric acid, when measured by either HPLC or the Scott colorimetric procedure. In the process of optimizing the procedure for the measurement of uronic acids, it was shown by HPLC that on average, only 30% of uronic acid polymers were hydrolysed to monomers after treatment with 12 mol dm^{-3} sulfuric acid for 1 h, followed by 2 mol dm^{-3} sulfuric acid for 1 h and the losses were less than those observed for free uronic acids subjected to identical hydrolysis conditions. This indicates some protection from destruction of uronic acids in oligomer or polymer form. The extent of the loss of uronic acids in polymer form cannot be determined using monosaccharide test solutions subjected to identical acid hydrolysis conditions. It was found that acetate ions produced during treatment of galacturonic acids (and glucuronic acids) with sulfuric acid reflect destruction. Therefore, acetate ions were measured and the values used to calculate the amount of destruction of uronic acids during hydrolysis of uronic acid-containing polymers. Full experimental details and results will be presented elsewhere.

Values are given in Table 1 for the composition of a calibration mixture adjusted to compensate for incomplete hydrolysis of polymers and losses of monosaccharides. When

such a sugar mixture is used in the measurement of neutral sugars by GLC and uronic acids by the Scott procedure, accurate values for NSP are obtained without further correction. The corrections required for the measurement of neutral sugars by GLC and HPLC[9] are identical, whereas the measurement of uronic acids by HPLC requires a correction separate from that used in the Scott procedure.

The results obtained with the hydrolysis conditions given here (see Experimental) are compared in Table 3 with those obtained under the conditions previously reported from the Englyst procedure,[3] and with the results obtained by the conditions recommended by Selvendran from the measurement of cell-wall polysaccharides.[11] The observed values are very similar and, when correction factors are applied, accurate quantification is obtained under all three hydrolysis conditions. However, the hydrolysis conditions presented here are the most rapid and require smaller correction factors than those described previously for the Englyst procedure.[3]

We have shown that there is good agreement between values obtained for NSP by GLC and colorimetry,[12] and elsewhere we have shown that the neutral sugar[9] and uronic acid (unpublished results) constituents of NSP can be measured by HPLC. Each of the three procedures gives values for total, soluble and insoluble NSP. When using GLC or HPLC, these fractions are further divided into cellulose and non-cellulosic NSP with values for the individual sugars (Table 4). The information obtained by the GLC and HPLC procedure is valuable for the interpretation of physiological studies where diseases may relate to the type of NSP.

The GLC procedure described here and the colorimetric procedure described elsewhere[12] have been tested successfully in a collaborative trial organized by the UK Ministry of Agriculture, Fisheries and Food.[13]

References

1 *Dietary Fibre, Fibre-Depleted Foods and Disease*, eds., Trowell, H., Burkitt, D., and Heaton, K., Academic Press, London, 1985.
2 Englyst, H. N., Wiggins, H. S., and Cummings, J. H., *Analyst*, 1982, **107**, 307.
3 Englyst, H. N., and Cummings, J. H., *J. Assoc. Off. Anal. Chem.*, 1988, **71**, 808.
4 Englyst, H. N., Bingham, S. A., Runswick, S. A., Collinson, E., and Cummings, J. H., *J. Hum. Nutr. Dietet.*, 1988, **1**, 247.
5 Englyst, H. N., Bingham, S. A., Runswick, S. A., Collinson, E., and Cummings, J. H., *J. Hum. Nutr. Dietet.*, 1989, **2**, 253.
6 Holland, B., Unwin, I. D., and Buss, D. H., *Vegetables, Herbs and Spices; The Fifth Supplement to McCance & Widdowson's The Composition of Foods*, Royal Society of Chemistry, Cambridge, 4th edn., 1991.
7 Holland, B., Unwin, I. D., and Buss, D. H., *Cereals and Cereal Products; The Third Supplement to McCance & Widdowson's The Composition of Foods*, Royal Society of Chemistry, Nottingham, 4th edn., 1991.
8 Holland, B., Welch, A. A., Unwin, I. D., Buss, D. H., Paul, A. A., and Southgate, D. A. T., *McCance & Widdowson's The Composition of Foods*, Royal Society of Chemistry, Cambridge, 5th edn., 1991.
9 Quigley, M. E., and Englyst, H. N., *Analyst*, 1992, **117**, 1715.
10 Scott, R. W., *Anal. Chem.*, 1979, **51**, 936.
11 Selvendran, R. R., and DuPont, M. S., *J. Sci. Food Agric.*, 1980, **31**, 1173.
12 Englyst, H. N., and Hudson, G. J., *Food Chem.*, 1987, **24**, 63.
13 Wood, R., Englyst, H. N., Southgate, D. A. T., and Cummings, J. H., *J. Assoc. Off. Anal. Chem.*, 1992, in the press.

Paper 2/00583B
Received February 3, 1992
Accepted May 28, 1992

Determination of Neutral Sugars and Hexosamines by High-performance Liquid Chromatography With Pulsed Amperometric Detection

Michael E. Quigley and Hans N. Englyst
Medical Research Centre Dunn Clinical Nutrition Centre, 100 Tennis Court Road, Cambridge, UK CB2 1QL

Procedures are described using high-performance liquid chromatography with pulsed amperometric detection for the measurement of neutral sugars and amino sugars released upon acid hydrolysis of non-starch polysaccharides. One procedure measures the neutral sugars with near-baseline separation in a 36 min run. The second procedure measures amino sugars and all neutral sugars except rhamnose and arabinose, which co-elute under the conditions described, in a 40 min run. Neutral sugars released from non-starch polysaccharides are ionized at high pH and separated by anion-exchange chromatography using NaOH as the eluent. When hexosamines or *N*-acetylhexosamines are present, as in mycoprotein and mushrooms or in ileostomy effluent, separation is achieved isocratically using 0.1 mmol dm^{-3} NaOH. The sulfate ions present in the hydrolysate are prevented from reaching the analytical column by a pre-column guard. Post-column addition of 300 mmol dm^{-3} NaOH increases the analytical signal and minimizes baseline drift. When only neutral sugars are present in the hydrolysate a single dilution step is required before analysis. When neutral sugars and hexosamines are present, a simple two-step neutralization and dilution are performed before injection.

Keywords: *Neutral sugar; hexosamine; high-performance liquid chromatography; non-starch polysaccharide; ileostomy effluent*

High-performance liquid chromatography (HPLC) has been used for more than 15 years for the measurement of mono-, di- and oligosaccharides.[1–7] However, until recently HPLC could not adequately separate the complex mixture of hexoses and pentoses released by the acid hydrolysis of non-starch polysaccharides (NSP). In the development of a procedure for the measurement of NSP as an index of dietary fibre, gas–liquid chromatography (GLC) was chosen for the determination of the constituent sugars.[8,9] With the development of improved anion-exchange separations combined with pulsed amperometric detection (PAD), HPLC offers an attractive alternative. Here, we describe two HPLC techniques: one for the measurement of neutral sugars alone and the second for the measurement of hexosamines and neutral sugars.

Experimental

Reagents

High-purity de-ionized water (18 MΩ cm) was prepared 'in house' and filtered through 2 μm filters. Sodium hydroxide solution (50% m/v, low in carbonate) was purchased from BDH (Poole, Dorset, UK). Solution 1 is NaOH at 1.6 cm^3 dm^{-3} in high-purity water. Solution 2 is NaOH at 60 mm^3 dm^{-3} in high-purity water. In the preparation of these solutions, the water was sparged with helium for 5 min before and during addition of the appropriate volume of NaOH solution.

Chromatography

A Dionex Bio-LC gradient pump, Dionex Carbopac PA-1 (10 μm; 250 × 4 mm i.d.) equipped with a Dionex AG6 guard column and a Dionex Model PAD 2 detector were used for HPLC of neutral and amino sugars. Monosaccharide detection was carried out with the following pulse potentials and durations: E_1 = 0.05 V (t_1 = 300 ms); E_2 = 0.60 V (t = 120 ms); E_3 = −0.60 V (t_3 = 60 ms). The response time was 1 s. The output on the detector was set to 1000 nA. Separation of neutral sugars in the absence of amino sugars was achieved using isocratic elution with 23% v/v solution 1 in water from 0 to 3.5 min, a gradient from 23 to 1% solution 1 from 3.5 to 4.5 min, and isocratic elution with 1% solution 1 from 4.5 to 30 min at a flow rate of 1 cm^3 min^{-1}, followed by at least 6 min re-equilibration with the starting conditions before injection of the next sample. (Better resolution between rhamnose and arabinose was achieved using a higher proportion of solution 1 but this resulted in decreased resolution between xylose and mannose.) Isocratic separation of neutral and amino sugars was achieved with 16% v/v solution 2. After 40 min the column was purged with 100 mmol dm^{-3} NaOH for 5 min followed by 6 min re-equilibration with the starting conditions before the next sample was injected.

A Dionex Model DQP-1 single-piston pump was used to add 300 mmol dm^{-3} NaOH (NaOH at 24 cm^3 dm^{-3} in high-purity water) at a flow rate of 0.5 cm^3 min^{-1} to the column effluent before the PAD cell, which minimized baseline drift and increased the analytical signal. A Dionex Eluent De-gas Module was used to saturate the eluents with helium gas to minimize CO_2 absorption. Samples were transferred to Polyvial sample vials with 20 μm filters and injected with a Dionex automated sampler *via* a Dionex high-pressure valve. A Dionex AI-450 chromatography data-handling system was used to plot and integrate the results.

The presence of sulfate ions in the hydrolysate decreased retention times and resulted in co-elution of peaks in the chromatography. Sulfate ions, in amounts equivalent to those injected in the methods described here, are retained on an AG5 column for 80 s while monosaccharides are not retained. We therefore incorporated an AG5 guard column with column switching after 60 s to prevent sulfate ions from reaching the analytical column. Complete purging of sulfate ions from the column requires 19 min, well within the run time. Constant chromatographic retention times were achieved for a batch of at least 24 samples using the conditions described for neutral sugars only. When hexosamines were present, however, it was necessary to wash the column after each sample with 100 mmol dm^{-3} NaOH for 5 min followed by 6 min re-equilibration with the original eluent. After several batches of samples have been analysed, the elution times of the sugars begin to decrease with each subsequent injection. The analytical and guard columns can be re-generated completely by washing with 100 mmol dm^{-3} NaOH and 600 mmol dm^{-3} NaOAc for 1 h, followed by 1 mmol dm^{-3} NaOH for 1 h. To avoid contamination of the internal reference solution the 1 mmol dm^{-3} NaOH solution was not allowed to pass through the detector. Using this washing procedure the

same column has been used for the analysis of more than 3000 samples with no loss of performance. Since the completion of these studies we have used a recently developed Dionex Carbopac PA-100 column to separate the neutral sugars and hexosamines isocratically using a 2 mmol dm^{-3} NaOH eluent in less than 30 min, with similar resolution to that achieved using a Dionex Carbopac PA-1 column. When using this eluent the treatment of hydrolysates containing hexosamines is identical with that described for neutral sugars and hexosamines (see below).

Preparation of Standards and Treatment of Hydrolysates

In the procedure of Englyst *et al.*[10] for the measurement of NSP, starch is removed enzymically and the constituent sugars are released by acid hydrolysis. The choice of treatment required for measurement of the constituent sugars in these hydrolysates depends on either the presence or absence of hexosamines.

Neutral sugars only

To 150 mm^3 of hydrolysate, or standard sugar mixture (in 2 mol dm^{-3} sulfuric acid), 5 cm^3 of internal standard solution (15 mg dm^{-3} deoxygalactose in high-purity water) were added and mixed. The standard sugar mixture contained 95 mg of arabinose, 96 mg of fucose, 26 mg of rhamnose, 89 mg of xylose, 46 mg of mannose, 94 mg of galactose and 94 mg of glucose in 100 cm^3 of 2 mol dm^{-3} sulfuric acid. For calibration, the standard sugar mixture was assumed to contain 1 mg cm^{-3} of all sugars except rhamnose and mannose, where a value of 0.5 mg cm^{-3} was used. When the actual amount of sugars present was less, this was to correct for losses of sugars and incomplete hydrolysis of NSP.

Neutral and amino sugars

To 150 mm^3 of hydrolysate, or standard sugar mixture (in 2 mol dm^{-3} sulfuric acid), 1 cm^3 of internal standard solution (125 mg dm^{-3} deoxygalactose in 50 mmol dm^{-3} NaH_2PO_4) and 4 cm^3 of 0.16 mmol dm^{-3} NaOH were added and mixed. The pH of the final solution must be between 7.2 and 8.2. The standard sugar mixture contained 95 mg of arabinose, 99 mg of fucose, 89 mg of xylose, 92 mg of mannose, 94 mg of galactose, 94 mg of glucose, 90 mg of galactosamine (108 mg of galactosamine hydrochloride) and 93 mg of glucosamine (112 mg of glucosamine hydrochloride) in 100 cm^3 of 2 mol dm^{-3} sulfuric acid. Again, the value of 1 mg cm^{-3} for each sugar was used for the purpose of calibration.

Calculation of Neutral Sugars

The amounts of individual sugars (in g per 100 g of sample) are calculated as:

$$\frac{A_T \times m_I \times R_F \times 100}{A_I \times m_T} \times 0.89$$

where A_T and A_I are the peak areas of the sample and the internal standard, respectively; m_T is the mass of the sample (in mg); m_I is the mass of the internal standard if added to the whole sample (in mg; here 15 in the analysis of neutral sugars only and 25 in the analysis of neutral sugars and hexosamines); R_F is the response factor for individual sugars obtained from the calibration run with the sugar mixture treated in parallel with the samples; and 0.89 is the factor for converting the experimentally determined monosaccharides into polysaccharides. All calculations are performed with a computing integrator.

Results and Discussion

The destruction of sugars during acid hydrolysis was investigated by treating sugars with 2 mol dm^{-3} sulfuric acid at 100 °C for various times, and with 12 mol dm^{-3} sulfuric acid for 1 h at 35 °C followed by 2 mol dm^{-3} sulfuric acid at 100 °C for various times. The values obtained for neutral sugars were identical with those obtained by GLC.[10] It was found for both the hexosamines and the neutral sugars that the treatment with 12 mol dm^{-3} sulfuric acid caused extensive sulfation, which resulted in decreased recovery. However, on dilution to 2 mol dm^{-3} sulfuric acid and heating at 100 °C, increasing recovery was obtained between 0 and 60 min as a result of hydrolysis of the ester sulfate linkages. After 60 min of treatment with 2 mol dm^{-3} sulfuric acid no further increase in recovery of the hexosamines was observed, indicating complete desulfation. Prolonged hydrolysis, up to 360 min, with 2 mol dm^{-3} sulfuric acid had little effect on recovery, with less than 0.5% m/m of the amino sugars being destroyed per hour (Fig. 1). Complete de-acetylation and desulfation are achieved after 60 min at 100 °C in 2 mol dm^{-3} sulfuric acid. The *N*-acetylhexosamines are therefore measured as the corresponding hexosamines. The acetate ions released were measured after extraction with diethyl ether,[11] using propionate as internal standard, and quantified by GLC using a fused silica capillary column (25QC5/BP21 0.5 from Scientific Glass Engineering). Maximum values for acetate ions were found after 40 min of treatment with 2 mol dm^{-3} sulfuric acid, which remained constant even on prolonged boiling (up to 6 h). By comparing the molar ratio of acetate ions to glucosamine, it is possible to determine the degree of *N*-acetylation of a sample. For example, a mycoprotein sample was found to contain 43.3 μmol of acetate ions and 43.9 μmol of glucosamine per 100 mg of sample, which represents a degree of *N*-acetylation of 0.986. It should be noted, however, that acetate ions are produced upon destruction of pentoses, but not hexoses or hexosamines, and are released from *O*-acetylated sugars upon acid hydrolysis. The degree of *N*-acetylation can be determined by subtracting values for the experimentally determined alkali-labile *O*-acetyl groups[12] and the acetate ions produced by destruction of the pentoses present in the sample. Alternatively, it is possible to determine the degree of *N*-acetylation by the picric acid method of Neugabauer *et al.*[13]

Samples of guar gum, mucin, chitin and cellulose, and the NSP residue from haricot bean, oat bran, mycoprotein, wheat bran, soya bran, wholemeal flour, carrot, cabbage, garden pea, sugar beet, mushroom and ileostomy effluent, and a test solution of monosaccharides (containing 30 mg of each sugar) were subjected to treatment with 12 mol dm^{-3} sulfuric acid at 35 °C for 1 h and then 2 mol dm^{-3} sulfuric acid at 100 °C for

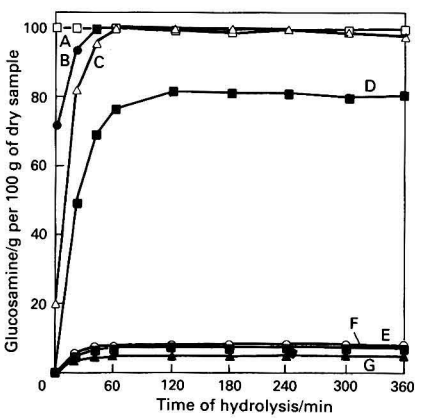

Fig. 1 A, Recovery of glucosamine from a test solution of sugars subjected to treatment with 2 mol dm^{-3} sulfuric acid at 100 °C. Observed recovery of glucosamine from: B, a test solution of glucosamine; C, a test solution of *N*-acetylglucosamine; D, chitin; E, mycoprotein; F, mushroom; and G, an ileostomy effluent subjected to treatment with 12 mol dm^{-3} sulfuric acid for 1 h followed by treatment with 2 mol dm^{-3} sulfuric acid at 100 °C is shown

various times; the sugars released were measured by HPLC. For the samples and the test solution, the time to maximum value for xylose, glucose, fucose, arabinose, mannose and galactose was very similar and the values were identical with those obtained by GLC.[10] The time required to reach maximum values for rhamnose (4–5 h) and hexosamines (2 h; Fig. 1) from the samples was different from that required for the test solution (1 h), indicating slow release of these sugars. For mucin, no difference in recovery was observed when the hydrolysis with 12 mol dm^{-3} sulfuric acid was omitted, whereas for chitin and mycoprotein dispersion with 12 mol dm^{-3} sulfuric acid was essential. When samples containing a mixture of neutral sugars and hexosamines are to be analysed, as in mushroom, mycoprotein and ileostomy effluent, separate acid hydrolysis is required for optimum release of monosaccharides, *i.e.*, 1 h of treatment with 2 mol dm^{-3} sulfuric acid for the neutral sugars but 2 h for hexosamines. For routine analytical purposes it is possible, however, to use one set of acid hydrolysis conditions and to apply correction factors for incomplete hydrolysis of polymers and destruction of sugars. These values for the incomplete recovery of sugars can be used either by post-analysis calculation or, more simply, by incorporation of these values into the sugar mixture used for the calibration of response factors (*e.g.*, 0.89 mg of xylose and 0.94 mg of glucose represent 1 mg of each sugar present in a sample after 1 h of treatment with 2 mol dm^{-3} sulfuric acid).

The treatment of acid hydrolysates for analysis by HPLC is minimal. The addition of internal standard is the only step required when neutral sugars alone are to be measured. The sulfate ions present in the hydrolysate are removed during the chromatography by a pre-column guard with column switching (see above). This obviates the need for the time-consuming removal of acids by treatment with resin[14] or by rotary evaporation.[15] Maintenance of pH between 7.2 and 8.2 before chromatography is critical when amino sugars are present. At lower pH, these sugars produce multiple peaks on chromatography using the elution conditions described here, and they are unstable at higher pH.

Fig. 2 shows chromatograms for a standard sugar mixture and an acid hydrolysate of NSP from cabbage, analysed by the procedure described for neutral sugars only; separation is near-baseline for all sugars. Fig. 3 shows the chromatograms obtained for a standard sugar mixture containing hexosamines and neutral sugars (except rhamnose), and an ileostomy effluent using the conditions described here for the measurement of neutral sugars and hexosamines. Rhamnose and arabinose co-elute under these conditions but can be measured separately by the neutral sugar method.

The NSP from a range of food samples (n = 86) were hydrolysed and analysed for neutral sugars by GLC and by HPLC using the procedure for neutral sugars only or the procedure for neutral sugars and hexosamines, as appropriate (Fig. 4). The values obtained for total neutral sugars by GLC and by HPLC for each sample were transformed to the mean and difference;[16] regression analysis showed no significant deviation (correlation coefficient = 0.014) from a slope of zero, indicating very close agreement of the two methods, with no bias. Within-batch relative standard deviations were between 2.1 and 4.3% for neutral sugars and between 3.2 and 4.0% for hexosamines in sugar mixtures containing 1 mg cm^{-3} of monosaccharides in 2 mol dm^{-3} sulfuric acid (n = 15). Using the conditions described here, the linear response range was found to be between 0.05 and 60 mg for fucose and between 0.1 and 120 mg for all other sugars present in the hydrolysate. Values obtained for the neutral sugar content of the NSP from a range of samples by GLC and by HPLC for neutral sugars only are given in Table 1. Table 2 gives values for NSP constituents obtained by HPLC analysis of test meals and of effluent from ileostomy subjects given a polysaccharide-free diet or with the same diet with added brown bread or mycoprotein.

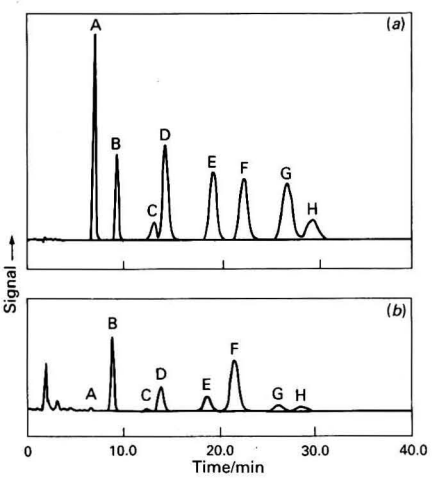

Fig. 2 High-performance liquid chromatogram of (*a*) a standard sugar mixture and (*b*) a cabbage hydrolysate analysed by the procedure described for neutral sugars only. A, Fucose; B, deoxygalactose (internal standard); C, rhamnose; D, arabinose; E, galactose; F, glucose; G, xylose; and H, mannose

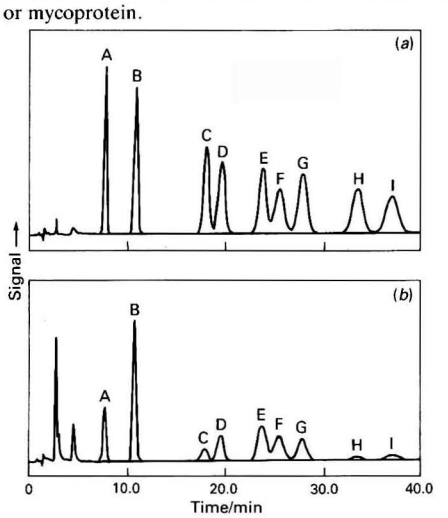

Fig. 3 High-performance liquid chromatogram of (*a*) a standard sugar mixture and (*b*) an ileostomy effluent analysed by the procedure described for neutral and amino sugars. A, Fucose; B, deoxygalactose (internal standard); C, arabinose. D, galactosamine; E, galactose; F, glucosamine; G, glucose; H, xylose; and I, mannose

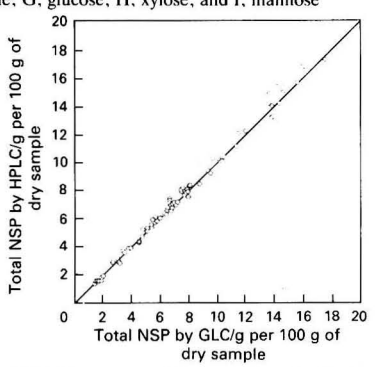

Fig. 4 Total NSP for a range of foods analysed by GLC and HPLC are compared. The line of unity is shown

Table 1 Values for neutral NSP constituents (g per 100 g of dry matter) obtained by GLC and HPLC

Sample	Method	Rhamnose	Fucose	Arabinose	Xylose	Mannose	Galactose	Glucose	Total
Apple	GLC	0.09	t*	0.94	0.82	0.28	0.89	4.48	7.50
	HPLC	0.17	t	0.94	0.90	0.51	0.97	4.04	7.53
Arabinogalactan	GLC	—	0.40	14.10	0.20	—	79.30	0.60	94.60
	HPLC	—	0.80	14.90	0.20	—	79.50	0.40	95.80
Baked beans	GLC	0.09	0.20	3.61	1.31	0.26	0.79	2.78	9.04
	HPLC	0.12	0.25	3.70	1.43	0.32	0.88	2.79	9.49
Banana	GLC	—	—	0.24	0.16	0.54	0.32	1.00	2.26
	HPLC	—	—	0.21	0.16	0.65	0.37	1.05	2.44
Barley flakes	GLC	—	—	2.08	4.23	0.27	0.32	6.80	13.70
	HPLC	—	—	2.08	4.03	0.30	0.33	6.77	13.51
Cabbage	GLC	0.42	0.13	3.29	1.19	0.81	2.62	9.09	17.55
	HPLC	0.44	0.17	3.31	1.26	0.84	2.69	8.84	17.55
Carrot	GLC	0.69	t	2.49	0.37	0.56	4.33	7.64	16.08
	HPLC	0.80	t	2.85	0.40	0.56	4.54	7.64	16.79
Cellulose	GLC	—	—	—	2.20	1.40	—	97.00	100.60
	HPLC	—	—	—	2.10	1.50	—	97.80	101.40
Corn flakes	GLC	—	—	0.23	0.18	0.07	0.10	0.40	0.98
	HPLC	—	—	0.20	0.20	0.01	0.12	0.46	0.99
Corn meal	GLC	—	—	0.54	0.40	t	0.15	0.55	1.64
	HPLC	—	—	0.39	0.42	t	0.20	0.73	1.74
Garden pea	GLC	0.16	0.04	3.11	1.28	t	0.80	5.79	11.18
	HPLC	0.14	0.03	3.22	1.37	t	0.73	5.67	11.16
Haricot bean	GLC	0.15	0.40	5.70	1.84	0.47	1.47	4.17	14.20
	HPLC	0.13	0.35	5.20	1.94	0.60	1.41	4.61	14.24
Instant potato	GLC	—	—	0.38	0.09	0.07	2.39	2.27	5.20
	HPLC	—	—	0.35	0.09	0.07	2.51	2.28	5.30
Wheat bran	GLC	—	—	8.22	14.99	0.34	1.25	10.16	34.96
	HPLC	—	—	8.14	15.23	0.29	1.12	10.35	35.13
White flour	GLC	—	—	0.86	1.19	0.19	0.53	0.68	3.45
	HPLC	—	—	0.85	1.16	0.17	0.48	0.65	3.31
Wholemeal bread	GLC	—	—	2.16	3.54	0.18	0.35	2.41	8.64
	HPLC	—	—	2.20	3.61	0.20	0.37	2.25	8.63
Xylan	GLC	—	—	7.80	57.30	—	1.60	18.10	84.80
	HPLC	—	—	7.90	57.70	—	1.40	17.90	84.90

* t = trace.

Table 2 Values for NSP constituents obtained by HPLC for test meals containing brown bread and mycoprotein and in effluents from ileostomy patients fed a polysaccharide-free diet (PSF), or test meals consisting of the PSF diet with added brown bread or mycoprotein (results in g per 100 g of dry matter)

Sample	Diet	GalNAc*	GlcNAc†	Fucose	Arabinose	Xylose	Mannose	Galactose	Glucose	Uronic acid	Total
Test meal	Bread	0.00	0.00	0.00	1.59	2.50	0.34	0.46	1.59	0.41	6.89
	Mycoprotein	0.00	9.22	0.00	0.16	0.00	2.96	0.81	8.45	2.85	24.45
Ileostomy effluent	PSF	1.61	2.78	1.31	0.11	0.00	0.35	1.99	0.42	0.32	8.89
	PSF + bread	1.27	2.26	1.20	3.80	5.45	1.23	2.35	3.09	0.66	21.31
	PSF + mycoprotein	0.99	8.55	0.85	0.39	0.00	2.11	1.94	5.28	1.12	21.23

* GalNAc = *N*-Acetylgalactosamine.
† GlcNAc = *N*-Acetylglucosamine.

We have developed a method (unpublished) for the measurement of the uronic acid constituents of NSP using HPLC. Combined with the methods described here, all the components of NSP can be measured using HPLC. In addition, the technique is suitable for measuring the complex mixture of neutral sugars and hexosamines found in ileostomy effluents and faecal samples, and thus provides a useful tool in interpretation of physiological studies.

References

1 Honda, S., *Anal. Biochem.*, 1984, **140**, 1.
2 Verhaar, L. A. Th., and Kuster, B. F. M., *J. Chromatogr.*, 1981, **220**, 313.
3 Honda, S., Suzuki, S., and Kakehi, K., *J. Chromatogr.*, 1984, **291**, 317.
4 Jandera, P., and Churacek, J., *J. Chromatogr.*, 1974, **98**, 55.
5 Ross, L. F., and Chapital, D. C., *J. Chromatogr. Sci.*, 1987, **25**, 112.
6 Wight, A. W., and van Nierkerk, P. J., *Food Chem.*, 1983, **10**, 211.
7 Wight, A. W., and Datel, J. M., *Food Chem.*, 1986, **21**, 167.
8 Englyst, H. N., Wiggins, H. S., and Cummings, J. H., *Analyst*, 1982, **107**, 307.
9 Englyst, H. N., and Cummings, J. H., *J. Assoc. Off. Anal. Chem.*, 1988, **71**, 808.
10 Englyst, H. N., Quigley, M. E., Hudson, G. J., and Cummings, J. H., *Analyst*, 1992, **117**, 1707.
11 Holdeman, L. V., Cato, E. P., and Moore, W. E. C., *Anaerobic Laboratory Manual*, Blacksburg, Virginia Polytechnic Institute and State University, 4th edn., 1977.
12 Voragen, A. G. J., Schols, H. A., and Pilnik, W., *Food Hydrocolloids*, 1986, **1**, 65.
13 Neugabauer, W. A., Neugabauer, E., and Brzezinski, R., *Carbohydr. Res.*, 1989, **189**, 363.
14 Garleb, K. A., Bourquin, L. D., and Fahey, G. C., *J. Agric. Food Chem.*, 1989, **37**, 1287.
15 Hardy, M. R., Townsend, R. R., and Lee, Y. C., *Anal. Biochem.*, 1988, **170**, 54.
16 Bland, J. M., and Altman, D. G., *Lancet*, 1986, February, 307.

Paper 2/00585I
Received February 3, 1992
Accepted May 28, 1992

ANALYST, NOVEMBER 1992, VOL. 117

High-performance Liquid Chromatographic Determination of 3α,5β-Tetrahydroaldosterone in Human Urine With Chemiluminescence Detection

Junichi Ishida, Shinji Sonezaki and Masatoshi Yamaguchi*
Faculty of Pharmaceutical Sciences, Fukuoka University, Nanakuma, Johnan-ku, Fukuoka 814-01, Japan
Takashi Yoshitake
Chemical Biotesting Centre, Chemical Inspection and Testing Institute, 3-822 Ishii Machi, Hita, Oita 877, Japan

A sensitive method for the determination of 3α,5β-tetrahydroaldosterone (THALD) in human urine is described. The method uses high-performance liquid chromatography with chemiluminescence detection. Urinary THALD, released by enzyme hydrolysis, is isolated and concentrated using a Sephadex G-25M column and Bond-Elut C_1 cartridges, and then oxidized by copper(II) acetate to form the corresponding glyoxal derivative. The glyoxal derivative is converted into the chemiluminescent quinoxaline by reaction with 4,5-diaminophthalhydrazide. The chemiluminescent quinoxaline is separated within 50 min on a reversed-phase column (TSKgel ODS-120T) with isocratic elution, followed by chemiluminescence detection; the chemiluminescence is produced by the reaction of the quinoxaline with hydrogen peroxide in the presence of potassium hexacyanoferrate(III) in alkaline solution. The detection limit for THALD is 0.6 pmol (220 pg) ml^{-1} in urine [1.5 fmol (0.53 pg) per 20 μl injection] at a signal-to-noise ratio of 3. This method permits the sensitive and precise determination of THALD in human urine (50 μl) from normal subjects and a patient with primary aldosteronism.

Keywords: *High-performance liquid chromatography; chemiluminescence detection; 3α,5β-tetrahydroaldosterone; human urine; 4,5-diaminophthalhydrazide*

Aldosterone (ALD) is the most biologically active mineralocorticosteroid secreted by the adrenal cortex and regulates the metabolism of sodium and potassium ions. The relationship between the concentration of ALD in body fluids and diseases such as primary aldosteronism, hypertension and inborn deficiencies of 21-hydroxylase, 11-hydroxylase and 3β-hydroxysteroid dehydrogenase has been studied.

3α,5β-Tetrahydroaldosterone (THALD) is a major metabolite of ALD found in urine.[1–3] The determination of urinary THALD provides an excellent index of ALD secretion,[4,5] and can be useful for the diagnosis and/or treatment of the diseases described above.

Radioimmunoassay[5–8] (RIA), gas chromatographic[9,10] (GC), and GC–mass spectrometric[11,12] (GC–MS) methods have been reported for the determination of THALD in human urine. Radioimmunoassay is not very selective for THALD because of the cross-reacting THALD antibody with tetrahydrocortisol and tetrahydrocortisone. Recently, an improved RIA method[13] has been investigated which was coupled with high-performance liquid chromatography (HPLC) to prevent the cross-reaction. The method, however, is still time consuming and requires a radioactive compound. Gas chromatographic methods are not sensitive and require large amounts of sample (10 ml of urine). Gas chromatographic–mass spectrometric methods require expensive equipment and rather tedious techniques.

Chemiluminescence detection has been successfully used with HPLC owing to its high sensitivity.[14–16] Recently, we found that 4,5-diaminophthalhydrazide (DPH) reacts selectively with glyoxal compounds to form chemiluminescent quinoxaline derivatives.[17] We have developed a sensitive method for the determination of THALD in minute amounts of human urine by HPLC with chemiluminescence detection. This method is based on the conversion of THALD into the corresponding glyoxal compound by oxidation with copper(II) acetate (Porter–Silber reaction).[18,19] The glyoxal compound is then derivatized with DPH into the chemiluminescent quinoxaline derivative (Fig. 1). The resulting derivative produces chemiluminescence by reaction with hydrogen peroxide in the presence of potassium hexacyanoferrate(III) in alkaline medium.

The present objective was to develop a sensitive and selective HPLC method with pre-column chemiluminescence derivatization with DPH for the determination of THALD in human urine after enzyme hydrolysis.

Experimental

Chemicals and Solutions

All chemicals and solvents were of analytical-reagent grade, unless stated otherwise. Water was de-ionized, distilled and further purified with a Milli-QII system (Japan Millipore, Tokyo, Japan). The compounds THALD and ALD were purchased from Sigma (St. Louis, MO, USA). Hydrogen peroxide (31% v/v) was purchased from Mitsubishi Gas Kagaku (Tokyo, Japan). 4,5-Diaminophthalhydrazide was synthesized as described previously;[20,21] it is now commercially available from Wako (Osaka, Japan).

Enzyme solution (β-glucuronidase/arylsulfatase from *Helix pomatia*) was obtained from Boehringer Mannheim–Yamanouchi (Tokyo, Japan). The solution contains about 100000 Fishmann units ml^{-1} of β-glucuronidase and about 800000 Roy units ml^{-1} of arylsulfatase.

The DPH solution (7.5 mmol l^{-1}) was prepared in 250 mmol l^{-1} hydrochloric acid containing 125 mmol of β-mercaptoethanol. This solution was used within 5 h. Copper(II) acetate solution (39 mmol l^{-1}) was prepared by dissolving 0.7 g of copper(II) acetate in 10 ml of water and diluting the solution to 100 ml with methanol. The solution was used within 1 month after preparation. Hydrogen peroxide (40 mmol l^{-1}) and potassium hexacyanoferrate(III) (30 mmol l^{-1}) solutions were prepared in water and 3.0 mol l^{-1} sodium hydroxide, respectively.

A Sephadex G-25M column (bed volume 9 ml, void volume

* To whom correspondence should be addressed.

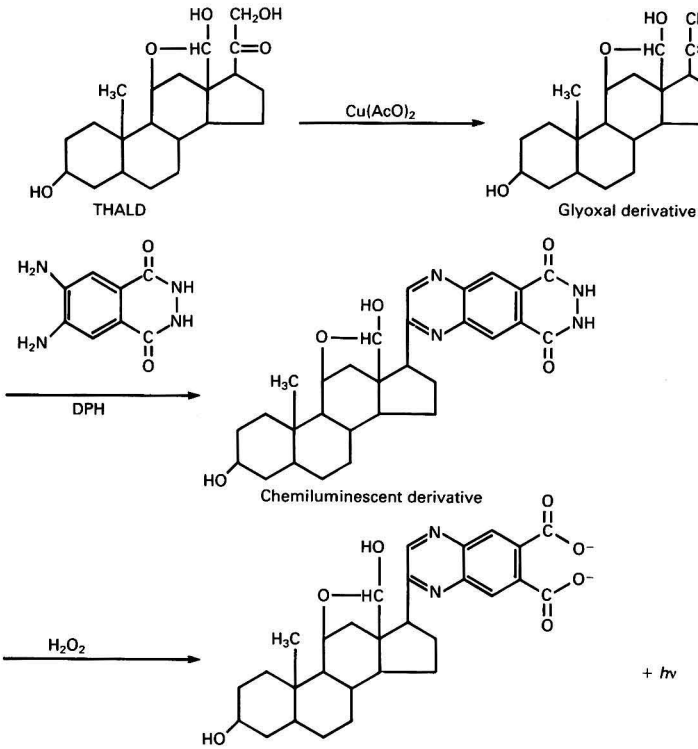

Fig. 1 Derivatization and chemiluminescence reaction of THALD with DPH

2.5 ml) (Pharmacia Fine Chemicals, Tokyo, Japan) was pre-equilibrated with 0.1 mol l^{-1} phosphate buffer (pH 7.0). A Bond-Elut C_1 cartridge (Analytichem International, Harbor City, CA, USA) was washed successively with methanol (5 ml) and water (5 ml) before use.

Urine Samples

Urine (24 h) from healthy volunteers in our laboratories and a patient with primary aldosteronism was collected without preservatives. The urine was frozen on dry-ice immediately after collection and kept at −40 °C. The urine was hydrolysed with β-glucuronidase/arylsulfatase in the usual manner for corticosteroid analysis.[22,23]

A 50 μl aliquot of urine was mixed with 50 μl of 0.5 mol l^{-1} acetate buffer (pH 5.0) and 8 μl of the enzyme solution. The mixture was incubated for 24 h at 37 °C. After hydrolysis, the urine was poured onto a Bond-Elut C_1 cartridge. The cartridge was washed with 2 ml of water and the adsorbed THALD was eluted with 1.5 ml of aqueous 50% methanol. To the eluate, 1.5 ml of 0.1 mol l^{-1} phosphate buffer (pH 7.0) were added and the mixture was applied to a Sephadex G-25M column. The column was washed with 3 ml of 0.1 mol l^{-1} phosphate buffer (pH 7.0) followed by 4 × 2 ml of the same buffer and this latter 8 ml were collected as containing THALD. The fraction was then poured onto another Bond-Elut C_1 cartridge and the analytes were eluted with 2 ml of aqueous 50% methanol. After 12 ml of diethyl ether had been added to the eluate, the mixture was shaken for 5 min and was then centrifuged for 5 min at 1000*g*. The upper layer (10 ml) was transferred into a screw-capped tube and evaporated to dryness under a stream of nitrogen gas. The residue, dissolved in 100 μl of methanol, was used as a sample solution.

Derivatization Procedure

A 100 μl portion of the sample solution was mixed with 20 μl of the copper(II) acetate solution. The mixture was allowed to stand at room temperature for 1 h, then 80 μl of the DPH solution were added and the mixture was heated at 80 °C for 40 min. After cooling, the mixture was briefly centrifuged at 1000*g* for 5 min and the supernatant was injected into the chromatograph.

The amounts of THALD were calibrated by means of the standard additions method: the acetate buffer solution (50 μl) added to urine was replaced with 50 μl of the buffer solution containing 2.5, 20 and 500 pmol each of THALD. The net peak heights due to THALD were plotted against the concentrations of the spiked THALD.

HPLC and Chemiluminescence Detection System

Fig. 2 shows a schematic diagram of the HPLC–chemiluminescence detection system. Chromatography was performed with a Hitachi (Tokyo, Japan) 655A-11 high-performance liquid chromatograph (P_1) equipped with a Rheodyne 7125 syringe-loading sample injector valve (I) (20 μl loop). Chromatograms were recorded with a SIC chromatocorder (REC) (System Instruments, Tokyo, Japan). The DPH derivatives of THALD and ALD were separated on a TSKgel ODS-120T reversed-phase column (250 × 4.6 mm i.d., particle size 5 μm) (Tosoh, Tokyo, Japan) by isocratic elution with acetonitrile–tetrahydrofuran–10 mmol l^{-1} ammonium acetate (1 + 1 + 8 v/v) as eluent (E). The flow rate of the eluent was 1.0 ml min^{-1}. The column temperature was ambient (18–25 °C).

The eluate from the HPLC column was mixed with the hydrogen peroxide solution by the first T-type mixing device

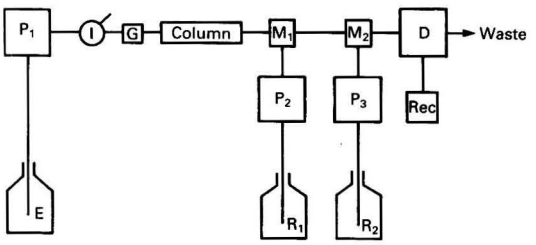

Fig. 2 Schematic flow diagram of the HPLC–chemiluminescence detection system. P_1–P_3, HPLC pumps; I, injection valve (20 μl); D, chemiluminescence detector; G, guard column; Column, TSKgel ODS-120T (250 × 4.6 mm i.d.; 5 μm); M_1 and M_2, mixing devices; Rec, recorder; E, mobile phase; R_1, hydrogen peroxide solution; and R_2, potassium hexacyanoferrate(III) solution. Flow rate: E, 1.0; R_1, 1.0; and R_2, 2.0 ml min^{-1}, respectively

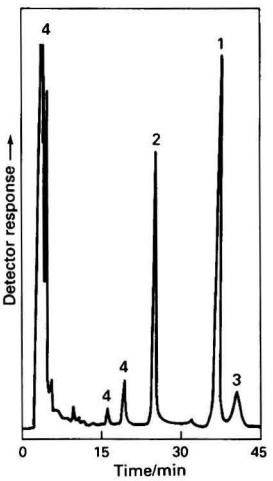

Fig. 3 Chromatogram of DPH derivatives of THALD and ALD. A portion (100 μl) of a standard mixture of THALD (1.0 nmol ml^{-1}) and ALD (5.0 nmol ml^{-1}) was treated according to the derivatization procedure. Peaks: 1 = THALD; 2 = ALD; 3 = by-product from ALD; and 4 = reagent blank

(M_1) and then with the potassium hexacyanoferrate(III) solution by the second T-type mixing device (M_2) delivered by two Hitachi L-6000 pumps (P_2 and P_3). The flow rates of the hydrogen peroxide (R_1) and potassium hexacyanoferrate(III) (R_2) solutions were 1.0 and 2.0 ml min^{-1}, respectively. The generated chemiluminescence was monitored with a Model 825-CL chemiluminescence detector (D) (Jasco, Tokyo, Japan) equipped with a 90 μl flow cell. Stainless-steel tubing (0.5 mm i.d.) was used for the HPLC system.

Results and Discussion

HPLC Conditions

Complete baseline separation of the DPH derivatives of THALD and ALD was achieved using a TSKgel ODS-120T reversed-phase column and acetonitrile–tetrahydrofuran–10 mmol l^{-1} ammonium acetate (1 + 1 + 8 v/v) as the eluent. Fig. 3 shows a typical chromatogram obtained with a standard mixture. The retention times for THALD and ALD were 37.0 and 25.0 min, respectively.

The other 21-hydroxycorticosteroids (cortisone, 18-hydroxycorticosterone, 18-hydroxydeoxycorticosterone, corticosterone, 11-deoxycortisol, deoxycorticosterone, 11-dehydrocorticosterone, 3α,5β- and 3α,5α-tetrahydrocortisol, 3α,5β-tetrahydrocortisone, 3α,5β-tetrahydro-11-deoxycortisol, 3α,5β- and 3α,5α-tetrahydrocorticosterone, 3α,5β- and 3α,5α-tetrahydro-11-deoxycorticosterone, prednisone, prednisolone, dexamethasone, betamethasone and beclomethasone) reacted with DPH to give corresponding derivatives under the present derivatization conditions. However, these derivatives were strongly retained and did not elute under the HPLC conditions used. Hence these compounds did not interfere in the determination of THALD. The HPLC column was washed with acetonitrile–water (3 + 2 v/v) after the analysis every day. Urinary steroids (progesterone, androstendione, pregnenolone, estrone, estradiol and estriol) other than 21-hydroxycorticosteroids did not give chemiluminescence.

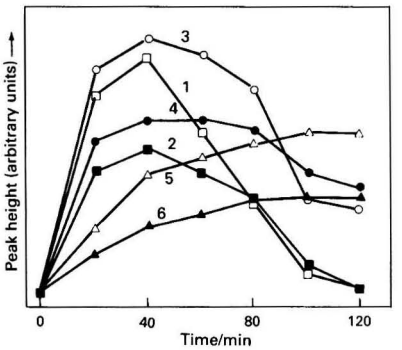

Fig. 4 Effect of reaction time and temperature on the chemiluminescence derivatization with DPH. Temperature: 1 and 2 = 100 °C; 3 and 4 = 80 °C; 5 and 6 = 60 °C. Compound: 1, 3 and 5 = THALD; 2, 4 and 6 = ALD

Derivatization Conditions

Both THALD and ALD are easily oxidized by copper(II) acetate to form the corresponding glyoxal compounds. The oxidation conditions were the same as those described by Görög and Szepesi[19] and Yamaguchi *et al.*[23]

The glyoxal compounds for THALD and ALD reacted with DPH in dilute hydrochloric acid, but not in neutral or alkaline solution; 0.25 mol l^{-1} hydrochloric acid was adopted to give the most intense peaks for the preparation of the DPH solution. β-Mercaptoethanol was used to facilitate the derivatization reaction. The peak heights for both the compounds were maximum at 0.125 mol l^{-1} β-mercaptoethanol in the DPH solution.

The DPH solution gave the most intense and constant peaks at concentrations >6.3 mmol l^{-1}; 7.5 mmol l^{-1} was used as a sufficient concentration. The derivatization reaction proceeded more rapidly as the reaction temperature was increased (60–80 °C). The peak heights became maximum after heating at 80 °C for 40 min. On the other hand, heating at 80–100 °C for more than 60 min caused a decrease in the peak heights. Therefore, heating at 80 °C for 40 min was adopted in the recommended precedure (Fig. 4).

The DPH derivatives in the final mixture were stable for at least 120 h in daylight at room temperature.

Chemiluminescence Reaction Conditions

The optimum chemiluminescence reaction conditions were examined by setting the flow rates of the hydrogen peroxide and potassium hexacyanoferrate(III) solutions at 1.0 and 2.0 ml min^{-1}, respectively. The chemiluminescence intensities were affected by the concentrations of hydrogen peroxide,

potassium hexacyanoferrate(III) and sodium hydroxide. The concentrations of these reagents were varied one at a time to establish the maximum intensity obtainable. Based on these experiments (Fig. 5), concentrations of 40 mmol l^{-1} hydrogen peroxide, 30 mmol l^{-1} potassium hexacyanoferrate(III) and 3.0 mol l^{-1} sodium hydroxide were selected.

Changes in the concentrations of acetonitrile and tetrahydrofuran in the eluent did not affect the peak heights significantly; this means that these organic solvents do not inhibit the chemiluminescence reaction.

The length of tubing between the second mixing device (M_2 in Fig. 2) and the detector affected the detector response. The peak heights increased with decreasing length of the tubing; 5 cm was selected as the shortest length usable.

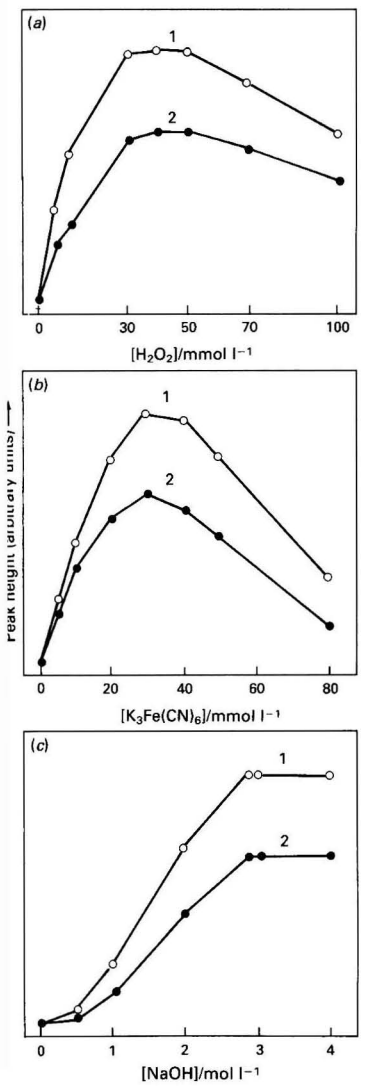

Fig. 5 Effects of (*a*) hydrogen peroxide, (*b*) potassium hexacyanoferrate(III) and (*c*) sodium hydroxide concentrations on the chemiluminescence peak heights. Curves (concentration of the compound): 1 = THALD (1.0 nmol ml^{-1}); 2 = ALD (5.0 nmol ml^{-1})

Determination of THALD in Human Urine

Clean-up of urine

Many large and broad peaks were observed at retention times between 3 and 35 min in the chromatogram obtained with a urine sample treated by conventional liquid–liquid extraction.[23] The peaks might be due to unknown urinary hydrophilic substances that reacted with DPH to give chemiluminescent products. Hence a Bond-Elut C_1 cartridge was used for sample pre-treatment to remove such hydrophilic substances. After the hydrophilic substances had been washed with 2 ml of water, the retained corticosteroids were effectively eluted with 1.5 ml of aqueous 50% methanol. The eluate was then applied to a Sephadex G-25M column to remove macromolecules such as proteins. The contaminants were eliminated from the column by washing with 3 ml of 0.1 mol l^{-1} phosphate buffer (pH 7.0), and the analytes were then eluted with 8 ml of the same buffer. Finally, in order to concentrate the sample, the eluate was applied to another Bond-Elut C_1 cartridge; THALD was successfully collected with a small amount of aqueous 50% methanol (2 ml) and was extracted with diethyl ether.

Chromatography

Figs. 6 and 7 show the chromatograms obtained with urine samples from a healthy volunteer and a patient with primary aldosteronism, respectively. The peak for THALD (retention time 37.0 min) was successfully separated from those of unknown urinary substances. The identification was carried out on the basis of the retention time in comparison with the standard compound, and co-chromatography with the standard using 10–25% v/v acetonitrile as eluent. When the oxidation step with copper(II) acetate was omitted, only peak 1 disappeared completely from the chromatogram (Figs. 6 and 7). These results indicate that peak 1 in Figs. 6 and 7 is the chemiluminescent derivative of THALD.

Aldosterone could not be measured precisely because its concentrations in urine were estimated to be 10–100 times less than those of THALD.

Linearity, Detection Limit, Recovery and Precision

A linear relationship was observed between the peak heights and the amounts of THALD added to urine, up to at least 10

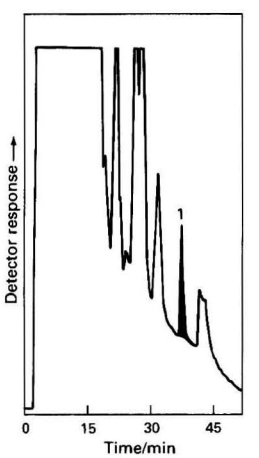

Fig. 6 Chromatogram obtained with healthy human urine. A portion (50 µl) of the urine sample (43.55 µg d^{-1}) was treated according to the procedure. Peaks: 1 = THALD; others = unknown endogenous substances in human urine and reagent blank. The shaded area disappeared when the oxidation step with copper(II) acetate was omitted

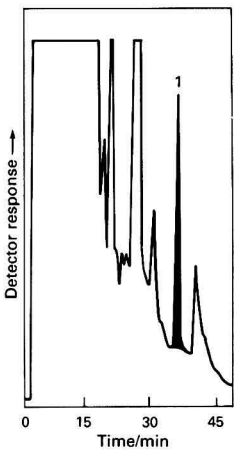

Fig. 7 Chromatogram obtained from a patient with primary aldosteronism. A portion (50 μl) of the urine sample (98.13 μg d^{-1}) was treated according to the procedure. Peaks: as in Fig. 6. The shaded area disappeared when the oxidation step with copper(II) acetate was omitted. The detector sensitivity was the same as that in Fig. 6

nmol (3.6 μg) ml^{-1}; the correlation coefficient of the calibration graph was >0.998. The linear range and correlation coefficient were independent of the urine used. The detection limit for THALD was 0.6 pmol (220 pg) ml^{-1} in urine [corresponding to 1.5 fmol (0.53 pg) per 20 μl injection volume] at a signal-to-noise ratio of 3. The detection limit in the urine matrix was determined by calculating the ratio of the peak height from the endogenous THALD and noise width. A recovery test was performed by adding 50 pmol of THALD to hydrolysed urine. The recovery of THALD was 56.9 ± 2.6% (mean ± standard deviation, $n = 7$); the main loss of THALD may be due to adsorption on the Sephadex G-25M column.

The within-day precision of the method was established by repeated determinations ($n = 7$) using normal human urine containing 24.87 μg d^{-1} (70.0 pmol ml^{-1}) of THALD. The relative standard deviation was 4.4%.

Urinary Excretion (24 h) of THALD From Healthy Volunteers and a Patient With Primary Aldosteronism

The urinary excretion of THALD from healthy volunteers and a patient with primary aldosteronism was determined by the proposed method (Table 1). The concentration of THALD from a patient with primary aldosteronism was about 2–5 times higher than those from normal subjects. The mean value and its standard deviation for THALD from healthy subjects were in good agreement with those obtained by other workers (Table 2). In comparison with the RIA and GC–MS methods in Table 2, the proposed method has sufficient selectivity and sensitivity for the determination of THALD in human urine. Moreover, the method does not require radioactive compounds and can be performed in conventional laboratories. One major problem with the method is the failure of internal standardization; we could not find a suitable compound among corticosteroids to use as an internal standard. However, good precision was obtained even using the standard additions method.

This study provides the first practical and sensitive HPLC method with chemiluminescence detection for the determination of THALD in a small volume of human urine (50 μl), and should be useful for biological and biomedical investigations of THALD. The method could be applicable to the determination of ALD in plasma, if the method gives complete separation of ALD from endogenous interfering substances; further studies are continuing.

Table 1 Urinary excretion (24 h) of THALD from healthy volunteers and a patient with primary aldosteronism

Subject	Age	Sex*	THALD/ μg d^{-1}†
Normal	21	F	24.39
	22	F	19.77
	22	F	41.09
	21	M	54.34
	21	M	20.54
	21	M	31.62
	22	M	43.55
	23	M	44.28
	23	M	61.73
	23	M	24.87
	26	M	20.68
	32	M	54.61
			Mean: 36.71
			SD: 14.35
Primary aldosteronism	63	F	98.13

* F, female; M, male.
† Duplicate determinations.

Table 2 Comparison of urinary excretion (24 h) of THALD from normal subjects obtained with the proposed HPLC and other methods

Method	Ref.	No. of subjects	THALD concentration/ μg d^{-1} (mean ± SD)
RIA	5	45	53.3
RIA	6	12	25.88 ± 16.50
RIA	7	43	29.1 ± 12.8
RIA	13	8	36.9 ± 9.5
GC–MS	12	20	34.16 ± 23.98
HPLC	This work	12	36.71 ± 14.35

The authors are grateful to Dr. M. Nakamura (Faculty of Pharmaceutical Sciences, Fukuoka University) for helpful suggestions and T. Ueda for his skilful assistance. The authors thank Dr. M. Haji, School of Medicine, Kyusyu University, for the supply of a urine sample from a primary aldosteronism patient.

References

1 Ulick, S., Laragh, J. H., and Lieberman, S., *Trans. Assoc. Am. Physicians*, 1958, **71**, 225.
2 Flood, C., Layne, D. S., Ramcharan, S., Rossipal, E., Tait, J. F., and Tait, S. A., *Acta Endocrinol.*, 1961, **36**, 237.
3 Cope, C. L., Nicolis, G., and Fraser, B., *Clin. Sci.*, 1961, **21**, 367.
4 Bauknecht, H., Vecsei, P., Endres, H., and Hattenbach, A., *Am. J. Obstet. Gynecol.*, 1982, **144**, 28.
5 Delassalle, A., Cesselin, F., Carayon, S., Legrand, S., Antreassian, J., Lagoguey, A., Legrand, J. C., and Desgrez, P., *Steroids*, 1977, **29**, 725.
6 Kohl, K. H., Vecsei, P., and Abdelhamid, S., *Acta Endocrinol.*, 1978, **87**, 596.
7 Gomez-Sanchez, C. E., and Holland, O. B., *J. Clin. Endocrinol. Metab.*, 1981, **52**, 214.
8 Lewicka, S., and Vecsei, P., *Clin. Endocrinol.*, 1985, **22**, 123.
9 Posadas, C., Blair, A. J., Jr., and McCann, D. S., *Clin. Chim. Acta*, 1973, **45**, 299.
10 Nicolis, G. L., Wotiz, H. H., and Gabrilove, J. L., *J. Clin. Endocrinol.*, 1968, **28**, 547.
11 Miyazaki, T., Mizukoshi, H., Fujizaki, M., and Kamidate, T., *Endocrinol. Jpn.*, 1985, **32**, 505.
12 Koopman, B. J., Lokerse, I. J. G., Verweij, H., Nagel, G. T., van der Molen, J. C., Drayer, N. M., and Wolthers, B. G., *J. Chromatogr.*, 1986, **378**, 283.

13 Holland, O. B., Risk, M., Brown, H., Komes, K., Dube, P., and Swann, C., *J. Chromatogr.*, 1987, **385**, 393.
14 Kobayashi, S., and Imai, K., *Anal. Chem.*, 1980, **52**, 424.
15 MacDonald, A., and Nieman, T. A., *Anal. Chem.*, 1985, **57**, 936.
16 Kawasaki, T., Maeda, M., and Tsuji, A., *J. Chromatogr.*, 1985, **328**, 121.
17 Ishida, J., Sonezaki, S., and Yamaguchi, M., *J. Chromatogr.*, 1992, **598**, 203.
18 Porter, C. C., and Silber, R. H., *J. Biol. Chem.*, 1950, **185**, 201.
19 Görög, S., and Szepesi, G., *Anal. Chem.*, 1972, **44**, 1079.
20 Ishida, J., Yamaguchi, M., Nakahara, T., and Nakamura, M., *Anal. Chim. Acta*, 1990, **231**, 1.
21 Williams, R. L., and Shalaby, S. W., *J. Heterocycl. Chem.*, 1973, **10**, 891.
22 Kawasaki, T., Maeda, M., and Tsuji, A., *J. Chromatogr.*, 1982, **232**, 1.
23 Yamaguchi, M., Yoshitake, T., Ishida, J., and Nakamura, M., *Chem. Pharm. Bull.*, 1989, **37**, 3022.

Paper 2/02012B
Received April 21, 1992
Accepted July 13, 1992

High-performance Liquid Chromatographic Determination of Selenium in Coal After Derivatization to 2,1,3-Benzoselenadiazoles

Muhammad Y. Khuhawar, Rasool B. Bozdar and Mushtaq A. Babar
Institute of Chemistry, University of Sindh, Jamshoro, Sindh, Pakistan

High-performance liquid chromatography was examined for the determination of selenium after derivatization to 2,1,3-benzoselenadiazoles using 1,2-diaminobenzene, 1,2-diamino-4-nitrobenzene (NDAB), 2,3-diaminonaphthalene and 3,3′-diaminobenzidine as derivatizing agents. Elution was carried out using a mixture of chloroform and hexane, with ultraviolet spectrophotometric detection. The 2,1,3-benzoselenadiazoles were extracted into toluene. Linear calibrations were obtained for 0–4 μg of selenium in 10 cm³ of solution and the detection limits were 20–50 ng of selenium in 10 cm³ of solution. The method was applied to the determination of selenium in coal samples and a shampoo using NDAB as the derivatizing reagent in acidic solution.

Keywords: *High-performance liquid chromatography; selenium determination; coal*

The determination of trace amounts of selenium is of considerable biological and environmental interest.[1,2] A number of analytical methods have been reported, including atomic absorption spectrometry using an air–acetylene flame,[3] electrothermal atomic absorption spectrometry[4–8] and hydride generation atomic absorption spectrometry.[7,8] The most selective methods for the determination of selenium are probably those that involve the solvent extraction of selenium as a 2,1,3-benzoselenadiazole after reaction with 1,2-diaminobenzene and its derivatives (Fig. 1). These methods are mostly based on the use of spectrophotometry,[9–11] spectrofluorimetry[12,13] or gas chromatography (GC)[14,15] for the determination of trace amounts of selenium in a variety of materials. Several methods are available which involve high-performance liquid chromatography (HPLC) with spectrofluorimetric, spectrophotometric or electrochemical detection for the determination of selenium.[16–21] Schwedt and Sehwaz[16] have determined selenium in drinking, lake and drain waters. The selenium in the sample was converted into a 2,1,3-benzoselenadiazole by reaction with 4-chloro-1,2-diaminobenzene and selenium diethyldithiocarbamate and was then determined by HPLC. A limit of detection of 0.3 μg dm^{-3} was reported. Shibata *et al.*[18] have used 2,3-diaminonaphthalene for the determination of selenium by HPLC with spectrofluorimetric detection. They have claimed detection limits at the femtogram level; however, the method suffers from the fact that the reagent has to be purified extensively before use and de-aeration of the eluent (acetonitrile) is necessary.

Selenium is usually present in coal with sulfur as trace constituents. The formation of 2,1,3-benzoselenadiazoles with 1,2-diaminobenzene and its derivatives is useful, because their reaction with selenium(IV) is highly selective, quantitative and yields a stable product. The formation of the 2,1,3-benzoselenadiazoles occurs over a wide range of concentration and pH, and the products have high molar absorptivities in the ultraviolet (UV) region. It was, therefore, considered desirable to examine the reagents 1,2-diaminobenzene (DAB), 1,2-diamino-4-nitrobenzene (NDAB), 2,3-diaminonaphthalene (DAN) and 3,3′-diaminobenzidine (DABZ) for the determination of selenium using HPLC with UV detection. In this work, it was not expected that a similar detection limit to

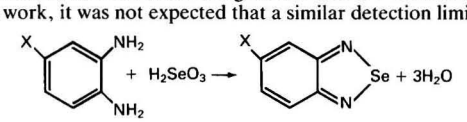

o-Diamine 2,1,3-Benzoselenadiazole

Fig. 1 Reaction of selenium(IV) with aromatic 1,2-diamines

that reported using spectrofluorimetric detection would be achieved, but rather that the developed method would not suffer from background emission, which requires an extensive clean-up procedure. The aim was to obtain a stable background at the wavelength selected for the 2,1,3-benzoselenadiazoles; in addition, the excess reagent should not interfere with the quantitative determination of selenium. The work initially involved the preparation of pure 2,1,3-benzoselenadiazoles in order to optimize the conditions for the quantitative elution of these compounds from the HPLC column. The optimum conditions for the formation of 2,1,3-benzoselenadiazoles in aqueous solution were investigated in order to develop an HPLC method for the determination of selenium.

Experimental

1,2-Diaminobenzene dihydrochloride (Sigma), NDAM (Fluka), 2,3-diaminonaphthalene dihydrochloride (Fluka) and DABZ (Fluka) were used. 2,1,3-Benzoselenadiazole (PS), 5-nitro-2,1,3-benzoselenadiazole (NPS), naphtho[2,3-d]-2,1,3-selenadiazole (BPS) and 5-(3,4-diaminophenyl)-2,1,3-benzoselenadiazole (DAPPS) were prepared from DAB, NDAB, DAN and DABZ, respectively, as described elsewhere.[22,23]

Spectrophotometric studies in chloroform were carried out using a Hitachi Model 220 spectrophotometer in the range 600–240 nm using 1 cm³ quartz cuvettes, against chloroform.

A Hitachi Model 655A liquid chromatograph equipped with a variable-wavelength UV monitor, a Rheodyne Model 7125 injector and a Model 561 recorder or a Model D2500 integrator was used. An Si 100 column (5 μm) (200 × 4.6 mm i.d.). (Hewlett-Packard) was used.

Solutions of the diamines (1% m/v) were freshly prepared in 0.1 mol dm^{-3} hydrochloric acid each week and kept at 5 °C when not in use. A stock standard selenium solution containing 1 mg cm^{-3} of selenium was prepared by dissolving selenium dioxide in 0.1 mol dm^{-3} hydrochloric acid. The working solutions were prepared by appropriate dilution of the stock solution before use.

Extraction Procedure

An aqueous solution (10 cm³) of selenium containing 0.1–4.0 μg of selenium(IV) was transferred into a 50 cm³ separating funnel and the pH of the solution was adjusted to 1–2 with hydrochloric acid. The reagent solution (1% m/v) (2 cm³) (DAB, NDAB, DABZ or DAN) was added and the mixture was kept at room temperature (30 °C) for 40 min. Toluene (2

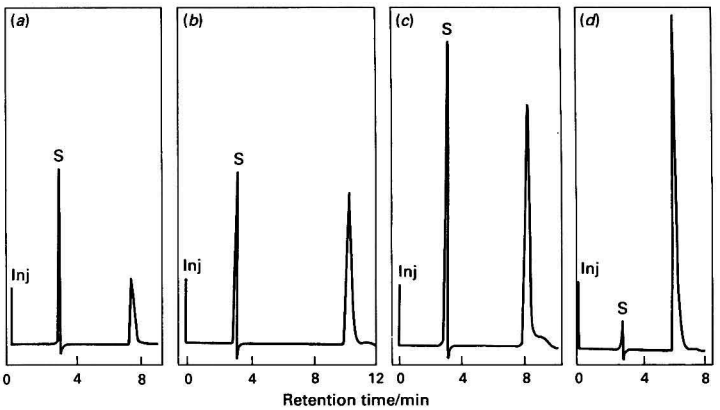

Fig. 2 HPLC traces of (*a*) PS; (*b*) NPS; (*c*) BPS; and (*d*) DAPPS. Column: Si 100 (5 μm) (200 × 4.6 mm i.d.). Eluent for (*a*), (*b*) and (*c*), 10% chloroform in hexane; and for (*d*), 40% chloroform in hexane. Flow rate, 1 cm^3 min^{-1}. Detection, UV at (*a*) 332 nm; (*b*) 343 nm; (*c*) 262 nm; and (*d*) 340 nm

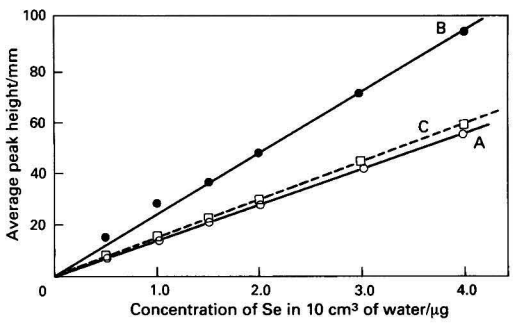

Fig. 3 Calibration graphs for the extraction of selenium using: A, DAB; B, NDAB; and C, DAN as derivatizing reagents. Conditions as in Fig. 2

cm^3) was then added, the mixture was shaken thoroughly and the two layers were allowed to separate. An aliquot (5 mm^3) of the organic phase was injected onto the column, using the optimized conditions for elution.

Analysis of Shampoo

A new bottle of Galorapel Shampoo (Abbott, Karachi, Pakistan) was shaken for 3 min. A sample (2 g) was transferred into a beaker and nitric acid (100 cm^3) was added. The contents were heated gently until most of the oxides of nitrogen had been evolved and the volume of the solution had been reduced to 1–2 cm^3. Concentrated hydrochloric acid (10 cm^3) was added to the residue and the mixture was heated on a water-bath for 1 h to reduce selenium(VI) to selenium(IV). The mixture was cooled and the volume was adjusted to 50 cm^3 with water. The solution (0.2 cm^3) was diluted to 10 cm^3 with 0.1 mol dm^{-3} hydrochloric acid, after which 2 cm^3 of 1% m/v NDAB solution were added and the extraction procedure described above was followed. The amount of selenium in the sample was evaluated from a calibration graph prepared from known amounts of selenium.

Analysis of Coal Samples

Coal samples from Lakhra coal mines (Habib and Indus coal mines) were collected at different depths, where digging was being carried out. The sample (0.5–1 kg) was crushed, mixed and sub-divided into four parts. A portion was taken and again sub-divided. A sample (5 g) was then transferred into a beaker and nitric acid (100 cm^3) was added. The contents were heated gently on a hot-plate. Further nitric acid was added, if required, to complete the oxidation. The mixture was concentrated to about 1–2 cm^3, hydrochloric acid (10 cm^3) was added and the contents were heated on a water-bath for 1 h. The solution was filtered and the volume of the filtrate was adjusted to 25 cm.[3] The solution (5 cm^3) was diluted to 10 cm^3 with water, then 2 cm^3 of the NDAB derivatizing reagent (1% m/v) were added and the extraction procedure described above was followed.

Table 1 Analysis of coal samples (Lakhra coal mines)

Name of mine	Depth of sample collection/m	Selenium content/ μg g^{-1}*
Habib	58	2.35 ± 0.04
Habib	29	1.37 ± 0.15
Habib	48	2.05 ± 0.15
Indus	70	1.65 ± 0.17
Indus	58	2.75 ± 0.02
Indus	41	2.05 ± 0.10

* 95% confidence limits (n = 3).

Results and Discussion

The spectrophotometric studies of PS, NPS, BPS and DAPPS were carried out in chloroform to determine the characteristics of the absorption curves of the 2,1,3-benzoselenadiazoles and to establish a suitable wavelength for the determination of selenium by HPLC with UV detection. The 2,1,3-benzoselenadiazoles exhibit a series of high intensity π–π* transitions within the UV region, which could be used for the spectrophotometric detection of a particular species: PS, NPS, BPS and DAPPS have maximum absorbances at 332, 343, 262 and 340 nm, respectivily, with molar absorptivities of 2.9×10^4, 1.8×10^4, 2.2×10^4 and 5.7×10^4 dm^3 mol^{-1} cm^{-1}, respectively. These bands were considered suitable for spectrophotometric detection.

The optimum conditions for the quantitative elution of the 2,1,3-benzoselenadiazoles from the HPLC column were investigated. Solutions of PS, NPS, BPS and DAPPS (0.5 mg cm^{-3}), after appropriate dilution, were injected onto the HPLC column. The 2,1,3-benzoselenadiazoles were eluted with a mixture of chloroform and hexane. It was observed that PS, NPS and BPS exhibited symmetrical peaks with elution in a reasonable time (12 min), when eluted with 10% chloroform in hexane. However, DAPPS required elution with 40% chloroform in hexane (Fig. 2).

In order to examine whether the response of the detector was quantitative for the 2,1,3-benzoselenadiazoles injected, PS, NPS, BPS and DAPPS were injected and the average peak height of at least two injections was determined. Linear calibrations were obtained for 25–900 ng of the 2,1,3-benzoselenadiazoles injected.

The reagents DAB, NDAB and DAN react with selenium(IV) quantitatively to form PS, NPS and BPS, respectively, when an excess of the reagent solution is added. A 2 cm^3 volume of the reagent solution (1% m/v) was therefore added and proved to be adequate. The reaction was found to be complete in 40 min at room temperature (30–35 °C) and pH 1–2 and was used throughout this work.

Linear calibration graphs (Fig. 3), for the extraction and subsequent determination of selenium(IV) by HPLC with UV detection, were obtained for 0.1–4.0 μg of selenium(IV) in 10 cm^3 of water for each of the reagents. The correlation coefficients (r) for DAB, NDAB and DAN were 0.999, 0.979 and 0.998, respectively. The limits of detection (at least three times the background noise) for selenium(IV) were also ascertained, following the extraction procedure, and were found to be 50, 50 and 20 ng of selenium in 10 cm^3 of water using DAB, NDAB and DAN, respectively. Test solutions containing 0.8–3.5 μg of selenium(IV) in a volume of 10 cm^3 were analysed using DAB, NDAB and DAN and the relative error was found to be within 0–10, 0–5 and 0.8–3.2%, respectively.

A shampoo and several coal samples (Lakhra) were analysed in order to determine their selenium content. The amount of selenium in the shampoo was found to be 0.48 ± 0.02% m/v. The amount of selenium in the shampoo as indicated on the bottle was about 0.55% m/v. The results of the determination of selenium in coal samples are summarized in Table 1. The selenium contents in the samples were in the range 1.37–2.75 ± 0.02–0.17 μg g^{-1}.

Conclusion

This work has demonstrated that HPLC with UV detection can be used for the determination of selenium after derivatization to 2,1,3-benzoselenadiazoles. The proposed method is in parallel with the reported methods for the determination of selenium using GC.[14]

The 2,1,3-benzoselenadiazoles formed have high molar absorptivities in the UV region and can be quantitatively eluted with a mixture of chloroform and hexane. The analysis of test solutions of selenium with DAB, NDAB and DAN yields a relative error in the range ±0–5%, but the error is slightly higher with DAB. Selenium can be determined in shampoo and coal samples with a relative standard deviation of less than 2.2% (n = 4). A stable baseline was obtained and excess reagent did not interfere with the quantitative determination of selenium.

References

1 Schwaz, K., and Fottoz, C. M., *J. Am. Chem. Soc.*, 1957, **79**, 3292.
2 Rapits, S. E., Kaiser, G., and Tölg, G., *Fresenius Z. Anal., Chem.*, 1983, **316**, 105.
3 Lin, W., Huang, L., Zhaoo, S., Hung, G., Wu, J., and Zhang, L., *Lihua Jianvan Huaxue Fence*, 1989, **25**, 34.
4 Neve, J., Hanocq, M., and Molle, L., *Fresenius' Z. Anal. Chem.*, 1981, **308**, 448.
5 Woo, I. H., Nishyama, H., Hashimoto, Y., and Lee, Y. K., *Bunseki Kagaku*, 1985, **34**, 595.
6 Donaldson, E. M., *Talanta*, 1988, **35**, 633.
7 Welz, B., Melcher, M., and Neve, J., *Anal. Chim. Acta*, 1984, **165**, 131.
8 Bunker, V. W., and Delves, H. T., *Anal. Chim. Acta*, 1987, **201**, 231.
9 Keshavan, B., Nagaraja, P., and Raj, S. S., *J. Indian Chem. Soc.*, 1988, **65**, 507.
10 Kastarka, B., *Mikrochim. Acta, Part I* 1989, 337.
11 Motoharu, T., and Takuji, K., *Talanta*, 1965, **12**, 211.
12 Maher, W. A., *Talanta*, 1982, **29**, 1117.
13 Nakagawa, T., Aoyama, E., Hasegawa, N., Kobayashi, N., and Tanaka, H., *Anal. Chem.*, 1989, **61**, 233.
14 Toei, T., and Shimoishi, Y., *Talanta*, 1981, **28**, 967.
15 Zeng, O., Xu, P., Xiong, G., and Liu, Y., *Talanta*, 1986, **33**, 443.
16 Schwedt, G., and Sehwaz, A., *J. Chromatogr.*, 1978, **160**, 309.
17 Eggers, H., and Russel, H. A., *Chromarographia*, 1988, **9**, 17.
18 Shibata, Y., Masalushi, M., and Keichiro, F., *Anal. Chem.*, 1984, **56**, 1527.
19 Aelvot, C., and Hanocq, M., *Analusis*, 1986, **14**, 523.
20 Hanada, K., and Dallas, R., *Anal. Chem.*, 1988, **60**, 2283.
21 Aelvot, C., and Hanocq, M., *Analusis*, 1989, **17**, 131.
22 Parker, C. A., and Harvey, L. G., *Analyst*, 1961, **86**, 54.
23 Parker, C. A., and Harvey, L. G., *Analyst*, 1962, **87**, 558.

Paper 1/06352I
Received December 19, 1991
Accepted June 9, 1992

On-line Microwave Sample Pre-treatment for Hydride Generation and Cold Vapour Atomic Absorption Spectrometry

Part 1. The Manifold

Dimiter L. Tsalev,* Michael Sperling and Bernhard Welz†
Department of Applied Research, Bodenseewerk Perkin-Elmer GmbH, W-7770 Überlingen, Germany

An analytical system for automated on-line pre-treatment of liquid samples in a microwave oven for flow injection cold vapour and hydride generation atomic absorption spectrometry has been designed and evaluated. The system is based on a focused microwave oven and a new manifold with two coils. A reaction coil and a ballast-load coil are placed and oriented within the digestor in a manner providing a reliable long-term operation and increased reaction time. Samples are mixed with an appropriate oxidation reagent and loaded on an autosampler; all further operations of sample uptake, digestion, measurement, calibration and data processing are performed automatically with a sample throughput rate of 20–40 h^{-1}. For the determination of mercury at ng l^{-1} levels using amalgamation the sample throughput decreased to 7–20 h^{-1}. Introducing hot sample digests into the mercury/hydride system resulted in an increased sensitivity, particularly for peak height absorbance.

Keywords: *Flow injection; on-line sample digestion; microwave digestion; hydride generation atomic absorption spectrometry; cold vapour atomic absorption spectrometry*

Flow injection (FI) is a very efficient approach for introducing and processing liquid samples in atomic absorption spectrometry (AAS).[1] For hydride generation AAS (HGAAS) in particular, there are numerous advantages of the FI approach, such as smaller sample size, higher sample throughput, better tolerance to chemical interferences, improved absolute limits of detection, lower consumption of reagents and ease of automation.[2] Most of these advantages are equally valid for the cold vapour (CV) technique for the determination of mercury. However, the rate-limiting step in these analyses is the sample pre-treatment, which is typically carried out off-line and is aimed at liberating the analyte element from its chemical bonding to the organic matrix and thus transforming all of the analyte species into a well-defined oxidation state, such as Hg^{II}, Se^{IV}, Te^{IV}, As^{III}, Sb^{III}, Bi^{III} and Pb^{IV}. Sample pre-treatment and acid digestion of organic matter are also typically required prior to preconcentration of trace elements from biological and environmental samples for flame or electrothermal AAS.

Microwave digestion was introduced into atomic spectroscopy in 1975 by Abu-Samra *et al.*[3] and has been established during the last decade as a fast and efficient technique for acid digestion of various samples for trace element determination.[4–6]

Microwave ovens could be expected to be ideally suited for FI as they would be able to heat liquids flowing within a non-conductive plastic tubing instantaneously. Surprisingly, however, there are only a few reports on microwave digestion of samples in FI for flame AAS.[7–10] On examining the literature pertinent to on-line sample pre-treatment by microwave,[7–11] resistance oven,[12,13] and thermostatic-bath heating,[14–18] it became apparent that this approach, although very attractive and promising, was not as simple and straightforward, as anticipated. Among the problems faced were: (*i*) inhomogeneity of power distribution within the microwave cavity; (*ii*) short reaction times; (*iii*) incomplete digestion of organic matter; (*iv*) evolution of gases during digestion; (*v*) pressure build-up; (*vi*) disturbance of flow; (*vii*) high percentages of non-absorbed power; and (*viii*) effects of sample composition and mass on power absorption and digestion.

The aim of this study was to design and evaluate an analytical system for automated on-line pre-treatment of liquid samples for FI in combination with CVAAS and HGAAS.

Experimental

Instrumentation

The analytical system was assembled from commercially available instruments and accessories. A Perkin-Elmer Model 2100 atomic absorption spectrometer (Perkin-Elmer, Überlingen, Germany) equipped with a FIAS-200 flow injection system and an AS-90 autosampler was operated by means of an Epson EL 3s personal computer and the data were printed with an Epson LQ-850+ printer. A Maxidigest MX 350 microwave station with TX 31 Maxidigest programmer (Prolabo, Paris, France) and an Ismatec peristaltic pump (Ismatec, Wertheim-Mondfeld, Germany) were incorporated in the FI system, as shown in Fig. 1. An amalgamation

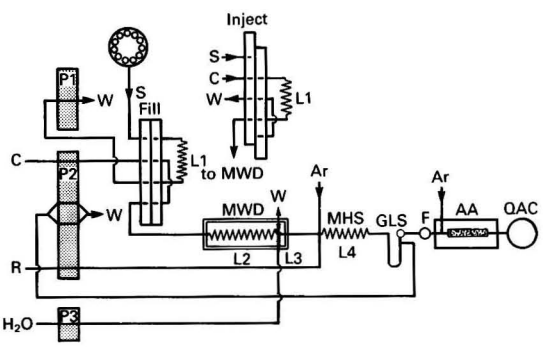

Fig. 1 Schematic diagram of the manifold and the instrumental set-up for on-line microwave digestion and mercury determination using CVAAS. P1 and P2, peristaltic pumps of FIAS-200 system; P3, Ismatec peristaltic pump; L1, sample coil; L2, reaction coil; L3, 'dummy load' coil; L4, MHS reaction coil; MWD, microwave digestor; MHS, mercury/hydride system manifold; GLS, gas–liquid separator; F, filter; AA, amalgamation accessory; S, sample; C, carrier; R, reductant; W, waste; and QAC, quartz absorption cell (for details see text)

* On leave from Faculty of Chemistry, University of Sofia, Sofia 1126, Bulgaria.

† To whom correspondence should be addressed.

Table 1 Flow injection manifold coils, conduits and flow rates

Coil or peristaltic pump tubing	Description
Sample coil (L1)	0.9 mm i.d.; Teflon PFA; 0.5, 1 or 2 ml volume
Reaction coil (L2)	1.07 mm i.d. × 1.7 mm o.d.; PTFE; 10.2 m long
'Dummy load' coil (L3)	1.33 mm i.d. × 1.93 mm o.d.; PTFE; 2.3 m long
MHS reaction coil (L4)	1.0 mm i.d.; PTFE; 10 cm (100 cm for Se)
Sample conduit	2.06 mm i.d., 'violet–violet'; 6.0 ml min^{-1}; 100 rev min^{-1} of P1
Carrier conduit	1.52 mm i.d.; 'blue–yellow'; 8.5 ml min^{-1}; 120 rev min^{-1} of P2
Reductant conduit	1.14 mm i.d., 'red–red'; 6.1 ml min^{-1}; 120 rev min^{-1} of P2
'Dummy coil' conduit	1.30 mm i.d., 'grey–grey'; 3.7 ml min^{-1}; 40 rev min^{-1} of P3
Waste from GLS	Two lines 'violet–violet'; 14.5 ml min^{-1} each; 120 rev min^{-1} of P2

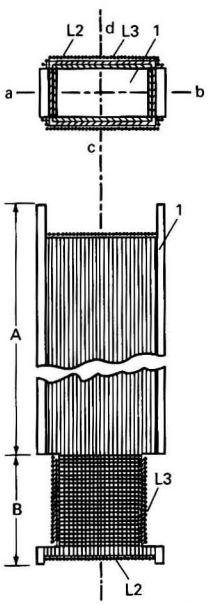

Fig. 2 PTFE shaft (1) with reaction coil (L2) and 'dummy load' coil (L3) wound in two perpendicular planes as detailed in the text. The upper part of the shaft (A) is situated in the chimney of the MWD while the lower part (B) resides within the irradiated zone of the MWD. Two orientations of the shaft within the MWD are possible: a–b ('parallel') and c–d ('perpendicular')

accessory for the FIAS-200 system was used in some determinations of sub-μg l^{-1} levels of mercury. Vessels with samples mixed with reagents were loaded on the sample tray of the AS-90 autosampler. Usually, Tray C with 44 vessels of 50 ml each was used but in most applications sample consumption was only 2–3 ml and a sample tray with higher capacity, *e.g.*, Tray B with 98 test-tubes of 15 ml, could have been employed. Most AAS instrumental parameters were set as recommended by the manufacturer[19] unless given otherwise. The manifold components and flow rates are listed in Table 1. The arrangement of the reaction coil (L2) and the ballast load ('dummy load') coil (L3) within the microwave digestor (MWD) is shown in more detail in Fig. 2.

Between the gas–liquid separator (GLS) and the quartz absorption cell a poly(tetrafluoroethylene) (PTFE) filter holder was placed with a PTFE micropore membrane filter

Table 2 FIAS-200 programme for the determination of hydride-forming elements and mercury without amalgamation. Sample coil L1 = 0.5 or 1 ml

	Time/s		Pump 1/ rev	Pump 2/ rev		
Step	0.5 ml	1 ml	min^{-1}	min^{-1}	Valve position	Read/ s
1	15	30	100	120	Fill	—
2	25	40	—	120	Inject	—
3	50	50	—	120	Inject	0

Table 3 FIAS-200 programme for mercury determination with amalgamation: sample coil, 2 ml; steps 2 and 3 can be repeated 3 or 5 times for higher preconcentration and sensitivity; prefill time, 10 s

						Amalgamation remotes		
Step	Time/ s	Pump 1/rev min^{-1}	Pump 2/rev min^{-1}	Valve position	Read/ s	Heat	Cool	Purge
1	10	120	120	Fill	—	—	On	—
2	30	120	120	Fill	—	—	On	—
3	30	—	120	Inject	—	—	—	On
4	65	—	120	Inject	—	—	—	On
5	12	—	40	Inject	0	On	—	—
6	5	—	120	Inject	—	—	On	On

(0.2 μm; 12 mm diameter, SU 7492, Gore-Tex, W. L. Gore & Associates, Putzbrunn, Germany). In mercury determinations using amalgamation a glass-fibre filter was used (50 mm diameter, SM 134 00-50s, Sartorius, Göttingen, Germany). The argon gas flow rate was 60 ml min^{-1} except in the amalgamation mode where a carrier gas flow rate of 15 ml min^{-1} and a purge gas flow rate of 300 ml min^{-1} were used. Optimized programmes for the determination of the hydride-forming elements and of mercury both with and without amalgamation are given in Tables 2 and 3.

Operation of the System

Liquid samples (urine, environmental waters) are mixed with an appropriate reagent and are loaded on the autosampler tray. With the valve in the 'fill' position the sample coil (L1) is washed and filled with the sample *via* pump 1 (P1). During this step the carrier (C) flows through the MWD and the mercury/hydride system (MHS) manifold.

In the 'inject' step, the sample plug is injected into the carrier stream (C) and passes through the reaction coil (L2) placed within the MWD. The hot effluent from the MWD is merged with the reductant flow (R) and an argon purge gas flow (Ar) in the MHS manifold; this passes through the MHS reaction coil (L4) and enters the GLS. The waste (W) from the GLS is continuously removed by means of pump 2 (P2). The gaseous phase passes through a filter (F) where the aerosol droplets are kept from entering the amalgamation accessory (AA) and/or the quartz absorption cell (QAC). An additional peristaltic pump (P3) provides a continuous flow of de-ionized water through the 'dummy load' coil (L3); this pump is switched on about 20 min before the start of operation and is switched off about 10 min after terminating the MWD heating at the end of measurements. Thus a complete cycle of sampling, pre-treatment in the MWD, vapour generation, amalgamation preconcentration (optional) and measurement proceeds automatically within 90–402 s (depending on the volume of L1 and the FIAS-200 programme).

Temperature Measurements

The temperature of the effluent from the MWD (Figs. 4–6) and in the GLS (Fig. 7) was measured by means of a digital thermocouple thermometer (Impact Tastotherm D 1200, B. Kummer, Freiburg, Germany). The NiCr–Ni thermocouple was inserted in a PTFE sleeve in order to avoid corrosion.

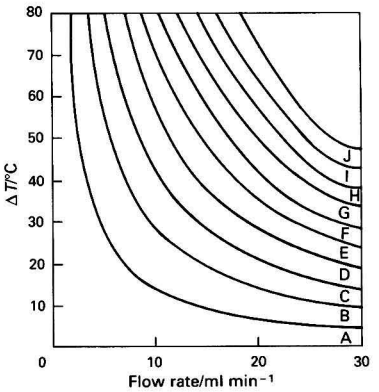

Fig. 3 Theoretical heating pattern of water: temperature increase (ΔT) *versus* the flow rate (F) at different MWD power settings (P), $\Delta T = (14.33 \times P)/F$. A, 10; B, 20; C, 30; D, 40; E, 50; F, 60; G, 70; H, 80; I, 90; and J, 100 W

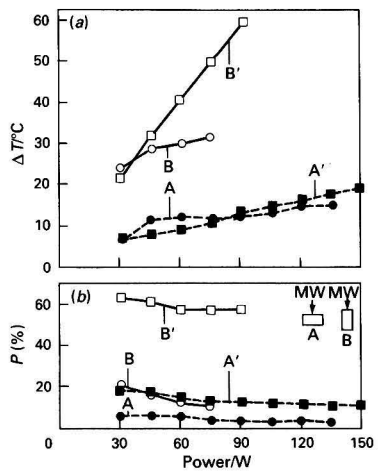

Fig. 4 Heating pattern of the 'dummy' coil. (*a*) Temperature increase (ΔT) due to MW heating; and (*b*) percentage of absorbed power (P%). A, Orientation c–d within the microwave cavity ('perpendicular'); B, orientation a–b ('parallel'). A and B, Flow rate, 3.7 ml min^{-1}; and A′ and B′, flow rate, 12.3 ml min^{-1}

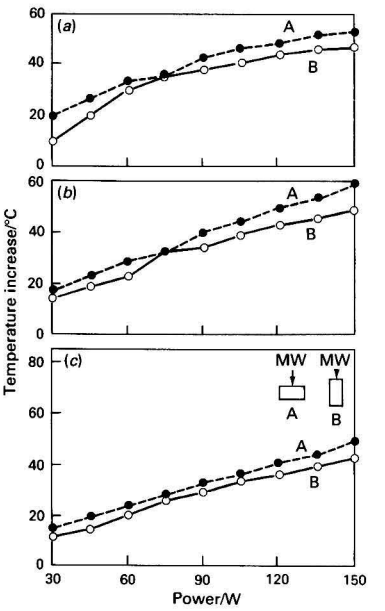

Fig. 5 Heating pattern of the reaction coil (temperature increase, ΔT); (*a*), (*b*) and (*c*), flow rates of 4.7, 15.5 and 24.3 ml min^{-1}, respectively. A, Orientation c–d within the microwave cavity ('perpendicular'); and B, orientation a–b ('parallel'). Flow rate through dummy coil, 3.7 ml min^{-1}

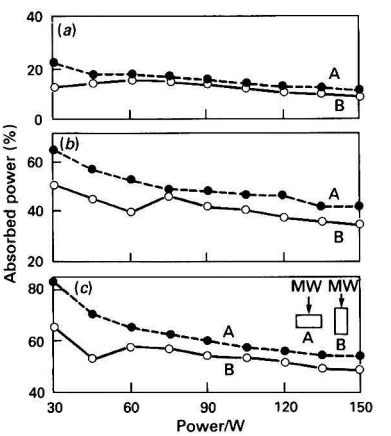

Fig. 6 Heating pattern of the reaction coil (percentage absorbed power). (*a*), (*b*) and (*c*), flow rates of 4.7, 15.5 and 24.3 ml min^{-1}, respectively. A, Orientation c–d within the microwave cavity ('perpendicular'); and B, orientation a–b ('parallel'). Flow rate through dummy coil, 3.7 ml min^{-1}

Reagents

Doubly de-ionized water was used throughout and all reagents were of analytical-reagent grade unless stated otherwise. The composition and concentration of oxidation reagents, reaction media, carrier and reductant are summarized in Table 4. Details will be discussed in Part 2 of this series.[20] Solutions of the sodium tetrahydroborate reductant and of strong oxidants [$K_2S_2O_8$, $(NH_4)_2S_2O_8$, bromination mixture] were prepared daily.

Results and Discussion

Optimization of the Manifold

As the FI manifolds are typically small and most commercial (and especially household) microwave ovens have a rather large irradiated space, the volume ratio of the oven to the reaction coil is unfavourably high and the power absorption inefficient. Moreover, the percentage of non-absorbed power with such small loads is rather high and its reflected portion could damage the magnetron or at least impair its performance. Considering these problems a so-called 'focused microwave digestor' was chosen for this work. It has a small irradiated zone (microwave cavity) approximately 31 mm in height and 48 mm in diameter, *i.e.*, with a volume of only about 56 cm^3. Preliminary experiments with reaction coil L2 reeled on a PTFE shaft and placed entirely within the microwave cavity have shown that the sample solution could be brought to the boil within 10 s, even at high flow rates and moderate power settings of less than one-third of the full power. This is not surprising if the expected heating pattern of water is considered.[4]

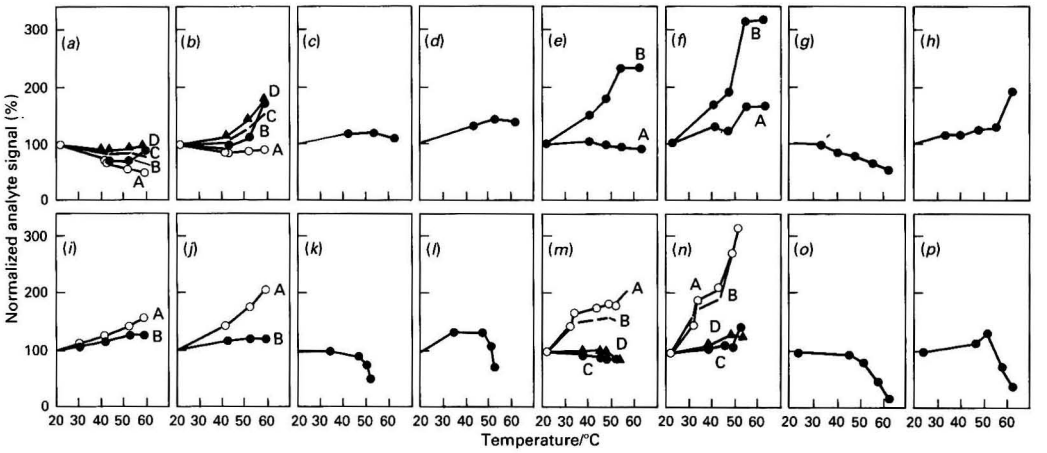

Fig. 7 Effect of temperature measured in the gas–liquid separator on the analyte signal. (*a*) Arsenic peak area, (*b*) arsenic peak height (arsenic species: A, As^{III}; B, As^{V}; C, monomethylarsonate; and D, dimethylarsinate). (*c*) Bismuth peak area, (*d*) bismuth peak height. (*e*) Antimony peak area, (*f*) antimony peak height (antimony species: A, Sb^{III}; and B, Sb^{V}). (*g*) Selenium peak area, (*h*) selenium peak height. (*i*) Mercury peak area, (*j*) mercury peak height (mercury: A, without and B, with amalgamation). (*k*) Lead peak area, (*l*) lead peak height. (*m*) Tin peak area, (*n*) tin peak height (reaction media for stannane generation: A and B, bromination mixture; C and D, peroxodisulfate; and B and D, 1% tartaric acid added). (*o*) Tellurium peak area, (*p*) tellurium peak height

Table 4 Reagents and concentrations used for studying effects of temperature

Analyte	Reaction medium	Carrier/ mol l^{-1}	Concentration of $NaBH_4$ (% m/v*)
As	0.5 mol l^{-1} HCl†	0.5 HCl	0.2
Bi	2.7 mmol l^{-1} $KBrO_3$–13.3 mmol l^{-1} KBr–2 mol l^{-1} HCl	0.1 HCl	0.1
Hg	1.3 mmol l^{-1} $KBrO_3$–6.7 mmol l^{-1} KBr–1 mol l^{-1} HCl	0.1 HCl	0.02
Pb	0.4 mol l^{-1} $(NH_4)_2S_2O_8$–0.015 mol l^{-1} HNO_3–0.01 mol l^{-1} CH_3COOH	0.1 HNO_3	0.2
Sb	1 mol l^{-1} HCl†	1 HCl	0.1
Se	0.1 mol l^{-1} HCl†	0.1 HCl	0.1
Sn	2.7 mmol l^{-1} $KBrO_3$–13.3 mmol l^{-1} KBr–0.01 mol l^{-1} HCl–1% tartaric acid	0.01 HCl	0.1
	or 1% m/v $K_2S_2O_8$–0.01 mol l^{-1} H_2SO_4–1% tartaric acid	0.01 H_2SO_4	0.1
Te	2 mol l^{-1} HCl†	1 HCl	0.02

* 0.05% m/v NaOH added as stabilizer except for mercury, 0.02%.
† No digestion; reaction medium for HG only.

Provided that the efficiency of power absorption is 100%, the increase of temperature (ΔT) of water at a flow rate of F (ml min^{-1}) could be expressed as

$$\Delta T = \frac{14.33 \times P}{F}$$

where P is the absorbed power in watts. This theoretical heating pattern of water is shown in Fig. 3. At flow rates of about 10 ml min^{-1}, which are common in CVAAS and HGAAS, aqueous samples could be heated to 80–90 °C within 3–4 s using a power of only 40–50 W.

In order to solve the problem with these short reaction times, we have adopted a construction with two coils, a reaction coil L2 and a ballast coil (the dummy load coil) L3, wound and situated in a different manner within the MWD, as shown in Fig. 2. The PTFE shaft (280 × 38 × 15 mm), with the two coils, was placed vertically within the cavity and the chimney of the MWD. The PTFE tubing of L2 and L3 was wound in two perpendicular directions. Two rows of the L3 tubing were wound around the lower part of the PTFE shaft, which was machined as a reel. This coil was expected to be in good thermal contact with the shaft and to absorb part of the incident microwave power, thus providing a ballast load (the dummy load) for the microwave digestor and a thermal and load buffer. The reaction coil L2 was wound along the PTFE shaft in such a manner that only part of the coil (about 14%) was situated within the microwave cavity. Thus the sample flow spent only a short time in the irradiated zone (about 0.35 s), then travelled along the PTFE shaft in the chimney part of the MWD and again back into the MWD cavity. This process was repeated 18 times, which is the number of rows of L2. In this way, the reaction time was increased to 46 s, whereas the actual irradiation time was confined to only 6.3 s (at a carrier flow rate of 8.5 ml min^{-1}, which was the optimum for this system).

It is noteworthy that there were two rotational positions of the shaft within the irradiated zone that entailed somewhat different heating patterns (see Figs. 4–6). Orientation 2 (a–b, parallel) was preferred and adopted in further work because of the better absorption of microwave power by the flow of the dummy coil. As can be seen in Fig. 4, about 10–20% of the incident power was absorbed at a flow rate of 3.7 ml min^{-1} and up to 60% at a flow rate of 12.3 ml min^{-1}. The lower flow rate of 3.7 ml min^{-1} was used in all further work. Thus the dummy coil provided a constant ballast load for the MWD that was highly independent of the heating of the reaction coil and helped to reduce the non-absorbed, reflected power.

The maximum power available with this MWD was 300 W and power settings in excess of 90–120 W resulted in pronounced bubble formation and flow disturbances through both coils. A better tolerance to bubble formation was observed at higher flow rates. Under analytical conditions the heating of the carrier and of the sample zone obviously depended also on the chemical composition of the solution.

The manifold, and particularly the long reaction coil, contributed significantly to the dispersion in the system. The peak height sensitivity, when using a sample loop L1 of 1 and 0.5 ml, was decreased by a factor of 2 and 4, respectively. Therefore, a 1 ml sample volume was preferred for all further work. In practice, the sample consumption was about 3-fold

higher because the sample loop was rinsed with the sample during step 1 of the FIAS-200 programme. Employing a large filter and filter holder (50 *versus* 12 mm) entailed an additional 2-fold decrease of peak height sensitivity and was hence incorporated in the system only for mercury determinations using amalgamation.

Effect of Temperature on the Analytical Signal

The elevated temperature of the effluents from the MWD had some positive effects, but also caused some problems. The temperature of the sample plug was between 50 and 90 °C, and hence some 5–20 °C higher than the temperature of the carrier. Measurements of the carrier temperature over time indicated fluctuations between ±1 and ±3 °C, probably due to an inhomogeneous distribution of microwaves in the irradiated zone and/or non-smooth coupling of the microwave power with the transported liquid. This could be expected to contribute to an impaired precision of measurements, as observed for high power settings in the peak-height mode.

A pronounced effect of temperature on analytical signals was found in HGAAS and CVAAS as is shown in Fig. 7. These observations are in agreement with published data which show that heating of the reaction vessel[21–24] or of the gas–liquid separator[21,25] has a positive effect on the sensitivity of As,[22,25] Hg,[23] In,[24] Sb[21,22] and Se.[21] Cooling below room temperature on the other hand was reported to improve the performance for elements with thermally unstable hydrides such as bismuth[22,26,27] and thallium.[24] The temperature effects shown in Fig. 7 could be explained by improved hydride generation kinetics and better stripping of gaseous products from the solution in the GLS. Indeed, the temperature effects were more pronounced with analyte species that exhibited kinetic problems in hydride generation, such as As^{V}, Sn^{IV} and with less volatile hydrides such as methylated arsenic species. On the other hand the picture was possibly complicated by side effects such as partial decomposition of less stable hydrides of Bi, Pb and Te, or by hydrolysis of hydrides with more acidic character such as H_2Se and H_2Te. Finally it must be kept in mind that there was a significant *a priori* peak broadening and hence loss of peak height absorbance due to the dispersion in the long conduits for on-line sample pre-treatment. The apparent gain in sensitivity of the signals due to heating (as shown in Fig. 7) partly compensated for the previous loss that resulted from the on-line sample pre-treatment. The peaks became sharper, *i.e.*, higher and narrower, which resulted in the improved peak height sensitivity; they were also shifted to earlier appearance times and were thus better located within the integration period of 50 s (the maximum available with the current instrument software). Consequently peak area was measured more accurately and precisely due to better peak sampling. In the determination of mercury, if the amalgamation technique was used, the analyte element was collected on a gold absorber and released instantaneously upon heating. Thus, all the kinetic effects due to dispersion and heating, *etc.*, were eliminated, which is apparent in Fig. 7.

A warm-up time of 15–20 min was needed in order to avoid sensitivity drift during measurements and to improve long-term precision. After 2–3 h of continuous operation the filter became wet and had to be replaced by a dry filter; this operation took less than 1 min and could be performed during a blank run even without turning the system off.

More details on the chemistry of sample pre-treatment and applications of the system will be given in Part 2 of this series.[20] The application to mercury determination in urine and environmental waters is described elsewhere.[28]

Conclusion

The proposed manifold for on-line sample pre-treatment with two coils, a reaction and a ballast-load coil, placed in the microwave oven provided two main features: a stable and reliable long-term operation and an increased reaction time of the sample in the MWD. Microwave heating was found to be highly compatible with HGAAS and CVAAS techniques. Introducing hot samples into the MHS manifold compensated at least in part for the peak broadening and loss of peak height sensitivity due to dispersion in the long conduits for on-line sample pre-treatment. These effects were most pronounced for analytes in higher oxidation states such as As^{V}, Sb^{V} and Sn^{IV}. At high power settings, however, there were increasing problems with aerosol formation and impaired precision of (peak height) measurements.

References

1 *Flow Injection Atomic Spectroscopy*, ed. Burguera, J. L., Marcel Dekker, New York and Basel, 1989.
2 Welz, B., and Schubert-Jacobs, M., *At. Spectrosc.*, 1991, **12**, 91.
3 Abu-Samra, A., Morris, J. S., and Koirtyohann, S. R., *Anal. Chem.*, 1975, **47**, 1475.
4 *Introduction to Microwave Sample Preparation: Theory and Practice*, eds. Kingston, H. M., and Jassie, L. B., American Chemical Society, Washington, DC, 1988.
5 Matusiewicz, H., and Sturgeon, R. E., *Prog. Anal. Spectrosc.*, 1989, **12**, 21.
6 de la Guardia, M., Salvador, A., Burguera, J. L., and Burguera, M., *J. Flow Injection Anal.*, 1988, **5**, 121.
7 Burguera, M., Burguera, J. L., and Alarcón, O. M., *Anal. Chim. Acta*, 1986, **179**, 351.
8 Burguera, M., Burguera, J. L., and Alarcón, O. M., *Anal. Chim. Acta*, 1988, **214**, 421.
9 Carbonell, W., de la Guardia, M., Salvador, A., Burguera, J. M., and Burguera, M., *Anal. Chim. Acta*, 1990, **238**, 417.
10 Haswell, S. J., and Barclay, D., *Analyst*, 1992, **117**, 117.
11 Ninkamp, S., and Schwedt, G., *Anal. Chim. Acta*, 1990, **236**, 345.
12 Appleton, J. M. H., Tyson, J. F., and Mounce, R. P., *Anal. Chim. Acta*, 1986, **179**, 269.
13 Aoyagi, M., Yasumasa, Y., and Nishida, A., *Anal. Chim. Acta*, 1988, **214**, 229.
14 Korenaga, T., and Ikatsu, H., *Analyst*, 1981, **106**, 653.
15 Goto, M., Shibakawa, T., Arita, T., and Ishii, D., *Anal. Chim. Acta*, 1982, **140**, 179.
16 Korenaga, T., and Ikatsu, H., *Anal. Chim. Acta*, 1982, **141**, 301.
17 de Andrade, J. C., Rocha, J. C., and Baccan, N., *Analyst*, 1984, **109**, 645.
18 Birnie, S. E., *J. Autom. Chem.*, 1988, **10**, 140.
19 *Recommended Analytical Conditions for the Perkin-Elmer FIAS-200, Applied Atomic Spectroscopy 2.3 E*, Bodenseewerk Perkin-Elmer, Überlingen, 1989.
20 Tsalev, D. L., Sperling, M., and Welz, B., *Analyst*, 1992, **117**, 1735.
21 Goulden, P. D., and Brooksbank, P., *Anal. Chem.*, 1974, **46**, 1431.
22 Fujita, K., and Takada, T., *Talanta*, 1986, **33**, 203.
23 Carillo, F., Bonilla, M., and Cámara, C., *Microchem. J.*, 1986, **33**, 2.
24 Yan, D., Yan, Z., Cheng, G., and Li, A., *Talanta*, 1984, **31**, 133.
25 Pierce, F. D., Lamoreaux, T. C., Brown, H. R., and Fraser, R. S., *Appl. Spectrosc.*, 1976, **30**, 38.
26 Dong, S. L., *Anal. Chem.*, 1982, **54**, 1682.
27 Crock, J. G., *Anal. Lett.*, 1986, **19**, 1367.
28 Welz, B., Tsalev, D. L., and Sperling, M., *Anal. Chim. Acta*, 1992, **261**, 91.

Paper 2/01928K
Received April 13, 1992
Accepted July 24, 1992

On-line Microwave Sample Pre-treatment for Hydride Generation and Cold Vapour Atomic Absorption Spectrometry

Part 2.* Chemistry and Applications

Dimiter L. Tsalev,† Michael Sperling and Bernhard Welz‡
Department of Applied Research, Bodenseewerk Perkin-Elmer GmbH, W-7770 Überlingen, Germany

A system for on-line treatment of liquid samples in a microwave oven digestor was evaluated for use with cold vapour (CV) and hydride generation (HG) atomic absorption spectrometry (AAS). Various oxidation mixtures were tested and those based on bromination (bromate–bromide–acid) and peroxodisulfate (persulfate–acid–complexing agent) were found to be compatible with and most appropriate for CVAAS and HGAAS. The composition of reagents and the analytical conditions were optimized for the determination of mercury, arsenic, bismuth, lead and tin in urine and environmental waters. The limits of detection were 0.01 and 0.2 μg l^{-1} for mercury, with and without amalgamation, respectively, 0.5 μg l^{-1} for arsenic, 0.07 μg l^{-1} for bismuth and 0.1 μg l^{-1} for tin and the sample throughput was between 13 and 30 h^{-1}.

Keywords: *Hydride generation and cold vapour atomic absorption spectrometry; on-line sample preparation; microwave digestion; urine analysis; water analysis*

On-line microwave digestion was *a priori* expected to be associated with serious problems. A literature search on sample pre-treatment for trace element determinations revealed that a complete decomposition of organic matter could be achieved only under vigorous conditions using an excess of acid mixtures, high temperature and pressure, long digestion times, the presence of catalysts, *etc.*[1–5] Even pressurized microwave digestion, while dramatically speeding-up the sample decomposition, does not completely oxidize the organic matter if reaction times are short.[5–7] The only examples of on-line microwave digestion for detection by flame atomic absorption spectrometry (AAS) are partial decomposition and homogenization of blood samples in order to facilitate nebulization for the determination of Cu, Fe and Zn[8] and an acid extraction of Pb from slurried powdered samples.[9]

An increase of reaction time up to several minutes and pressurization of the sample plug by means of high-pressure valves and stop-flow conditions could obviously be applied but at the expense of a reduced sample throughput and more complicated hardware. Therefore, only liquid samples of low organic content (urine, water) and a mild oxidation treatment are used here. Attempts to handle samples with high protein content such as milk and blood serum have proved unsuccessful because of the formation of bulky, adhesive precipitates within the manifold.

Fortunately, AAS does not usually call for complete decomposition of the organic matter. All that is required in hydride generation AAS (HGAAS) and cold vapour AAS (CVAAS) is that the analyte element is released from its chemical bond with the matrix and transformed into an ionic or loosely bound species that can be reduced to the hydride or to elemental mercury by the sodium tetrahydroborate reductant. For some hydride-forming elements it is also of importance that they are transformed into a certain oxidation state, such as As^{III}, Sb^{III}, Se^{IV}, Te^{IV} and Pb^{IV}.

The first part of this series described the design and optimization of the flow injection (FI) system for on-line microwave digestion with HGAAS and CVAAS.[10] The aim of this work was to evaluate the system further with the analysis of real samples such as urine and environmental waters. Most attention was given to the HGAAS determination of arsenic, bismuth, lead and tin.

* For Part 1 of this series, see ref. 10.

† On leave from the Faculty of Chemistry, University of Sofia, Sofia 1126, Bulgaria.

‡ To whom correspondence should be addressed.

Experimental

Instrumentation

A Perkin-Elmer Model 2100 atomic absorption spectrometer was used with an automatic system for on-line sample preparation based on FI techniques that have been described in detail in Part 1 of this series.[10] The instrumental parameters for the determination of Hg, Bi, Sn, Pb and As are compiled in Table 1. The programme for the FIAS-200 FI accessory with a sample loop of 1 ml was given in Part 1.[10] Under these conditions the sample consumption was about 3 ml per determination and the sample throughput was around 30 h^{-1}.

Reagents

All reagents were of analytical-reagent grade unless otherwise stated, and doubly de-ionized water (18 MΩ cm^{-1}) was used throughout.

Stock standard solutions (1000 mg l^{-1} of the analyte element) were made up from Titrisol (Merck, Darmstadt, Germany) or Fixanal (Riedel-de Haen, Seelze, Germany) concentrates. The stock solution for Sn^{II} was in 5 mol l^{-1} HCl, the stock solutions for As^{V}, Bi^{III}, Hg^{II} and Pb^{II} were in dilute nitric acid. All stock solutions were further diluted with de-ionized water as appropriate.

Stock solutions of peroxodisulfates were prepared daily and were diluted according to Table 2 prior to the analysis.

Table 1 Instrumental parameters

	Analyte				
Parameter	Hg	Bi	Sn	Pb	As
Wavelength/nm	253.6	223.1	286.3	283.3	193.7
Bandpass/nm	2	2	2	0.7	0.7
HCL* current/mA	—	5	30	—	—
EDL† power/W	6	—	—	10	8
Quartz cell temperature/°C	200	800	900	900	900

* HCL = hollow cathode lamp.
† EDL = electrodeless discharge lamp.

Table 2 Optimum composition of reagents

Analyte	Digestion mixture	Carrier/mol l^{-1}	$NaBH_4$ concentration* (% m/v)
As	2% m/v $K_2S_2O_8$–0.4 mol l^{-1} NaOH	Water	0.2
Bi	2.7 mmol l^{-1} $KBrO_3$–13.3 mmol l^{-1} KBr–2 mol l^{-1} HCl	0.1 HCl	0.1
Hg	1.35 mmol l^{-1} $KBrO_3$–6.65 mmol l^{-1} KBr–1 mol l^{-1} HCl	0.1 HCl or water	0.02
Pb	0.4 mol l^{-1} $(NH_4)_2S_2O_8$–0.015 mol l^{-1} HNO_3–0.01 mol l^{-1} CH_3COOH	0.01 HNO_3	0.2
Sn	2.7 mmol l^{-1} $KBrO_3$–13.3 mmol l^{-1} KBr–9 mmol l^{-1} HCl–1% tartaric acid or 1% m/v $K_2S_2O_8$–0.01 mol l^{-1} H_2SO_4–1% tartaric acid	0.01 HCl 0.01 H_2SO_4	0.1 0.1

* 0.05% m/v NaOH added as stabilizer (except for mercury, 0.02%) and 0.08% of antifoam added in urine analyses (except for mercury, 0.04%).

Potassium peroxodisulfate, $K_2S_2O_8$, was 4% m/v, and ammonium peroxodisulfate, $(NH_4)_2S_2O_8$, was 45.6% m/v (2 mol l^{-1}).

A stock solution of bromination digestion mixture (BDM) was prepared each week by dissolving 2.23 g of $KBrO_3$ and 8.0 g of KBr in 100 ml of water. Samples and standards were prepared to contain 1–4% v/v of BDM, according to Table 2. Upon acidification the BDM evolved bromine, hence solutions were acidified only immediately before their analysis.

Reductant solution was prepared daily from sodium tetrahydroborate, $NaBH_4$ (for Synthesis grade, Riedel-de Haen), according to Table 2 and was stabilized with sodium hydroxide, NaOH. For the analysis of urine, an antifoaming agent (Dow Corning, Antifoam 110 A) was added to the reductant solution.

Results and Discussion

General Characteristics of Oxidation Reagents

The preferred approach in this work was to pre-mix samples with the digestion reagents directly in the autosampler vessels; this was in order to avoid the need for acid-resistant valves and complicated manifolds for merging sample and reagent flows. The general guidelines for selection of oxidation mixtures were: (*i*) high oxidation potential; (*ii*) rapid oxidation; (*iii*) compatibility with HGAAS and CVAAS techniques; (*iv*) stability on storage (at least short-term); and (*v*) no formation of solid reaction products.

Oxidation mixtures based on permanganate ($KMnO_4$), peroxodisulfates [$K_2S_2O_8$ or $(NH_4)_2S_2O_8$], hydrogen peroxide (H_2O_2) and bromate ($KBrO_3$) were tested. Oxidation reagents were acidified or made alkaline, as appropriate, and catalysts, Os^{VIII} or Fe^{II}, were added to some reagents.

Permanganate-based reaction mixtures were abandoned because of their numerous side effects. With this reagent hydrated manganese(IV) oxides were gradually deposited on the surface of sample vessels, conduits and other manifold components, resulting in instability of solutions, adsorption of analytes, cross-contamination and drift in measurements. Moreover, the manifold had to be complicated by an extra channel supplying hydroxylamine hydrochloride to reduce the excess of MnO_4^- and Mn^{IV} before the reaction of the sample flow with $NaBH_4$.

The oxidation mixture of H_2O_2 + Fe^{II} (Fenton's reagent)[2] was found to suppress tin and lead absorbance markedly at elevated temperatures and was, therefore, also abandoned in further work.

Oxidation mixtures based on bromate–bromide[11,12] and peroxodisulfate[2,13,14] have proved most successful and will be discussed further with the individual elements.

Determination of Mercury

The bromination reagent originally proposed by Farey and co-workers[11,12] was adopted with slight modifications in the determination of mercury. A dichromate–nitric acid stabilizer was added to preserve mercury in the samples and the concentration of BrO_3^-–Br^- reagent was increased by a factor of two and four compared with the levels used previously in the analyses of water and urine, respectively. Diluted urine samples contained, for example, 2.7 mmol l^{-1} $KBrO_3$, 13.3 mmol l^{-1} KBr, 1 mol l^{-1} HCl, 50 mg l^{-1} $K_2Cr_2O_7$ and 0.1 mol l^{-1} HNO_3. In this reaction medium, various mercury species (eight compounds were investigated[15]) were oxidized and stabilized in solution probably in the form of Hg^{II}–bromo complexes. The efficiency of this pre-treatment should be expected to be very high, as all organomercurials tested were recovered almost quantitatively, *i.e.*, 92–102% from 1 + 2 diluted urine without amalgamation and 94–111% from 1 + 5 diluted urine with amalgamation. Results for reference urine samples and pre-analysed environmental waters (river, lake, rain) were in good agreement with certified values. The limits of detection (3σ) were about 0.2 μg l^{-1} without amalgamation and 0.01 μg l^{-1} with amalgamation for a 10 ml sample. A detailed account for on-line sample pre-treatment for the determination of mercury has been published elsewhere.[15]

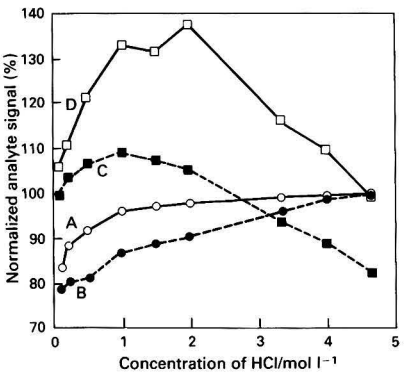

Fig. 1 Effect of HCl concentration on bismuth signal. A and C, integrated absorbance; B and D, peak height absorbance; A and B, without heating; and C and D, heating at 60 W microwave power. Reaction medium: 2.7 mmol l^{-1} $KBrO_3$ and 13.3 mmol l^{-1} KBr in various concentrations of HCl

Determination of Bismuth

A peroxodisulfate oxidation mixture with 2% m/v $K_2S_2O_8$ in 1 mol l^{-1} H_2SO_4 provided a 6–7% better sensitivity compared with the bromination reagent in Bi determinations, but sample solutions with added peroxodisulfate reagent proved to be unstable on storage and the signal began to drop within less than 30 min. This effect could be due to oxidation of Bi^{III} to Bi^{V} and hydrolysis of Bi^{V} species. Therefore, bromination treatment was preferred for further evaluation.

The effect of the acid concentration on the analyte element signal is shown in Fig. 1. Heating at a microwave power of 60 W (approximately 55 °C measured in the gas–liquid separator) caused a shift of the signal maximum to lower HCl concentrations: from about 3 to 1 mol l^{-1} HCl using integrated absorbance for signal evaluation, and from >4 to 2 mol l^{-1} HCl using peak height absorbance. This could be an indication of kinetic problems with the generation of bismuthine (BiH_3) and its stripping from solution. Elevated temperatures could be expected to cause two opposite effects: improved kinetics of bismuthine generation but also an increased decomposition rate of BiH_3, which is known to be among the thermally unstable hydrides.[16] This might well be the reason for the observed dependence of the analytical signal on the applied microwave digestion (MWD) power (Fig. 2). The peak height absorbance was more strongly affected than the integrated absorbance; the height-to-area ratio increased slightly (about 1.2-fold) but only up to power settings of 45–60 W (<50 °C); above these temperatures the sensitivity and precision were significantly impaired.

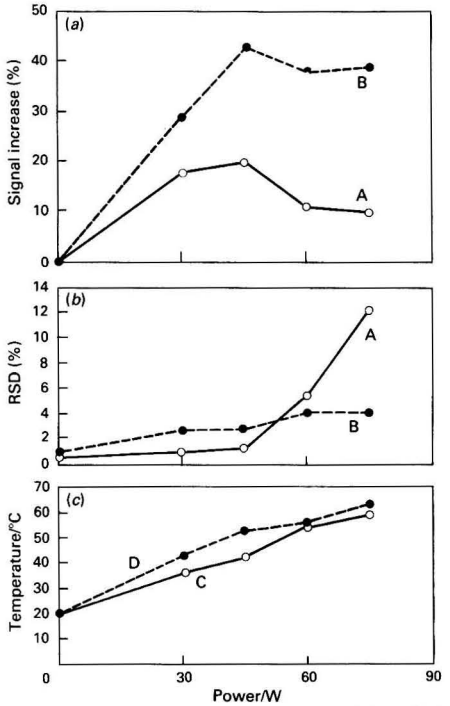

Fig. 2 Effect of the applied microwave power on: (*a*) sensitivity, (*b*) precision and (*c*) temperature of liquid in the GLS. Reagents, 5 μg l^{-1} Bi in BDM and 2 mol l^{-1} HCl. A, Integrated absorbance; B, peak height absorbance; C, mean temperature of the carrier flow (0.1 mol l^{-1} HCl) and D, the maximum temperature of the sample zone (BDM, 2 mol l^{-1} HCl)

Table 3 Recovery test for bismuth; 3.3 μg l^{-1} of Bi added to eight different samples of 1 + 2 diluted urine. Diluent, BDM–HCl; MWD, 60 W

	Recovery (%) ($\bar{x} \pm \sigma$, $n = 8$)	
Acidity of HCl/mol l^{-1}	Integrated absorbance	Peak height absorbance
0.5	97 ± 1	97 ± 3
1.0	96 ± 2	97 ± 3
1.5	96 ± 2	99 ± 2
2.0	95 ± 2	102 ± 3

Urine samples were diluted 1 + 2 or 1 + 3 with the bromination reagent containing 2.7 mmol l^{-1} $KBrO_3$ and 13.3 mmol l^{-1} KBr in 2 mol l^{-1} HCl. Recovery of added bismuth was between 95 and 102% (Table 3) and the limit of detection (3σ) was about 0.07 μg l^{-1} in diluted samples (approximately 0.3 μg l^{-1} in urine).

The precision was tested in a run over 150 min in which four water samples (3–10 μg l^{-1} of Bi) and eight urine samples (spiked with 10 μg l^{-1} of Bi) were analysed repeatedly six times. For the water samples, the relative standard deviations (RSDs) were between 0.8 and 1.7% in integrated absorbance and 1.5–4.6% in peak height absorbance. For the urine samples, the RSDs were 1.0 and 4.0% in integrated and peak height absorbance, respectively.

The bismuth content of 'spot' samples of morning urine from eight male donors was below the detection limit of 0.3 μg l^{-1} of Bi. Analytical results for two certified reference materials, water and urine, were in good agreement with the certified values (Table 4). In conclusion, this technique eliminated the need for lengthy off-line digestions of urine[17,18] and provided improved limits of detection of around 0.3 μg l^{-1} *versus* 2.5 μg l^{-1} obtained with direct HGAAS procedures.[19] The on-line procedure could be applied to monitoring therapy with bismuth-containing pharmaceutical preparations and occupational exposure.[3,4,19] The sample throughput of 30 h^{-1} is fairly competitive with that of electrothermal (ET) AAS procedures.[20,21]

Determination of Tin

The generation of stannane (SnH_4) should be tolerant towards oxidants, as both Sn^{II} and Sn^{IV} are reduced to the hydride,[22,23] and Sn^{IV} is the common oxidation state of inorganic tin in solution. Problems might arise, however, from organically bound tin in environmental waters[23–26] and urine.[23,24,27]

Both oxidation mixtures, the bromination reagent with 2.7 mmol l^{-1} $KBrO_3$ and 13.3 mmol l^{-1} KBr in 10 mmol l^{-1} HCl with 1% tartaric acid, and the peroxodisulfate reagent with 1% $K_2S_2O_8$ in 50 mmol l^{-1} H_2SO_4 with tartaric acid were found to be suitable for the determination of tin. The second reagent proved to be more efficient in the decomposition of organic matter and was preferred for 1 + 1 or 1 + 2 dilutions of urine. As can be seen from the peak shapes in Fig. 3, foaming was less of a problem in the presence of the peroxodisulfate reagent. Erratic peaks were observed with the bromination reagent due to excessive foam formation. Increasing the

Table 4 Determination of bismuth in certified reference materials (in μg l^{-1})

Sample	Reference value	This procedure*
NIST SRM† 1643b Trace Elements in Water	(11)‡	Area: 10.2 ± 0.3 (2.9%; $n = 4$) PKHT: 9.6 ± 0.1 (1.5%; $n = 4$)
Seronorm, batch No. 009024 (Trace Elements in Urine)	24§ 24.2 (22.4–26.0)¶	Area: 25.1 ± 1.7 (6.8%; $n = 5$) PKHT: 24.4 ± 1.4 (5.9%; $n = 5$)

* Mean ± SD (RSD and number of analyses in parentheses); Area = integrated absorbance, PKHT = peak height absorbance.
† NIST SRM = National Institute of Standards and Technology Standard Reference Material.
‡ Information value.
§ Recommended value.
¶ Analytical value (range of all values in parentheses).

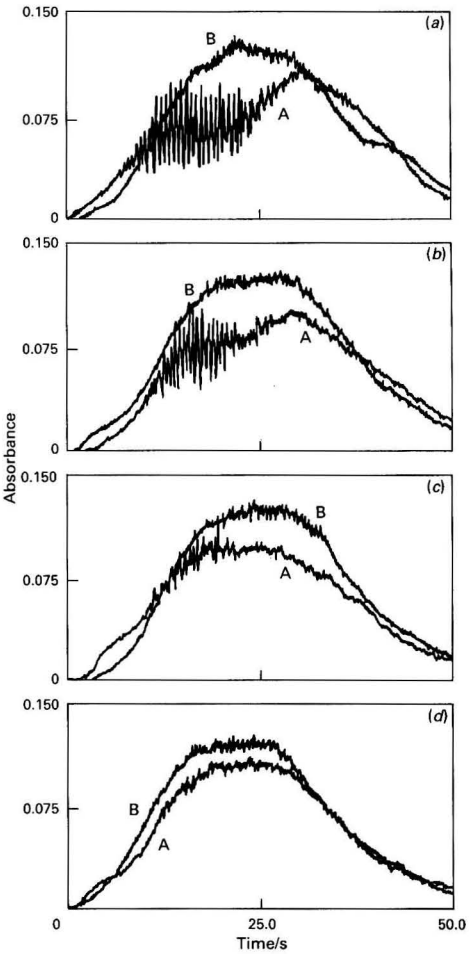

Fig. 3 Effect of foam formation on peak shape for 10 μg l^{-1} Sn added to urine at different dilutions: (*a*) 1 + 1; (*b*) 1 + 2; (*c*) 1 + 3; and (*d*) 1 + 4. Urine diluent: A, BDM + 2% tartaric acid; and B, 2% $K_2S_2O_8$ in 90 mmol l^{-1} H_2SO_4 + 2% tartaric acid. Microwave power, 60 W; pH, 1.7; and reductant, 0.1% $NaBH_4$ + 0.05% NaOH + 0.04% antifoam

concentration of the antifoaming agent added to the $NaBH_4$ reductant up to 0.08% could cure the problem of excessive foam formation when the bromination reagent was used.

A serious problem with stannane generation is the well documented effect of pH on the tin signal (shown in Fig. 4). It was found that the pH was under fairly good control in the presence of 1% tartaric acid. In addition to its buffering action, which facilitates pH adjustment, tartaric acid could also be expected to prevent hydrolysis by complexing Sn^{IV}, the resulting effect being improved hydride generation kinetics.[28] Accordingly, a significant enhancement of peak height sensitivity was observed in the presence of tartaric acid (Fig. 5) and an improved stability of sample solutions on storage.

The determination of tin in urine was complicated by a somewhat different dependence of the signal on the pH of the digestion mixture compared with that of the standard solutions, as can be seen in Fig. 4(*a*). The optimum pH for the determination of tin was about 2.0 for standard solutions (curves A and B) and around 1.6 for urine samples. In addition it was observed that urine samples and standards were adjusted to different pH values upon the addition of the

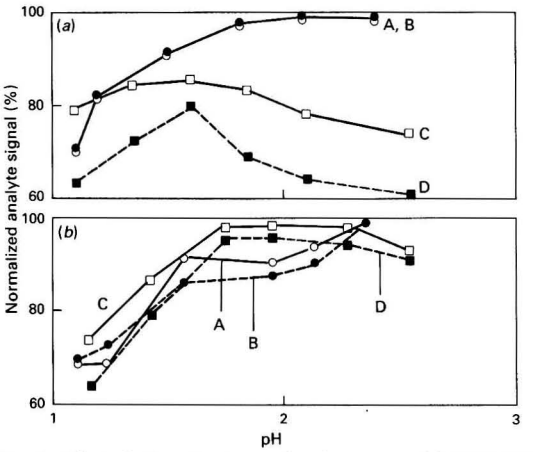

Fig. 4 Effect of pH on tin signal. Digestion reagent: (*a*) BDM (2.7 mmol l^{-1} $KBrO_3$ and 13.3 mmol l^{-1} KBr in 0.01 mol l^{-1} HCl + 1% tartaric acid); and (*b*) 1% $K_2S_2O_8$ in 45 mmol l^{-1} H_2SO_4 + 1% tartaric acid. A and C, integrated absorbance; B and D, peak height absorbance; A and B, standards in digestion reagent; and C and D, 1 + 1 diluted urine in digestion reagent

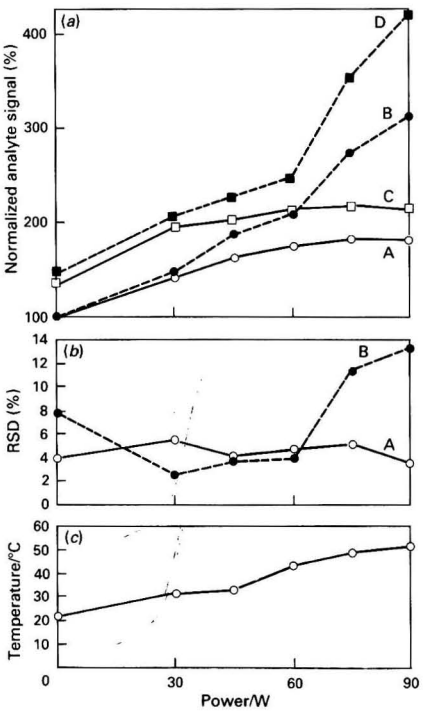

Fig. 5 Effect of the applied microwave power on: (*a*) sensitivity; (*b*) precision; and (*c*) temperature of liquid in the GLS. Reagents, 10 μg l^{-1} Sn in BDM and 0.01 mol l^{-1} HCl. A and C, integrated absorbance; B and D, peak height absorbance; A and B, without tartaric acid; and C and D, with 1% tartaric acid

same amount of reagent, and there were even pH variations among different urine samples. By using the same experimental conditions the pH of 16 urine samples was found to vary between 1.53 and 1.78 with an average and standard deviation of 1.64 ± 0.08, whereas the pH of the standards was within the range 1.42–1.50. An additional complication came from the somewhat different foaming of individual urine samples.

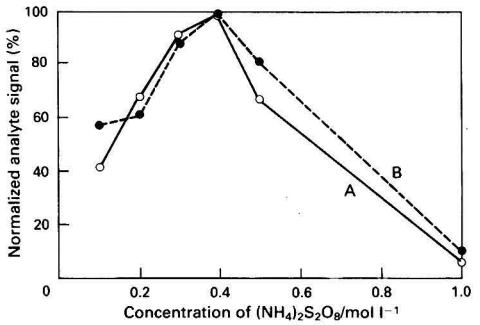

Fig. 6 Effect of the oxidant concentration on: A, integrated absorbance; and B, peak height absorbance signal, for lead in 0.01 mol l^{-1} HNO_3 without heating

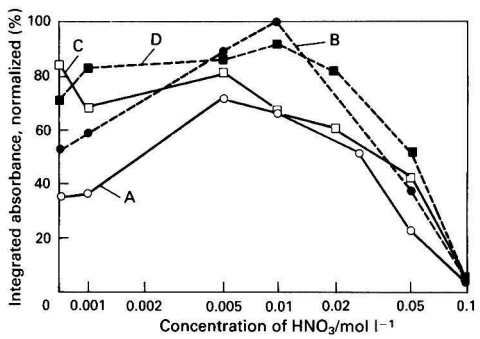

Fig. 7 Effect of nitric acid concentration on the integrated absorbance signal for lead. Concentration of $(NH_4)_2S_2O_8$: A, 0.2; B, 0.3; C, 0.4; and D, 0.5 mol l^{-1} (without heating)

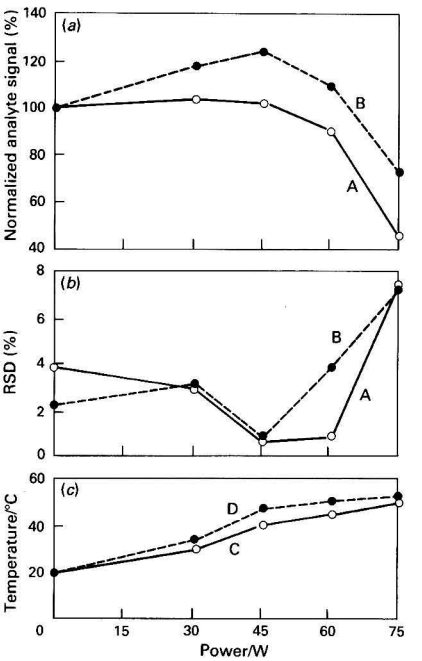

Fig. 8 Effect of the applied microwave power on: (*a*) sensitivity; (*b*) precision; and (*c*) temperature of liquid in the GLS. Reagent, 20 μg l^{-1} of Pb in peroxodisulfate digestion mixture. A, Integrated absorbance; B, peak height absorbance; C, mean temperature of the carrier flow (0.01 mol l^{-1} HNO_3); and D, the maximum temperature of the sample zone

Therefore, in the above example the recovery of tin additions ranged from 76 to 100% in integrated absorbance with an average of 86 ± 7%. Hence it was necessary to carry out standard additions calibration for the determination of tin in urine; this was adopted at the expense of a lower sample throughput rate of about 13 h^{-1}. Precision was also impaired by the calibration procedure and by the substantial blank values corresponding to about 0.4 μg l^{-1} of Sn. The precision for 5–6 measurements within a 2 h run in terms of RSD was 4.6–10% in integrated absorbance and 4.8–5.5% in peak height absorbance at 7–14 μg l^{-1} Sn levels in urine.

A detection limit (3σ) of 0.1 μg l^{-1} of Sn was obtained in 1 + 1 diluted urine. The tin content of 'spot' samples of morning urine from nine male donors ranged from <0.2 to 7.2 μg l^{-1} (mean and standard deviation 2.3 ± 2.4 μg l^{-1}; median 1.4 μg l^{-1}). These levels are in good agreement with previously published values of 1.0 μg l^{-1} (range 0.56–1.6 μg l^{-1}; $n = 11$)[23] and 5.1 ± 1.3 μg l^{-1} (range <2–11 μg l^{-1}; median 5.0 μg l^{-1}; $n = 9$).[29,30]

Determination of Lead

The problems associated with the determination of lead are similar to those with tin, but more severe. Efforts have been made to overcome these difficulties bearing in mind the toxicological and environmental significance of lead monitoring.[3,4] Lead in urine can be both inorganically[27] and organically bound[31] and the various lead species react differently with the $NaBH_4$ reductant.[31–33]

The presence of a strong oxidant in the reaction medium is essential for the determination of lead by HGAAS in order to convert the analyte element into a reactive form, *i.e.*, Pb^{IV}.[34,35] The bromination mixture and the H_2O_2–Fe^{II} reagent were rejected because of their depressive effect on the lead signal. Peroxodisulfate was found to be an appropriate oxidant, in agreement with the literature data.[34,35] Careful optimization of the oxidant concentration (Fig. 6) and of sample acidity (Fig. 7) was found to be essential. It can be assumed that the generation of plumbane is kinetically limited at lower pH whereas hydrolysis of Pb^{IV} can take place at higher pH values.

Sample solutions with added reagents could be better stabilized in the presence of 0.01 mol l^{-1} acetic acid. This stabilization could be explained by complexation of the Pb^{IV} by acetate. Acetic acid at concentrations higher than 0.05 mol l^{-1}, however, strongly suppressed the lead signal.

Microwave heating had a moderate effect on the lead signal (Fig. 8). At a lower setting of 45 W, peak height absorbance increased by a factor of 1.25 and precision was significantly improved. Characteristic concentrations were 0.07 and 0.9 μg l^{-1} in integrated and peak height absorbance, respectively. The relative effect of heating with a microwave power of 45 W (Fig. 9) is most pronounced in peak height absorbance and at low pH. Owing to the thermal instability of plumbane, the applied MWD power should be confined to values around 45 W.

The pH of samples and standard solutions should be contolled within a narrow interval between 1.45 and 1.60 as shown in Fig. 10. The problem with pH control is even more pronounced for the determination of lead than in the determination of tin. Recoveries of lead were also lower than those for tin: a recovery of 52–84% was obtained, for example, from 1 + 2 diluted urine. Addition of a catalyst, such as 5 mg l^{-1} of Os^{VIII},[2] did not improve the efficiency of sample pre-treatment and lead recovery. Higher dilution factors improved the recovery but involved larger errors because of the significant blank values of about 4 μg l^{-1}. The studies on lead were, therefore, terminated at that stage.

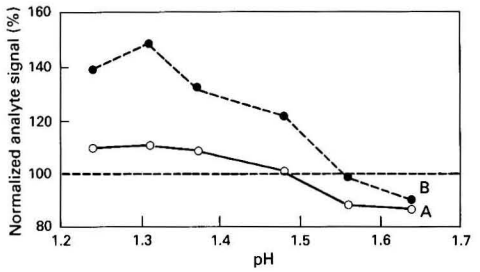

Fig. 9 Relative effect of microwave heating (45 W) on the analyte signal *versus* pH. Absorbance at each point is normalized *versus* non-heating (0 W) conditions ($A_{45W}/A_{0W} \times 100\%$). A, Integrated absorbance; and B, peak height absorbance

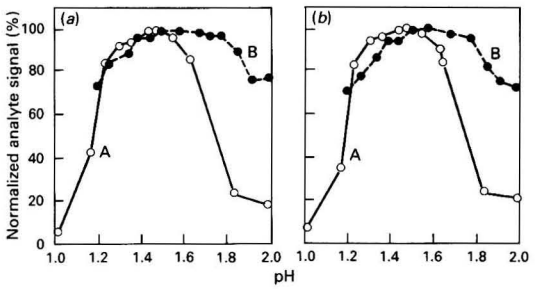

Fig. 10 Effect of pH on lead signal. Digestion reagent: 0.4 mol l^{-1} $(NH_4)_2S_2O_8$ in 0.015 mol l^{-1} HNO_3 and 0.01 mol l^{-1} CH_3COOH. Microwave power 45 W. (*a*) Integrated absorbance; (*b*) peak height absorbance. A, Standards in digestion reagent; and B, 1 + 2 diluted urine in digestion reagent

Determination of Arsenic

Methylated compounds of arsenic are common constituents of biological and environmental materials.[36] They are very resistant to chemical attack[4,37] and are reduced by $NaBH_4$ to the corresponding alkylarsines such as CH_3AsH_2 and $(CH_3)_2AsH$, which do, however, behave very differently compared with inorganic arsenic in respect of their rate of evolution and stripping from solutions.[38] All oxidation mixtures studied in this work failed in the on-line oxidation of monomethylarsonate (MMA) and dimethylarsinate (DMA). The only promising reagent was alkaline peroxodisulfate, which was adapted from recent work of Atallah and Kalman.[14] The optimum composition of the reagent was found to be 2% m/v $K_2S_2O_8$ in 0.4 mol l^{-1} NaOH. At a microwave power of 75 W the characteristic concentrations were 0.052 and 0.87 μg l^{-1} of As^V for integrated and peak height absorbance, respectively. Recoveries for MMA were 116 ± 12% in integrated and 99 ± 10% in peak height absorbance (n = 8). The DMA recoveries were 106 ± 9% in integrated and 94 ± 10% in peak height absorbance for eight measurements within a 2 h run. However, working with an alkaline digestion mixture involved some serious problems: (*i*) mixing of sample and oxidation mixture must be on-line in order to avoid precipitation of urine phosphates on basification; (*ii*) an extra neutralization channel should be introduced into the manifold (2 ml min^{-1} of 5 mol l^{-1} HCl) in order to acidify sample digests before hydride generation; (*iii*) arsenic had to be determined in its pentavalent oxidation state, which was less sensitive by a factor of 4 compared with trivalent arsenic; (*iv*) employment of many reagents contributed to increased blank values of 0.7–1 μg l^{-1} thus impairing the detection limits to about 0.5 μg l^{-1}. Attempts to reduce pentavalent arsenic on-line to its trivalent oxidation state were unsuccessful for urine samples.

Conclusions

The most successful oxidation mixtures for on-line microwave digestion are those containing bromate–bromide and peroxodisulfate. Careful optimization of the digestion mixture was needed for each analyte. Determinations of mercury and bismuth in water and urine were straightforward; lead and tin caused significant problems, which was to be expected, because of their sensitivity to the pH of the solution and because of differences in foaming of individual urine samples. Therefore the standard additions method had to be used for calibration in tin and lead determinations. Modifications of the present manifold are needed in order to perform determinations of arsenic in urine.

References

1 Gorsuch, T. T., *The Destruction of Organic Matter*, Pergamon Press, London, 1970.
2 Bock, R., *A Handbook of Decomposition Methods in Analytical Chemistry*, International Textbook Co., Glasgow, 1979.
3 Tsalev, D. L., and Zaprianov, Z. K., *Atomic Absorption Spectrometry in Occupational and Environmental Health Practice, Analytical Aspects and Health Significance*, CRC Press, Boca Raton, FL, vol. 1, 1983.
4 Tsalev, D. L., *Atomic Absorption Spectrometry in Occupational and Environmental Health Practice, Determination of Individual Elements*, CRC Press, Boca Raton, FL, vol. 2, 1984.
5 *Introduction to Microwave Sample Preparation: Theory and Practice*, eds. Kingston, H. M., and Jassie, L. B., American Chemical Society, Washington, DC, 1988.
6 Pratt, K. W., Kingston, H. M., MacCrehan, W. A., and Koch, W. F., *Anal. Chem.*, 1988, **60**, 2024.
7 Nakashima, S., Sturgeon, R. E., Willie, S. N., and Berman, S. S., *Analyst*, 1988, **113**, 159.
8 Burguera, M., Burguera, J. L., and Alarcón, O. M., *Anal. Chim. Acta*, 1986, **179**, 351.
9 Carbonell, V., de la Guardia, M., Salvador, A., Burguera, J. M., and Burguera, M., *Anal. Chim. Acta*, 1990, **238**, 417.
10 Tsalev, D. L., Sperling, M., and Welz, B., *Analyst*, 1992, **117**, 1729.
11 Farey, B. J., Nelson, L. A., and Rolph, M. G., *Analyst*, 1978, **103**, 656.
12 Farey, B. J., and Nelson, L. A., in *Atomic Absorption Spectrometry*, ed. Cantle, J. E., Elsevier, Amsterdam, 1982, pp. 82–84.
13 Ninkamp, S., and Schwedt, G., *Anal. Chim. Acta*, 1990, **236**, 345.
14 Atallah, R. H., and Kalman, D. A., *Talanta*, 1991, **38**, 167.
15 Welz, B., Tsalev, D. L., and Sperling, M., *Anal. Chim. Acta*, 1992, **261**, 91.
16 Fujita, K., and Takada, T., *Talanta*, 1986, **33**, 203.
17 Rooney, R. C., *Analyst*, 1976, **101**, 749.
18 Froomes, P. R. A., Wan, A. T., Harrison, P. M., and McLean, A. J., *Clin. Chem. (Winston-Salem, N.C.)*, 1988, **34**, 382.
19 Chou, P. P., Jaynes, P. K., and Bailey, J. L., *J. Anal. Toxicol.*, 1984, **8**, 158.
20 Bertholf, R. L., and Renoe, B. W., *Anal. Chim. Acta*, 1982, **139**, 287.
21 Jin, L. Z., and Ni, Z. M., *Can. J. Spectrosc.*, 1981, **26**, 219.
22 Castillo, J. R., and Mir, J. M., *Microchem. J.*, 1989, **39**, 119.
23 Braman, R. S., and Tompkins, M. A., *Anal. Chem.*, 1979, **51**, 12.
24 Weber, G., *Fresenius' Z. Anal. Chem.*, 1985, **321**, 217.
25 Donard, O. F. X., Rapsomanikis, S., and Weber, J. H., *Anal. Chem.*, 1986, **58**, 772.
26 Andreae, M. O., and Byrd, J. T., *Anal. Chim. Acta*, 1984, **156**, 147.
27 Weber, G., *J. Trace Elem. Electrolytes Health Dis.*, 1988, **2**, 61.
28 Mandjukov, P. B., Djarkova, V., and Tsalev, D. L., in *CAS–6, Colloquium Atomspektrometrische Spurenanalytik*, ed. Welz, B., Bodenseewerk Perkin-Elmer, Überlingen, 1991, pp. 597–608.
29 Yokoi, K., Kimura, M., Hirakata, H., Someya, Y., Sekine, K., and Itokawa, Y., *Nippon Eiseigaku Zasshi*, 1987, **42**, 881.
30 Yokoi, K., Kimura, M., Sekine, K., and Itokawa, Y., *Trace Nutr. Res.*, 1988, No. 4, 133.

31 Yamauchi, H., Arai, F., and Yamamura, Y., *Ind. Health*, 1981, **19**, 115.
32 D'Ulivo, A., Fuoco, R., and Papoff, P., *Talanta*, 1986, **33**, 401.
33 Chau, Y. K., Wong, P. T. S., Bengert, G. A., and Dunn, J. L., *Anal. Chem.*, 1984, **56**, 271.
34 Castillo, J. R., Mir, J. M., Martinez, C., Val, J., and Colón, M. P., *Mikrochim. Acta*, 1985, **I**, 253.
35 Castillo, J. R., Mir, J. M., Val, J., Colón, M. P., and Martínez, C., *Analyst*, 1985, **110**, 1219.
36 Braman, R. S., and Foreback, C. C., *Science*, 1973, **182**, 1247.
37 Buchet, J. P., Lauwerys, R., and Roels, H., *Int. Arch. Occup. Environ. Health*, 1980, **46**, 11.
38 Anderson, R. K., Thompson, M., and Culbard, E., *Analyst*, 1986, **111**, 1143.

NOTE—Ref. 10 is to Part 1 of this series.

Paper 2/02108K
Received April 24, 1992
Accepted July 24, 1992

Factorial Design Approach to Microwave Dissolution

A. A. Mohd
School of Applied Sciences, Institut Teknologi Mara, Shah Alam 40000, Malaysia
J. R. Dean* and W. R. Tomlinson
Department of Chemical and Life Sciences, University of Northumbria at Newcastle, Ellison Building, Newcastle upon Tyne, UK NE1 8ST

A fractional factorial design has been used to explore the variables that affect microwave dissolution using perfluoroalkoxy (PFA)-Teflon digestion vessels. Optimum operating conditions for National Research Council of Canada, certified reference material TORT-1 Lobster Hepatopancreas and National Institute of Standards and Technology, Standard Reference Material (SRM) 1575 Pine Needles, were obtained using this procedure. The optimum conditions found for each variable are: 0.25 g sample mass, 6 ml of concentrated hydrochloric acid, 6 ml of concentrated nitric acid, 3 ml of concentrated hydrofluoric acid and 90% microwave power for a total dissolution time of 15 min. Results for Ca, Fe, Cu and Zn in TORT-1 and Ca and Fe in SRM 1575 were in agreement with the certified values.

Keywords: *Fractional factorial design; microwave dissolution; acid digestion; direct current plasma atomic emission spectrometry; biological material*

The elemental analysis of solid samples has traditionally been carried out using wet or dry ashing methods;[1–3] both methods are relatively time consuming. The recent use of microwave heating[4–6] to speed up the dissolution process in both sealed and open vessels is, therefore, advantageous. However, as with every new technique there is the need to investigate the optimum parameters that affect the dissolution process.[7–15] For microwave dissolution the need is to optimize: (*i*) the amount of sample; (*ii*) the type and amount of acid to be used, singularly and in combination; (*iii*) the microwave power; and (*iv*) the time of the dissolution. These operating parameters can be effectively and efficiently optimized using a factorial design approach.[16] Factorial design allows a consideration of the over-all number of experiments and possible interaction effects between the variables. The approach adopted in this paper is based on a fractional factorial design using a parametric model.[16–19]

This paper describes the optimization of a microwave oven dissolution procedure for the analysis of two biological reference materials. Elemental analysis was achieved using a sequential direct current plasma for atomic emission spectrometry.

Experimental

Instrumentation

All reference materials were digested in a microwave oven (Model Floyd RMS-150, PS Analytical, Sevenoaks, Kent, UK). The Floyd RMS-150 system consists of an oven, rotary table, extraction fan, remote control console, power range 0–100% (600 W) and 12 digestion vessels made from perfluoroalkoxy (PFA)-Teflon. The digestion vessels (80 ml capacity) incorporate a double-wall design and use disposable PFA rupture discs to ensure safe operation up to a precise pressure limit of 1380 kPa (200 lb in^{-2}).

The elements Ca, Zn, Cu and Fe were determined using a direct current plasma atomic emission spectrometer (PS Analytical). The slit settings throughout the analysis for all elements were 200 μm (vertical) and 100 μm (horizontal). The emissions of Ca, Cu, Fe and Zn were measured at their optimum wavelengths of 393.3, 324.7, 259.9 and 213.8 nm, respectively. The linear range, linearity and detection limits for all the elements were initially determined using an appropriate concentration of standard solution at the optimum emission wavelength. Touchstone software (PS Analytical) was used for data collection and handling.

Reagents

All chemicals used were of analytical-reagent grade [BDH (now Merck), Poole, Dorset, UK]. Stock standard solutions (1000 μg ml^{-1}) of Ca, Cu, Fe and Zn were prepared from $CaCl_2 \cdot 6H_2O$, $CuSO_4 \cdot 5H_2O$, $Fe(NO_3)_3 \cdot 9H_2O$ and $ZnCl_2$, respectively. Concentrated nitric (70.5%), hydrochloric (35%) and hydrofluoric (48%) acids were used for microwave dissolution. Distilled, de-ionized water from a Millipore system was used for all dilutions. All calibrated flasks and beakers [poly(propylene)] were cleaned by soaking in a 10% nitric acid bath for at least 12 h and thoroughly rinsed in distilled, de-ionized water.

Reference Materials

Validation was carried out using two reference materials, National Research Council of Canada (NRCC) marine biological reference material TORT-1 Lobster Hepatopancreas and National Institute of Standards and Technology (NIST) Standard Reference Material (SRM) 1575 Pine Needles. The reference materials were obtained from the Laboratory of the Government Chemist, Teddington, Middlesex, UK. The reference materials used were primarily intended for evaluating reliability of analytical methods for the determination of major, minor and trace elements in plant and animal materials.

Analytical Protocol

The reference materials were digested according to the experimental design derived as outlined below. The TORT-1 and SRM 1575 were accurately weighed into the PFA-Teflon digestion vessels, which had previously been acid cleaned then thoroughly rinsed with distilled, de-ionized water and dried. To each vessel was added the appropriate volume and combination of acids. The nature of the PFA-Teflon digestion vessels limits the acid choice to concentrated hydrochloric, nitric and hydrofluoric acids.[20] After fitting the rupture discs, all 12 vessels were subjected to microwave power for a pre-selected time period. The microwave oven was always operated with its full complement of 12 digestion vessels.

The digestion vessels were removed and allowed to cool prior to manual venting. The contents of each vessel were then

* To whom correspondence should be addressed.

quantitatively transferred through Whatman No. 40 ashless filter-paper into 50 ml calibrated flasks and made up to the mark with distilled, de-ionized water. The digestion of all samples was carried out in duplicate with two acid blanks included for every acid combination. The blanks were treated in the same way as the samples. To investigate extraction efficiencies and obtain information on recovery levels the samples were spiked with a 1 μg ml^{-1} concentration of each respective element.

Experimental Design

Factorial design is required in order to establish the optimum conditions and also to obtain information about the interrelationships between the variables. The application of a statistical approach using a fractional factorial design and a parametric model to optimize microwave dissolution can both reduce the development time and provide less ambiguous data. The statistically optimized design repertoire and randomized permutation of experiments were obtained using dedicated software.[21] The six variables considered were: (*i*) the total solution volume and sample mass; (*ii*) the volume of concentrated hydrochloric acid; (*iii*) the volume of concentrated nitric acid; (*iv*) the volume of concentrated hydrofluoric acid; (*v*) the microwave oven power; and (*vi*) the time of dissolution. The variable parameters involving the volume of nitric acid were considered at three levels, *i.e.*, 1, 3 and 9 ml, whereas the variable parameters involving the volume of hydrochloric acid, volume of hydrofluoric acid, ratio of total solution volume to sample mass, microwave power and time of dissolution were considered at only two levels, *i.e.*, 1 and 9 ml, 1 and 3 ml, 4 and 84 ml g^{-1}, 30 and 90%, and 5 and 15 min, respectively. The selection of the appropriate operating conditions for each variable is an important consideration for the analyst. Each variable must not be outside the effective operating capabilities of the microwave oven and dissolution vessels. The analyst must consider what is the likely interdependence of the variables prior to generation of the parametric model. This allows a more simple and smaller repertoire of experiments to be considered.

A linear equation representing a response surface containing nine terms was generated:

$$y = B_0 + B_1V_1 + B_2V_2 + B_3V_3 + B_4V_4 + B_5V_5 + B_6V_6 + B_7V_2V_3 + B_8V_5V_6 \quad (1)$$

where y is the response, B_1–B_8 are parametric coefficients, B_0 is the intercept, V_1 is the ratio of total solution volume to sample mass, V_2 is the volume of concentrated hydrochloric acid, V_3 is the volume of concentrated nitric acid, V_4 is the volume of concentrated hydrofluoric acid, V_5 is the microwave power and V_6 is the time of dissolution.

The variable parameters involving acid combinations allowed an insight into their dependence (B_2–B_4) and the necessity for *aqua regia* (B_7). In addition, microwave power and time of extraction (B_8) were investigated because of their interdependence. From the parametric equation, the experimental design software was used to generate 21 sets of statistically significant experiments of variable level combinations. Multilinear regression[22] was used to determine the parametric coefficients (B_n) from eqn. (1), after measurement of the emission response for selected elements.

Table 1 Experimental design repertoire

Sample mass/g	Volume of HCl/ ml	Volume of HNO_3/ ml	Volume of HF/ ml	Power (%)	Time/ min
0.250	9.0	9.0	1.0	30	5
0.750	1.0	3.0	3.0	30	5
0.250	9.0	1.0	3.0	30	15
0.250	9.0	1.0	1.0	90	5
0.750	1.0	9.0	3.0	90	5
0.750	1.0	1.0	1.0	30	15
0.250	1.0	9.0	1.0	30	15
0.750	9.0	9.0	3.0	90	5
0.250	1.0	3.0	3.0	90	15
0.750	9.0	1.0	1.0	90	15
0.250	1.0	1.0	1.0	90	5
0.750	9.0	9.0	1.0	90	15
0.250	9.0	9.0	3.0	30	15
0.250	1.0	9.0	3.0	90	15
0.750	1.0	9.0	1.0	30	5
0.750	9.0	1.0	3.0	30	5
0.250	1.0	1.0	3.0	30	5
0.750	1.0	1.0	3.0	30	15
0.750	1.0	9.0	3.0	30	15
0.750	1.0	1.0	1.0	90	15
0.750	9.0	9.0	3.0	90	15

Results and Discussion

Optimization of Microwave Dissolution

The spectrometer was tuned to obtain maximum sensitivity for each element prior to analysis. Two test elements were

Table 2 Experimental design repertoire analytical results for recovery

Sample number	SRM 1575		TORT-1			
	Fe (%)	Ca (%)	Cu (%)	Zn (%)	Fe (%)	Ca (%)
1	90.4	62.9	100.5	94.9	84.4	106.3
2	82.5	13.2	96.1	79.1	40.9	41.7
3	94.2	64.9	104.1	109.6	90.3	106.6
4	86.4	86.3	87.7	66.1	100.0	102.5
5	86.3	51.7	89.7	96.6	58.6	90.2
6	57.3	11.2	103.2	72.3	68.8	19.7
7	88.3	67.6	59.2	49.2	85.5	46.9
8	86.8	51.2	104.1	77.4	103.2	105.1
9	71.1	72.4	108.9	113.6	61.3	23.0
10	71.9	84.4	101.1	105.1	106.5	102.8
11	59.1	86.3	87.7	51.4	41.4	28.7
12	96.5	82.4	97.9	77.4	93.0	107.4
13	109.5	59.5	99.5	88.7	94.6	101.5
14	99.7	87.1	109.6	98.3	88.7	102.5
15	81.3	53.4	96.8	72.9	66.1	92.3
16	77.9	48.0	104.6	80.2	114.5	95.1
17	76.7	20.5	94.3	61.0	66.7	23.6
18	69.0	9.8	101.4	86.4	38.7	6.6
19	87.9	51.0	110.7	78.5	97.8	101.8
20	49.5	8.0	97.5	99.4	43.0	3.9
21	83.3	98.8	101.6	83.1	113.4	98.3

Table 3 Regression coefficients, determined from eqn. (1), for Ca in TORT-1

Descriptor	Variable	Beta value	Standard error	Parametric coefficient (B_n)	Standard error	$t(11)$	p-level
	Mass	0.065	0.220	0.101	0.342	0.296	0.773
V_1	Volume: mass	0.069	0.296	0.001	0.005	0.232	0.821
V_2	**Volume of HCl**	**1.175**	**0.195**	**0.114**	**0.019**	**6.014**	**0.000**
V_3	**Volume of HNO_3**	**0.958**	**0.181**	**0.096**	**0.018**	**5.292**	**0.000**
V_4	Volume of HF	0.060	0.0868	0.023	0.034	0.696	0.501
V_5	Power	0.022	0.211	0.000	0.003	0.107	0.916
V_6	Time	−0.127	0.189	−0.010	0.015	−0.671	0.516
V_2V_3	**HCl × HNO_3**	**−0.898**	**0.179**	**−0.011**	**0.002**	**−5.004**	**0.000**
V_5V_6	Time × power	0.044	0.271	0.000	0.000	0.163	0.873

Table 4 Regression coefficients, determined from eqn. (1), for Fe in TORT-1

Descriptor	Variable	Beta value	Standard error	Parametric coefficient (B_n)	Standard error	$t(11)$	p-level
	Mass	−0.526	0.320	−0.514	0.312	−1.645	0.128
V_1	Volume: mass	−0.769	0.431	−0.008	0.005	−1.786	0.102
V_2	**Volume of HCl**	**1.543**	**0.284**	**0.094**	**0.017**	**5.432**	**0.000**
V_3	**Volume of HNO_3**	**0.978**	**0.263**	**0.061**	**0.016**	**3.714**	**0.003**
V_4	Volume of HF	0.106	0.126	0.026	0.031	0.837	0.420
V_5	Power	−0.257	0.307	−0.002	0.002	−0.837	0.420
V_6	Time	0.145	0.275	0.007	0.013	0.527	0.609
V_2V_3	**HCl × HNO_3**	**−0.719**	**0.261**	**−0.005**	**0.002**	**−2.758**	**0.019**
V_5V_6	Time × power	0.145	0.394	0.000	0.000	0.367	0.721

Table 5 Regression coefficients, derived from eqn. (1), for Zn in TORT-1

Descriptor	Variable	Beta value	Standard error	Parametric coefficient (B_n)	Standard error	$t(11)$	p-level
	Mass	**1.209**	**0.429**	**0.842**	**0.300**	**2.816**	**0.017**
V_1	**Volume: mass**	**1.739**	**0.577**	**0.014**	**0.004**	**3.009**	**0.012**
V_2	Volume of HCl	−0.394	0.381	−0.017	0.017	−1.034	0.323
V_3	Volume of HNO_3	−0.658	0.353	−0.029	0.016	−1.864	0.089
V_4	Volume of HF	0.300	0.169	0.052	0.029	1.769	0.105
V_5	Power	−0.116	0.411	−0.001	0.002	−0.282	0.783
V_6	Time	−0.406	0.369	−0.014	0.013	−1.099	0.295
V_2V_3	HCl × HNO_3	−0.350	0.350	−0.002	0.002	−1.001	0.338
V_5V_6	Time × power	0.977	0.529	0.000	0.000	1.847	0.092

Table 6 Regression coefficients, derived from eqn. (1), for Cu in TORT-1

Descriptor	Variable	Beta value	Standard error	Parametric coefficient (B_n)	Standard error	$t(11)$	p-level
	Mass	0.665	0.569	0.287	0.246	1.168	0.267
V_1	Volume: mass	0.649	0.766	0.003	0.004	0.848	0.414
V_2	Volume of HCl	−0.222	0.505	−0.006	0.013	−0.439	0.669
V_3	Volume of HNO_3	−0.539	0.468	−0.015	0.013	−1.150	0.274
V_4	Volume of HF	0.451	0.225	0.049	0.024	2.007	0.070
V_5	Power	−0.370	0.546	−0.001	0.002	−0.679	0.511
V_6	Time	−0.409	0.489	−0.009	0.010	−0.836	0.421
V_2V_3	HCl × HNO_3	0.191	0.464	0.001	0.001	0.413	0.687
V_5V_6	Time × power	0.828	0.701	0.000	0.000	1.181	0.262

Table 7 Regression coefficients, derived from eqn. (1), for Ca in SRM 1575

Descriptor	Variable	Beta value	Standard error	Parametric coefficient (B_n)	Standard error	$t(11)$	p-level
	Mass	**−1.069**	**0.289**	**−1.205**	**0.326**	**−3.702**	**0.003**
V_1	**Volume: mass**	**−0.988**	**0.388**	**−0.013**	**0.005**	**−2.546**	**0.027**
V_2	**Volume of HCl**	**1.221**	**0.256**	**0.086**	**0.018**	**4.764**	**0.001**
V_3	**Volume of HNO_3**	**1.104**	**0.237**	**0.080**	**0.017**	**4.649**	**0.001**
V_4	Volume of HF	−0.051	0.114	−0.014	0.032	−0.445	0.665
V_5	Power	0.172	0.277	0.002	0.002	0.622	0.547
V_6	Time	0.083	0.248	0.005	0.014	0.335	0.744
V_2V_3	**HCl × HNO_3**	**−0.642**	**0.235**	**−0.006**	**0.002**	**−2.728**	**0.019**
V_5V_6	Time × power	0.170	0.355	0.000	0.000	0.478	0.642

Table 8 Regression coefficients, derived from eqn. (1), for Fe in SRM 1575

Descriptor	Variable	Beta value	Standard error	Parametric coefficient (B_n)	Standard error	$t(11)$	p-level
	Mass	−0.163	0.293	−0.093	0.168	−0.555	0.590
V_1	Volume: mass	0.214	0.394	0.001	0.003	0.542	0.598
V_2	**Volume of HCl**	**0.599**	**0.260**	**0.021**	**0.009**	**2.303**	**0.042**
V_3	**Volume of HNO_3**	**0.789**	**0.241**	**0.029**	**0.009**	**3.272**	**0.007**
V_4	**Volume of HF**	**0.265**	**0.115**	**0.038**	**0.017**	**2.295**	**0.042**
V_5	Power	−0.120	0.281	−0.001	0.001	−0.427	0.678
V_6	Time	0.007	0.252	0.000	0.007	0.029	0.977
V_2V_3	HCl × HNO_3	−0.465	0.239	−0.002	0.001	−1.948	0.077
V_5V_6	Time × power	−0.008	0.361	−0.000	0.000	−0.022	0.983

Table 9 Significant variable descriptors determined by multilinear regression

Reference material	Mass	Volume: mass	Volume of HCl	Volume of HNO_3	Volume of HF	Power	Time	HCl × HNO_3	Time × power
SRM 1575	Ca	Ca	Ca, Fe	Ca, Fe	Fe	—	—	Ca	—
TORT-1	Zn	Zn	Ca, Fe	Ca, Fe	—	—	—	Ca, Fe	—

selected (Fe and Ca) in the two reference materials to allow for simplification of the analytical protocol; Zn and Cu were also determined in TORT-1. The experimental design parameters and their elemental response (extrapolated from a five-point analytical working curve) are shown in Tables 1 and 2. The chronological listing of the experimental design parameters represents the statistically randomized order in which the experimental treatments were undertaken.

Multilinear regression, based on the least-squares fit, was used to calculate the parametric coefficients B_n from eqn. (1). Tables 3–8 show the coefficients of regression for Fe, Ca, Cu and Zn in TORT-1 and Ca and Fe in SRM 1575. The significant variables calculated from the parametric equation are highlighted in bold type in Tables 3–8. The beta values represent the regression coefficients after the variables have been standardized to remove scale effects.[23] The term significant is used to describe those coefficients where the observed magnitude is not a result of random error. Significance is determined at a confidence level of 0.05, *i.e.*, 95% confidence limit. In Tables 3–8 a coefficient with a probability (p) level of less than 0.05 will be considered significant. Calcium and Fe show maximum dependence on the operating variables irrespective of sample type.

Table 9 summarizes the significant variables for the determination of Ca and Fe in SRM 1575 and Ca, Fe, Cu and Zn in TORT-1. Copper in TORT-1 appears to be labile as no

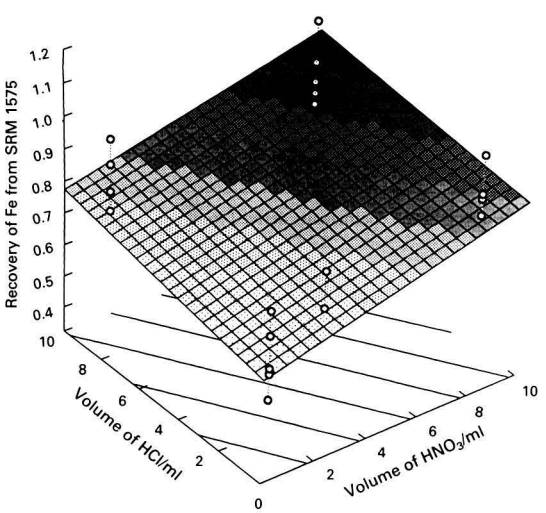

Fig. 1 Response surface for the recovery of Fe from SRM 1575. $z = 0.6354 + 0.0231x + 0.0138y$. Recovery expressed as fractional recovery, *i.e.*, 1.0 ≡ 100%

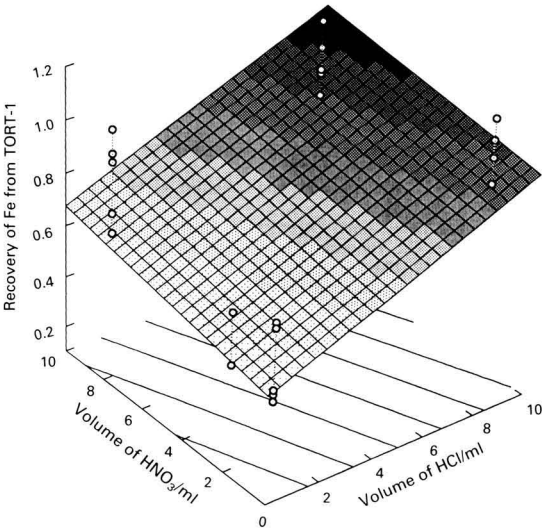

Fig. 2 Response surface for the recovery of Fe from TORT-1. $z = 0.5097 + 0.04448x + 0.01653y$. Recovery expressed as fractional recovery, *i.e.*, 1.0 ≡ 100%

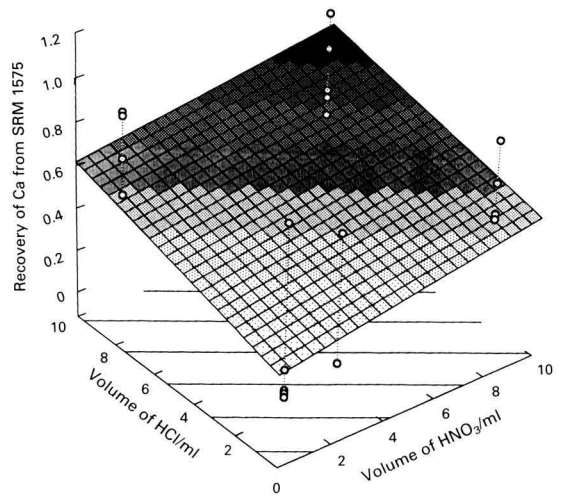

Fig. 3 Response surface for the recovery of Ca from SRM 1575. $z = 0.3057 + 0.02288x + 0.03102y$. Recovery expressed as fractional recovery, *i.e.*, 1.0 ≡ 100%

significant variables are observed whilst excellent recoveries are obtained. Of the remaining analytes it is readily observed that the main variables are the independent volumes of HCl and HNO_3. However, negative beta values for HCl–HNO_3 interaction in Tables 3, 4 and 7, for Ca and Fe in TORT-1 and Ca in SRM 1575, respectively, indicate that the formation of *aqua regia* is antagonistic to the recovery of analytes. The property of *aqua regia* to dissolve matrices arises from the reactivity of nitrosyl chloride (NOCl) and/or free chlorine formation.[24] However, it is apparent from the response surfaces that the ideal combination of HCl and HNO_3 is not the 3 + 1 required to form *aqua regia* but equal volumes, for optimum extraction.

Examples of response surfaces for the microwave dissolution of Ca and Fe in SRM 1575 and TORT-1 shown in Figs. 1–4 were obtained with a sample mass of 0.25 g, 3 ml of concentrated HF and 90% microwave power for 15 min.

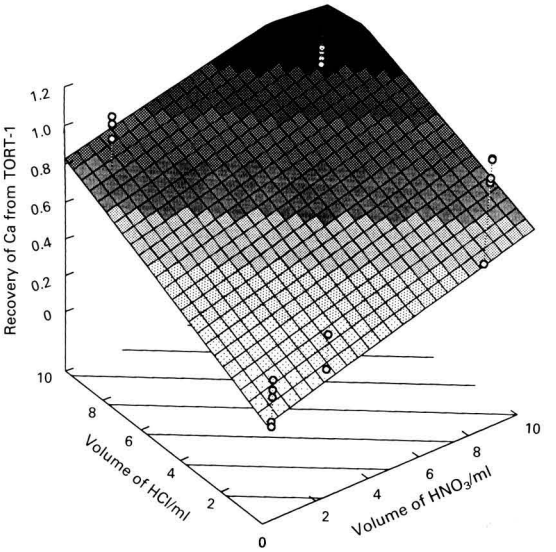

Fig. 4 Response surface for the recovery of Ca from TORT-1. $z = 0.1934 + 0.04869x + 0.06331y$. Recovery expressed as fractional recovery, *i.e.*, 1.0 ≡ 100%

Table 10 Optimized microwave dissolution conditions

Variable	Amount
Sample mass	0.25 g
Volume of HCl	6 ml
Volume of HNO_3	6 ml
Volume of HF	3 ml
Microwave power	90%
Time of dissolution	15 min

Table 11 Determination of minor elements in two reference materials

Reference material	Element	Certified value/ μg g^{-1}	Microwave digestion*/ μg g^{-1}
TORT-1	Ca†	0.895 ± 0.058	0.863
	Fe	186 ± 11	185
	Cu	439 ± 22	436
	Zn	177 ± 10	170
SRM 1575	Ca†	0.41 ± 0.02	0.390
	Fe	200 ± 10	196

* Average of duplicates.
† Concentration reported in per cent.

Table 12 Percentage recoveries of elements in two reference materials

Reference material	Element	Recovery* (%)
TORT-1	Ca	97
	Fe	97
	Cu	105
	Zn	98
SRM 1575	Ca	96
	Al	100
	Mn	96
	Fe	97

* Average of duplicates.

Accuracy of Microwave Dissolution

In order to ascertain the accuracy of the dissolution method, the two reference materials were analysed under optimum conditions (Table 10). The results, shown in Table 11, represent the average of duplicate analyses. All elements

determined are within the experimental limits of the certified values. This outlines the importance of optimizing the analytical procedure to digest samples of known composition.

Recovery Studies

The microwave dissolution procedure was evaluated for loss of analyte and contamination by the analysis of the reference materials with the addition of a known element concentration. The element spike was introduced after weighing the sample into the dissolution vessel. This ensures that the recovery of the element reflects the entire analytical methodology. Table 12 summarizes the recoveries obtained for the six elements that have been spiked to a 1 μg ml^{-1} level. The recoveries ranged from 96 to 105% indicating good analytical work-up with minimal contamination.

Conclusions

Fractional factorial experimental design based on a parametric model has been applied to optimize the operating variables of a microwave dissolution system. Subsequent elemental analysis using a direct current plasma atomic emission spectrometer has allowed the accurate determination of selected elements in two reference materials. The exploration of the effects of six variables on the analysis of four analytes has been accomplished using 21 treatments. The detrimental effects of *aqua regia* to effect dissolution are reported.

Financial support from the British Council, Kuala Lumpur, Malaysia, is acknowledged for A. A. M.

References

1 Uhrberg, R., *Anal. Chem.*, 1982, **54**, 1906.
2 Topper, K., and Kotuby-Amacher, J., *Commun. Soil Sci. Plant Anal.*, 1990, **21**, 1437.
3 Banuelos, G. S., and Pflaum, T., *Commun. Soil Sci. Plant Anal.*, 1990, **21**, 1717.
4 Kingston, H. M., and Jassie, L. B., *Introduction to Microwave Sample Preparation, Theory and Practice*, American Chemical Society, Washington, DC, 1988.
5 Matusiewicz, H., and Sturgeon, R. E., *Prog. Anal. Spectrosc.*, 1989, **12**, 21.
6 Kimber, G. M., and Kokot, S., *TrAC, Trends Anal. Chem. (Pers. Ed.)*, 1990, **9**, 203.
7 Matusiewicz, H., Sturgeon, R. E., and Berman, S. S., *J. Anal. At. Spectrom.*, 1989, **4**, 323.
8 Aysola, P., Anderson, P., and Langford, C. H., *Anal. Chem.*, 1987, **59**, 1582.
9 Fischer, L. B., *Anal. Chem.*, 1986, **58**, 261.
10 Vermer, G., Vandecasteele, C., and Dams, R., *Anal. Chim. Acta*, 1989, **220**, 257.
11 White, R. T., Jr., and Douthit, G. E., *J. Assoc. Off. Anal. Chem.*, 1985, **68**, 766.
12 Nieuwenhuize, J., Poley-Vos, C. H., van den Akker, A. H., and van Delft, W., *Analyst*, 1991, **116**, 347.
13 Finch, C. R., Pennington, H. D., Lyons, C. G., and Littau, S. E., *Commun. Soil Sci. Plant Anal.*, 1990, **21**, 583.
14 Bettinelli, M., and Baroni, U., *Int. J. Environ. Anal. Chem.*, 1990, **43**, 33.
15 Binstock, D. A., Groshse, P. M., Gaskill, A., Jr., Sellers, C., Kingston, H. M., and Jassie, L. B., *J. Assoc. Off. Anal. Chem.*, 1991, **74**, 360.
16 Brereton, R. G., *Chemometric Applications of Mathematics and Statistics to Laboratory Systems*, Ellis Horwood, Chichester, 1990.
17 Bayne, C. K., and Rubin, I. B., *Practical Experimental Designs and Optimization Methods for Chemists*, VCH, Deerfield Beach, FL, 1986.
18 Deming, S. N., and Morgan, S. L., *Experimental Design: a Chemometric Approach*, Elsevier, Amsterdam, 1987.
19 Massart, D. L., Vandeginste, B. G. M., Deming, S. N., Michotte, Y., and Kaufman, L., *Chemometrics: a Textbook*, Elsevier, Amsterdam, 1988.
20 Floyd Inc., 5440 Highway 55 East, Lake Wylie, SC 29710, USA.
21 Goldsmith, P. L., CAED, ICI Fibres, Harrogate, North Yorkshire, UK.
22 Smith, G. L., *Anal. Proc.*, 1991, **28**, 150.
23 "CSS: Statistica", Release 3.0F, Statsoft UK, Letchworth.
24 Cotton, A. F., Wilkinson, G., and Gaus, P. L., *Basic Inorganic Chemistry*, Wiley, Chichester, 2nd edn., 1987, p. 219.

Paper 2/01379G
Received March 16, 1992
Accepted July 14, 1992

Determination of Cadmium in Biological Samples by Inductively Coupled Plasma Atomic Emission Spectrometry After Extraction With 1,5-Bis(di-2-pyridylmethylene) Thiocarbonohydrazide

J. M. Espinosa Almendro, C. Bosch Ojeda, A. Garcia de Torres and J. M. Cano Pavón*
Department of Analytical Chemistry, Faculty of Sciences, University of Málaga, 29071 Málaga, Spain

An inductively coupled plasma atomic emission spectrometric method for the determination of trace amounts of cadmium after extraction of the metal into isobutyl methyl ketone containing 1,5-bis(di-2-pyridylmethylene) thiocarbonohydrazide is described. The optimum extraction conditions were evaluated from a critical study of the effects of pH, concentration of extractant, shaking time and ionic strength. The detection limit for cadmium is 0.1 ng ml^{-1} and the calibration is linear from 0.2 to 140 ng ml^{-1}. The relative standard deviation for ten replicate measurements is 2.9% for 2 ng ml^{-1} of cadmium. Results from the analysis of some certified biological reference materials are given.

Keywords: *Solvent extraction; inductively coupled plasma atomic emission spectrometry; cadmium; biological samples*

Liquid–liquid extraction is one of the most frequently used sample pre-treatment techniques for the determination of trace metals by inductively coupled plasma atomic emission spectrometry (ICP-AES). The extraction serves the dual purposes of concentration of the metals of interest and their separation from an interfering matrix. The extent of concentration achieved depends on the ratio of the aqueous to organic phase volume. On the other hand, isolation from the matrix significantly decreases any background signal caused by concomitants.

Occupational exposure to cadmium represents a continuing problem of significant magnitude. The initial effects of cadmium poisoning are proteinuria, leading to kidney stones and osteomalacia. Chronic cadmium inhalation produces pulmonary emphysema[1] and liver and kidney damage.[2,3] Levels of cadmium in the blood, urine, liver and kidneys are important indicators of human exposure to this metal; blood levels are considered to reflect recent exposure, but are not representative of body burden, whereas urine concentrations are suggested to indicate the cadmium body-burden of persons subjected to either low-level or industrial exposure.[4,5] Cadmium can be determined in the clinical laboratory by several methods: neutron activation analysis and X-ray fluorescence analysis have been used for the measurement of cadmium in the liver[6,7] and kidneys;[3,8] however, these techniques are not always practical for a number of reasons including the radiation hazard. The recommended method for cadmium determination in the clinical laboratory is electrothermal atomic absorption spectrometry.[9–11]

Inductively coupled plasma atomic emission spectrometry has been widely recognized as a technique suitable for the determination of trace elements, with particular advantages because of its multi-element capability, large dynamic range and effective background correction. However, several problems have been indicated by researchers, *e.g.*, spectral interferences due to matrix components, nebulizer blockage due to the high solids content of the solution or analyte emission enhancement. In this paper an ICP-AES method is described for the determination of trace amounts of cadmium in biological materials after extraction of the metal into isobutyl methyl ketone (IBMK) containing 1,5-bis(di-2-pyridylmethylene) thiocarbonohydrazide (DPTH). The complex formed is soluble in IBMK, so much so that it allows the use of aqueous-to-organic phase volume ratios of up to 30 (*i.e.*, much higher than those typically afforded by other extractants) and hence the determination of concentrations down to 30 times lower than those afforded by the direct non-extractive method. In addition, the extraction step enhances the selectivity.

* To whom correspondence should be addressed.

Experimental

Apparatus

The ICP-AES measurements were made on a Perkin-Elmer Plasma 40 sequential emission spectrometer. The system was controlled by an IBM XT-286 computer which was used in developing the method and in acquiring and storing the data. A standard torch and a Meinhard concentric glass nebulizer (controlled by a peristaltic pump working at a flow rate of 1 ml min^{-1}) were used during the experiments.

All pH measurements were made with the aid of a Crison Digit-501 pH-meter supplied with a combined glass–calomel electrode.

Separating funnels were shaken on a Gallenkamp flask agitator.

A Panasonic (National) microwave oven, Model NN-8507, and a Parr Microwave Acid Digestion Bomb, Model 4782, were used for sample digestion.

Reagents

All chemicals were of analytical-reagent grade or better. Glass distilled and de-ionized water was used throughout.

The ligand for the DPTH solution was synthesized as described elsewhere.[12] A stock solution in IBMK was prepared by dissolving 0.1 g of DPTH in 9 ml of *N*,*N*-dimethylformamide and diluting to 100 ml with IBMK. The solution was found to remain stable for more than 1 week.

A stock solution of cadmium(II) was prepared from the nitrate (Merck, *pro analysi*) and standardized using complexometry. Standards of working strength were made by appropriate dilution as required.

An acetic acid–acetate buffer of pH 5.6 was prepared by mixing 4.8 ml of 0.2 mol l^{-1} AcOH and 45.2 ml of 0.2 mol l^{-1} NaOAc in a 100 ml calibrated flask and making up to the mark with distilled water.

A 1 mol l^{-1} solution of $NaClO_4$ was also used.

Procedures

All glassware and plasticware were acid cleaned (25% v/v nitric acid) prior to use.

Sample Preparation

The certified reference materials (CRMs) analysed to determine the accuracy of the proposed procedure were: National Institute of Standards and Technology (NIST) Standard Reference Materials (SRMs) 2670 Toxic Metals in Freeze-Dried Urine and 1577a Bovine Liver; Community Bureau of Reference (BCR) CRM 186 Pig Kidney; National Research Council Canada (NRCC) CRMs DOLT-1 Dogfish Liver, DORM-1 Dogfish Muscle and TORT-1 Lobster Hepatopancreas. These samples were first dried in accordance with the norms of the respective analysis certificates. Each dried sample (with the exception of SRM 2670) was mineralized according to the following procedure. A 0.200–0.600 g amount of the powdered sample was placed in the reaction pump together with 4 ml of 65% nitric acid. Then, after 30 min, 2 ml of 37% HCl were added and the digestion pump was shut and placed in the microwave oven, where it was kept at 360 W for 4 min, followed by 10 min at 180 W. The oven was allowed to cool for the same time as the programme duration (14 min) after it was opened. After digestion, the solutions were evaporated to a small volume (1–2 ml), neutralized with sodium hydroxide, and finally diluted with de-ionized water to 50 ml in a calibrated flask. Finally, three identical volumes of each were taken for the determination of cadmium. The determination of this metal was carried out by the recommended procedure. The SRM 2670 did not require mineralization, the sample was prepared from concentrates according to the directions supplied.

Recommended Procedure

Volumes of sample or standard solutions containing 0.03–2.10 μg of cadmium were placed in separating funnels, together with 0.5 ml of 1 mol l^{-1} $NaClO_4$ and 5 ml of acetic acid–acetate buffer of pH 5.6. Then, 5 ml of 0.1% DPTH in IBMK were added (the maximum volume ratio of the aqueous to organic phase was 30:1, for a single-stage extraction of 99–100%). The mixture was shaken vigorously on the mechanical agitator at 3000 rev min^{-1} for 5 min. The phases were allowed to separate, and the solvent layer was transferred into a poly(propylene) centrifuge tube (some samples may need centrifugation for up to 5–20 min to improve the separation between the layers). The organic phase was inserted into the plasma bulk by means of a peristaltic pump and cadmium was determined according to the instrumental conditions given in Table 1. Triplicate analyses of each sample were made and the cadmium concentration was determined from the calibration graph; alternatively, the standard additions method could also be applied satisfactorily.

Results and Discussion

Optimization of Extraction Conditions

Extraction of metal ions by an organic reagent is known to be dependent on several factors such as the type and amount of reagent, organic solvent, chemical form of metal ion, pH of solution and shaking time. We have investigated the extraction process in order to obtain optimum conditions. The IBMK has a significant solubility in water but was chosen as the organic solvent because of its high extraction efficiency for the cadmium(II)–DPTH complex.

The effect of pH on the extraction of cadmium is shown in Fig. 1. As can be seen, the optimum pH range for quantitative extraction is about 4.0–10.7. All subsequent studies were carried out at pH 5.6; this pH was adjusted using an acetic acid–acetate buffer solution. The volume of the added buffer (3–8 ml) had no effect. Increasing the ionic strength produced no significant changes on the extraction. However, in order to facilitate the phase separation a concentration of 3.3×10^{-3} mol l^{-1} $NaClO_4$ was used in all experiments.

The extraction behaviour of cadmium(II) was examined by a single extraction of a fixed amount of this ion with varying concentrations of DPTH in the organic phase while keeping its final volume at 5 ml. A 220-fold molar excess of the reagent over cadmium was required for quantitative extraction; therefore, 5 ml of 2.30×10^{-3} mol l^{-1} (0.1%) reagent solution were sufficient for the analytical procedure.

The minimum shaking time was determined by varying the shaking time from 1 to 15 min, a time of 4 min was found to be sufficient; however, prolonged shaking had no adverse effect on the extraction; thus a shaking time of 5 min was selected for this study.

The extraction of cadmium was found to be quantitative up to an aqueous-to-organic phase volume ratio of 30, above which phase separation was inadequate and the method was thus inefficient. Such a high phase ratio results in a sensitivity 30 times higher than that of the direct non-extractive method.

Under these optimum conditions, the recovery factors for the extraction of cadmium were calculated by means of a series of experiments in which the atomic emission of cadmium in the organic phase was compared with that of a

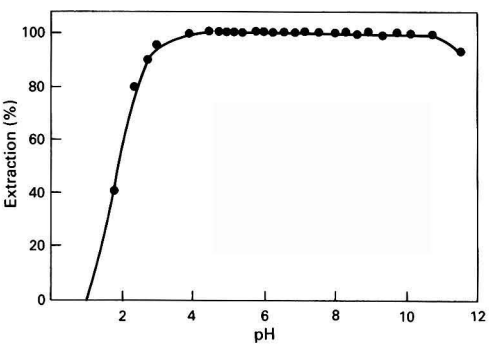

Fig. 1 Effect of pH on the extraction of Cd^{II} with DPTH in IBMK in the presence of perchlorate. $[Cd]_{initial} = 60$ μg, $[DPTH]_0 = 2.3 \times 10^{-3}$ mol l^{-1}, $[ClO_4^-] = 0.75$ mol l^{-1}; shaking time, 10 min

Table 1 Operating conditions for the ICP

Wavelength: 228.802 nm
Background correction: −0.040, +0.056 nm
R.f. generator: frequency 40 MHz, incident power 1.1 kW
Photomultiplier voltage: 600 V
Plasma gas flow rate: 12 l min^{-1}
Auxiliary gas flow rate: 0.6 l min^{-1}
Nebulizer gas flow rate: 0.4 l min^{-1}
Plasma viewing height: 15 mm above the induction coil
Integration time: 100 s
Read delay: 20 s
Peristaltic pump flow rate: 1 ml min^{-1}

Table 2 Determination of cadmium in biological samples

	Amount of cadmium/μg g^{-1}	
Sample	Found	Certified
CRM 186 Pig Kidney	2.65 ± 0.13	2.71 ± 0.15
DOLT-1 Dogfish Liver	3.79 ± 0.20	4.18 ± 0.28
TORT-1 Lobster Hepatopancreas	28.6 ± 3.2	26.3 ± 2.1
DORM-1 Dogfish Muscle	0.098 ± 0.010	0.086 ± 0.012
SRM 1577a Bovine Liver	0.44 ± 0.08	0.44 ± 0.06
SRM 2670 Toxic Metals in Freeze-Dried Urine	0.099 ± 0.020*	0.088 ± 0.003*

* In μg ml^{-1}.

standard prepared in water-saturated IBMK. In all instances, cadmium in the range 0.03–2.1 μg was extracted completely by a single extraction.

Selection of Measurement Conditions

The following wavelengths were investigated: 214.438, 228.802, 226.502, 361.051, 326.106, 231.284 and 479.992 nm. The 228.802 nm cadmium line was chosen because for the other wavelengths studied either the intensity was poorer or the background was higher compared with that at 228.802 nm. After the wavelength had been selected, background-correction points were chosen by consideration of the standards, blank and sample matrices.[13] Other experimental variables were established to achieve the best signal-to-noise ratios. The operating conditions for the spectrometer are recorded in Table 1.

Calibration Graph: Precision and Detection Limit

Under the optimum conditions, a linear calibration graph was obtained from 0.2 to 140 ng ml^{-1} of cadmium (aqueous phase) when an aqueous-to-organic phase volume ratio of 30 was used. Ten determinations of standard solutions containing 2 ng ml^{-1} of cadmium gave a relative standard deviation of 2.9% ($p = 0.05$). On the other hand, the detection limit, defined as the concentration of analyte giving a signal equivalent to three times the standard deviation of the blank plus the net blank intensity, was measured to be 0.1 ng ml^{-1}.

Sample Analysis

In order to test the accuracy and applicability of the proposed method to the analysis of real samples, some biological reference materials were analysed. Matrix interference was verified by comparison of the slopes of the calibration graphs with those using the standard additions method. Only for SRM 2670 were matrix effects apparent for the ICP measurements and quantification was performed with the standard additions method. The results are given in Table 2 as the average of three replicates. As can be seen, the cadmium concentrations determined by the proposed method are in close agreement with the certified values. The estimated practical detection limit, based on the combined effects of the digestion method, the imprecision and instability of the instrument and the variability of the biological materials, is 0.7 ng ml^{-1}.

Conclusion

The proposed method is efficient for the accurate determination of cadmium in biological materials. The main advantages offered by the fast solvent extraction of cadmium prior to its atomization are the suppression of interferences and an increase in the sensitivity by preconcentration of the analyte.

The authors thank the Comision de Investigacion Cientifica y Tecnica (CICYT) for supporting this study (Project PB90-0805).

References

1 Davison, A. G., Fayers, P. M., Taylor, A. J., Venables, K. M., Darbyshire, J., and Kickering, C. A., *Lancet*, 1988, **1**, 663.
2 Shalkh, Z. A., Ellis, K. J., Subramanian, K. S., and Greenberg, A., *Toxicology*, 1990, **63**, 53.
3 Kostial, K., *Trace Elements in Human and Animal Nutrition*, Academic Press, New York, 5th edn., 1986, vol. 2, ch 5, pp. 184–197.
4 Friberg, L., Kjelltrom, T., Nordberg, G., and Piscator, M., *Handbook on the Toxicology of Metals*, Elsevier, Amsterdam, 1979, p. 335.
5 Lauwerys, R. R., *Industrial Chemical Exposure: Guidelines for Biological Monitoring*, Biomedical Publications, Davis, CA, 1983, p. 17.
6 Roels, H., Lauwerys, R., Buichet, J. P., Bernard, A., Chettle, D., Harvey, T. C., and Haddad, I. K., *Environ. Res.*, 1981, **26**, 217.
7 Harvey, T. C., Thomas, B. J., McLellan, J. S., and Fremlin, J. H., *Lancet*, 1975, **1**, 1269.
8 Chystofferson, J. O., Welinder, H., Spang, G., Mattsson, S., and Skerfving, S., *Environ. Res.*, 1987, **42**, 489.
9 Tsalev, D. L., Dimitrov, T. A., and Mandjukov, P. B., *J. Anal. At. Spectrom.*, 1990, **5**, 189.
10 *Atomic Absorption Spectrometry*, ed. Haswell, S. J., Elsevier, Amsterdam, 1992.
11 Smeyers-Verbeke, J., Yang, Q., Penninck, W., and Vendervoot, F., *J. Anal. At. Spectrom.*, 1990, **5**, 393.
12 Bonilla, J. R., Garcia de Torres, A., and Cano, J. M., *Microchem. J.*, 1983, **28**, 132.
13 Ediger, R. D., and Fernandez, F. J., *At. Spectrosc.*, 1980, **1**, 1.

Paper 2/02730E
Received April 9, 1992
Accepted July 13, 1992

Structural Analysis of the Non-dialysable Urinary Glucoconjugates of Normal Men

Oluwole O. Adedeji*
Nuffield Department of Clinical Biochemistry, John Radcliffe Hospital, Oxford, UK

Enzymic methods were employed to analyse the structure of the non-dialysable urinary glucoconjugates of ten healthy males. The excretion of the urinary glucoconjugates was determined from the glucosyl : galactosyl ratio after acid hydrolysis, and a mean value of 0.27 was obtained. The results of the specific actions of α- and β-glucosidases showed that the non-dialysable urinary glucoconjugates contain a branched α-glucan fraction with 1,4- and 1,6-glucosidic bonds, and a β-glucan fraction containing 1,4-glucosidic bonds.

Keywords: *Stuctural analysis; non-dialysable urinary glucoconjugates; enzymic method; α-glucan; β-glucan*

Lloyd and co-workers[1,2] described the presence of non-dialysable conjugates of glucose and galactose in urine from normal people and observed that the glucosyl : galactosyl ratio could be used as a valid index of the 24 h excretion of glucosyl molecules. They found the value of the glucosyl : galactosyl ratio in normal males to be 0.24 ± 0.01, and the range to be 0.15–0.33. Honda *et al.*[3] also described the non-dialysable glucoconjugates in urine, and they reported a mean glucosyl : galactosyl ratio of 0.22 for normal subjects, although the results for men were not recorded separately.

The object of the work described here was to obtain further information on the structure of non-dialysable conjugates of glucose in the urine of normal males. Because of the complexity of the mixtures of glycoconjugates present in urine it was considered appropriate to attempt to use enzymic methods to obtain information about the glucosidic bonds.

Experimental

Samples

The subjects were ten healthy male laboratory workers with ages ranging from 24 to 60 years. They were chosen at random and the urine samples were collected in the course of their normal daily life.

Methods

The 24 h urine was collected in a plastic container with merthiolate (100 mg l^{-1}) as preservative to prevent the growth of micro-organisms. This was kept at 4 °C during collection and dialysed immediately on completion. Dialysis was carried out in Visking seamless tubing (Scientific Instrument Centre, London, UK), which had been sterilized and freed of plasticizers by boiling, and was subsequently stored at 4 °C in sodium azide (0.01%). The urine samples were dialysed at 4 °C against running tap water for 48 h, followed by dialysis against three changes of distilled water over 18 h. The dialysed urine was lyophilized and kept at −18 °C in air-tight containers. Approximately 200 mg of urine powder were obtained from 1 l of urine.

Preparation of the Amyloglucosidase Resistant Fraction

A 100 mg amount of dialysed urine powder was dissolved in 5 ml of distilled water. The solution was added to 10 ml of acetate buffer (0.1 mol l^{-1}, pH 4.0) and 7.2 U of amyloglucosidase (BCL, London, UK), and mixed. The mixture was incubated at 30 °C for 3 h. When there was no increase in the glucose production, the incubation mixture was heated over a boiling-water bath for 5 min to stop the action of the enzyme. The mixture was dialysed as above, freeze-dried and stored at −18 °C.

Acid Hydrolysis

A 0.1 ml aliquot of a solution of carbohydrate was added to 1 ml of 1 mol l^{-1} H_2SO_4 (final concentration of glycogen, 0.12 mg ml^{-1} or in terms of urine powder, 1.0 mg ml^{-1}), and thoroughly vortex mixed. The incubation mixture was heated in a tube with a tight-fitting cap at 100 °C for 6 h.[4] The hydrolysate was allowed to cool, and then neutralized with 1 ml of 0.5 mol l^{-1} triethanolamine–HCl, pH 7.5, plus 2 mol l^{-1} KOH, and assayed for glucose and galactose.

Amyloglucosidase E.C. 3.2.1.3 (1,4-α-D-Glucan Glycohydrolase, from *Aspergillus niger*)

A 0.1 ml aliquot of carbohydrate solution was added to 0.5 ml of 0.1 mol l^{-1} acetate buffer (pH 4) and 0.15 ml of distilled water (final concentration of glycogen, 0.78 mg ml^{-1} or for urine powder, 6.7 mg ml^{-1}). To this 0.02 ml (2.8 U) of amyloglucosidase was added and the mixture incubated at 30 °C for 3 h.[5] The hydrolysate was assayed for glucose.

α-Glucosidase, E.C. 3.2.1.20, β-Amylase, E.C. 3.2.1.2 and Pullulanase, E.C. 3.2.1.41 (all from BCL)

α-Glucosidase (3.9 U ml^{-1}) and β-amylase (65 U ml^{-1}) were added to 0.5 ml of carbohydrate solution (final concentration of glycogen, 0.78 mg ml^{-1} or for urine powder 6.7 mg ml^{-1}) in citrate buffer (6 mmol l^{-1}, pH 5) containing glutathione (6–8 mg in 50 ml) and serum albumin (25 mg in 50 ml). The mixture was incubated at 30 °C for 3 h.[5,6] The glucose released was then assayed.

Pullulanase (2.4 U ml^{-1}) was added to the mixture of α-glucosidase, β-amylase and dialysed urine powder in citrate buffer and incubated at 30 °C for 3 h. The glucose was then assayed. The β-amylase and pullulanase were used to hydrolyse glycogen and the reducing sugars of the hydrolysate were determined by the Somogyi–Nelson copper reduction method.[7]

Phosphorylase a, E.C. 2.4.1.1 (BCL)

A 40 μl aliquot of glycogen solution (6 mg ml^{-1}) or of urine powder solution (50 mg ml^{-1}) in 20 mmol l^{-1} phosphate buffer, pH 6.8, was added to 1 ml of phosphorylase a (20 U ml^{-1}) in the same buffer and incubated at 30 °C for 1 h.

* Present address: Clinical Chemistry Department, Royal Hallamshire Hospital, Sheffield, UK S10 2JF.

Glucose-1-phosphate (G1P) was then assayed spectrophotometrically.[5]

Pullulanase (3.0 U ml^{-1}) was added to the incubation mixture of phosphorylase (20 U ml^{-1}) and carbohydrate solutions in phosphate buffer, pH 6.8, and left at 30 °C for 1 h; G1P was then assayed.

β-Glucosidase, E.C. 3.2.1.21 and Cellulase, E.C. 3.2.1.4 (both from Sigma, Poole, Dorset, UK)

A 0.1 ml aliquot of carbohydrate solution (cellobiose, 0.02 mg ml^{-1} or dialysed urine powder, 50 mg ml^{-1}) was added to 0.5 ml of 0.1 mol l^{-1} Na_2HPO_4–0.2 mol l^{-1} citric acid buffer (pH 4.5) and thoroughly mixed. β-Glucosidase (0.06 U ml^{-1}) was added and the mixture incubated at 30 °C for 3 h. The glucose was assayed enzymically.

β-Glucosidase (0.06 U ml^{-1}) and cellulase (0.12 U ml^{-1}) were added to solutions of dialysed urine powder (6.7 mg ml^{-1}) and amyloglucosidase resistant fraction (6.7 mg ml^{-1}) in 0.1 mol l^{-1} Na_2HPO_4–0.2 mol l^{-1} citric acid buffer (pH 4.5). The mixtures were thoroughly mixed and incubated at 30 °C for 3 h. The glucose released in the hydrolysates was then assayed.[5]

Assays

Glucose

Glucose was determined spectrophotometrically with hexokinase and glucose-6-phosphate dehydrogenase.[5] The formation of reduced nicotinamide adenine dinucleotide phosphate (NADPH), as measured by the change in absorbance at 340 nm, is proportional to the amount of glucose.

Galactose

Galactose was determined spectrophotometrically with D-galactose dehydrogenase.[5] The formation of reduced nicotinamide adenine dinucleotide (NADH), as measured by the change in absorbance at 340 nm, is proportional to the amount of D-galactose.

Glucose-1-phosphate

The G1P was assayed by adding 25 μl of the incubation mixture to 1.2 ml of 50 mmol l^{-1} KH_2PO_4–10 mmol l^{-1} ethylenediaminetetraacetic acid (EDTA)–1 mmol l^{-1} $MgCl_2$–NADP (0.5 mg ml^{-1})–glucose-1,6-diphosphate (10 μg). The formation of NADPH, as measured by the change in absorbance at 340 nm after addition of phosphoglucomutase and glucose-6-phosphate dehydrogenase, is proportional to the amount of G1P released.[5]

Copper reduction method of Somogyi–Nelson

Reducing sugars were determined after de-proteinizing the incubation mixture with equal volumes of 50% m/v $ZnSO_4 \cdot H_2O$ and 0.15 mol l^{-1} $Ba(OH)_2 \cdot 8H_2O$, adjusted to equivalence after titration with phenolphthalein as indicator. The supernatant was added to an equal volume of the mixture of copper reagents A and B (Reagent A: 25 g of anhydrous Na_2CO_3, 25 g of Rochelle salt, 20 g of $NaHCO_3$ and 200 g of anhydrous Na_2SO_4 were dissolved in 800 ml of water and diluted to 1 l. Reagent B: 15% m/v $CuSO_4 \cdot 5H_2O$ in water containing 1–2 drops of concentrated H_2SO_4 per 100 ml.). Both the blanks (water) and standards were treated in the same way. The solutions were mixed and heated for 20 min in a boiling-water bath. After cooling, arsenomolybdate reagent was added in an amount equal to the volume of the mixture as the reagents A and B. The samples were thoroughly mixed and diluted with water to a volume 25 times the starting volume. A stable colour developed and was read at 500 nm after 5 min.[7]

Table 1 Acid hydrolysis of glycogen and non-dialysable urinary glucoconjugates of normal men (200 mg of urine powder were obtained from 1 l of urine; results given are $\bar{x} \pm$ standard error of the mean)

Sample	Glucose*/ mmol g^{-1}	Conversion† (%)	Galactose*/ mmol g^{-1}	Glucosyl : galactosyl ratio‡
Glycogen	5.60 ± 0.10	90.76 ± 3.00	—	—
Subjects§				
1(*a*)	61.33 ± 8.78	—	217.44 ± 68.46	0.28 ± 0.04
1(*b*)	58.21 ± 6.16	—	185.27 ± 23.13	0.31 ± 0.03
Over-all $\bar{x}$ ($n = 10$)	56.56 ± 6.51	—	204.98 ± 27.02	0.27 ± 0.03
Range	43.4–64.2	—	160.2–258.1	0.23–0.31

* These values were not corrected for possible losses during acid hydrolysis.

† Based on approximate value of glucose content of glycogen of 6.12 mmol g^{-1}, assuming an average relative molecular mass of 162.

‡ Because the losses are the same for glucose and galactose, the glucosyl : galactosyl ratio is unaffected by them.

§ The values for 1(*a*) and 1(*b*) were for the same man; samples were taken with an interval of 12 months between them, and the values are not significantly different ($p > 0.05$).

Table 2 Actions of α-glucosidases on glycogen and non-dialysable urinary glucoconjugates (results given are mean ± standard error of the mean with the ranges in parentheses)

	Glycogen		Glucoconjugate	
Enzyme	mmol g^{-1}	Conversion (%)	mmol g^{-1}	Conversion (%)
Amyloglucosidase	5.19 ± 0.06 Glucose	92.68 ± 1.07	19.00 ± 3.49 Glucose	33.95 ± 6.17 (26.24–40.70)
α-Glucosidase and β-amylase	2.85 ± 0.01 Glucose	50.89 ± 0.18	15.67 ± 4.41 Glucose	25.92 ± 4.93 (18.35–33.34)
α-Glucosidase, β-amylase and pullulanase	5.58 ± 0.02 Glucose	95.55 ± 0.34	27.37 ± 8.20 Glucose	43.86 ± 5.50 (35.74–51.30)
Phosphorylase*	1.48 ± 0.07 G1P	26.43 ± 1.25	10.50 ± 0.23 Glucose $n = 2$	18.56 ± 0.41
Phosphorylase* and pullulanase	2.52 ± 0.05 G1P	45.00 ± 0.89	20.95 ± 1.23 Glucose $n = 2$	37.02 ± 2.17

* Urine powder samples from five subjects were added together and the results are the means of n experiments.

Results

Acid Hydrolysis

The component monosaccharides of glycogen and the non-dialysable urinary glucoconjugates were released by acid hydrolysis prior to their determination. The yield of glucose obtained after acid hydrolysis of glycogen (as a test glucan)

was 5.60 mmol g^{-1}, representing 90.76% recovery (Table 1). This value was less than 100% because some losses are to be expected on heating sugars in strong acids. However, uncorrected values obtained after acid hydrolysis were taken as the monosaccharide contents of glycogen and urinary glucoconjugates.

The values obtained for the urinary glucoconjugates were: glucose, 56.56 mmol g^{-1}; galactose, 204.98 mmol g^{-1}; and a mean glucosyl : galactosyl ratio of 0.27 ± 0.03.

Enzymic Hydrolysis

Actions of α-glucosidases

Amyloglucosidase. A quantitative yield of glucose (92.68% conversion) was obtained by the action of amyloglucosidase on glycogen (Table 2). The action of the enzyme on non-dialysable urinary glucoconjugates produced 33.95% conversion to glucose; suggesting that only a fraction of the urinary glucoconjugates was susceptible to the action of amyloglucosidase.

β-Amylase and α-glucosidase. A 50.89% conversion of glycogen to glucose was obtained by the actions of β-amylase and α-glucosidase. The enzymes hydrolysed non-dialysable urinary glucoconjugates to produce 25.92% conversion to glucose, which is significantly less than that obtained with amyloglucosidase ($p < 0.05$).

β-Amylase, pullulanase and α-glucosidase. The actions of these enzymes on glycogen resulted in 95.55% conversion to glucose, whereas their actions on non-dialysable urinary glucoconjugates produced 43.86% conversion to glucose, which is not significantly different from that obtained by the action of amyloglucosidase ($p > 0.05$).

Phosphorylase a and pullulanase. The action of phosphorylase a on glycogen resulted in 26.43% conversion to G1P, and the production of phosphorylase limit dextrins. Phosphorylase and pullulanase acted on glycogen to produce 45.00% conversion to G1P. The increase in the amount of G1P released by the combined actions of phosphorylase a and pullulanase on glycogen was because the pullulanase removed α-1,6-glucosidic bonds in the phosphorylase limit dextrins, and, thus, allowed further phosphorolysis.

The actions of phosphorylase a alone and in combination with pullulanase on non-dialysable urinary glucoconjugates resulted in 18.56 and 37.02% conversions to glucose, respectively. Glucose was produced in these experiments because phosphatases present in the dialysed urine hydrolysed the G1P that was released by phosphorylase a. The hydrolysis of the urinary glucoconjugates that were obtained with phosphorylase a and pullulanase is not significantly different from that of amyloglucosidase ($p > 0.05$).

Actions of β-glucosidase

β-D-Glucosidase. β-D-Glucosidase completely hydrolysed cellobiose (a test β-glucan) to glucose. However, the enzyme did not hydrolyse either the non-dialysable urinary glucoconjugates or the amyloglucosidase resistant fraction. In the presence of dialysed urine, β-D-glucosidase acted on cellobiose to produce 85.27% conversion to glucose (Table 3). This result suggests that the constituents of dialysed urine must have caused about 16% inhibition of the enzymic action.

Cellulase and β-D-glucosidase. The combined actions of cellulase and β-D-glucosidase on the non-dialysable urinary glucoconjugates produced 46.06% conversion to glucose (Table 4). Further, 86.95% of the amyloglucosidase resistant fraction was hydrolysed by cellulase and β-D-glucosidase. The latter result is comparable to that of the conversion of cellobiose to glucose by β-D-glucosidase in the presence of dialysed urine. Thus, inhibitory constituents of the dialysed urine could have prevented complete hydrolysis of the amyloglucosidase resistant fraction.

Table 3 Action of β-D-glucosidase on cellobiose and the non-dialysable urinary glucoconjugates (results given are mean ± standard error of the mean)

Substrate	Glucose	Conversion (%)
Cellobiose ($n = 4$)	5.91 ± 0.03	101.20 ± 0.51
Non-dialysable urinary glucoconjugates	0	0
Cellobiose in the presence of dialysed urine ($n = 2$)	4.98 ± 0.03	85.27 ± 0.51

* Based on the theoretical value of glucose of 5.84 mmol g^{-1} of cellobiose.

Table 4 Actions of cellulase and β-D-glucosidase on non-dialysable urinary glucoconjugates and amyloglucosidase resistant fraction (results given are mean ± standard error of the mean)

	Glucose determined/mmol g^{-1}		
Substrate*	Acid hydrolysis	Cellulase and β-D-glucosidase	Conversion† (%)
Non-dialysable urinary gluco-conjugates ($n = 2$)	54.60	25.14 ± 0.73	46.06 ± 1.34
Amyloglucosidase resistant fraction ($n = 3$)	34.64	30.12 ± 0.49	86.95 ± 1.41

* Urine powder samples from five subjects were added together and the results are means of n experiments.

† Based on acid hydrolysis values.

Discussion

Acid Hydrolysis

The value obtained for the glucosyl : galactosyl ratio, 0.27, was in good agreement with previously reported values for normal men.[2] This result is also consistent with the fact that the glucosyl : galactosyl ratio could provide a valid basis for comparing urinary excretion of conjugated glucose. The range of the ratio for ten healthy males studied, 0.23–0.30, is also comparable to the reported values.[2]

Enzymic Hydrolysis

Amyloglucosidase

Based on the specificity of amyloglucosidase,[5] the fraction of the non-dialysable urinary glucoconjugates that was hydrolysed must be the α-glucan component. This fraction, possibly, contains α-1,4- and α-1,6-glucosidic bonds.

β-Amylase and α-glucosidase

These enzymes are specific for α-1,4-glucosidic bonds.[5] Therefore, the hydrolysis of non-dialysable urinary glucoconjugates by the enzymes confirms the presence of an α-glucan fraction with 1,4-glucosidic bonds.

β-Amylase, pullulanase and α-glucosidase

The conversion of non-dialysable urinary glucoconjugates to glucose increased after the addition of pullulanase to the incubation mixture of glucoconjugates, β-amylase and α-glucosidase. This is because pullulanase hydrolyses α-1,6-glucosidic bonds[8] in the glucoconjugates to allow further hydrolysis by β-amylase and α-glucosidase. Therefore, this result confirms that the α-glucan fraction of the urinary glucoconjugates is a branched molecule containing 1,4- and 1,6-glucosidic bonds.

Phosphorylase a and pullulanase

Based on the specificities of phosphorylase a and pullulanase, the results of their actions on non-dialysable urinary glucoconjugates provide further evidence of the presence of a branched α-glucan fraction with 1,4- and 1,6-glucosidic bonds. Also, the pattern of actions of these enzymes on glycogen was similar to that on the urinary α-glucan, which is an indication of the similarity in their structures.

Actions of α-glucosidases

The results of actions of α-glucosidases show that a substantial fraction of the non-dialysable urinary gluconconjugates was resistant to the enzymes that cleave α-glucosidic bonds. Therefore, the actions of the enzymes that are specific for β-glucosidic bonds were investigated with the non-dialysable urinary glucoconjugates.

β-D-glucosidase

The absence of any hydrolysis of the non-dialysable urinary glucoconjugates or the amyloglucosidase resistant fraction by β-D-glucosidase suggests that they might not be suitable substrates for this enzyme (Table 3).

Cellulase and β-D-glucosidase

The results in Table 4 show that a fraction of the non-dialysable urinary glucoconjugates was susceptible to the actions of cellulase and β-D-glucosidase. This fraction was further shown to be the amyloglucosidase resistant component, which was almost completely hydrolysed by these enzymes. The explanation for these results is that cellulase must have hydrolysed the β-glucan fraction of urinary glucoconjugates to produce cellobiose, and β-D-glucosidase acted on the cellobiose to release glucose.[9,10] As cellulase hydrolyses only β-1,4-glucosidic bonds the β-glucan fraction must, therefore, contain 1,4-bonds.

Conclusion

In this study, non-dialysable urinary glucoconjugates of normal men were shown to consist of two components. An α-glucan fraction (with 1,4- and 1,6-glucosidic bonds) and a β-glucan fraction (with 1,4-glucosidic bonds) are the components of the urinary glucoconjugates.

References

1 Lloyd, P., and Randle, P. J., *Diabetologia*, 1982, **23**, 470.
2 Lloyd, P., Hockaday, T. D. R., and Randle, P. J., *Diabetologia*, 1984, **27**, 433.
3 Honda, S., Susuki, S., Kakehi, K., Honda, A., and Takai, T., *J. Chromatogr.*, 1981, **226**, 341.
4 Kennedy, J. F., and White, C. A., *Bioactive Carbohydrates in Chemistry, Biochemistry and Biology*, Ellis Horwood, Chichester, 1983, ch. 4, pp. 66–87.
5 *Methods in Enzymatic Analysis*, ed. Bergmeyer, H. U., Verlag Chemie, New York, London, 1974, vol. 3.
6 Lee, E. Y. C., and Whelan, W. J., *Biochem. J.*, 1965, **95**, 27P.
7 *Fundamentals of Clinical Chemistry*, ed. Tietz, N. W., W. B. Saunders, Philadelphia, PA, 1976, ch. 6, p. 245.
8 Bender, H., and Wallenfels, K., *Biochem. Z.*, 1965, **334**, 79.
9 Conchie, J., Gelman, A. J., and Levy, G. A., *Biochem. J.*, 1967, **103**, 609.
10 Clarke, A. E., and Stone, B. A., *Biochem. J.*, 1966, **99**, 582.

Paper 2/02183H
Received April 28, 1992
Accepted July 27, 1992

Potentiometric Titration of Sodium Sulfate in Sodium Sulfite Solutions

Brent Walton
Quality-Control Department, Manro Products Limited, Stalybridge, Cheshire, UK SK15 1PH

A novel potentiometric titration procedure has been developed for the determination of sodium sulfate impurity in sodium sulfite solutions using 0.1 mol l^{-1} lead nitrate solution as the titrant. Sodium sulfite was effectively removed by reaction with formaldehyde solution, leaving only sulfate to react quantitatively with the standard 0.1 mol l^{-1} lead nitrate solution. Commercially available sodium sulfite solutions are manufactured to contain 18–20% m/m Na_2SO_3 and during method development the lowest level of sodium sulfate impurity measured was 0.3% m/m in a laboratory-prepared 18% m/m sodium sulfite solution. The potentiometric titration results agreed closely with those of a traditional gravimetric procedure, with no difference when the sodium sulfate level was 2.5% m/m and only 0.3% m/m maximum difference in absolute terms, when the sodium sulfate level was at 9% m/m. At low concentrations of sodium sulfite (*i.e.*, about 0.2% m/m) the detection limit for the sodium sulfate impurity is 0.02% m/m.

Keywords: *Sodium sulfate; sodium sulfite; impurity; potentiometric titration; formaldehyde*

Pure sodium sulfite is used in the food industry as a preservative and in the photographic industry; these industries demand that the sodium sulfate impurity that is present is kept to an absolute minimum. The manufacture of sodium sulfite involves passing sulfur dioxide into sodium hydroxide solution.

$$2NaOH + SO_2 \rightarrow Na_2SO_3 + H_2O$$

In the surfactant industry, excess of sulfur dioxide can be effectively removed from gas streams by passage through sodium hydroxide solutions in order to produce sodium sulfite. This is an efficient process that prevents sulfur dioxide being passed into the atmosphere and, hence, leads to a cleaner environment.

Sodium sulfite is prone to oxidation by molecular oxygen (or air) producing sodium sulfate as an impurity. This reaction is catalysed by certain ions, such as Fe^{2+} and Cu^{2+} and inhibited by phenol, glycerol, sodium thiosulfate and Sn^{2+} (Sn^{II} ions).[1] Low levels of sulfur trioxide (SO_3) react with sodium hydroxide to generate the impurity sodium sulfate.

The standard method for the determination of sulfate is the gravimetric procedure involving its precipitation as barium sulfate.[2] This procedure when adopted to determine sodium sulfate in sodium sulfite solutions took at least 3 h to complete, by an experienced analyst. Sodium sulfite had to be removed by boiling with concentrated hydrochloric acid to produce sulfur dioxide.

Determination of the sodium sulfate impurity in sodium sulfite solutions proved unsuccessful using 0.01 mol l^{-1} lead nitrate solutions as the titrant and dithizone as the indicator.[3] Attempts to develop an analytical method involving ion chromatography to convert the sodium sulfate and sodium sulfite salts into their corresponding acids and then use potentiometric titration with 1 mol l^{-1} cyclohexylamine in methanol also proved difficult as the sodium sulfate concentration was underestimated.[4,5]

A rapid and accurate potentiometric titration procedure was developed which could be used to determine sodium sulfate in sodium sulfite solutions in only 20 min. Under the conditions of the titration, sulfite ions were precipitated by lead ions producing lead sulfite that would interfere with the determination. However, addition of formaldehyde prior to the titration, rapidly and effectively removed the sulfite ions as the hydrogen sulfite addition compound.

This improved procedure allowed less experienced analysts to monitor the production of sodium sulfite and also allowed plant operators to make any necessary plant parameter changes in accordance with the sodium sulfate concentrations.

A similar potentiometric titration was used by Crabb and Persinger[6] to determine sulfate in anionic surfactants.

Experimental

Apparatus

Metrohm 686 Titroprocessor and 665 Dosimat

Platinum single wire electrode with an Ag–AgCl reference electrode containing 3 mol l^{-1} potassium chloride as electrolyte.

Equipment and electrodes are available from V. A. Howe (Banbury, Oxon, UK; UK Metrohm Agents).

Reagents

The following chemicals of analytical-reagent grade were obtained from Merck (formerly BDH) (Poole, Dorset, UK).

AnalaR sodium sulfate (99.9% *m/m purity*). This was used to standardize the 0.1 mol l^{-1} lead nitrate solution.

AnalaR potassium hexacyanoferrate(II) *trihydrate*, $K_4Fe(CN)_6 \cdot 3H_2O$.

AnalaR potassium hexacyanoferrate(III), $K_3Fe(CN)_6$.

AnalaR hydrochloric acid solution, 1 mol l^{-1}.

Formaldehyde solution, 40% *m/v*. General Purpose Grade.

Industrial methylated spirit (*IMS*). Obtained from BP Chemicals (London, UK).

Lead nitrate solution, 0.1 mol l^{-1}. Obtained from P & R Laboratory Supplies (St. Helens, Merseyside, UK).

Sodium sulfite (*ACS Reagent*). Obtained from Aldrich (Gillingham, Dorset, UK).

Procedure

The 0.1 mol l^{-1} lead nitrate solution was standardized by weighing 10 g amounts, separately, of a 7% m/m sodium sulfate solution into 150 ml beakers. Each amount taken was diluted to 25 ml with de-ionized water and then 75 ml of IMS were added. The IMS minimizes the solubility of the lead sulfate precipitate produced during the titration. Then, 0.5 ml of 0.1 mol l^{-1} potassium hexacyanoferrate(III) and 2.5 ml of 0.005 mol l^{-1} potassium hexacyanoferrate(II) were pipetted into the same beaker and the pH of the solution was reduced to 3.0 using 1 mol l^{-1} hydrochloric acid solution. Both the standard and sample solutions should be made acidic (pH 3.0–3.3) before titration in order to prevent the precipitation of lead hydroxide. The platinum single-wire electrode and the Ag–AgCl reference electrode are positioned in the prepared

solution and the redox titration carried out with the 0.1 mol l^{-1} lead nitrate solution. Blank determinations were performed under the same conditions.

During the titration the potential remains nearly constant because the ratio of hexacyanoferrate(III) to hexacyanoferrate(II) remains constant. However, when all the sulfate has reacted with the lead ions to produce lead sulfate, the first increment of excess of lead ions produces lead hexacyanoferrate(II), $Pb_2Fe(CN)_6$, and a large potential change is observed indicating the end-point.

Sodium sulfite samples were analysed by accurately weighing about 2 g into a 150 ml beaker and adding, initially, 5 ml of 40% m/v formaldehyde solution. The solution was diluted to 25 ml with de-ionized water and then 75 ml of IMS were added. The remainder of the procedure is the same as that for the standardization. The same blank value was used for the analysis of the sample.

Results and Discussion

The preparation stage for the potentiometric titration involves the effective removal of sodium sulfite by the formation of the hydrogen sulfite addition compound with formaldehyde.

Sulfite ions (SO_3^{2-}) are removed completely by the equilibrium reaction in eqn. (1) being driven to the right as indicated.

$$SO_3^{2-} + H_2O \rightleftharpoons HSO_3^- + OH^- \quad (1)$$

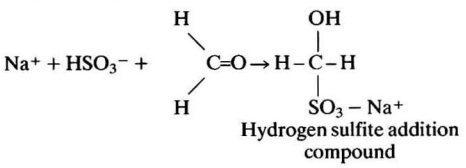

Hydrogen sulfite addition compound

For the potentiometric titration with 0.1 mol l^{-1} lead nitrate solution the hydrogen sulfite addition compound does not react. Lead(II) ions react quantitatively with the available sulfate ions to produce lead sulfate.

If after the preparation stage and after reducing the pH to 3.0 the solution appears cloudy, then repeat the preparation stage, using a smaller amount of sodium sulfite solution. For an accurate analysis, all samples of sodium sulfite, that have been treated with formaldehyde and the pH reduced to 3.0 prior to titration, must be totally clear.

The following ions have been identified as interferents in the potentiometric titration method. Phosphate ions interfere and will be titrated as apparent sulfate. Free Fe^{II} and Fe^{III} ions interfere because they react with hexacyanoferrate(III) and hexacyanoferrate(II) ions, respectively, forming a blue precipitate: $K^+Fe^{3+}[Fe(CN)_6]$. Under alkaline conditions Fe^{II} and Fe^{III} are effectively removed as their hydroxides.

To control the titration with a 0.1 mol l^{-1} lead nitrate solution, an incremental addition step of 0.10 ml and a drift value of 30 mV min^{-1} were used which relates to the kinetics of the titration reaction. The end-point corresponds to the largest potential break on the inflection curve.

The accuracy of the proposed method was established by performing the analysis with the traditional gravimetric procedure involving the precipitation of sulfate as barium sulfate. The comparative results are shown in Table 1.

Sample 2 was provided by William Blythe (Accrington, Lancashire, UK)[7] and had been previously analysed for sodium sulfate by the traditional gravimetric method. Results for an interlaboratory study are shown in Table 2.

The results show that the values obtained with the proposed potentiometric method are in good agreement with those obtained using the traditional gravimetric method for the determination of sodium sulfate in sodium sulfite solutions.

Table 1 Determination of sodium sulfate in sodium sulfite solutions by two independent analytical methods

Sample number	Potentiometric titration method (% m/m)	Gravimetric method (as $BaSO_4$) (% m/m)
1	1.9	1.9
2	2.0	2.1
3	2.5	2.5
4	5.1	5.3
5	8.7	9.0

Table 2 Interlaboratory comparison of results for sulfate (as $BaSO_4$)

	Potentiometric titration method (Manro Products) (% m/m)	Gravimetric method (as $BaSO_4$)	
Sample number		Company Manro Products (% m/m)	Company William Blythe (% m/m)
2	2.0	2.1	2.0

Standard Additions

A known amount of sodium sulfate was added to a known mass of sample 2 to evaluate the recovery of sodium sulfate. The results were expressed as a percentage of the original sample mass of sodium sulfite taken.

Theoretical result = 3.3% m/m sodium sulfate
Experimental result = 3.3% m/m sodium sulfate

Precision of the Proposed Potentiometric Titration Method

Nine analyses were performed on a sample of sodium sulfite solution giving

$$\text{mean } (\bar{x}) = 1.90\% \text{ m/m}$$

and sample standard deviation $(\sigma_{n-1}) = 0.0662\%$ m/m

Using the t distribution, the population mean (μ) at 95% confidence limits is

$$\mu = 1.90 \pm 0.05\% \text{ m/m}$$

We are 95% sure that the population mean lies in the range 1.85–1.95% m/m. It is important to perform all the comparative analyses on the same day, as the sodium sulfate concentration in sodium sulfite solution increases with time as a result of oxidation.

This potentiometric titration is a suitable analytical method for the continuous monitoring of the manufacture and final approval of sodium sulfite solutions as a sample analysis takes only 20 min.

Thanks to S. Barker of William Blythe Limited for assisting in providing sodium sulfite samples and allowing an interlaboratory comparison of the analytical methods. I. Johnson of William Blythe Limited is also acknowledged for his comments on the uses of sodium sulfite on a general basis.

References

1 Chambers, C., and Holliday, A. K., *Modern Inorganic Chemistry. An Intermediate Text*, Butterworth, Sussex, 1975, p. 291.
2 Vogel, A. I., *Textbook of Quantitative Inorganic Analyses*, Longman, London, 4th edn., 1978, pp. 504–507.
3 Longman, G. F., *The Analysis of Detergents and Detergent Products*, Wiley, Surrey, 1978, pp. 441–443.

4 Yamaguchi, S., Nukui, S., Mitsugi, K., and Konishi, K., *J. Am. Oil Chem. Soc.* (*Soap, Deterg. Cosmet., Tech. J.*), 1977, **55**, 359.
5 Yamaguchi, S., *J. Am. Oil Chem. Soc.* (*Soap, Deterg. Cosmet., Tech. J.*), 1978, **55**, 673.
6 Crabb, N. T., and Persinger, H. E., *J. Am. Oil Chem. Soc.*, 1967, **44**, 229.
7 Barker, S., personal communication, William Blythe Limited, Accrington, Lancashire, UK.

Paper 2/02352K
Received May 7, 1992
Accepted July 24, 1992

Photochemical Determination of Ascorbic Acid Using Unsegmented Flow Methods

Antonio Sanz-Martínez,* Angel Ríos and Miguel Valcárcel†
Department of Analytical Chemistry, Faculty of Sciences, University of Córdoba, E-14004 Córdoba, Spain

Several continuous-flow manifolds were developed in order to implement the photochemical reaction between ascorbic acid and Methylene Blue. Each design has special features that make it suitable for a specific application. The reaction was carried out in the reactor coil or flow cell depending on which region was irradiated. The analyte was determined at the microgram per millilitre level, with relative standard deviations ranging from 1.8 to 5.0%. Various types of samples were analysed using the proposed methodology.

Keywords: *Ascorbic acid; photochemical reaction; flow injection*

Photochemical reactions have been used to develop a number of analytical methods, particularly in pharmaceutical analysis.[1] These reactions have mostly been used for post-column derivatization in high-performance liquid chromatography (HPLC) in order to improve detection of some type of solute. However, they have not yet been used widely in other hydrodynamic analytical techniques such as flow injection (FI). Some interesting applications have been suggested in the few references available in this context. Thus, the oxalate–Fe^{III} system was used for the kinetic amperometric determination of oxalate[2] that was subsequently applied to the determination of this anion in urine samples.[3] Also individual phenothiazine compounds[4] and mixtures thereof[5] were assayed by photochemical spectrofluorimetric methods with ultraviolet irradiation of the reaction coil or flow cell. Nitrite was also determined amperometrically by its inhibitory effect on the photochemical reaction between iodine and ethylenediaminetetraacetic acid,[6] and thioridazine was determined in pharmaceutical compounds by using an open–closed configuration.[7]

White and Fitzgerald reported the continuous determination of ascorbic acid by photobleaching of Methylene Blue (MB) in an apparatus including a reaction zone that was irradiated with a photolysis lamp,[8] and subsequently used it in dye-sensitized continuous photochemical analysis.[9] In this paper we describe the development of various flow methods based on the photochemical reaction between ascorbic acid and MB for different types of applications. In addition, the reaction coil or the flow cell was also irradiated. For this latter purpose, a special photometric flow cell was designed that allowed for irradiation *via* two optical fibres. The reaction plug was stopped in the flow cell in order to monitor the photochemical reaction continuously.

Experimental

Reagents

Aqueous stock solutions of 1×10^{-4} mol l^{-1} MB (CI 52015, Aldrich), and 0.1 g l^{-1} ascorbic acid (Merck) were used. The latter was standardized titrimetrically with *N*-bromosuccinimide.[10] Hydrochloric acid was used to adjust the pH of the samples and reagents.

Apparatus

Photometric measurements were made on a Perkin-Elmer Lambda 1 spectrophotometer equipped with a Perkin-Elmer R100 recorder. A commercially available 700 W tungsten lamp featuring variable irradiation intensity and an optical fibre made of methyl acrylate of 0.5 mm diameter (supplied by RS components) were used. A Gilson Minipuls-3 peristaltic pump and two Rheodyne 5041 rotary valves were also used.

A special Hellma photometric flow cell housing two optical fibre guides was designed and built (Fig. 1). Essentially, it is a Hellma 178.10 QS photometric flow cell (inner volume 18 μl) containing two holes in the top which allow the stream passing through the optical light path to be irradiated *via* the two optical fibres.

Manifolds

Fig. 2 is a schematic diagram of the flow configurations employed. In Fig. 2(*a*) and (*b*) the sample–reagent mixture was irradiated in the reactor coil (250 cm length, 0.5 mm i.d.). This reactor was immersed in a thermostatically controlled water-bath (at 23 °C), 5 cm below the water level and 18 cm away from the radiation source. Fig. 2(*a*) shows the reversed FI (rFI) manifold, in which the sample containing the ascorbic acid acted as the carrier whilst the MB solution was injected. Fig. 2(*b*) shows the merging zones manifold, where identical volumes of sample and reagent were injected simultaneously into water carrier streams at pH 3.3, and then synchronously merged before reaching the irradiated reactor.

The third manifold [Fig. 2(*c*)] is similar to that shown in Fig. 2(*a*), but includes a special flow cell that was designed for this laboratory and was supplied by Hellma; this allowed the detection point to be irradiated. A schematic diagram of this flow cell can be seen in Fig. 1. It has two holes that act as guidelines for the light from the lamp to be directed into the flow cell through optical fibres. This assembly allows the photochemical reaction to be monitored in real time provided that the flow is stopped as the injected MB plug reaches the detector.

Results and Discussion

The photochemical reaction between MB and ascorbic acid has been well known for several years.[11,12] The MB is reduced to yield a colourless compound. The reaction can be monitored photometrically at 650 nm, where MB shows maximum absorbance. The reaction can be influenced by several experimental variables that were optimized by using the proposed flow systems.

The pH plays a major role in the reaction, because it determines both the redox potential of ascorbic acid and the sample and reagent stability. Thus, the influence of this variable was studied from 2 to 5.5, and an optimum pH of 3.3 was selected. The concentration of MB providing the best analytical response was 4.3×10^{-5} mol l^{-1}. No significant influence from the temperature (23 °C was the final working value), or the dissolved oxygen was detected.

* Permanent address: Department of Analytical Chemistry, Faculty of Sciences, University of Murcia, Spain.
† To whom correspondence should be addressed.

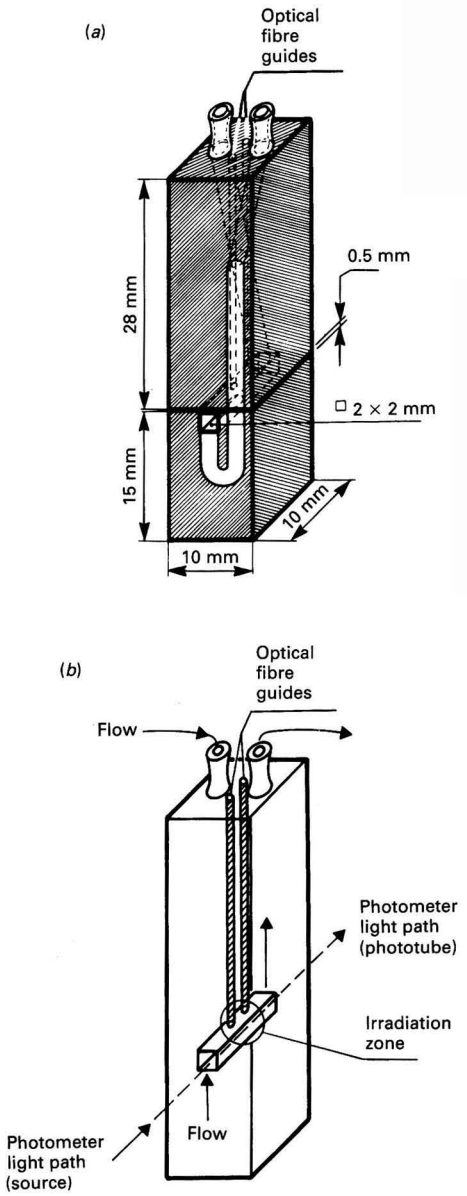

Fig. 1 Photometric flow cell furnished with two optical fibre guides for continuous monitoring of the photochemical reaction that takes place at the detection point. (*a*) General view and dimensions; (*b*) details of the irradiation and detection zone

Light acts as a reagent that can be readily manipulated. Although ultraviolet light has no effect, visible light triggers the photochemical reaction. The radiation intensity also has a decisive effect: values from 2400 to 8850 lux were tested, the maximum reaction rate being obtained at 8850 lux (light source output). It was found that approximately 20% of this intensity was lost through the optical fibre arrangement.

Under the above optimum chemical and irradiation conditions, the automated determination of ascorbic acid was carried out using the manifolds shown in Fig. 2 as described below.

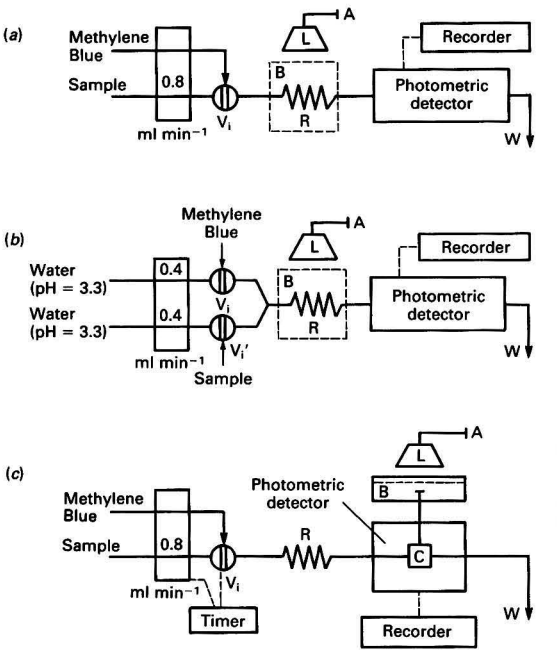

Fig. 2 Schematic diagram of the FI manifolds used: with irradiation of the reactor [reversed FI (*a*) and merging zones (*b*) modes]; with irradiation of the flow cell (*c*). L = Radiation source; A = intensity regulator; B = thermostated water-bath; C = flow cell furnished with optical fibre guides; D = optical fibre bundle; V_i = injection valve; and R = reaction coil

With Irradiation of the Reaction Coil

Two basic manifolds were developed in order to automate the photochemical reaction with irradiation on the reactor located before the detector by using the reversed flow mode [Fig. 2(*a*)] and the merging zones mode [Fig. 2(*b*)]. In both cases, the flow rate and reactor length were the main FI variables as they dictated the irradiation time; they also had an adverse effect on the sampling frequency. Taking into account these two opposite effects, 0.8 ml min^{-1} and 250 cm were chosen as the compromise flow rate and reaction coil length, respectively.

Reversed flow mode

An injected volume of 345 μl was necessary in order to achieve maximum sensitivity. Thus, the following calibration equation was arrived at under the optimum experimental conditions:

$$\Delta A = 3.71 \times 10^{-2}C + 1.05 \times 10^{-3} \quad (r = 0.9985)$$

where ΔA is the absorbance difference between the blank (without irradiation) and that measured when the photochemical reaction took place (in the presence of light); and C is the concentration of ascorbic acid in the samples, expressed in μg ml^{-1}. The determination range achieved was 0.5–5 μg ml^{-1}, and the detection limit was 0.4 μg ml^{-1}. The relative standard deviation (RSD) for 3.0 μg ml^{-1} ($n = 11$; $P = 0.05$) was 2.4%. Table 1 lists the results obtained by applying this procedure to different synthetic samples of ascorbic acid.

This procedure can be readily adapted for the continuous monitoring of ascorbic acid in samples (it should be of interest to process control and test solution studies). For this purpose, the injection valve in Fig. 2(*a*) was replaced with a confluence point for the incoming MB and sample streams. All experimental variables were kept constant as in the reversed FI method described above, except the flow rate, which was increased to 1.8 ml min^{-1} for more efficient monitoring of the variation in the analyte concentration. Fig. 3(*a*) shows the

Table 1 Results obtained for the determination of ascorbic acid in synthetic samples by reversed FI with irradiation of the reaction coil

Concentration added/ μg ml^{-1}	Concentration found/ μg ml^{-1}	Error (%)
2.24	2.32	+3.4
1.07	1.09	+1.8
5.00	5.04	+0.8
2.00	2.05	+2.5
0.50	0.48	−4.0
3.00	2.92	−2.5

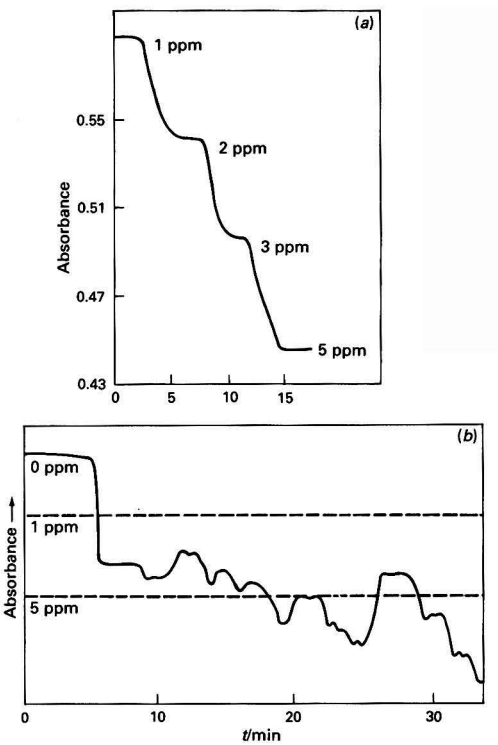

Fig. 3 Completely continuous technique for monitoring ascorbic acid. (*a*) Calibration run; (*b*) simulation of continuous monitoring of ascorbic acid

calibration graph recorded from standard solutions of ascorbic acid, whereas Fig. 3(*b*) shows a simulation of the continuous monitoring of this compound. The synthetic sample was drawn from a 2 l container which initially held 1000 ml of distilled water. Another vessel containing a solution of ascorbic acid was fixed to this tank. Periodically, different volumes of ascorbic acid or distilled water were added to the container in such a way that the ascorbic acid concentration was altered.

Merging zones approach

Volumes of 300 μl of both MB and sample were injected simultaneously into two acidified water streams (pH = 3.3) flowing at 0.4 ml min^{-1}. The other experimental variables were kept constant. Under these conditions, the following calibration equation was obtained:

$$\Delta A = 7.62 \times 10^{-3}C + 1.09 \times 10^{-2} \quad (r = 0.9939)$$

for a determination range of the analyte between 2.5 and 15 μg ml^{-1}, and an RSD of 1.8% ($n = 11$, $P = 0.05$) for 5 μg ml^{-1} of ascorbic acid. The detection limit was 0.7 μg ml^{-1} and the sampling frequency 25 h^{-1}. The results found in the analysis of synthetic samples are given in Table 2.

Table 2 Results obtained for the determination of ascorbic acid in synthetic samples by using the merging zones approach with irradiation of the reaction coil

Concentration added/ μg ml^{-1}	Concentration found/ μg ml^{-1}	Error (%)
2.00	2.05	+2.5
5.00	4.99	−0.2
15.00	14.77	−1.5
8.00	8.12	+1.5
10.00	9.72	−2.8
4.00	3.91	−2.2

Table 3 Features of merit of the determination of ascorbic acid by irradiating the flow cell and stopping the flow for 120 (A_1), 180 (A_2), 240 (A_3) and 300 (A_4) s at two different concentrations of MB

	Slope	Intercept	Regression coefficient	Concentration range/ μg ml^{-1}	Sampling frequency/ h^{-1}
[*MB*] = 25 μg ml^{-1}					
A_1	-5.3×10^{-4}	0.692	0.9831		15
A_2	-6.5×10^{-4}	0.666	0.9913	40–200	12
A_3	-7.3×10^{-4}	0.645	0.9948		10
A_4	-8.11×10^{-4}	0.628	0.9967		8
[*MB*] = 14 μg ml^{-1}					
A_1	-1.3×10^{-3}	0.390	0.9646		15
A_2	-1.5×10^{-3}	0.380	0.9796	20–100	12
A_3	-1.6×10^{-3}	0.370	0.9888		10
A_4	-1.7×10^{-3}	0.368	0.9910		8

With Irradiation of the Flow Cell

The manifold shown in Fig. 2(*c*) was used for this purpose. It is similar to that in Fig. 2(*a*), but includes a special flow cell (Fig. 1) that was used to develop and monitor the photochemical reaction simultaneously. In order to ensure a high reaction yield, the flow had to be stopped as the injected plug reached the detector. For this purpose, a timer was used to synchronize the functioning of the pump and injection valve, the flow being stopped 90 s after the MB plug was injected. The irradiation time affected the amount of product formed and hence the sensitivity of the determination, but inordinately long periods of time diminished the sampling frequency. Maximum sensitivity was achieved for an irradiation time of 300 s. After this period of time, the flow was resumed and, 20 s later, the next plug of MB was injected.

Ascorbic acid was determined from the increase in signal obtained over the 300 s during which the flow was stopped using the following equation:

$$\Delta A = 0.368 - 1.68 \times 10^{-3}C \quad (r = 0.9910)$$

For a determination range between 20 and 100 μg ml^{-1}, a detection limit of 8.7 μg ml^{-1}, and an RSD of 2.0% was obtained for 11 samples containing 50 μg ml^{-1} ($P = 0.05$). Different calibration equations were obtained by stopping the flow for shorter intervals and using various concentrations of MB (Table 3). Better sensitivity and regression were achieved with longer stop times, but to the detriment of the sampling

Table 4 Results obtained for the determination of ascorbic acid in synthetic samples with irradiation of the flow cell

(*a*) *By use of the maximum signal*

Concentration added/ μg ml^{-1}	Concentration found/ μg ml^{-1}	Error (%)
20.0	20.1	+0.5
40.0	40.2	+0.5
60.0	59.3	−1.2
80.0	81.7	+2.1
100.0	100.7	+0.7

(*b*) *By use of the kinetic method (reaction-rate)*

Concentration added/ μg ml^{-1}	Concentration found/ μg ml^{-1}	Error (%)
20.0	19.7	−1.5
40.0	40.5	+1.2
60.0	58.9	−1.8
80.0	81.2	+1.5
100.0	102.3	+2.3
150.0	149.0	−0.7
200.0	204.2	+2.1

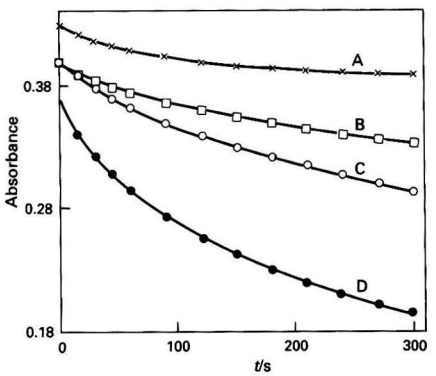

Fig. 4 Absorbance–time curves obtained by irradiating a flow cell containing various concentrations of ascorbic acid: A, 10; B, 20; C, 40; and D, 100 μg ml^{-1}

frequency. The sensitivity also increased with decreasing concentrations of MB, but regressions were less favourable. By using the above calibration equation, several synthetic samples containing different concentrations of ascorbic acid were analysed. The results obtained are listed in Table 4(*a*).

The main advantage of this method is the possibility of monitoring the photochemical reaction continuously from the beginning, which in turn allows the kinetics to be studied. In this case, the rate constant was calculated from the absorbance–time recordings obtained when the flow was stopped through the graph $\log(A_t - A_\infty) = f(t)$, where A_t is the absorbance at time t and A_∞ the absorbance at equilibrium. The slope of the straight line thus obtained is $-k/2.303$, where k is the rate constant under pseudo first-order kinetic conditions. This constant was found to be 0.56 ± 0.01 min^{-1}. The kinetic determination of ascorbic acid was accomplished from initial reaction-rate measurements under experimental conditions, that allowed the following kinetic equation to be obeyed:

$$v = k[\text{ascorbic acid}] \quad \text{(excess MB)}$$

Fig. 4 shows some typical recordings obtained at different concentrations of ascorbic acid.

This procedure allowed the determination of the analyte at concentrations from 20 to 200 μg ml^{-1}, with an RSD of 2.4% for a concentration of 40 μg ml^{-1} (n = 11; P = 0.05). Table 4(*b*) shows the results obtained in the analysis of various samples containing ascorbic acid.

Table 5 Maximum tolerated ratios of foreign species to analyte in the determination of 5 μg ml^{-1} of ascorbic acid

Species	Maximum tolerated ratio [foreign species]/[ascorbic acid]
Lactic acid	20
Citric acid	20
Benzoic acid	30
Oxalic acid	30
Succinic acid	30
Aspartic acid	30
Tartaric acid	30
Sucrose	10
Glucose	20
Fructose	20
Galactose	30
Alanine	30
Cysteine	30
Thiamine	30
Creatinine	20
Urea	30
Sodium acetate	60
Sodium sulfite	0.8

Table 6 Determination of ascorbic acid in real samples

Sample	*N*-Bromosuccinimide method/mg l^{-1}	Photochemical flow method*/ mg l^{-1}	Difference (%)
Pharmaceutical preparations			
Redoxon	979.8	987.6	+0.8
Citrovit	959.1	940.0	−2.0
Treasury	438.9	424.1	−3.3
Home-made orange juice	767.3	756.2	−1.4
Home-made lemon juice	635.1	623.1	−1.9
Boxed orange juice	585.2	589.5	+0.7

* By use of the merging zones approach.

Comparison of Results

Four different methods were developed in order to determine ascorbic acid photochemically. The reversed FI and completely continuous methods can be used for 'quasi' continuous monitoring of the analyte in abundant samples or process lines, where changes in the analyte concentration must be strictly controlled. These methods provide the maximum sensitivity. The merging zones method is suitable when only a limited amount of sample is available and features the highest sampling frequency and precision. Finally, the stopped-flow method with irradiation of the flow cell is better suited than the other methods to the kinetic and theoretical studies of the photochemical reaction concerned.

We studied the influence of concomitant species on the determination of ascorbic acid in real samples. The results obtained by using the four methods were similar. Table 5 shows the tolerated levels of foreign species, which, except for sodium sulfite, are higher than those at which the acid usually occurs in both natural and commercially available products. Nevertheless, the real [sulfite]/[ascorbic acid] levels in the samples are normally lower than the maximum tolerated ratio found in this case. Neither carbohydrates, preservatives nor acidifiers interfered with the determination. In order to check

the applicability of the proposed methods, they were applied to various real samples and the results obtained were compared with those provided by the conventional titration with *N*-bromosuccinimide.[10] All results are listed in Table 6.

Conclusion

Photochemical reactions used in unsegmented flow systems have a great analytical potential. Light acts as a reagent that allows reactions to be manipulated readily. It is a clean, cheap and 'flexible' reagent that can be applied to the reactor coil or even the cell where detection is to be performed; it takes place thanks to the optical fibre technology. As reported, ascorbic acid can be determined photochemically by reaction with MB using various flow methods. Each of the proposed methods has special features that make it suitable for a given application. The methodology can also be extended to similar applications involving other chemical systems.

One of the authors (A. S.-M.) gratefully acknowledges support from Comunidad Autónoma de Murcia.

References

1 Birks, J. W., *Chemiluminescence and Photochemical Reaction Detection in Chromatography*, VCH, New York, 1989.
2 León, L. E., Ríos, A., Luque de Castro, M. D., and Valcárcel, M., *Anal. Chim. Acta*, 1990, **234**, 227.
3 León, L. E., Ríos, A., Luque de Castro, M. D., and Valcárcel, M., *Analyst*, 1990, **115**, 1549.
4 Chen, D., Ríos, A., Luque de Castro, M. D., and Valcárcel, M., *Analyst*, 1991, **116**, 171.
5 Chen, D., Ríos, A., Luque de Castro, M. D., and Valcárcel, M., *Talanta*, 1991, **38**, 1227.
6 Liu, R. M., and Liu, D. J., *Analyst*, 1991, **116**, 497.
7 Tena, M. T., Luque de Castro, M. D., and Valcárcel, M., *J. Autom. Chem.*, 1991, **13**, 111.
8 White, V. R., and Fitzgerald, J. M., *Anal. Chem.*, 1972, **44**, 1267.
9 White, V. R., and Fitzgerald, J. M., *Anal. Chem.*, 1975, **47**, 903.
10 Barakat, M. Z., Bassioni, M., and El-Wakil, M., *Analyst*, 1972, **97**, 466.
11 Lund, H., and Lieck, H., *Klin. Wochenschr.*, 1937, **16**, 555.
12 Lund, H., and Trier, E., *Klin. Wochenschr.*, 1939, **18**, 80.

Paper 2/02812C
Received May 29, 1992
Accepted July 24, 1992

Studies on the Application of Photochemical Reactions in a Flow Injection System

Part 2.* Simultaneous Determination of Iron(II) and Iron(III) Based on the Photoreduction of the Iron(III)–Phenanthroline Complex

Ren-Min Liu, Dao-Jie Liu and Ai-Ling Sun
Department of Chemistry, Liaocheng Teachers College, Liaocheng, Shandong, People's Republic of China

An automated procedure for the simultaneous determination of iron(II) and iron(III) was developed, involving the use of a laboratory-built flow-through photochemical reactor in a flow injection system based on the photoreduction of the iron(III)–1,10-phenanthroline complex. Optimum analytical conditions were established. A 100 mm^3 sample injection gave linear working ranges of 0.1–120 ppm of iron(II) and 0.2–120 ppm of total iron. The sample throughput was 40–60 h^{-1}. The proposed method was applied to the determination of iron(II) and iron(III) in synthetic mixtures of standard iron(II) and iron(III) and the catalyst for synthetic ammonia manufacture.

Keywords: *Photochemical reaction; iron(II) and iron(III) simultaneous determination; flow injection*

Photochemical analysis has been used increasingly in various fields, owing to its high selectivity and sensitivity. However, relatively few photochemical analysis methods have been combined with modern analytical techniques. Flow injection(FI) offers high sample throughput, cost-effective performance and versatility. The combination of FI techniques with photochemical analysis could provide a novel means for studies on photochemical analysis.[1–5] The amperometric determination of oxalate based on the photochemical reaction taking place in the reaction coil of an FI system that was irradiated with visible light has been reported.[1] An alternative approach to the photochemical determination of this analyte was based on the use of an amperometric flow cell with several inlet optical fibre leads, which irradiated the sample only in the flow cell.[2] A similar use of a photochemical reaction in FI, with unstable compounds such as phenothiazines, under ultraviolet (UV) radiation was reported recently.[3] The method was simpler than those reported previously. Another recently used FI system involving photochemical reaction is based on on-line photo-oxidation of organoarsenicals to inorganic arsenic.[4] The arsenate generated by oxidation of the organoarsenicals is reduced to arsine and continuously detected by atomic absorption spectrometry. In our previous work,[5] a flow-through photochemical reactor was constructed and used in an FI system for the determination of nitrite based on the photochemical reaction between iodine and ethylenediaminetetraacetic acid (EDTA).

The iron(III)–1,10-phenanthroline (phen) complex can be reduced to the iron(II)–phen complex, which shows a red colour when irradiated with light.[6,7] Stucki[8] studied this photochemical reaction and established a photochemical analysis method for the determination of iron(III), but it required 36 h for one determination. Yan *et al.*[9,10] also studied this photochemical reaction and proposed the following mechanism. When no organic complexant is present in the system, the mechanism is:

$$H_2O \rightleftharpoons H^+ + OH^-$$

$$Fe(OH)^{2+} \xrightarrow{h\nu} Fe^{2+} + {}^{\cdot}OH$$

$$2{}^{\cdot}OH \rightarrow H_2O + \tfrac{1}{2}O_2$$

When a carboxylic acid or other organic complexant is present in the system, the mechanism is as follows:

$$-CO-O-Fe^{3+} \xrightarrow{h\nu} Fe^{2+} + CO_2$$

Based on this study, they established a photochemical analysis method for the determination of iron(II) and iron(III). The time taken for the reaction was about 30 min.

In this work, a flow-through photochemical reactor was constructed and used for the study of the photochemical reduction of the iron(III)–phen complex in an FI system. An FI method for the simultaneous determination of iron(II) and total iron was established based on the photochemical reduction of the iron(III)–phen complex and the spectrophotometric determination of the iron(II)–phen complex at 510 nm. The proposed method shows high selectivity, sensitivity and speed.

Experimental

Apparatus

A schematic diagram of the FI system is shown in Fig. 1. The flow system was assembled with polyethylene tubing (0.8 mm i.d.). The peristaltic pump was supplied by Jiangsu Electroanalytical Instrument Plant. For sample injection (S_1 and S_2 in Fig.1), a dual six-way rotary valve was used. A flow-through photochemical reactor (laboratory built, shown in Fig. 2) was used in the FI system. A Hitachi Model 220A spectrophotometer was used as the detector with a 1 cm flow cell with a volume of 18 mm^3. Detection was effected at 510 nm. The pulses produced by the pump were suppressed by an air damper, D, placed just behind the pump. All polyethylene tubing was wrapped with aluminium foil to prevent exposure of the solution to light, so that the photoreduction of the iron(III)–phen complex was not accelerated outside of the photochemical reactor.

Reagents

All the solutions were prepared with distilled, de-ionized water.

Iron(III) stock solution, 1000 μg cm^{-3}. Prepared with Fe_2O_3 of spectroscopic grade.

Iron(II) stock solution, 1000 μg cm^{-3}. Prepared with ammonium iron(II) sulfate of analytical-reagent grade.

Carrier solution. Dissolve 8.2 g of anhydrous sodium acetate and 0.71 g of potassium sodium tartrate in 400 cm^3 of water and adjust the pH to about 4.7. Dissolve 1.0 g of 1,10-phenanthroline in this solution and dilute to 500 cm^3.

* For Part 1 of this series, see ref. 5.

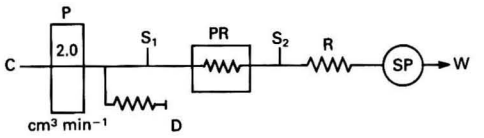

Fig. 1 Schematic diagram of the FI system. P, Peristaltic pump; D, damper coil (500 cm length; 1.0 mm i.d.); S_1 and S_2, sample solutions (100 mm^3); PR, photochemical reactor; R, reaction coil for iron(II) and phen (80 cm); SP spectrophotometric detector with flow cell (18 mm^3 volume); W, waste; and C, carrier solution

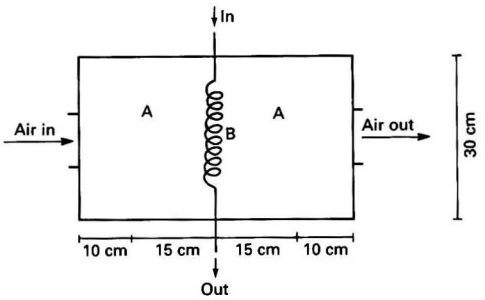

Fig. 2 Schematic diagram of the flow-through photochemical reactor. A, Light source, one is a GGY-125 W fluorescent high-pressure mercury lamp and the other is a GGZ-125 W Vitalight lamp; B, quartz reaction tube (200 cm × 0.8 mm i.d.)

Procedure

Use the flow system illustrated in Fig. 1. Inject the sample solution into the carrier stream at the two points S_1 and S_2 simultaneously using the dual six-way rotary injection valve. Allow the sample plug from S_1 to pass through the photochemical reactor, then allow the two sample plugs to pass through the flow-through cell in the detector. Read the absorbance at 510 nm. Obtain the iron(II) absorbance of the iron(II)–phen complex from the first peak and the total iron absorbance of the iron(II)–phen complex from the second peak.

Prepare a series of mixed standard solutions containing iron(II) and iron(III) and inject these solutions into the carrier stream as described for sample solutions.

Use the peak height as a measure of absorbance throughout the sample and calibration runs.

Results and Discussion

Iron(II) reacts with phen to form an iron(II)–phen complex, which has an absorption maximum at 510 nm, a wavelength at which the absorption of the iron(III)–phen complex is negligible. However, the iron(III)–phen complex can be reduced to the iron(II)–phen complex by a photochemical reaction. The system described (Fig. 1) is a single-channel system with a photochemical reactor that effects the reduction of the iron(III)–phen complex. The introduction of a sample into the carrier stream simultaneously at two injection points (S_1 and S_2) gives a double-peak response on the recorder, as illustrated in Fig. 3. The first peak height obtained corresponds to iron(II) whereas the second peak height corresponds to total iron.

Light Source of the Photochemical Reactor

The reaction rate depends on the irradiation wavelength. Yan *et al.*[9] studied the photochemical reduction of the iron(III)–phen complex in detail. The effective wavelength of photoreduction of the iron(III) was <300 nm when no organic ligand was present in the system and >300 nm and between 420 and 450 nm with acetic acid present in the system. A GGZ 125 W Vitalight lamp and a GGY 125 W fluorescent high-pressure mercury lamp were used as the light sources for the photochemical reactor in this experiment.

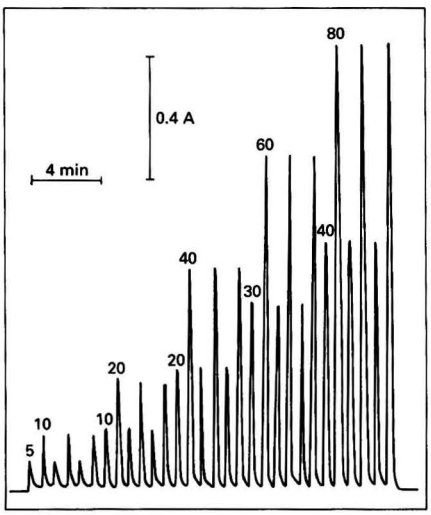

Fig. 3 Recorder signals for mixed standard solutions of iron(III) and iron(II) with the double-injection FI system. Values above the peaks indicate the concentration in ppm. The first peak corresponds to iron(II) and the second peak corresponds to total iron

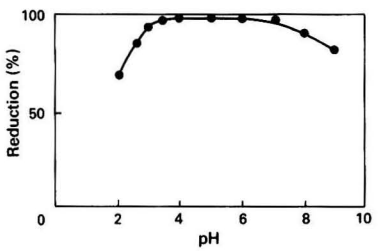

Fig. 4 Influence of pH. The percentage reduction values were calculated with respect to the absorbance of 5.0 ppm of iron(III)/absorbance of 5.0 ppm of iron(II)

Effect of pH

Iron(II) reacts with phen to form the red iron(II)–phen complex in the pH range 2.0–9.0. The photoreduction efficiency for 5.0 ppm of iron(III) in this pH range was measured (Fig. 4). The results showed that more than 95% of the iron can be reduced to iron(II) in the pH range 3.0–7.0. A buffer solution with a pH of about 4.7 was adopted for the determination.

Length of Reaction Tube

A quartz tube was used as the reaction tube for the photochemical reaction and its length was found to have a significant effect on the photoreduction of the iron(III)–phen complex. The extent of the reduction can be controlled by adjusting the length of the reaction tube when the power of the lamp and its distance from the reaction coil are kept constant. The influence of the reaction tube on the reduction of 5.0 ppm of iron(III) was studied. Fig. 5 shows that more than 95% of the iron(III) can be reduced to iron(II) when the reaction tube was longer than 175 cm. A reaction tube 200 cm long was adopted for the determination.

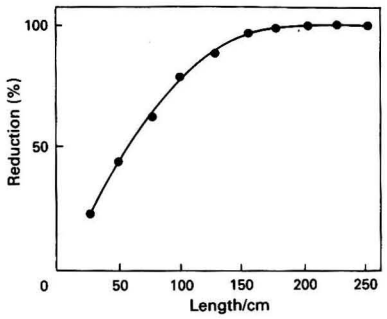

Fig. 5 Influence of the length of the photochemical reaction tube. The reduction (%) of iron(III) was calculated as for Fig. 4

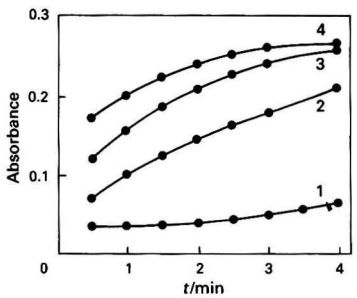

Fig. 6 Influence of tartrate, citrate and salicylate. 1, 0.1 mol dm^{-3} sodium acetate; 2, 0.1 mol dm^{-3} sodium acetate + 0.01 mol dm^{-3} salicylic acid; 3, 0.1 mol dm^{-3} sodium acetate + 0.01 mol dm^{-3} sodium citrate; and 4, 0.1 mol dm^{-3} sodium acetate + 0.01 mol dm^{-3} potassium sodium tartrate

Effect of Tartrate

The effects of tartrate, citrate and salicylate on the photoreduction of the iron(III)–phen complex were studied. Volumes of 5 cm^3 of 1.0 mol dm^{-3} sodium acetate and 0.1 mol dm^{-3} potassium sodium tartrate (or sodium citrate or salicylic acid) were placed in a 50 cm^3 beaker, the pH was adjusted to about 4.7, and the solution was transferred into a 50 cm^3 calibrated flask and 1.0 cm^3 of 1.0×10^{-3} mol dm^{-3} iron(III) and 5.0 cm^3 of 0.2% phen solution were added. The mixture was diluted to volume and then transferred into a quartz beaker and irradiated with a GGY 125 W fluorescent high-pressure mercury lamp. A 0.5 cm^3 volume of the solution was removed by pipette at intervals of 30 s and the absorbance was measured at 510 nm. Fig. 6 shows that the photoreduction of the iron(III)–phen complex can be accelerated significantly by tartrate, citrate and salicylate, particularly tartrate. The mechanism of the acceleration is not clear.

The effect of the concentration of tartrate was also studied and the results are shown in Fig. 7. A concentration of 5.0×10^{-3} mol dm^{-3} potassium sodium tartrate was adopted in subsequent work.

Effect of Foreign Ions

The interference of various foreign ions was studied by adding them to 5.0 ppm of iron(II) and iron(III). The results (relative error <5%) are given in Table 1.

Calibration

According to the proposed procedure, the calibration graph was established with standard solutions of iron(III) and iron(II) (Fig. 3). The first peak height corresponds to the absorbance of iron(II) and the second peak height to the absorbance of total iron. A 100 mm^3 sample injection gave linear working ranges of 0.1–120 ppm of iron(II) and 0.2–120 ppm of total iron.

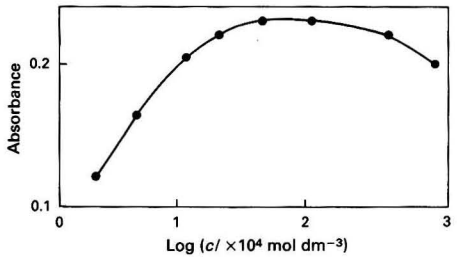

Fig. 7 Influence of tartrate concentration

Table 1 Interferences in the determination of iron(III) and total iron

Element	Maximum tolerable concentration (ppm)
Alkali and alkaline earth metals, Ni, Zn, As, Al, Cd, Sb, Mn^{II}, Pb^{II}, Cr^{III}, Sn^{II}	500
Cu^{II}, Ag	200
Hg^{II}, Co^{II}, Mo^{VI}	100
Bi^{III}	25

Table 2 Simultaneous determination of iron(II) and iron(III) in synthetic mixtures of standard iron(II) and iron(III)

Added (ppm)			Found (ppm)		
Fe^{II}	Fe^{III}	Total*	Fe^{II}	Total	Fe^{III}†
8.00	8.00	16.0	8.02	16.1	8.1
8.00	39.6	47.6	7.96	47.3	39.3
16.0	8.00	24.0	15.9	24.2	8.3
16.0	39.6	55.6	16.0	55.7	39.7
40.0	8.00	48.0	39.8	47.7	7.9
40.0	39.6	79.6	39.8	80.1	40.3
0	39.6	39.6	0.18	39.6	39.5
40.0	0	40.0	40.0	40.0	0

* Fe^{II} + Fe^{III}.
† Calculated by subtraction of Fe^{II} from total iron.

Applications

Table 2 shows the results obtained with the proposed method for synthetic mixtures of standard iron(II) and iron(III). The precision for the determination of iron(II) and iron(III) was measured by analysing the samples listed in Table 2 six times. The relative standard deviations for all samples were <0.84%.

Iron oxides are used as catalysts in the industrial process for the manufacture of ammonia and the ratio of the iron valency states has a significant effect on the characteristics of these catalysts. It has been reported that the optimum iron(III) to iron(II) ratio is about 2:1.[11,12] The proposed method was used for the determination of the ratio of the iron valency states of these catalysts.

A 0.1 g amount of catalyst was weighed accurately and dissolved in 5 cm^3 of concentrated hydrochloric acid. The solution was transferred into a 1000 cm^3 calibrated flask, diluted to volume and analysed by the proposed method. The results are given in Table 3.

The samples were also analysed by the dichromate titrimetric method, as follows. A 0.15–0.20 g amount of sample was weighed and dissolved in 10 cm^3 of concentrated hydrochloric acid and heated nearly to boiling. Tin(II) chloride

Table 3 Results for iron speciation analysis in catalysts for synthetic ammonia manufacture

	Fe^{II} : Fe^{III}*		
Sample No.	Dichromate titrimetric method	Proposed method	Relative error (%)
1	0.60	0.597	−0.5
2	0.62	0.618	−0.3
3	0.64	0.646	+0.9
4	0.68	0.672	−1.2

* Molar ratio.

solution (10% m/v) was added to the solution dropwise to reduce iron(III) to iron(II) until the yellow colour disappeared, then 1–2 drops were added in excess. The solution was cooled to room temperature in an ice–water bath and 10 cm^3 of 5% m/v mercury(II) chloride were added immediately to oxidize the excess of tin(II). The solution was shaken until homogeneous and set aside for 3–5 min, then diluted to about 150 cm^3. A 15 cm^3 volume of a mixture of sulfuric acid, water and orthophosphoric acid (1.5 + 7 + 1.5 v/v) and 5–6 drops of 0.2% m/v sodium diphenylamine-4-sulfonate as indicator were added and the solution was titrated with 16.67 mmol dm^{-3} $K_2Cr_2O_7$ solution until the solution became purple. The total amount of iron can be calculated from the volume of $K_2Cr_2O_7$ required.

For the determination of iron(II), no tin(II) chloride or mercury(II) chloride solutions were added.

The amount of iron(III) can be calculated from the difference between the total iron and iron(II) contents. The results are given in Table 3, and show that the results obtained by the proposed method are in accordance with those of the titrimetric dichromate method.

References

1 Leon, L. E., Rios, A., Luque de Castro, M. D., and Valcárcel, M., *Analyst*, 1990, **115**, 1549.
2 Leon, L. E., Rios, A., Luque de Castro, M. D., and Valcárcel, M., *Anal. Chim. Acta*, 1990, **234**, 227.
3 Chen, D., Rios, A., Luque de Castro, M. D., and Valcárcel, M., *Analyst*, 1991, **116**, 171.
4 Atallah, R. H., and Kalman, D. A., *Talanta*, 1991, **38**, 167.
5 Liu, R.-M., and Lu, D.-J., *Analyst*, 1991, **116**, 497.
6 Novak, J., and Ared, H., *Talanta*, 1964, **11**, 898.
7 David, P. G., Richardson, J. G., and Wehry, E. L., *J. Inorg. Nucl. Chem.*, 1972, **34**, 1333.
8 Stucki, J. W., *Soil. Sci. Am. J.*, 1981, **45**, 638.
9 Yan, K., Sha, D., and Tan, M., *Kexue Tongbao*, 1986, **31**, 238.
10 Yan, K., Sha, D., and Tan, M., *Fenxi Huaxue*, 1987, **15**, 1019.
11 Almquist, J. A., and Cristtendem, E. D., *Ind. Eng. Chem.*, 1926, **18**, 1307.
12 Bridge, G. L., Pole, G. R., Beinlich, A. W., and Thomson, H. L., *Chem. Eng. Prog.*, 1947, **43**, 291.

NOTE—Ref. 5 is to Part 1 of this series.

Paper 1/06324C
Received December 17, 1991
Accepted May 28, 1992

Photochemical Method for the Determination of Hydrogen Peroxide and Glucose

Tomás Pérez-Ruiz, Carmen Martínez-Lozano, Virginia Tomás and Otilia Val
Department of Analytical Chemistry, Faculty of Sciences, University of Murcia, Murcia 30071, Spain

Reduction of hydrogen peroxide was achieved with leuco-phloxin in the presence of haematin. The leuco dye was generated through the photochemical reaction between phloxin and ethylenediaminetetraacetic acid. The method involves measuring the time to reach the end-point of the photochemical titration, *i.e.*, the photolysis time necessary for the total reduction of the peroxide. The method can be extended to the determination of substrate–enzyme systems that produce hydrogen peroxide, *e.g.*, glucose–glucose oxidase. The assay is linear between 0.12 and 4.61 μg cm^{-3} for hydrogen peroxide ($r = 0.9992$) and between 3.99 and 43.2 μg cm^{-3} for glucose ($r = 0.9989$). The detection limit, defined as three times the standard deviation of the reagent blank, was 0.03 μg cm^{-3} for hydrogen peroxide and 1.0 μg cm^{-3} for glucose.

Keywords: *Hydrogen peroxide determination; glucose determination; photochemical reduction; phloxin*

Hydrogen peroxide is important in clinical, environmental and biological studies and it is used in many industrial and related processes as an oxidizing, bleaching and sterilizing agent. For these reasons it is important that improved methods be developed for the determination of trace amounts of hydrogen peroxide. In addition, such methods are also potentially useful for the monitoring of processes or for the indirect determination of other substances. For example, one can monitor the activities of enzymes that specifically catalyse the oxidation of biological materials in the presence of oxygen with the formation of hydrogen peroxide. The substrates or the enzymes in these reactions can be indirectly determined by the measurement of hydrogen peroxide.[1]

Hydrogen peroxide is usually determined at the micromolar level after reaction with a chromogenic hydrogen donor and a coupling agent in the presence of peroxidase[2,3] or by decomposition with peroxidase and oxidation of an indicator compound.[4] However, other procedures for the determination of hydrogen peroxide are based on its decomposition, which is promoted by a transition metal, with concomitant oxidation of a marker substrate to form a product that yields the analytical signal.

The most sensitive methods for the determination of hydrogen peroxide involve chemiluminescence,[5,6] spectrophotometry[7,8] and spectrofluorimetry.[9–12] Continuous-flow analysis,[13,14] flow injection[15–17] and kinetic methods[18] have also been reported.

We have developed a photochemical assay for hydrogen peroxide that is sensitive and very simple to perform. It is based on the photochemical reduction of this peroxide in the presence of haematin with leuco-phloxin (Phl_{red}), which is generated by the photochemical reaction between phloxin (Phl_{ox}) and ethylenediaminetetraacetic acid (EDTA). The photochemical assay was also used for the determination of glucose by measuring the hydrogen peroxide formed by the glucose oxidase (GOD)-catalysed reaction.

Experimental

Reagents

All chemicals were of analytical-reagent grade and solutions were prepared using doubly distilled water. Hydrogen peroxide was obtained from Merck (Perhydrol, 30%). Stock solutions were standardized by titration with permanganate which, in turn, had been standardized against oxalate according to Kolthoff and Sandell.[19] Standard glucose solutions (1×10^{-3}–1×10^{-6} mol dm^{-3}) were made by subsequent dilution of 0.1 mol dm^{-3} glucose (Sigma). Phloxin (tetrachlorotetrabromofluorescein; CI 45410) solution (4.6×10^{-4} mol dm^{-3}) was prepared by dissolving the commercial product (Geigy) in water. Haematin solution (0.05 mg cm^{-3}) was prepared by dissolving 1 mg of haematin (Sigma) in 0.5 cm^3 of 0.2 mol dm^{-3} NaOH and then diluting to 20 cm^3 with 0.15 mol dm^{-3} sodium tetraborate buffer (pH 8.5); this solution was prepared freshly each day. Glucose oxidase solution (40 U cm^{-3}) (1 U = 16.67 nkat) was prepared by dilution of the commercial product (Sigma), Type V, 138 U cm^{-3} [from *Aspergillus niger* in 0.1 mol dm^{-3} sodium acetate buffer (pH 4) containing 0.002% thimerosal as preservative]. All solutions were stored in a refrigerator to minimize degradation.

Photolysis Device

The arrangement of the apparatus is shown in Fig. 1. An electronic voltage regulator was used to obtain close voltage control for a stable radiation source. A Sylvania 250 W, 24 V halogen lamp was used as the source of visible radiation. The light produced was passed through a small water-cooled chamber which was arranged so that several neutral-density filters could be used. A lens system was used to focus the light on the reaction cell, which was thermostated at 30 ± 0.5 °C. A magnetic stirrer was used to stir the solution in the cell. The bleaching of Phl_{ox} was followed using a spectrophotometer equipped with a light-guide cell (Metrohm 662) connected to a recorder (Linseis 6512). All components were arranged in a fixed geometry to ensure a constant incident radiation intensity on the photolysis cell.

Procedures

Determination of hydrogen peroxide

To 5 cm^3 of 0.15 mol dm^{-3} sodium tetraborate buffer (pH 8.5), 4 cm^3 of 0.1 mol dm^{-3} EDTA, 2 cm^3 of 2.3×10^{-4} mol dm^{-3} Phl_{ox} and 1 cm^3 of 0.05 mg cm^{-3} haematin in the

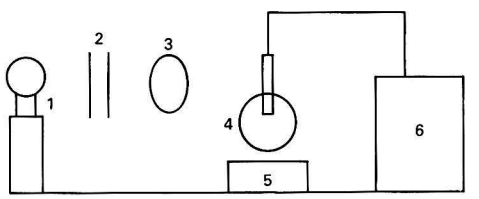

Fig. 1 Schematic diagram of the photolysis device used for the determination of hydrogen peroxide. 1, Lamp; 2, cooling system; 3, lens; 4, reaction cell; 5, magnetic stirrer; and 6, spectrophotometer

reaction cell was added an appropriate volume of hydrogen peroxide solution (standard and samples) to give a final hydrogen peroxide concentration of between 0.12 and 4.61 μg cm^{-3}. The solution was diluted to 20 cm^3 with doubly distilled water and kept at 30 ± 0.5 °C by thermostatic control. Oxygen was removed from the solution by bubbling pure nitrogen (99.99%) through the solution. The halogen lamp and the spectrophotometric titration unit recorder were switched on simultaneously, and the absorbance–photolysis time curve was recorded until the decrease in absorbance was sufficient to yield a linear graph (see Fig. 5).

The shapes of the graphs permit the evaluation of the time required for total reduction of hydrogen peroxide. The time is related to concentration by calibration with standard solutions.

Determination of hydrogen peroxide in milk

The samples (1 g of solid or 10 cm^3 of liquid), after dilution with doubly distilled water (5 cm^3), were spiked with hydrogen peroxide, then 2 mol dm^{-3} trichloroacetic acid (2 cm^3) was added and the samples were left to stand for 5 min. The curdled milk samples were then gravity filtered and the pH of the filtrates was adjusted to 8.5 with 2 mol dm^{-3} sodium hydroxide before being accurately diluted to 25 cm^3 with water. Suitable aliquots were then analysed following the procedure described above.

Determination of glucose

To 5 cm^3 of 0.15 mol dm^{-3} sodium tetraborate buffer (pH 8.5), 4 cm^3 of 0.1 mol dm^{-3} EDTA, 2 cm^3 of 2.3×10^{-4} mol dm^{-3} Phl_{ox} and 1 cm^3 of 0.05 mg cm^{-3} haematin in the reaction cell were added 1 cm^3 of 40 U cm^{-3} GOD and an appropriate volume of glucose solution (standard or samples) to give a final concentration between 4 and 43 μg cm^{-3}. The solution was diluted to 20 cm^{-3} with doubly distilled water and the amount of glucose present was obtained following the procedure described for hydrogen peroxide.

Results and Discussion

When a solution containing Phl_{ox} and EDTA in the absence of oxygen is illuminated at a suitable pH, photoreduction of the dye occurs and the pink colour disappears:

$$Phl_{ox} + EDTA \xrightarrow{h\nu} Phl_{red} + \text{EDTA oxidation products} \quad (1)$$

The reaction proceeds at an adequate rate only if the light is sufficiently intense. If air is passed through the colourless solution, the dye is oxidized and the solution returns to its original pink colour. Fig. 2 shows the absorption spectra of the dye before photoreduction and then after oxidation with oxygen of the Phl_{red} formed by photoreduction. As the two spectra coincide, it is concluded that Phl_{ox} does not undergo irreversible breakdown during the photochemical reaction.

The stoichiometry was determined by adding an excess of EDTA, at various pH values, photolysing until the dye was completely decolorized and titrating the remaining EDTA with zinc solution. The molar ratio of Phl_{ox} to EDTA was 1 : 1.

The rate of photoreduction of Phl_{ox} by EDTA is very dependent on pH, as shown in Fig. 3. Variations in temperature between 20 and 60 °C were found to have very little influence on the rate of the photochemical process.

Photogeneration of Leuco-phloxin (Phl_{red})

In the presence of an excess of EDTA, the rate of generation of Phl_{red} is given by

$$d[Phl_{red}]/dt = \sum_{\lambda} \phi_{\lambda} I_{abs} \quad (2)$$

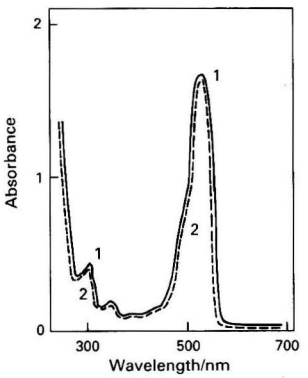

Fig. 2 Absorption spectra for 2.5×10^{-5} mol dm^{-3} Phl_{ox} with 8×10^{-3} mol dm^{-3} EDTA in sodium tetraborate buffer (pH 8.5). Curve 1: before the photochemical process. Curve 2: after the photochemical process and re-oxidation with oxygen

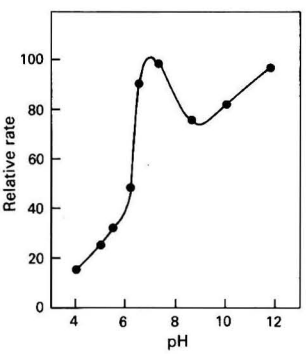

Fig. 3 Rate of photoreduction as a function of pH

The intensity of absorbed radiation can be obtained by application of the Beer–Lambert law;

$$d[Phl_{red}]/dt = \sum_{\lambda} \phi_{\lambda} I_{0\lambda} \{1\text{-}\exp(-2.3\varepsilon_{\lambda} b[Phl_{ox}])\} \quad (3)$$

where λ refers to each of any photochemically active wavelengths incident on the sample, ϕ_{λ} is the quantum yield at a given wavelength, ε_{λ} the molar absorptivity of Phl_{ox}, $I_{0\lambda}$ is the intensity of the incident radiation and b is the pathlength.

When the absorbance of the solution is greater than 2.0 the exponential term becomes smaller than 0.01. For this condition, eqn. (3) reduces to

$$d[Phl_{red}]/dt \approx \sum_{\lambda} \phi_{\lambda} I_{0\lambda} \quad (4)$$

This means that for a sufficiently large concentration of photogenerator Phl_{ox}, the rate of formation of Phl_{red} becomes independent of the concentration of the generator. The concentration of Phl_{red} at time t, c_t, can be obtained by integration of eqn. (4) over the photolysis time interval Δt, and is given by

$$c_t = \Delta t \sum_{\lambda} \phi_{\lambda} I_{0\lambda} \quad (5)$$

As the generation is carried out with no dilution, the amount of Phl_{red} formed is directly proportional to the time of photolysis, Δt. This is the fundamental basis for the linear relationship found between the photolysis time to the end-point and the amount of sample originally taken for the photochemical determination.

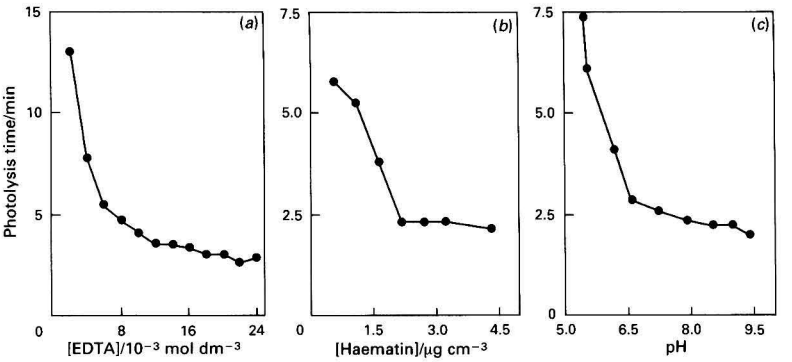

Fig. 4 Effect of the reaction variables on the photolysis time necessary for the reduction of 12 μg of hydrogen peroxide. (*a*): $[Phl_{ox}]$ = 2.3×10^{-5} mol dm^{-3}; [haematin] = 2.5 μg cm^{-3}; and 0.04 mol dm^{-3} sodium tetraborate buffer (pH 8.5). (*b*): $[Phl_{ox}]$ = 2.3×10^{-5} mol dm^{-3}; [EDTA] = 0.02 mol dm^{-3}; and 0.04 mol dm^{-3} sodium tetraborate buffer (pH 8.5). (*c*): $[Phl_{ox}]$ = 2.3×10^{-5} mol dm^{-3}; [EDTA] = 0.02 mol dm^{-3}; and [haematin] = 2.5 μg cm^{-3}

Photochemical Determination of Hydrogen Peroxide

The product of photoreduction of Phl_{ox} by EDTA, *i.e.*, Phl_{red}, is a strong reductant and reacts rapidly with hydrogen peroxide in the presence of haematin with reconversion into Phl_{ox}. When hydrogen peroxide is added to a solution of Phl_{ox}, EDTA and haematin at pH 8.5 and illuminated, the photoreduced Phl_{red} is oxidized; Phl_{ox} is then photoreduced again by EDTA and the cycle is repeated until all of the peroxide is reduced:

$$Phl_{ox} + EDTA \xrightarrow{h\nu} Phl_{red} \quad (6)$$

$$Phl_{red} + H_2O_2 \xrightarrow{Haematin} Phl_{ox} + H_2O \quad (7)$$

Haematin was required for the reaction in eqn. (7) as shown in Fig. 4(*b*). It has been observed that haematin has peroxidase activity.[20,21] The most likely mechanism of haematin catalysis is one in which haematin forms a haematin–peroxide complex, which degrades to a ferryl–oxo compound and hydroxyl radical, both of which are capable of oxidizing Phl_{red}.[22,23] De-aeration of the solution was essential as dissolved oxygen was also reduced by Phl_{red}.

Effect of Reaction Variables

This study was carried out by altering each variable in turn while keeping the others constant. The optimum reaction conditions chosen were those that yielded a minimum and constant photolysis time.

The influence of pH and the initial concentrations of EDTA and haematin on the rate of the over-all redox process is presented in Fig. 4. The photolysis time necessary for the total reduction of a fixed amount of hydrogen peroxide reaches minimum values at [EDTA] $>1.6 \times 10^{-2}$ mol dm^{-3}, [haematin] >2 μg cm^{-3} and pH >8.

The Phl_{ox} concentration must be at least 9×10^{-6} mol dm^{-3} so that the absorbance of the solution in the photolysis cell will be greater than 2.0.

The recommended conditions, therefore, are 0.02 mol dm^{-3} EDTA, 2.3×10^{-5} mol dm^{-3} Phl_{ox}, 2.5 μg cm^{-3} haematin and pH 8.5 (sodium tetraborate buffer) at 30 ± 0.5 °C.

The determination of various amounts of hydrogen peroxide with photogenerated Phl_{red} is shown in Fig. 5. The end-point (complete reduction) can be determined with great accuracy. The descending portion of the curves measures the decrease in absorbance beyond the equivalence point. A calibration graph was constructed of the time required for complete reduction of hydrogen peroxide *versus* its concentration.

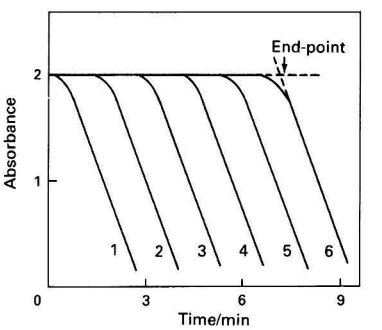

Fig. 5 Determination of the end-point for the determination of hydrogen peroxide. Curves 1–6 correspond to 2.4, 9.6, 16.8, 24.0, 31.2 and 38.4 μg of hydrogen peroxide, respectively, in a final volume of 20 cm^3

The light intensity was adjusted by using neutral-density filters in order to achieve a photolysis time necessary to arrive at the end-point of the determination in the range 1–15 min.

Calibration

The concentration of hydrogen peroxide covered by the method is 0.12–4.61 μg cm^{-3}. For higher levels of hydrogen peroxide the photolysis times needed are too long and it is advisable to dilute the sample. The regression equation of the calibration graph is

$$\Delta t(\text{min}) = 3.52\,[H_2O_2\ (\mu g\ cm^{-3})] + 0.09$$

and the correlation coefficient is 0.9992. The statistical study performed on two series of ten samples containing 0.73 and 3.64 μg cm^{-3} of hydrogen peroxide yielded relative standard deviations of 1.24 and 0.59%, respectively.

Interferences

The possible effects of various ions or substances on the determination of hydrogen peroxide following the proposed procedure are shown in Table 1. The limiting concentration of a foreign ion or substance was taken as that value which caused an error of not more than 3% in the assay. If metal ions that form stable EDTA complexes are present, preliminary

Table 1 Influence of other substances on the determination of hydrogen peroxide (2.43 μg cm^{-3})

Species added	Limiting ratio of added species to hydrogen peroxide
NO_3^-, SO_4^{2-}, Br^-, Cl^-, glucose	1000*
ClO_4^-	200
HPO_4^{2-}	100
Ba^{II}	50
Ca^{II}	30
Mg^{II}	20
Zn^{II}	10
Ni^{II}, Co^{II}, Fe^{III}	0.1
Ascorbic acid	0.1
Cu^{II}, Mo^{VI}	0.01

* Maximum molar ratio tested.

Table 2 Determination of hydrogen peroxide in milk samples

Milk type	H_2O_2 added/ μg cm^{-3}	H_2O_2 found ± SD/μg cm^{-3}	Recovery (%)
Liquid pasteurized, sample 1 (full cream)	7.6	7.55 ± 0.05	99.3
	1.5	1.55 ± 0.05	103.3
Liquid pasteurized, sample 2 (skimmed, low fat)	7.6	7.64 ± 0.05	100.5
	1.5	1.53 ± 0.03	102.2
Evaporated, sample 1 (full cream)	6.1	6.01 ± 0.06	98.5
	2.0	2.04 ± 0.07	102.0
Powdered, sample 1 (full cream)	6.1	5.93 ± 0.12	97.2
	2.0	1.98 ± 0.04	99.0

Table 3 Determination of glucose in fruit juices

Fruit juice sample	Glucose/g dm^{-3}	
	Photochemical method	Reference method
Orange	19.8	19.4
Pineapple	21.0	21.3
Apple	29.8	29.6
Pear	52.0	51.8
Mixed fruit	54.5	53.8
Grape	80.0	79.2
Kiwi	190.0	190.3

addition of EDTA is necessary; sufficient EDTA must be added to the test sample to fix the metal ions as chelates and to leave a sufficient amount of free EDTA.

Analysis of Milk Samples

The samples consisted of different brands of skimmed (low fat), full-cream liquid pasteurized, powdered and evaporated milks sold in supermarkets. All samples were previously spiked with different amounts of hydrogen peroxide and analysed following the proposed procedure.

The results obtained are given in Table 2. The data are presented as means ± SD obtained from three replicate determinations, and are in good agreement with the amounts added to each sample.

Determination of Glucose

Using glucose–glucose oxidase as the hydrogen peroxide-generating system it was possible to determine glucose. It was found that a GOD concentration of higher than 1 U cm^{-3} was necessary to obtain maximum signals in the range of glucose concentration studied. Under the recommended conditions, there was a linear relationship between glucose concentration and photolysis time over the range 3.99–43.2 μg cm^{-3} (r = 0.9989).

The photochemical method was successfully applied to the determination of glucose in fruit juices. The beverages were also analysed by a routine method described by Werner *et al.*[24] including GOD, diammonium 2,2′-azinobis(3-ethylbenzothiazoline-6-sulfonate) and peroxidase. Correlation between the two methods gave a linear regression $y = 1.002x - 0.379$ (r = 0.9999, n = 7), where x is the result obtained with the photochemical method and y that with the reference method. Results obtained based on triplicate analyses are reported in Table 3.

Conclusion

The results presented in this paper clearly demonstrate that Phl_{red}, generated by the photochemical reaction between Phl_{ox} and EDTA, can be used in the determination of hydrogen peroxide. The method is rapid, simple and convenient and has also been extended to the analysis of substrate–enzyme systems that produce hydrogen peroxide.

This investigation was supported by a grant from the Spanish DGICYT (PB90-0008).

References

1 Seitz, W. R., *CRC Crit. Rev. Anal. Chem.*, 1981, **13**, 1, and references cited therein.
2 Tamaoku, K., Murau, Y., Akiura, K., and Ohkura, Y., *Anal. Chim. Acta*, 1982, **136**, 121.
3 Allain, C. C., Poon, L. S., Chan, S. G., Richmond, W., and Fu, P. C., *Clin. Chem. (Winston-Salem N.C.)*, 1974, **20**, 470.
4 Salomon, L., and Johnson, J., *Anal. Chem.*, 1959, **31**, 453.
5 Scott, G., Seitz, W. R., and Ambrose, W. R., *Anal. Chim. Acta*, 1980, **115**, 221.
6 Shaw, F., *Analyst*, 1980, **105**, 11.
7 Shiga, M., Saito, M., and Kina, K., *Anal. Chim. Acta*, 1983, **153**, 191.
8 Frew, J. E., Jones, P., and Scholes, G., *Anal. Chim. Acta*, 1983, **155**, 139.
9 Guilbault, G. G., Brignac, P., and Zimmer, M., *Anal. Chem.*, 1968, **40**, 190.
10 Lazrus, A. L., Kok, G. L., Gitlin, S. N., Lind, J. A., and McLare, S. E., *Anal. Chem.*, 1985, **57**, 917.
11 Kieber, R. J., and Helz, G. R., *Anal. Chem.*, 1986, **58**, 2312.
12 Ebermann, R., and Couperus, A., *Anal. Biochem.*, 1987, **165**, 414.
13 Kok, G. L., Holler, T. P., López, M. B., Nachtrieb, H. A., and Yuan, M., *Environ. Sci. Technol.*, 1978, **12**, 1072.
14 Lee, J. H., Tang, I. N., and Weinstein-Lloyd, J. B., *Anal. Chem.*, 1990, **62**, 2381.
15 Růžička, J., and Hansen, E. H., *Flow Injection Analysis*, Wiley, New York, 1988, p. 351 and references cited therein.
16 Hool, K., and Nieman, T., *Anal. Chem.*, 1988, **60**, 834.
17 Genfa, Z., Dasgupta, P. K., Edgemond, W. S., and Marx, J. N., *Anal. Chim. Acta*, 1991, **243**, 207.
18 Peinado, J., Toribio, F., and Pérez-Bendito, D., *Anal. Chem.*, 1986, **58**, 1725.
19 Kolthoff, I. M., and Sandell, E. B., *Textbook of Quantitative Inorganic Analysis*, Macmillan, New York, 1963, p. 564.
20 Ames, B. N., Cathcart, R., Schwiers, E., and Hochstein, P., *Proc. Natl. Acad. Sci. USA*, 1981, **78**, 6858.
21 Howell, R. R., and Wyngaarden, J. B., *J. Biol. Chem.*, 1960, **235**, 3544.
22 *The Biological Chemistry of Iron*, eds. Dunford, H. B., Araiso, T., Job, D., Richard, J., Rutter, R., Hager, L. P., Wever, R., Kast, W. M., Boeleus, R., Ellfork, N., and Ronnberg, M., Reidel, Dordrecht, 1982.
23 Dunford, H. B., *Adv. Inorg. Biochem.*, 1982, **4**, 41.
24 Werner, W. H., Rey, G., and Wielinger, H., *Fresenius' Z. Anal. Chem.*, 1970, **252**, 224.

Paper 2/00578F
Received February 3, 1992
Accepted May 7, 1992

Novel Indicator System for the Photometric Titration of Ionic Surfactants in an Aqueous Medium. Determination of Anionic Surfactants With Distearyldimethylammonium Chloride as Titrant and Tetrabromophenolphthalein Ethyl Ester as Indicator

Shoji Motomizu, Mitsuko Oshima and Yun-hua Gao
Department of Chemistry, Faculty of Science, Okayama University, Tsushimanaka, Okayama 700, Japan
Shinsuke Ishihara and Kouji Uemura
Kyoto Electronics, Shinden, Kisshoin, Minamiku, Kyoto-shi 601, Japan

A photometric titration method for anionic surfactants with tetrabromophenolphthalein ethyl ester (TBPE) as indicator was examined. In the presence of a non-ionic surfactant (Triton X-100), TBPE was dissolved in an acidic aqueous medium giving a yellow colour in the acidic form (TBPE·H). When a bulky cation (Q^+) was added, TBPE·H reacted with Q^+ to form an ion associate (Q^+·$TBPE^-$), and the colour changed from yellow to blue. Distearyldimethylammonium ion was the preferred titrant. The titrant was added to a solution of anionic surfactant at pH 3.2, and absorbance changes were monitored with a fibre-optic sensor with a 640 nm interference filter. Anionic surfactants at concentrations from 5×10^{-6} to 2×10^{-4} mol dm^{-3} could be determined, and the standard deviations and the relative standard deviations for ten replicate titrations of 25 cm^3 of 2×10^{-4} mol dm^{-3} of various anionic surfactants were 0.03–0.15 cm^3 and 0.30–1.65%, respectively.

Keywords: *Photometric titration; anionic surfactant; aqueous medium; tetrabromophenolphthalein ethyl ester; distearyldimethylammonium salt*

As batchwise methods, liquid–liquid extraction–spectrophotometric methods are commonly used for the determination of micro-amounts of anionic surfactants. Such methods are based on the liquid–liquid extraction of ion associates with cationic dyes such as Methylene Blue and Ethyl Violet.[1–4] An automated spectrophotometric method with Methylene Blue was reported by Kawase *et al.*,[5] and it was applied to the determination of anionic surfactants at concentrations up to 1.25 mmol dm^{-3}. Recently, very sensitive and less time-consuming flow injection methods coupled with liquid–liquid extraction of ion associates have been developed and applied to the determination of anionic surfactants at μg dm^{-3} levels.[6–8]

Various types of surfactants are widely used in many fields, such as the textile, pulp, leather, mining and manufacturing industries, and the determination of ionic surfactants at concentrations of several millimolar or more is often necessary in process and quality control and in waste water control. In such instances, two-phase titration methods have been widely used.[9–11]

A two-phase titration method for anionic surfactants with a cationic titrant was first introduced by Epton.[12,13] Since then, various indicators and titrants have been examined.[11] Eppert and Liebscher[14] developed a two-phase titration method with Septonex (carbethoxypentadecyltrimethylammonium bromide) and a cationic dye, Dimethyl Yellow, which was applied to the determination of oil-soluble sulfonic acids and sulfonates.[14]

Recently, Hasegawa and co-workers[16–18] developed an automated two-phase titrator system, which was essentially based on Epton's method and utilized a porous poly(tetrafluoroethylene) (PTFE) membrane as a separator for a chloroform phase. The system is very useful for automated two-phase titrations. However, the phase separator system is troublesome and its maintenance is tedious.

Hosoi and Motomizu[19,20] developed a colour reaction of quaternary ammonium ions (Q^+) with an anionic dye, tetrabromophenolphthalein ethyl ester (TBPE·H), in the presence of non-ionic surfactants in aqueous medium. The reaction mechanism at pH 4 is

$$\underset{\text{yellow}\ (\lambda_{max} = 430\ \text{nm})}{(\text{TBPE·H})_m} + Q^+ \rightleftharpoons \underset{\text{blue}\ (\lambda_{max} = 600\text{–}610\ \text{nm})}{(Q^+\cdot\text{TBPE}^-)_m} + H^+$$

where $(\ )_m$ denotes the species in a micelle phase and TBPE·H and Q^+·$TBPE^-$ are the protonated species of TBPE and the ion associate of $TBPE^-$ and Q^+, respectively. This colour reaction is very sensitive for long-chain quaternary ammonium ions. However, in a batchwise method, the sensitivities are not identical in quaternary ammonium ions and the calibration graphs are slightly curved.

This paper describes an automated titration method for the determination of anionic surfactants at micromolar concentrations in an aqueous medium using a photometric detector, the indicator system of which is based on the colour reaction of TBPE with a titrant (Q^+).

Experimental

Reagents

Tetrabromophenolphthalein ethyl ester (TBPE) indicator solution. A 1×10^{-3} mol dm^{-3} TBPE solution was prepared by dissolving 70 mg of TBPE (potassium salt) (Wako Pure Chemical Industries) in 100 cm^3 of ethanol.

Quaternary ammonium titrant solutions. Distearyldimethylammonium chloride ($DSDMA^+Cl^-$) (Tokyo Kasei Kogyo) was dried to constant mass at 50 °C under reduced pressure (about 400 Pa) before use, and the dried salt was dissolved in ethanol to give a 1.25×10^{-2} mol dm^{-3} stock solution. A titrant solution (5×10^{-4} mol dm^{-3} $DSDMA^+Cl^-$) was prepared by diluting the stock solution with distilled water. Other quaternary ammonium salts (listed in Table 2) were dried under reduced pressure in a similar manner, and the dried salts were dissolved in distilled water.

Anionic surfactants. Sodium dodecyl sulfate (LS) (99.9%), sodium linear-dodecylbenzenesulfonate (DBS) (99.0%), and

sodium dodecane-1-sulfonate (DS) (99.0%) were purchased from Wako Pure Chemical Industries and sodium di-2-ethylhexylsulfosuccinate (SSS) (96.3%) from Kanto Chemical. These anionic surfactants were dried at 50 °C to constant mass under reduced pressure before use. They were dissolved in distilled water to give a 2×10^{-3} mol dm^{-3} stock solution, and were used after accurate dilution.

Non-ionic surfactant, Triton X-100 (TX-100). A 50 cm^3 volume of TX-100 (Rohm & Haas) was dissolved in hot distilled water. The solution was cooled and sufficient distilled water was added to bring the volume to 500 cm^3.

Buffer solutions. Monochloroacetate buffer solutions (1 mol dm^{-3}) and acetate buffer solutions (1 mol dm^{-3}) were used to adjust the pH of reaction solutions to 2.2–4.0.

Apparatus

Absorbance changes were measured with a Kyoto Electronics AT-310J automatic titrator with an APB-310 auto piston burette and a fibre-optic sensor. pH values were measured with a Corning Ion Analyzer 250 with a combined electrode. Beakers of 50 cm^3 were used and solutions in the beakers were stirred continuously with a magnetic stirrer bar during titration.

Standard Procedure

A 25 cm^3 volume of sample solution containing anionic surfactant at concentrations up to 2×10^{-4} mol dm^{-3} was placed in a 50 cm^3 beaker and 1 cm^3 each of 0.63% TX-100, 1.25×10^{-4} mol dm^{-3} TBPE and 1 mol dm^{-3} buffer solution (pH 3.2) were added. The mixture was titrated with DSDMA$^+$ (5.0×10^{-4} mol dm^{-3}) with continuous recording of the absorbance until the colour changed from yellow to blue. The absorbance changes were monitored with a fibre-optic sensor with a 630 nm interference filter. End-points were read from the inflection points using differential curves. Calibration graphs were prepared by using working solutions of LS containing 0–2.0×10^{-4} mol dm^{-3} of LS.

Results and Discussion

Indicator System

Yamamoto and Motomizu[21] reported flow injection spectrophotometric methods for the determination of ionic surfactants, based on the reaction of quaternary ammonium ions with dibasic anionic dyes such as Bromocresol Green, Bromothymol Blue, Bromocresol Purple (BCP), Bromochlorophenol Blue and Bromophenol Blue. Of these dyes, BCP was found to be the most suitable for the determination of anionic surfactants.

In this work, such dibasic anionic dyes were examined for use as indicator systems. When a CDMBA$^+$Cl$^-$ (cetyldimethylbenzylammonium chloride) solution was used as a titrant, the precipitates of the ion associates of anionic surfactants with CDMBA$^+$ occurred near the equivalence point, as shown in Fig. 1(*a*). This result shows the possibility of a precipitation titration, and anionic surfactants (LS$^-$) at concentrations from 5×10^{-5} to 2×10^{-4} mol dm^{-3} could be titrated with the CDMBA$^+$ solution, although the reproducibility of the titrant was not good. In the presence of non-ionic surfactants such as TX-100 and Brij 58, the precipitates did not appear during the titration. However, the absorbance change at 640 nm was very slow at pH 8 with BCP and also with other dyes as indicators, and a clear end-point was not observed with any of the indicators, as shown in Fig. 1(*b*) as an example. As a result, attempts to titrate anionic surfactants with quaternary ammonium ions as titrant and dibasic anionic dyes as indicator were all unsuccessful.

As other possible triphenylmethane dyes, a monobasic anionic dye, TBPE, was examined. In the presence of 0.025% v/v TX-100, the absorbance near 605 nm increased with increasing concentration of quaternary ammonium ion, DSDMA$^+$ [Fig. 2(*a*)], and the calibration graph for DSDMA$^+$ was linear up to 8×10^{-6} mol dm^{-3}. This colour reaction was considered to be based on the formation of an ion associate of a quaternary ammonium ion Q$^+$ with TBPE$^-$.

The reaction scheme is

$$\underset{\lambda_{max} = 420\ nm}{\{TBPE{\cdot}H\}_m} + Q^+ \rightleftharpoons \underset{\lambda_{max} = 605\ nm}{\{Q^+{\cdot}TBPE^-\}_m} + H^+ \quad (1)$$

where $\{\ \}_m$ denotes mixed micelles of TBPE·H and its ion associate Q$^+$·TBPE$^-$ with TX-100.

The blue colour resulting from the reaction of Q$^+$ with TBPE$^-$ faded on adding anionic surfactants (AS$^-$) according to the reaction

$$\underset{\lambda_{max} = 605\ nm}{\{Q^+{\cdot}TBPE^-\}_m} + AS^- + H^+ \rightleftharpoons \underset{\lambda_{max} = 420\ nm}{\{Q^+{\cdot}AS^- + TBPE{\cdot}H\}_m} \quad (2)$$

As is shown in Fig. 2(*b*), the absorbance at 605 nm decreased with increasing concentration of anionic surfactant,

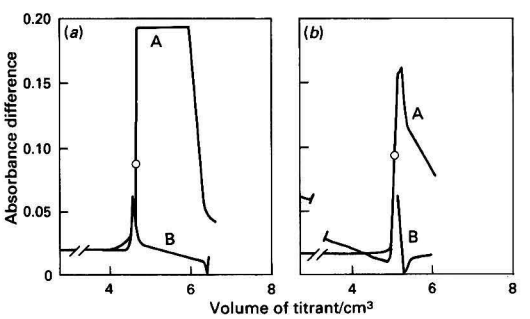

Fig. 1 Titration curves for the titration of LS$^-$ with CDMBA$^+$ in the presence and absence of TX-100. A, Absorbance curves, B, differential curves. Circles indicate end-points. Sample, 25 cm^3 of 1×10^{-4} mol dm^{-3} LS$^-$; titrant, 5×10^{-4} mol dm^{-3} CDMBA$^+$; indicator, 5×10^{-6} mol dm^{-3} BCP; pH = 8.1. (*a*) Without TX-100, and (*b*) with 0.025% v/v TX-100

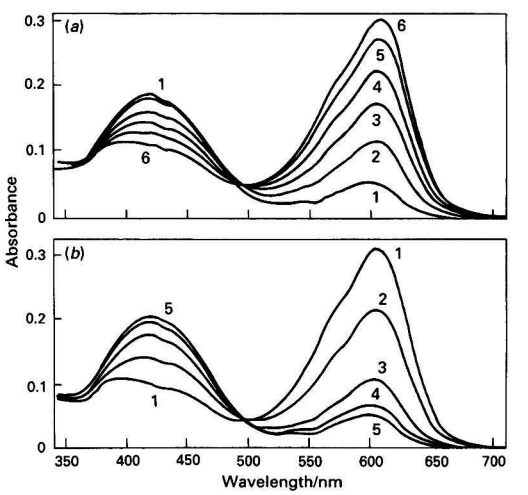

Fig. 2 Absorption spectra of TBPE in the presence of DSDMA$^+$ and in the presence of both DSDMA$^+$ and LS$^-$. TBPE: 1.0×10^{-5} mol dm^{-3}; TX-100: 0.025%; pH 3.2. (*a*) [DSDMA$^+$]/10^{-5} mol dm^{-3}; 1, 0; 2, 0.2; 3, 0.4; 4, 0.6; 5, 0.8; and 6, 1.0. (*b*) DSDMA$^+$: 1.0×10^{-5} mol dm^{-3}; [LS$^-$]/10^{-5} mol dm^{-3}: 1, 0; 2, 0.25; 3, 0.50; 4, 0.75; and 5, 1.00

LS^-. The reactions shown by eqns. (1) and (2) are thought to involve the extraction of ion associates into micelles and we therefore call such reactions 'micelle extraction'. By using the colour change based on this micelle extraction, the photometric titration of anionic surfactants was examined.

Effect of pH

The pH of sample solutions containing LS^- was varied from 2.2 to 4.0. Table 1 shows the results obtained using blank and sample (LS^-) solutions. The end-points could not be observed at pH 2.2. The acid dissociation constant of TBPE·H is known to be about 4.2, and therefore the titrant $DSDMA^+$ cannot be exchanged for the H^+ of TBPE·H at pH 2.2. At pH >3.6, $DSDMA^+$ can easily be exchanged for the H^+ of TBPE·H, and the end-points of blank solutions could not be determined from differential curves and were considered to be zero. Fig. 3 shows examples of the titration curves of LS^- with $DSDMA^+$. At pH 4.0, the absorbance near the end-points changed abruptly, and reproducible end-points could be obtained from the differential curves. In this instance, however, more accurate end-points are taken as the intersection of extrapolated linear portions as is shown in Fig. 3(*f*), and the volume of the blank solution is the deflection point of the differential curve in Fig. 3(*c*). For the automated determination of end-points, titration at pH 2.6–3.6 is recommended.

Table 1 Effect of pH on the end-points of the titration of LS. End-points were determined from the differential curves. Titrant, 5.0×10^{-4} mol dm^{-3} $(C_{18}H_{37})_2N(CH_3)_2^+$ ($DSDMA^+$); sample, 25 cm^3 of 2×10^{-4} mol dm^{-3} LS^-; indicator, 5.0×10^{-6} mol dm^{-3} TBPE; TX-100, 0.025%

	Titrant/cm^3*		
pH	Blank	Sample	Net
2.2	No EP†	No EP†	—
2.6	0.49 ± 0.05	10.61 ± 0.03	10.12
2.9	0.37 ± 0.02	10.53 ± 0.02	10.16
3.2	0.33 ± 0.01	10.36 ± 0.02	10.03
3.6	0.00‡	10.18 ± 0.02	10.18
4.0	0.00‡	10.06 ± 0.06	10.06

* Mean values of three replicates; ± values are the largest deviations from the mean values.
† End-points were not determined from the differential curves.
‡ Absorbances increased linearly with increasing titrant volume.

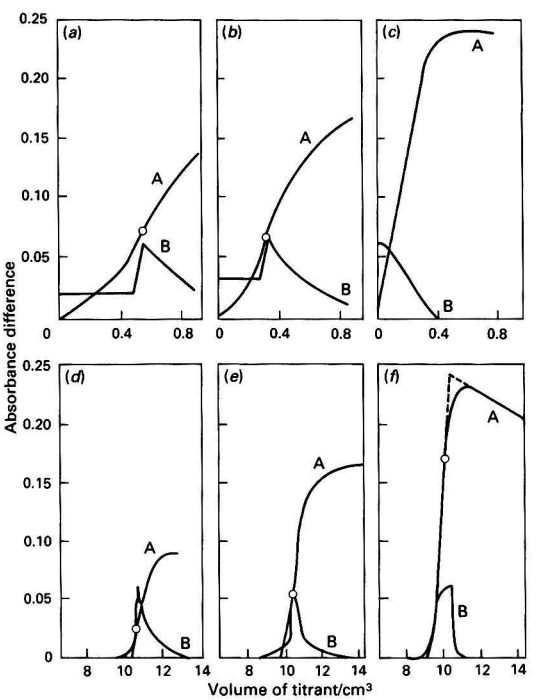

Fig. 3 Effect of pH on titration curves. A, Absorbance curves; B, differential curves; circles indicate end-points. (*a*) and (*d*): pH 2.6; (*b*) and (*e*): pH 3.2; (*c*) and (*f*): pH 4.0 TBPE: 5.0×10^{-6} mol dm^{-3}; TX-100: 0.025% v/v. Titrant: 5×10^{-4} mol dm^{-3} $DSDMA^+$. Samples: (*a*)–(*c*) LS = 0, (*d*)–(*f*) 2.0×10^{-4} mol dm^{-3} LS^-

Effect of Amount of TBPE Indicator

The concentrations of TBPE were varied from 1×10^{-6} to 1×10^{-5} mol dm^{-3}. As is shown in Fig. 4(*a*), at low concentrations of TBPE the absorbance changes were very small and the end-points were beyond the expected volume of the titrant. At higher concentrations of TBPE, the solutions became turbid near the end-points [Fig. 4(*c*)] and the reproducibility of the end-points became worse.

Effect of Amount of Non-ionic Surfactants

The protonated species of the indicator, TBPE·H, is less soluble in water, and therefore the solutions of TBPE become turbid in water at pH <4. However, in the presence of non-ionic surfactants such as TX-100, TBPE dissolved in water even at pH <4. When more than 0.01% v/v TX-100 was present, a 1×10^{-5} mol dm^{-3} TBPE solution became clear,

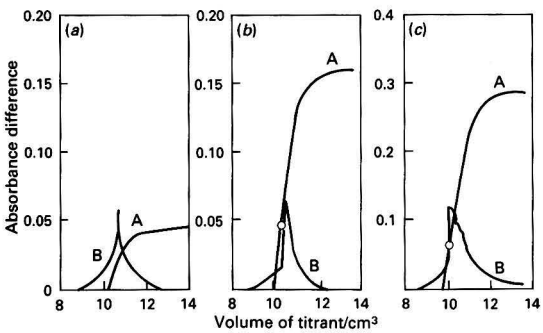

Fig. 4 Effect of TBPE concentration on titration curves. A, Absorbance curves; B, differential curves; circles indicate end-points. Titrant: 5.0×10^{-4} mol dm^{-3} $DSDMA^+$; sample: 25 cm^3 of 2.0×10^{-4} mol dm^{-3} LS^-. pH 3.2; TX-100: 0.025%. Indicator (TBPE): (*a*) 2.5×10^{-6}; (*b*) 5.0×10^{-6}; and (*c*) 1.0×10^{-5} mol dm^{-3}

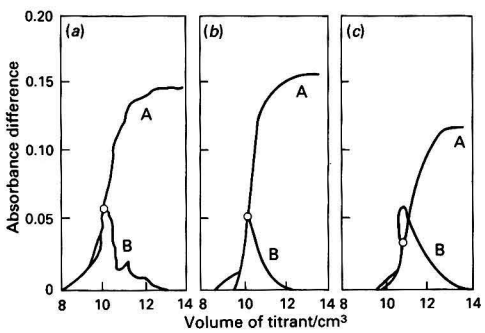

Fig. 5 Effect of non-ionic surfactant concentration on titration curves. A, Absorbance curves; B, differential curves; circles indicate end-points. Non-ionic surfactant (TX-100): (*a*) 0.01; (*b*) 0.025; and (*c*) 0.030%. TBPE: 5.0×10^{-6} mol dm^{-3}; other conditions as in Fig. 4

Table 2 Quaternary ammonium ions examined as titrants. Titrant, 5×10^{-4} mol dm^{-3} Q^+; sample, 25 cm^3 of 2×10^{-4} mol dm^{-3} LS^-; pH, 3.2; TBPE, 5.0×10^{-6} mol dm^{-3}; TX-100, 0.025%

Quaternary ammonium salt (Q^+)	Abbreviation	Titrant/cm^3* Blank	Titrant/cm^3* Sample
Distearyldimethylammonium chloride	$DSDMA^+$	0.33 ± 0.01	10.36 ± 0.02
Stearyltrimethylammonium chloride	$STMA^+$	0.79 ± 0.02	11.14 ± 0.02
Cetyltrimethylammonium chloride	$CTMA^+$	0.83 ± 0.03	10.57 ± 0.06
Tetradecyltrimethylammonium chloride	$TDTMA^+$	>3	11.61
Dodecyltrimethylammonium chloride	$DDTMA^+$	—†	—†
Tetrapentylammonium chloride	TPA^+	—†	—†

* Mean values of three replicates; ± values are the largest deviations from the mean values.
† End-points were not determined from the differential curves.

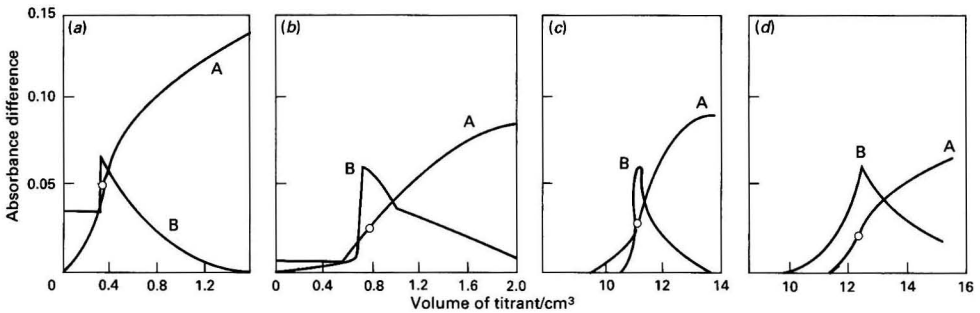

Fig. 6 Titration curves obtained with $STMA^+$ as the titrant. A, Absorbance curves; B, differential curves; circles indicate end-points. (*a*) 5.0×10^{-4} mol dm^{-3} $DSDMA^+$, $[LS^-] = 0$; (*b*) 5.0×10^{-4} mol dm^{-3} $STMA^+$, $[LS^-] = 0$; (*c*) 5.0×10^{-4} mol dm^{-3} $STMA^+$, $[LS^-] = 2.0 \times 10^{-4}$ mol dm^{-3}; and (*d*) 5.0×10^{-4} mol dm^{-3} $STMA^+$, $[DS^-] = 2.0 \times 10^{-4}$ mol dm^{-3}. TBPE: 5.0×10^{-6} mol dm^{-3}; pH 3.2; TX-100: 0.025%. Sample: 25 cm^3

Table 3 Linearity of calibration graphs. Titrant, 5.0×10^{-4} mol dm^{-3} $DSDMA^+$; sample, 25 cm^3 of LS^-; TBPE, 5.0×10^{-6} mol dm^{-3}; TX-100, 0.025%

$[LS^-]/10^{-4}$ mol dm^{-3}	Titrant/cm^3* pH 4.0	pH 3.2	pH 2.6
0.0	0.00	0.33 ± 0.01	0.49 ± 0.06
0.5	2.46 ± 0.02	2.84 ± 0.00	3.06 ± 0.01
1.0	4.91 ± 0.05	5.30 ± 0.02	5.55 ± 0.04
2.0	9.89 ± 0.05	10.36 ± 0.02	10.61 ± 0.03
Regression curve†			
$y = (10^5/2)$ $kx + b$	$k = 0.989$, $b = 0.00$	$k = 1.00$, $b = 0.33$	$k = 1.017$, $b = 0.49$

* Mean values of three replicates; ± values show the largest deviations from the mean values.
† y = Volume of titrant (cm^3); x = concentration of LS^- (mol dm^{-3}); k = slope of regression curve; b = volume of titrant for blank (cm^3)

Table 4 Linearity of calibration graphs at low concentrations of anionic surfactants. Titrant, (A) 5.0×10^{-4} mol dm^{-3} $DSDMA^+$ and (B) 5.0×10^{-5} mol dm^{-3} $DSDMA^+$; sample, 25 cm^3 of LS^-; TBPE, 5.0×10^{-6} mol dm^{-3}; TX-100, 0.025%; pH, 3.2

$[LS^-]/10^{-5}$ mol dm^{-3}	Titrant/cm^3* A	B
0.0	0.33 ± 0.01	1.44 ± 0.15
0.5	0.57 ± 0.01 (0.24)	4.05 ± 0.05 (2.61)
1.0	0.84 ± 0.06 (0.51)	6.54 ± 0.23 (5.10)
2.0	1.38 ± 0.02 (1.05)	11.80 ± 0.26 (10.36)
Regression curve†		
$y = (10^6/2)$ $kx + b$	$k = 0.100$, $b = 0.33$	$k = 1.030$, $b = 1.44$

* Mean values of three replicates; ± values show the largest deviations from the mean values. Figures in parentheses are net volumes of the titrant.
† See Table 3.

and with increasing amount of TX-100 the colour change became less sharp and the reproducibility of the end-points decreased [Fig. 5(*c*)]. In the present procedure, sample solutions were continuously stirred during the titration and air bubbles were present in the solutions. These bubbles were easily adsorbed on the surface of the optical sensor and the glass wall of the titration vessel when small amounts of non-ionic surfactants were present in the sample solutions. The bubbles adsorbed on the surface of the sensor interfered with the accurate measurement of the absorbances, as shown in Fig. 5(*a*). Such phenomena are explained as follows: in the presence of increasing amounts of TX-100, the surface tension of solutions becomes lower and air bubbles become less adsorbed on the surface of the sensor. When more than 0.02% v/v TX-100 was added to the sample solutions, hardly any air bubbles were adsorbed on the sensor and they were collected on the surface of the sample solutions. Considering these results, 0.025% v/v TX-100 was adopted in the standard procedure.

Selection of Quaternary Ammonium Salt as Titrant

Quaternary ammonium salts, listed in Table 2, were examined as titrants. The results of blank tests showed that the longer the alkyl chains of the quaternary ammonium ions (Q^+), the higher is the reactivity of Q^+ with TBPE and the better is the reproducibility of the titration. Fig. 6 shows the titration curves for LS^- and DS^- with $STMA^+$ (stearyltrimethylammonium) as titrant. The absorbance increase was smaller in the titration with $STMA^+$ than with $DSDMA^+$. By using $STMA^+$

the differential curve for DS^- showed a broader peak than for LS^-, which indicates that LS^- forms a more stable ion associate with Q^+ than DS^-. In the standard procedure, $DSDMA^+$ was adopted owing to its high reactivity and the good reproducibility of the titration.

Determination Ranges for Anionic Surfactants

Table 3 shows the data for the calibration graphs of LS^- at concentrations up to 2×10^{-4} mol dm^{-3}, obtained at various pH values with 5×10^{-4} mol dm^{-3} $DSDMA^+$ as titrant. The linearity of each calibration graph was very good, and each value of the intercept on the ordinate was in good agreement with the experimental value for each blank test.

Table 4 shows the data for the calibration graphs of LS^- at concentrations up to 2×10^{-5} mol dm^{-3}, which were obtained with 5×10^{-4} and 5×10^{-5} mol dm^{-3} $DSDMA^+$ solutions as titrants. Both calibration graphs showed good linearity, and

Table 5 Reproducibility test for the determination of various anionic surfactants. Titrant, 5.0×10^{-4} mol dm^{-3} $DSDMA^+$; sample, 25 cm^3 of 2×10^{-4} mol dm^{-3} anionic surfactant; pH, 3.2; TBPE, 5.0 ± 10^{-6} mol dm^{-3}; TX-100, 0.025%

Sample (2×10^{-4} mol dm^{-3})	Titrant/cm^3*	SD†/cm^3	RSD‡ (%)
LS^-	10.57	0.03	0.30
DBS^-	10.39	0.04	0.41
SSS^-	9.99	0.08	0.84
DS^-	9.28	0.15	1.65

* Mean values of ten replicates.
† Standard deviations.
‡ Relative standard deviations.

Table 6 Determination of anionic surfactants in commercial samples

Sample No.*	Anionic surfactants/mg cm^{-3}	
	Expected†	Found‡
1	277.5	208.1 ± 1.9
2	165.0	120.6 ± 1.1
3	234.6	188.4 ± 0.9
4	278.1	212.5 ± 1.3

* Samples 1 and 2, synthetic detergents for washing; samples 3 and 4, synthetic detergents for kitchen. The total content of the detergents in sample 1 is 37% and the surfactants are sodium linear-alkylbenzenesulfonates, sodium alkyl sulfates and others. The total content of the detergents in sample 2 is 22% and the surfactants are sodium α-sulfocarboxylic esters and others. The total content of the detergetns in sample 3 is 23% and the surfactants are sodium linear-alkylbenzenesulfonates, sodium alkyl sulfates and others. The total content of the detergents in sample 4 is 27% and the surfactants are metal salts of linear-alkylbenzenes and others.
† These values were calculated from the indicated total contents of detergents.
‡ These values were calculated by assuming that anionic surfactants in the samples were DBS^-.

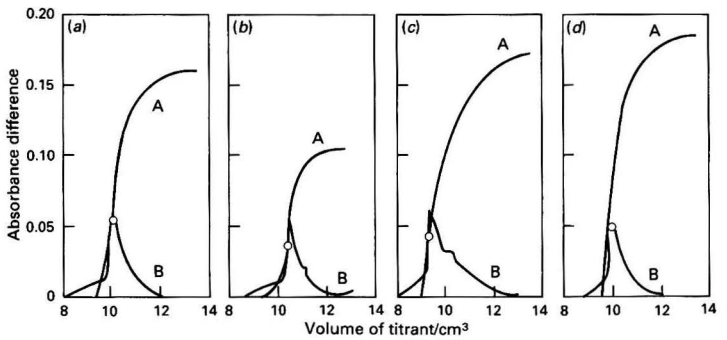

Fig. 7 Titration curves for various anionic surfactants (AS^-). A, Absorbance curves; B, differential curves; circles indicate end-points. AS^- (2.0×10^{-4} mol dm^{-3}): (*a*) LS^-; (*b*) DBS^-; (*c*) DS^-; and (*d*) SSS^-. Conditions as in Fig. 6

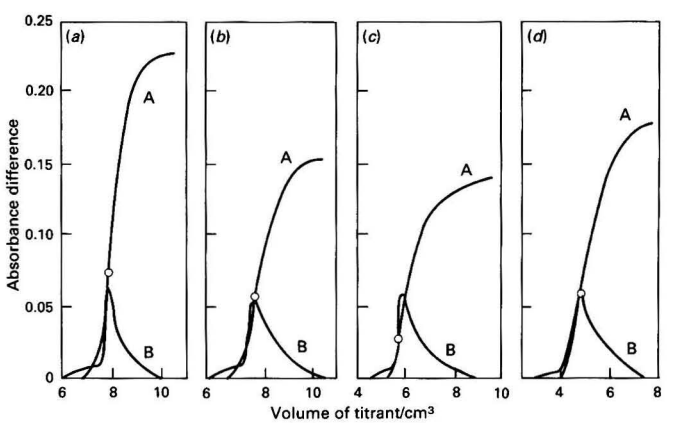

Fig. 8 Titration curves for commercial synthetic detergents. A, Absorbance curves; B, differential curves; circles indicate end-points. Commercial samples: (*a*) and (*b*) are synthetic detergents for washing; (*c*) and (*d*) are synthetic detergents for the kitchen. Conditions as in Fig. 6. The contents of the detergents are shown in Table 6

the intercepts on the ordinates were in good agreement with the experimental values. The net amounts of $DSDMA^+$ titrated were almost identical in both procedures with 5×10^{-4} and 5×10^{-5} mol dm^{-3} $DSDMA^+$ solutions, and also the percentage variances of the volume of the titrant were almost identical in both procedures. From these results, anionic surfactants at concentrations at the 1×10^{-6} mol dm^{-3} level can be determined by titration with $DSDMA^+$.

Application of the DSDMA Titration Method to the Determination of Anionic Surfactants in Synthetic Detergents

Various types of anionic surfactant were titrated with $DSDMA^+$. Each titration curve gave a clear end-point, as is shown in Fig. 7.

Table 5 shows the results obtained using various types of anionic surfactant. All these anionic surfactants could be determined by the standard titration method with $DSDMA^+$, and the standard deviations and the relative standard deviations are good, except for DS^-.

The method was applied to the determination of anionic surfactants in commercially available synthetic detergents for washing. The titration curves for the samples show clear end-points, as illustrated in Fig. 8, and the deviations of the experimental values are about 0.6–0.9%.

However, the contents of anionic surfactants obtained are 75–80% of the values expected from the stated total contents of detergents (Table 6). The reason why the experimental values are 20–25% lower than those expected is that the molecular mass of the anionic surfactants in the samples is unknown and different from that of DBS^-, and that some of the detergents in the samples are non-ionic and do not react with $DSDMA^+$.

Conclusion

A novel indicator system for the titration of anionic surfactants in an aqueous medium was developed. The colour change at the end-points was very clear, and the standard deviations and relative standard deviations for ten replicate determinations of 2×10^{-4} mol dm^{-3} LS^- were 0.03 cm^3 and 0.3%, respectively. By using the proposed titration method, anionic surfactants at micromolar levels can be determined.

This work was supported by a Grant-in-Aid for Scientific Research, No. 03453043, from the Ministry of Education, Science and Culture, Japan.

References

1 American Public Health Association, American Water Works Association and Water Pollution Control Federation, *Standard Methods for the Examination of Water and Waste Water*, Washington, DC, 17th edn., 1989, pp. 5–59.
2 *Japanese Industrial Standard*, JIS K 0102, Japanese Standards Association, Tokyo, 1991.
3 Motomizu, S., Fujiwara, S., Fujiwara, A., and Tôei, K., *Anal. Chem.*, 1982, **54**, 392.
4 Yamamoto, K., and Motomizu, S., *Analyst*, 1987, **112**, 1405.
5 Kawase, J., Nakae, A., and Yamanaka, M., *Anal. Chem.*, 1979, **51**, 1640.
6 Motomizu, S., Hazaki, Y., Oshima, M., and Tôei, K., *Anal. Sci.*, 1987, **3**, 265.
7 Motomizu, S., Oshima, M., and Kuroda, T., *Analyst* 1988, **113**, 747.
8 Motomizu, S., and Korechika, K., *Bunseki Kagaku*, 1989, **38**, T143.
9 International Organization for Standardization, ISO 2271, 1972; 6121, 1979.
10 *Japanese Industrial Standard*, JIS K 3362, Japanese Standards Association, Tokyo, 1990.
11 Schmitt, T. M., *Analysis of Surfactants*, Marcel Dekker, New York, 1992, p. 344.
12 Epton, S. R., *Nature (London)*, 1947, **160**, 795.
13 Epton, S. R., *Trans. Faraday Soc.*, 1948, **44**, 226.
14 Eppert, G., and Liebscher, G., *Z. Chem.*, 1978, **18**, 188.
15 Markó-Monostory, B., and Börzsönyi, S., *Tenside Detergents*, 1985, **22**, 5.
16 Hasegawa, A., Yamanaka, M., Tsuji, K., and Tamura, S., *Bunseki Kagaku*, 1982, **31**, 508.
17 Hasegawa, A., Yamanaka, M., and Tsuji, K., *Bunseki Kagaku*, 1983, **32**, 474.
18 Takano, S., Hasegawa, A., and Ohotsuka, H., *Bunseki Kagaku*, 1988, **37**, 137.
19 Hosoi, Y., and Motomizu, S., *Bunseki Kagaku*, 1989, **38**, 205.
20 Hosoi, Y., and Motomizu, S., *Bunseki Kagaku*, 1989, **38**, 211.
21 Yamamoto, K., and Motomizu, S., *Anal. Chim. Acta*, 1991, **246**, 333.

Paper 2/01696F
Received March 31, 1992
Accepted May 27, 1992

Oxo[5,10,15,20-tetra(4-pyridyl)porphyrinato]titanium(IV): An Ultra-high Sensitivity Spectrophotometric Reagent for Hydrogen Peroxide

Chiyo Matsubara, Naoki Kawamoto and Kiyoko Takamura*
Department of Pharmacy, Tokyo College of Pharmacy, 1432-1, Horinouchi Hachioji, Tokyo 192-03, Japan

The water-soluble titanium(IV)–porphyrin complex, oxo[5,10,15,20-tetra(4-pyridyl)porphyrinato]titanium(IV) [$TiO(tpypH_4)^{4+}$], was found to enhance the spectrophotometric determination of trace amounts of hydrogen peroxide. A 0.05 mol dm^{-3} hydrochloric acid solution containing $TiO(tpypH_4)^{4+}$ was used (the Ti–TPyP reagent), the absorbance of which decreased at 432 nm as hydrogen peroxide was added. This was due to the consumption of the $TiO(tpypH_4)^{4+}$ complex following the formation of peroxo[5,10,15,20-tetra(4-pyridyl)porphyrinato]titanium(IV). The decrease in absorbance at 432 nm (ΔA_{432}) was proportional to the concentration of hydrogen peroxide, from 1.0×10^{-8} to 2.8×10^{-6} mol dm^{-3}, in the sample solution (25 pmol–7.0 nmol per assay). The reaction was accelerated by hydrogen ions; the presence of 1.6 mol dm^{-3} perchloric acid was found to promote complexation to the greatest extent. A ΔA_{432} of 1.9×10^5 was found for 1 mol dm^{-3} hydrogen peroxide. A measurement precision of 1.2% for 1.0×10^{-6} mol dm^{-3} hydrogen peroxide ($n = 8$) was obtained. The reagent can be used for the determination of hydrogen peroxide in water samples such as tap water and rainwater over the range from 1.05×10^{-7} to 3.34×10^{-5} mol dm^{-3}.

Keywords: *Hydrogen peroxide determination; titanium(IV)–porphyrin complex; oxo[5,10,15,20-tetra-(4-pyridyl)porphyrinato]titanium(IV) reagent; spectrophotometry; hydrogen peroxide in water*

Recently, hydrogen peroxide in water has become of concern as the terminal product of the hydroperoxy radical in photochemical reactions. Hydrogen peroxide at high concentrations in the atmosphere affects human health, and can cause irritation to the eyes and skin. Moreover, hydrogen peroxide has an important function in heterogeneous processes as an oxidant, producing sulfuric and nitric acids in the atmosphere and rain. Its concentration varies widely and ranges from less than 1×10^{-8} mol dm^{-3} in relatively clean rainwater to more than 1×10^{-5} mol dm^{-3} in polluted rainwater.[1]

The determination of hydrogen peroxide is carried out in clinical assays of body fluids. By development of enzymic techniques, trace amounts of hydrogen peroxide can be quantitatively produced through the oxidation of the biological substances present.

For environmental and clinical analysis, the chemiluminescence of luminol or spectrophotometry using chromogens of peroxidase, such as the 4-aminoantipyrine–phenol system, is generally used.[2–4] However, results with these methods are affected considerably by the reducible substances that are present, as they are based on oxidative condensation reactions of the fluorophores and chromogens with hydrogen peroxide using peroxidase, which has a low selectivity to hydrogen donors.[5] Therefore, methods providing high selectivity would not require peroxidase or be based on redox reactions.

In a previous study, in order to prevent the interference from reducible substances, colour development systems based on the formation of a titanium(IV) complex with hydrogen peroxide and pyridylazo compounds were developed.[6–9] The apparent molar absorption coefficient (ε) for hydrogen peroxide in these systems is about 1×10^4 m^2 mol^{-1}; this was, however, inadequate for determining hydrogen peroxide when present at trace amounts. The use of ligands having larger ε values compared with the pyridylazo pigments was considered as a means for achieving greater sensitivity in measurement.

Certain water-soluble porphyrins have been used for the highly sensitive spectrophotometric determination of various metal ions,[10–13] as porphyrins have a strong absorption band at 400–450 nm, *viz.* the Soret band. A very highly sensitive method for hydrogen peroxide was thus established using porphyrins as the ligands for complex formation.

In this paper, a method was developed for determining trace amounts of hydrogen peroxide using the oxo[5,10,15,20-tetra(4-pyridyl)porphyrinato]titanium(IV) complex, [TiO(tpyp) as the basic form and $TiO(tpypH_4)^{4+}$, the protonated form]. An acid solution of $TiO(tpypH_4)^{4+}$ (Ti–TPyP reagent) was used for this determination.

Experimental

Reagents

The TiO(tpyp) complex synthesized according to the method of Inamo *et al.*[14] was specially supplied by Tokyo Kasei Industries. The Ti–TPyP reagent (5.0×10^{-5} mol dm^{-3}) was prepared by dissolving 34.03 mg of the TiO(tpyp) complex in 1000 cm^3 of 0.05 mol dm^{-3} hydrochloric acid. A standard hydrogen peroxide solution (0.100 mol dm^{-3}) was prepared by diluting 5.5 cm^3 of 30% v/v hydrogen peroxide to 500 cm^3 with water. The solution was standardized by titration with potassium permanganate. All reagent solutions were prepared with distilled, de-ionized water.

Procedure

To a 250 mm^3 sample of water, 250 mm^3 of 4.8 mol dm^{-3} perchloric acid and 250 mm^3 of Ti–TPyP reagent were added. The mixed solution was then allowed to stand for 5 min at room temperature. A sample solution was prepared by diluting this solution to 2.50 cm^3 with water. The absorbance at 432 nm was measured (A_S). A blank solution was prepared in a similar manner, using distilled water instead of the sample with its absorbance designated as A_B. The difference in absorbance was determined as follows: $\Delta A_{432} = A_B - A_S$. Based on the value obtained, the hydrogen peroxide content was determined.

Apparatus

The absorbance was measured with a UVIDEC-660 spectrophotometer (Japan Spectroscopic) using quartz cells of 1 cm pathlength.

* To whom correspondence should be addressed.

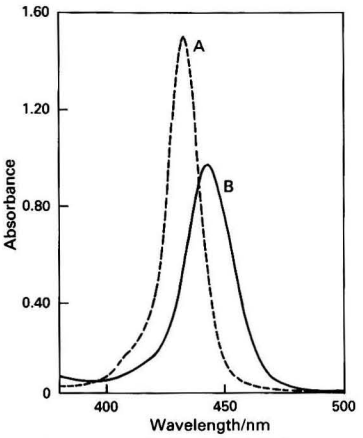

Fig. 1 Absorption spectra of: A, the Ti–TPyP reagent; and B, the $TiO_2(tpypH_4)^{4+}$ complex. $[HClO_4]$, 0.5 mol dm^{-3}; [Ti–TPyP], 5×10^{-6} mol dm^{-3}; and $[H_2O_2]$, 1×10^{-5} mol dm^{-3}

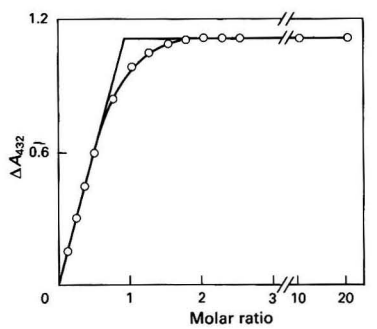

Fig. 2 Molar ratio method for determining the composition of the $TiO_2(tpypH_4)^{4+}$ complex. $[HClO_4]$, 0.5 mol dm^{-3}; and [Ti–TPyP], 5×10^{-6} mol dm^{-3}

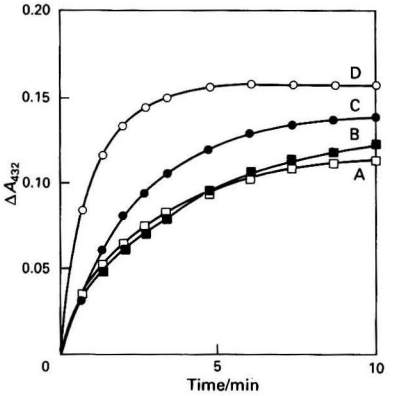

Fig. 3 Effect of acid for promoting formation of the $TiO_2(tpypH_4)^{4+}$ complex. Acids: A, HCl; B, H_2SO_4; C, HNO_3; and D, $HClO_4$. Concentration of acid up to time of reaction, 1.6 mol dm^{-3}; [Ti–TPyP], 5×10^{-6} mol dm^{-3}; and $[H_2O_2]$, 1×10^{-6} mol dm^{-3}

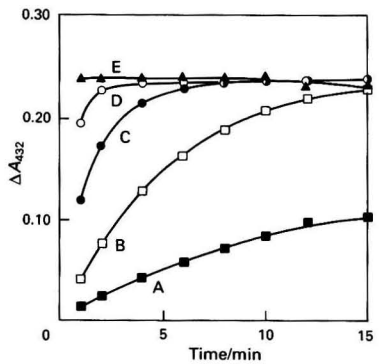

Fig. 4 Effect of concentration of perchloric acid on complex formation reaction. Concentration of $HClO_4$ up to time of reaction: A, 0.4; B, 0.8; C, 1.2; D 1.6; and E, 2.0 mol dm^{-3}. [Ti–TPyP], 5×10^{-6} mol dm^{-3}; and $[H_2O_2]$, 1×10^{-6} mol dm^{-3}

Results and Discussion

Ti–TPyP Reagent

The absorption spectrum of the Ti–TPyP reagent in 0.5 mol dm^{-3} perchloric acid is shown as curve A in Fig. 1.

The sharp peak, having a maximum at 432 nm, suggests the presence of only the $TiO(tpypH_4)^{4+}$ complex. Essentially the same peak was noted for $TiO(tpypH_4)^{4+}$ by Inamo *et al.*[14] When hydrogen peroxide was added to the Ti–TPyP reagent, the absorption peak decreased significantly in proportion to the concentration of hydrogen peroxide added, this being due to consumption of $TiO(tpypH_4)^{4+}$ accompanied by the formation of $TiO_2(tpypH_4)^{4+}$. The ΔA_{432} (degree of the decrease of absorbance at 432 nm) per mol dm^{-3} of hydrogen peroxide was 1.9×10^5. Following the addition of hydrogen peroxide to the Ti–TPyP reagent, the absorbance at 432 nm decreased and a new absorption peak was observed at 450 nm, as shown by curve B in Fig. 1. This peak was assigned to peroxo[5,10,15,20-tetra(4-pyridyl)porphyrinato]titanium(IV) $[TiO_2(tpypH_4)^{4+}]$[14] and its absorbance was proportional to the concentration of hydrogen peroxide. The apparent molar absorptivity was 1.1×10^5 m^2 mol^{-1}. This value was only half that for ΔA_{432}. Thus, based on the decrease in absorbance at 432 nm, trace amounts of hydrogen peroxide can be determined with greater sensitivity, and accordingly, this should be possible using the ΔA_{432} value.

The molar ratio method (at 432 nm) was used to determine the composition of the peroxo complex.[15] It can be seen from Fig. 2, that a monoperoxo complex with hydrogen peroxide is formed from $TiO(tpypH_4)^{4+}$ as follows:

$$TiO(tpypH_4)^{4+} + H_2O_2 \rightarrow TiO_2(tpypH_4)^{4+} + H_2O$$

The equilibrium constant for this reaction was $4.0 (\pm 0.4) \times 10^6$ dm^3 mol^{-1} at 25 °C,[14] which should be sufficient for determining the hydrogen peroxide content.

The Ti–TPyP reagent appeared useful for spectrophotometrically determining trace amounts of hydrogen peroxide, and thus additional experiments were conducted to decide on the optimum conditions for the method.

Optimization of the Measurement Conditions

Effect of acid

The use of various strong acids was found to enhance complex formation. Their effects on the rate of increase in ΔA_{432} were examined using a 1.0×10^{-6} mol dm^{-3} standard hydrogen peroxide solution. The results for hydrochloric, sulfuric, nitric and perchloric acids are shown in Fig. 3. With 1.6 mol dm^{-3} perchloric acid, a maximum value for ΔA_{432} was attained within 5 min, whereas the other acids showed less than 80% of the final value for ΔA_{432} even after standing for 10 min. Perchloric acid was thus considered best for the enhancement of the reaction.

The ΔA_{432} value was affected by the concentration of the perchloric acid that catalysed the peroxide substitution. Thus,

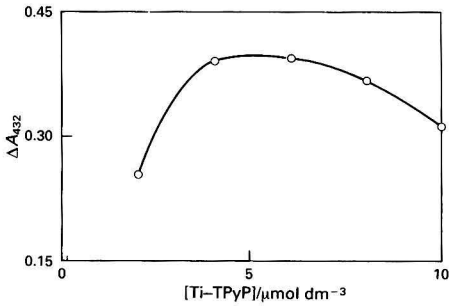

Fig. 5 Effect of concentration of the Ti–TPyP reagent on complex formation. Concentration of $HClO_4$ up to time of reaction, 1.6 mol dm^{-3}; and [H_2O_2], 2 × 10^{-6} mol dm^{-3}

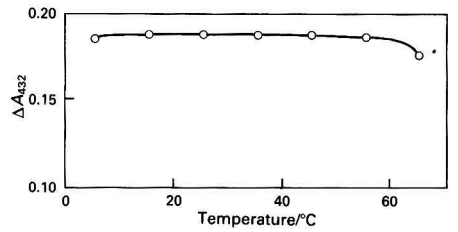

Fig. 6 Effect of the temperature of incubation on complex formation of mixture of sample solution and Ti–TPyP reagent. Concentration of $HClO_4$ up to time of reaction, 1.6 mol dm^{-3}; [Ti–TPyP], 5 × 10^{-6} mol dm^{-3}; and [H_2O_2], 1 × 10^{-6} mol dm^{-3}

the effect of the concentration of this acid on ΔA_{432} was examined while maintaining the concentrations of the Ti–TPyP reagent and hydrogen peroxide constant. As shown in Fig. 4, the ΔA_{432} value was constant over the range 1.6–2.0 mol dm^{-3}, irrespective of whether or not the standing time exceeded 3 min. A slight increase in A_S (decrease in ΔA_{432}) was noted after 15 min for 2.0 mol dm^{-3} perchloric acid.

The effects of perchlorate anion concentration on ΔA_{432} were also investigated. The ΔA_{432} value was found to be constant over the range from 1 × 10^{-4} to 0.5 mol dm^{-3}. The concentration was maintained at 1.6 mol dm^{-3} for complex formation, and subsequently diluted to 0.5 mol dm^{-3} for measurement of the absorbance.

Effect of reagent concentration

The concentration of the Ti–TPyP reagent affected the ΔA_{432} value, and thus a suitable concentration of this reagent was sought. A concentration of Ti–TPyP reagent of 5 × 10^{-6} mol dm^{-3} for complex formation was considered optimum as the ΔA_{432} value was at a maximum (Fig. 5).

Temperature of incubation

The effect of temperature on complex formation was examined. Virtually no dependence could be detected from 5 to 55 °C (Fig. 6) and equilibrium was attained within 5 min. The absorbance remained virtually constant for 2 h at room temperature; therefore, room temperature was subsequently chosen as being best for the application of the Ti–TPyP reagent. The reagent was stable for 20 months under refrigeration with no detectable change in absorbance.

Determination of Hydrogen Peroxide

Based on the results given above, the conditions for the spectrophotometric determination of hydrogen peroxide using the Ti–TPyP reagent were decided as described under Experimental.

Table 1 Effect of inorganic foreign substances on the determination of hydrogen peroxide using the Ti–TPyP reagent

Substance added	Concentration/ mol dm^{-3}	H_2O_2 found* (%)
NaCl	1 × 10^{-2}	99.5
KCl	1 × 10^{-2}	101.0
$BaCl_2$	1 × 10^{-2}	99.8
NH_4Cl	1 × 10^{-2}	98.2
$NiCl_2$	1 × 10^{-2}	100.6
$CuCl_2$	1 × 10^{-2}	99.9
$MnCl_2$	1 × 10^{-3}	94.7
$CoCl_2$	1 × 10^{-4}	99.4
$FeCl_3$	1 × 10^{-5}	97.3
$CaCl_2$	1 × 10^{-2}	101.2
$MgCl_2$	1 × 10^{-2}	100.3
NaBr	1 × 10^{-2}	101.0
$NaNO_3$	1 × 10^{-2}	99.8
NaN_3	1 × 10^{-2}	101.7
Na_2SO_4	1 × 10^{-2}	98.3
NaH_2PO_4	1 × 10^{-2}	100.9
H_3BO_3	1 × 10^{-2}	99.6

* [H_2O_2] = 1.00 × 10^{-6} mol dm^{-3}.

Table 2 Determination of hydrogen peroxide in water samples

Sample source	H_2O_2 concentration/ mol dm^{-3}	Recovery* (%)
Well water	4.74 × 10^{-7}	90.6
Tap water	3.16 × 10^{-7}	84.0
Ion-exchanged water	1.05 × 10^{-7}	96.9
NANOpure II	2.63 × 10^{-7}	99.2
Rainwater sample No. 1	2.74 × 10^{-6}	97.2
Rainwater sample No. 2	9.16 × 10^{-6}	94.9
Rainwater sample No. 3	1.62 × 10^{-5}	106.5
Rainwater sample No. 4	2.91 × 10^{-5}	104.4
Rainwater sample No. 5	3.34 × 10^{-5}	104.2

* [H_2O_2] added: 3.00 × 10^{-7} mol dm^{-3}.

The ΔA_{432} value, as determined using the standard hydrogen peroxide solution, could be expressed as a linear relationship when plotted against concentration, $y = 1.9 \times 10^5x + 0.0097$ (y and x being the ΔA_{432} and molar concentration of hydrogen peroxide, respectively). The correlation coefficient was 0.999 over the range from 1.0 × 10^{-8} to 2.8 × 10^{-6} mol dm^{-3} (from 25 pmol to 7 nmol per assay). The relative standard deviation was 1.2% at 1.0 × 10^{-6} mol dm^{-3} hydrogen peroxide (2.5 nmol per assay).

Effects of Foreign Substances

The above results demonstrate that the Ti–TPyP reagent is applicable to the determination of hydrogen peroxide from various sources, such as environmental water and biological fluids. For assessment of its usefulness in environmental and clinical assays, the effects of certain foreign substances generally present in the above types of sample were examined (Table 1). Inorganic ions such as Na^+, K^+, Ca^{2+}, Ni^{2+}, Cl^-, Br^-, NO_3^- and $H_2PO_4^-$ did not noticeably affect the accuracy of the determination, even up to a concentration 10000-fold that of hydrogen peroxide. A decrease in ΔA_{432} was obtained with Fe^{3+} and Co^{2+} ions present at 100 and 1000 times the concentration of hydrogen peroxide, respectively. These metal ions might possibly catalyse the decomposition of hydrogen peroxide.

Determination of Hydrogen Peroxide in Water Samples

The proposed method was used to determine hydrogen peroxide in well water, tap water, ion-exchanged water and water treated by the NANOpureII system (Barnstead). The results are shown in Table 2. Hydrogen peroxide at ppb levels

was determined for 10 samples within 1 h. The recovery of 3.00×10^{-7} mol dm^{-3} (approximately 10 ppb) hydrogen peroxide was from 90 to 99%, except for tap water.

The concentration of hydrogen peroxide in rainwater was also measured and was found to range from 2.7×10^{-6} to 3.34×10^{-5} mol dm^{-3}. The recovery of 3.00×10^{-7} mol dm^{-3} hydrogen peroxide ranged from 94.9 to 106.5%.

Conclusions

The Ti–TPyP reagent was shown to be useful for spectrophotometrically determining trace amounts of hydrogen peroxide.

A comparison of ΔA_{432} per mol dm^{-3} of hydrogen peroxide with the molar absorptivity indicated that the sensitivity of the proposed method exceeded that of the peroxidase (POD)–4-aminoantipyrine–phenol method by 16 times.[16] Generally when using POD any reducible substances (such as ascorbic acid) present inhibit the colour development. In the proposed method, no enzyme is required for colour development through complex formation and, therefore, such substances do not affect the process significantly.

This method should find application to the determination of the composition of biological material using appropriate oxidizing enzymes to produce hydrogen peroxide.

References

1 Yoshizumi, K., Aoki, K., Nouchi, I., Okita, T., Kobayashi, T., Kamakura, S., and Tajima, M., *Atmos. Environ.*, 1984, **18**, 395.
2 Madsen, B. C., and Kromis, M. S., *Anal. Chem.*, 1984, **56**, 2849.
3 Beltz, N., Jaeschke, W., Kok, G. L., Gitlin, S. N., Lazrus, A. L., McLaren, S. E., Shakespeare, D., and Mohnen, V. A., *J. Atmos. Chem.*, 1987, **5**, 311.
4 van Zoonen, P., Kamminga, D. A., Gooijer, C., Velthorst, N. H., and Frei, R. W., *Anal. Chim. Acta*, 1985, **174**, 151.
5 Sharp, P., *Clin. Chim. Acta*, 1972, **40**, 155.
6 Matsubara, C., and Takamura, K., *Bunseki Kagaku*, 1980, **29**, 759.
7 Matsubara, C., Iwamoto, T., Nishikawa, Y., Takamura, K., Yano, S., and Yoshikawa, S., *J. Chem. Soc., Dalton Trans.*, 1985, **1**, 81.
8 Matsubara, C., Nishikawa, Y., Yoshida, Y., and Takamura, K., *Anal. Biochem.*, 1983, **130**, 128.
9 Matsubara, C., Nishikawa, Y., and Takamura, K., *Yakugaku Zasshi*, 1983, **103**, 884.
10 Itoh, J., Yotsuyanagi, T., and Aomura, K., *Anal. Chim. Acta*, 1975, **74**, 53.
11 Ishii, H., and Koh, H., *Bunseki Kagaku*, 1979, **28**, 473.
12 Omata, M., and Itoh, J., *Nihon Kagaku Kaishi*, 1988, **9**, 1578.
13 Endo, K., Igarashi, S., and Yotsuyanagi, T., *Chem. Lett.*, 1986, 1711.
14 Inamo, M., Funahashi, S., and Tanaka, M., *Inorg. Chem.*, 1983, **22**, 3734.
15 Yoe, J. H., and Jones, A. L., *Ind. Eng. Chem. Anal. Ed.*, 1944, **16**, 111.
16 Trinder, P., *Ann. Clin. Biochem.*, 1969, **6**(1–2), 24.

Paper 2/01225A
Received March 6, 1992
Accepted April 27, 1992

Spectrophotometric Determination of Hexamethylenetetramine

Gary L. Madsen and Bruno Jaselskis*
Department of Chemistry, Loyola University of Chicago, 6525 N. Sheridan Road, Chicago, IL 60626, USA

A spectrophotometric method has been developed for the quantitative determination of aqueous hexamethylenetetramine (HMT) alone, in the presence of large amounts of formaldehyde, and in the presence of urine. The method is based on the perchloric acid hydrolysis of HMT to formaldehyde, oxidation of formaldehyde by hydrous silver(I) oxide, and oxidation of silver(0) with iron(III) in the presence of FerroZine. Optimum conditions were developed and HMT was determined over the range from 3×10^{-7} to 3.3×10^{-6} mol dm^{-3}. The method developed is approximately 7.5 times more sensitive than the chromotropic acid method.

Keywords: *Hexamethylenetetramine determination; spectrophotometry; methenamine; formaldehyde interference; urine*

Hexamethylenetetramine (HMT), $(CH_2)_6N_4$, also known as 1,3,5,7-tetraazatricyclo[3.3.1.1^{3,7}]decane, urotropine, hexamine, hexamethyleneamine, formine, aminoform and methenamine (USAN rINN), is a relatively old common urinary tract antiseptic. This compound was described in the literature as early as 1859 by Butlerow[1] and was used as a urinary tract antiseptic by Nicolaier[2] as early as 1894. Hexamethylenetetramine has been used for the manufacture of the high explosives RDX and HMX and as a controlled source of anhydrous formaldehyde to provide methylene group cross-linking in the curing of phenol–formaldehyde resins. Other commercial uses of HMT include the hardening of proteins (such as in glues), corrosion inhibition, fuel tablets for camping stoves and as a preservative.

Many methods have been developed for the determination of milligram amounts of HMT including spectrophotometry,[3] infrared spectroscopy,[4] polarography,[5] specific gravity,[6] gravimetry,[7] bromimetry,[8] nuclear magnetic resonance spectroscopy,[9] gas chromatography,[10] acid–base,[11] amperometry,[12] potentiometry,[13] conductimetry,[14] coulometry[15] and complexometry.[16] This extensive chemistry is due largely to the development of methods to assay prescription tablets that contain at least 250 mg. Despite this activity, there are relatively few methods available for the determination of HMT at low microgram levels; the methods available include spectrophotometry,[17–21] polarography,[22] potentiometry,[23] high-performance liquid chromatography[24,25] and gas chromatography.[26] As most of these methods are indirect determinations based on determination of the amount of formaldehyde released after hydrolysis, only small amounts of formaldehyde can be present before HMT hydrolysis. To determine the amount of formaldehyde formed from hydrolysis of HMT, the small amount of formaldehyde originally present must be determined prior to hydrolysis and then subtracted from the amount of formaldehyde formed after hydrolysis.

This study describes: (*i*) the indirect determination of micro-amounts of HMT; (*ii*) the elimination of a large amount of formaldehyde interference in the presence of micro-amounts of HMT; and (*iii*) the condensation of ammonia with formaldehyde and the determination of the resulting HMT. The HMT is determined, after hydrolysis to formaldehyde, by the Al-Jabari–Jaselskis method.[27]

Experimental

Instrumentation

Spectrophotometric measurements were obtained using a Cary 14 spectrophotometer equipped with quartz cells of 1 cm pathlength. The pH measurements were made using a Fisher Accumet Model 830 pH meter.

Reagents

All chemicals were of analytical or primary standard reagent grade. Hexamethylenetetramine was purified by recrystallization from absolute ethanol. Before use, HMT was dried over phosphorus pentoxide for 4 h as described in the United States Pharmacopeia (USP) XXII standard method.[28] FerroZine, 3-(2-pyridyl)-5,6-diphenyl-1,2,4-triazine-*p*,*p*′-disulfonic acid monosodium salt monohydrate (Aldrich), was used. A 0.01 mol dm^{-3} stock solution was prepared by dissolving 0.511 g in 100 cm^3 of distilled water. Stock solutions of 0.004 mol dm^{-3} iron(III) and 0.075 mol dm^{-3} silver nitrate were prepared by dissolving 1.929 g of ammonium iron(III) sulfate dodecahydrate in 1 dm^3 of 0.09 mol dm^{-3} sulfuric acid and 1.274 g of silver nitrate in 100 cm^3 of distilled water. An acetate buffer solution of pH 3.5 was prepared by partially neutralizing 0.5 mol dm^{-3} acetic acid with concentrated sodium hydroxide. Nickel(II) solution was prepared by dissolving 0.727 g of nickel(II) nitrate in 100 cm^3 of distilled water to produce a 0.025 mol dm^{-3} solution. Formaldehyde solutions were prepared by diluting an appropriate amount of commercial 37% formaldehyde containing 10–15% methanol. Sodium tetrahydroborate(III) solution of 2.4 mol dm^{-3} was prepared daily by dissolving 90.8 mg in 1 cm^3 of 0.2% sodium hydroxide. Chromotropic acid, 4,5-dihydroxynaphthalene-2,7-disulfonic acid disodium salt dihydrate (Aldrich), reagent solution was prepared as described in the USP XXII standard method.[28]

Procedures

Determination of aqueous HMT or HMT monomandelate

Solid samples of purified HMT or HMT monomandelate were weighed and dissolved in distilled water and treated as aqueous samples. Aqueous samples were determined by placing sample aliquots of 400 mm^3, containing 0.016–0.16 μmol of HMT, into 50 cm^3 calibrated flasks. The samples were hydrolysed by adding 1 cm^3 of 1 mol dm^{-3} perchloric acid and heating the stoppered flasks at 60 °C in a water-bath for 10 min. After chilling the samples in iced water for 1 min, the perchloric acid was neutralized and the solutions were made basic with 500 mm^3 of 2.2 mol dm^{-3} sodium hydroxide. Silver(I) was added by pipetting 200 mm^3 of 0.075 mol dm^{-3} silver nitrate into the sample; after vigorous mixing, the solution was allowed to react for 10 min with hydrous silver oxide. A 2 cm^3 aliquot of 0.004 mol dm^{-3} acidic iron(III), 2 cm^3 of 0.1 mol dm^{-3} FerroZine and 6 cm^3 of pH 3.5 acetate buffer

* To whom correspondence should be addressed.

were added to each sample followed by vigorous mixing and dilution to volume with distilled water. After 10 min the absorbance of the iron(II)–FerroZine complex was measured at 562 nm using 1 cm pathlength cells. To obtain high precision results, the amount of time required for each step must be closely monitored. Each sample was given the same amount of reaction time in each step. Both standard samples and synthetic unknown samples were determined by analysing all of the samples at the same time.

Elimination of large amounts of formaldehyde interference

Formaldehyde was eliminated by either evaporation or tetrahydroborate reduction. Evaporation of samples was accomplished using aspirator vacuum in a vacuum desiccator containing Drierite. Aliquots of 50 mm^3 of HMT in the range 2.3–23 μg and up to 0.2 mol dm^{-3} formaldehyde were pipetted into 30 cm^3 test-tubes containing 20 mm^3 of 0.025 mol dm^{-3} nickel nitrate and 10 mm^3 of glacial acetic acid. The test-tubes were placed in a vacuum desiccator and were aspirated just to dryness. (Prolonged aspiration can cause some loss of the HMT.) The dry samples were redissolved in 400 mm^3 of distilled water and the remaining HMT was then determined as previously described for aqueous HMT samples.

The interference of formaldehyde was also eliminated by sodium tetrahydroborate reaction. Formaldehyde–HMT (50 mm^3) aliquots containing HMT in the range 2.3–23 μg and up to 0.2 mol dm^{-3} formaldehyde were placed in 25 cm^3 calibrated flasks containing 20 mm^3 of 2.40 mol dm^{-3} freshly prepared alkaline tetrahydroborate. After 15 min reaction the sample was acidified with 25 mm^3 of 2 mol dm^{-3} perchloric acid to destroy all remaining tetrahydroborate, diluted to about 400 mm^3 with distilled water, and analysed *via* hydrolysis for HMT as previously described for aqueous samples.

Determination of HMT in urine

Aliquots of 50 mm^3 of urine spiked with 0.096–0.48 μmol of HMT (0.27–1.35 mg cm^{-3}) were pipetted into 10 cm^3 test-tubes containing 20 mm^3 of 2.2 mol dm^{-3} sodium hydroxide and 550 mm^3 of 0.09 mol dm^{-3} silver nitrate. The test-tubes were stoppered, agitated and then heated at 60 °C for 10 min to accomplish the oxidation and precipitation of interferences. The samples were chilled, centrifuged and filtered through cotton-wool plugged Pasteur pipettes to remove the reduced silver and interferences. Aliquots of 100 mm^3 from each sample were placed in 25.0 cm^3 calibrated flasks containing 300 mm^3 of water, and the HMT was determined in the samples as previously described for aqueous samples. Larger aliquots of filtered samples can be taken for samples containing smaller amounts of HMT (300 mm^3 filtered sample for 0.090 mg cm^{-3} urine sample). Blanks for urine were determined on the filtered samples by proceeding with the HMT determination without hydrolysis.

Condensation of ammonia with formaldehyde for the indirect determination of ammonia

Ammonia samples and standards were quantitatively added to calibrated flasks so that the final diluted ammonia concentration was in the range 0.5–8.5 mmol dm^{-3}. Formaldehyde was quantitatively added to the flask to produce a diluted concentration of 0.10 mol dm^{-3}, the solution was diluted to volume with distilled water and mixed. The flask was immersed in a 60 °C water-bath for 4 h to ensure complete HMT condensation. The sample was then cooled to room temperature and a 50 mm^3 aliquot removed. The excess of formaldehyde was eliminated by either evaporation or chemical reduction and the remaining HMT was determined as described for aqueous samples.

Determination of blanks

Blanks were prepared for a particular determination by preparing a sample without HMT but similar in composition to the samples of interest. The blank samples were then carried through the determination procedure in exactly the same way as for the HMT containing samples.

Determination of HMT by the USP XXII chromotropic acid method[28]

Sample aliquots of 80.0 mm^3 containing 0.026–0.26 μmol of HMT were pipetted into 10 cm^3 calibrated flasks. A 5 cm^3 volume of dilute sulfuric acid (1 + 1) and 2.5 cm^3 of chromotropic acid reagent solution were added and mixed. The 10 cm^3 calibrated flasks were placed in a boiling water-bath for an accurately timed 30 min and then immediately cooled in iced water to room temperature. Dilute sulfuric acid (1 + 1) was added to volume, the solution mixed and the absorbance measured at 570 nm against a blank.

Results

Results for synthetic aqueous unknown samples containing pure HMT and HMT in the presence of formaldehyde are shown in Table 1 using both the proposed method and the USP XXII chromotropic acid method. Results for the determination of ammonia, related to HMT determined, are shown in Table 2. Urine samples containing HMT were determined by the method of standard additions in the final

Table 1 Determination of aqueous HMT alone and in the presence of formaldehyde

Method	Final HMT concentration/ ng cm^{-3}	Sample CH_2O concentration/ mol dm^{-3}	HMT determined using calibration graph/ ng cm^{-3}	Relative standard deviation (%) (n = 4)
Iron–FerroZine:				
	111	—	113 (102)*	1.07
	210	—	213 (102)	0.345
	367	—	370 (101)	0.242
Chromotropic acid:				
	1110	—	1140 (103)	0.159
	2100	—	2110 (100)	0.408
	3670	—	3560 (96.8)	0.233
Formaldehyde elimination by evaporation:				
	108	0.0297	109 (101)	0.718
	251	0.0933	251 (100)	0.650
	334	0.163	332 (100)	0.267
Formaldehyde elimination by chemical reduction:				
	108	0.0297	109 (101)	1.38
	251	0.0933	254 (100)	0.500
	334	0.163	334 (101)	0.706

* Values in parentheses in %.

Table 2 Determination of ammonia in simulated unknown samples

Method	Final NH_3 concentration/ ng cm^{-3}	HMT determined using calibration graph/ ng cm^{-3}	Relative standard deviation (%) (n = 3)
Formaldehyde elimination by evaporation:			
	33.3	33.4 (100)*	0.948
	48.9	50.5 (103)	0.969
	84.5	85.5 (101)	0.790
	107	109 (101)	0.685
Formaldehyde elimination by tetrahydroborate reduction:			
	33.3	34.1 (102)	0.580
	48.9	49.1 (100)	0.419
	84.5	85.7 (101)	0.249
	107	109 (102)	0.658

* Values in parentheses in %.

dilution range from 6×10^{-7} to 32×10^{-7} mol dm^{-3} HMT. The HMT in urine, at 6×10^{-7} mol dm^{-3} concentration final dilution (0.27 mg cm^{-3} of HMT originally) using three replicates, was determined with a relative standard deviation of 1.9%.

Discussion

The indirect determination of HMT is based on the quantitative hydrolysis of HMT and the subsequent determination of formaldehyde released. The determination requires the control of a number of variables: (*i*) the hydrolysis conditions of HMT; (*ii*) the oxidation of the resulting formaldehyde with hydrous silver oxide; (*iii*) the oxidation of the metallic silver produced by formaldehyde with iron(III) in the presence of FerroZine; and (*iv*) the separation of HMT from the large amounts of formaldehyde.

The hydrolysis of HMT has been studied[29] and is shown to proceed in strongly acidic sulfuric acid as follows:

$$C_6H_{12}N_4 + 2H_2SO_4 + 6H_2O \xrightarrow{\text{heat}} 6CH_2O + 2(NH_4)_2SO_4 \quad (1)$$

However, the hydrolysis of HMT with sulfuric acid coupled with the proposed procedure yields low results. Hydrochloric and nitric acids were not used as hydrochloric acid yields insoluble silver chloride and nitric acid produces undesirable nitrated compounds. Dilute perchloric acid (0.7–1.4 mol dm^{-3}) shows no interference and will quantitatively hydrolyse HMT when heated between 40 and 60 °C. At 60 °C, the HMT is hydrolysed within 7 min in 0.7 mol dm^{-3} perchloric acid and within 4 min in 1.4 mol dm^{-3} perchloric acid. The lower acid concentration was preferred for easier pH adjustment throughout the determination procedure.

The oxidation and determination of the resulting formaldehyde from the hydrolysis of HMT is essentially accomplished by the Al-Jabari–Jaselskis[27] procedure. Formaldehyde is oxidized by hydrous silver oxide and the reduced metallic silver is re-oxidized with iron(III) in the presence of a complexing agent, FerroZine (Fz), as shown in the following reactions:

$$6CH_2O + 12Ag^+ \xrightarrow[\text{pH 12–13}]{(OH-)} 12Ag^0 + 6HCOO^- \quad (2)$$

$$12Ag^0 + 12Fe^{3+} \xrightarrow{H^+} 12Fe^{2+} + 12Ag^+ \quad (3)$$

$$12Fe^{2+} + 36Fz^{2-} \xrightarrow{\text{pH 3–6}} 12Fe(Fz)_3^{4-} \quad (4)$$

The molar absorption coefficient (ε) of $Fe(Fz)_3^{4-}$ is 2.79×10^3 m^2 mol^{-1} at 562 nm.[27] The theoretical ε for HMT by use of this method should be 3.35×10^4 m^2 mol^{-1}. The experimentally determined values for different sets of runs lie in the range 3.14×10^4–3.22×10^4 m^2 mol^{-1}, which is somewhat lower than expected. We attribute this deviation to minor losses in the procedure. The most accurate results are obtained by determining unknowns along with standards and by the use of a calibration graph rather than the ε value.

Determination of HMT or HMT–mandelate in the presence of small amounts of formaldehyde is achieved readily by first determining the amount of formaldehyde before the hydrolysis and then the total amount of formaldehyde after the hydrolysis. The difference in the amount of formaldehyde is related to the HMT present. However, HMT in the presence of large amounts of formaldehyde or complex mixtures, such as urine, must be separated from interferences. The formaldehyde interference can be removed by either evaporation or chemical reduction.

As the boiling-point of formaldehyde is −20 °C and HMT sublimes at 260 °C, it would appear that the evaporation of formaldehyde to leave HMT should be readily achieved. However, during evaporation, formaldehyde polymerizes to form paraformaldehyde and some of the HMT is lost by sublimation. Paraformaldehyde is an interferent as it is oxidized by hydrous silver oxide. The formation of paraformaldehyde can be inhibited by the addition of glacial acetic acid, and the sublimation of HMT diminished by complexation with nickel. Dilute acetic acid (0.1 mol dm^{-3}) does not readily hydrolyse HMT as noted by Bose.[30] Evaporation requires approximately 2 h, with careful observation at the end of the evaporation.

The removal of formaldehyde can also be accomplished by chemical reduction to methanol with alkaline tetrahydroborate. The tetrahydroborate reduction has an advantage over evaporation by saving a considerable amount of time and requiring less careful attention. The reduction requires an excess (greater than 1 : 1 molar ratio) of tetrahydroborate and is achieved in less than 15 min. The excess of tetrahydroborate (an interferent) is destroyed by perchloric acid prior to the hydrolysis of HMT.

Following either method of formaldehyde removal, there remains a residual blank interference, which is proportional to the original amount of formaldehyde present. The amount of formaldehyde present in the sample must be determined and accounted for by the preparation of a blank calibration graph for the most accurate results.

The determination of HMT in urine samples is difficult due to the complexity of urine, which contains many different interfering components. Dilute urine samples tested with this procedure contained coloured interferences, which were too large for blank subtraction. However, removal of these interferences can be accomplished by chemical means. Richmond *et al.*[31] reported that HMT is very stable to hydrolysis under alkaline conditions. Thus, the interferences capable of reducing silver(I), in alkaline media, or forming precipitates, including chloride and small amounts of formaldehyde, can be removed by 'pre-reacting' the sample with hydrous silver oxide and heating the solution at 60 °C for 10–15 min. The filtered sample then appears to be free of spectrophotometric interferences and HMT can be determined by the method of standard additions or directly using a calibration graph prepared from similar samples. The samples tested correspond to original HMT concentrations in the urine of 0.27–1.35 mg cm^{-3}. Samples containing smaller amounts of HMT can be analysed as noted under Procedures. As physiological concentrations of HMT range from 0.6 to 1.7 mg cm^{-3}, as reported by Musher and Griffith,[32] this method is sufficiently sensitive for clinical applications.

We have also investigated the condensation reaction of ammonia with formaldehyde and the formation of HMT. This reaction can also be used for the indirect determination of ammonia. The formation of HMT requires approximately 4 h, a relatively high concentration of formaldehyde, pH control and mild heating. Kawasaki and Ogata[33] state that the maximum rate of formation occurs at pH 9.8 corresponding to a solution of ammonia and formaldehyde alone. Although micro-amounts of ammonia can be determined in this manner, as shown in Table 2, it is time consuming.

Interferences include any compounds that reduce silver(I) or iron(III) and any compound yielding formaldehyde on hydrolysis with dilute perchloric acid.

References

1 Butlerow, A., *Ann. Chem. Pharm.*, 1859, **111**, 249.
2 Nicolaier, A., *Zblt. Med. Wiss.*, 1894, **32**, 897.
3 Stankovic, V., *Chem. Zvesti*, 1963, **17**, 274.
4 Pawelczyk, E., and Marciniec, B., *Acta Pol. Pharm.*, 1978, **35**, 643.
5 Tokes, B., and Suciu, G., *Chim. Anal. (Bucharest)*, 1972, **2**, 193.
6 Sandu, M. A., Lozan, R. M., and Ropot, V. M., *Izv. Akad. Nauk Mold., SSR, Ser. Biol. Khim. Nauk*, 1988, **2**, 71.

7 Slusanschi, H., *Z. Lebensm. Unters. Forsch.*, 1960, **112**, 390.
8 Koszegi, D., and Salgo, E., *Magy. Kem. Foly.*, 1960, **66**, 142.
9 Turczan, J. W., and Goldwitz, B. A., *J. Assoc. Off. Anal. Chem.*, 1973, **56**, 669.
10 Strom, J. G., and Jun, H. W., *J. Pharm. Sci.*, 1977, **66**, 589.
11 Pentegova, I. A., and Dubrovina, G. I., *Metody Anal. Kontrolya Proizvod. Khim. Prom-sti.*, 1977, **8**, 34.
12 Marunina, A. T., *Tr. Kom. Anal. Khim., Akad. Nauk SSSR, Inst. Geokhim. Anal. Khim.*, 1963, **13**, 320.
13 Fishman, G. I., and Pevzner, I. D., *Zavod. Lab.*, 1970, **36**, 926.
14 Stransky, Z., Dolinek, J., and Pavlica, J., *Acta Univ. Palacki. Olomuc. Fac. Rerum Nat.*, 1978, **57**, 197.
15 Nikolic, K., and Velasevic, K., *Arh. Farm.*, 1985, **35**, 215.
16 Blazsek, A., and Biro, Z., *Rev. Med. (Tirgu-Mures, Rom.)*, 1968, **14**, 70.
17 Filipeva, S. A., Strelets, L. N., Petrenko, V. V., and Buryak, V. P., *Zh. Anal. Khim.*, 1989, **44**, 131.
18 Strom, J. G., and Jun, H. W., *J. Pharm. Sci.*, 1986, **75**, 416.
19 Rizzoli, C., *Boll. Soc. Ital. Biol. Sper.*, 1949, **25**, 433.
20 Taha, A. M., El-Rabbat, N. A., and Fattah, F. A., *Analyst*, 1980, **105**, 568.
21 Sawicki, E., Hauser, T. R., and McPherson, S., *Anal. Chem.*, 1962, **34**, 1460.
22 Zhantalai, B. P., and Ruch'eva, N. I., *Zh. Prikl. Khim. (Leningrad)*, 1966, **39**, 2339.
23 Koupparis, M. A., Efstathiou, C. E., and Hadjiioannou, T. P., *Anal. Chim. Acta*, 1979, **107**, 91.
24 Levin, J.-O., and Fängmark, I., *Analyst*, 1988, **113**, 511.
25 Nair, J. B., Delaney, M. F., and Combs, K. J., *Anal. Lett.*, 1983, **16**, 711.
26 Koga, M., Shinohara, R., and Akiyama, T., *Anal. Sci.*, 1985, **1**, 381.
27 Al-Jabari, G., and Jaselskis, B., *Talanta*, 1988, **35**, 655.
28 *The United States Pharmacopeia, The National Formulary*, United States Pharmacopeial Convention, Rockville, MD, 1990, p. 846.
29 Tada, H., *J. Am. Chem. Soc.*, 1960, **82**, 255.
30 Bose, S., *J. Indian Chem. Soc.*, 1957, **34**, 663.
31 Richmond, H. H., Myers, G. S., and Wright, G. F., *J. Am. Chem. Soc.*, 1948, **70**, 3659.
32 Musher, D. M., and Griffith, D. P., *Antimicrob. Agents Chemother.*, 1974, **6**, 708.
33 Kawasaki, A., and Ogata, Y., *Mem. Fac. Eng., Nagoya Univ.*, 1967, **19**, 1.

Paper 2/01096H
Received March 2, 1992
Accepted June 10, 1992

Batch and Flow Injection Spectrophotometric Determination of Aztreonam

M. I. González Martín, C. González Pérez and M. A. Blanco López
Departamento de Química Analítica, Nutrición y Bromatología, Facultad de Química, Universidad de Salamanca, Salamanca, Spain

A method for the spectrophotometric determination of aztreonam operating manually and by flow injection is reported. The method is based on the reaction with hydroxylamine to form hydroxamic acid and subsequent reaction with Fe^{III}, giving a red complex. The effect of the concentrations of the reagents was studied and the reaction conditions are discussed. Nickel(II) was used as a catalyst. The method was applied to the determination of aztreonam in pharmaceutical products.

Keywords: *Aztreonam determination; spectrophotometry; flow injection*

Aztreonam is a monocyclic β-lactam antibiotic characterized by its excellent efficacy against Gram-negative micro-organisms.

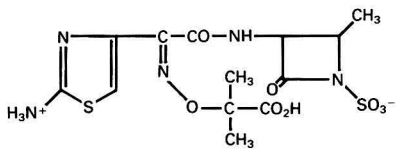

Most published methods for the determination of aztreonam, both in pharmaceutical products and in biological fluids, use high-performance liquid chromatography (HPLC).[1-4] Spectrophotometric methods have been used to a certain extent for the determination of penicillins and cephalosporins. For aztreonam, direct ultraviolet (UV) measurement has been performed, sometimes using the derivative mode.[5,6] Derivatization procedures have also been used with reagents such as sodium nitrite[7,8] and hydroxylamine,[9] which permit measurement of the visible region.

This paper describes a modification of the spectrophotometric method that employs hydroxylamine as reagent, leading to breakage of the β-lactam ring to form hydroxamic acid, which forms a red complex with Fe^{III}. Nickel(II) is used as the catalyst and the method permits the spectrophotometric determination of aztreonam in manual and flow-injection (FI) modes.

Experimental

Materials and Apparatus

A Shimadzu UV-160 UV/visible spectrophotometer with quartz cuvettes of 1 cm optical pathlength was used. pH measurements were made with a Crison Digit 501 pH meter.

The flow system (Fig. 1) was constructed with 0.5 mm i.d. poly(tetrafluoroethylene) (PTFE) tubing. A Gilson peristaltic pump was used as the propulsion system for continuous determination. For injection, a port with exchangeable loops of different capacities was used. Absorbance was measured with a Coleman 55 spectrophotometer equipped with a Hellma 178 QS cell of 1 cm optical pathlength and 18 μl internal volume.

A Tecator gas diffusion membrane was used.

Reagents for Manual Determination

A stock solution (1×10^{-3} mol l^{-1}) of aztreonam (Squibb Institute of Medical Research) was prepared by dissolving 43.3 mg of the solid in 100 ml of distilled water.

Hydroxylamine–nickel reagent was prepared by dissolving 34.77 g of hydroxylammonium chloride (Merck) and 3.27 g of nickel chloride (Merck) in about 200 ml of distilled water, adjusting the pH to 6.2 with NaOH and diluting to 250 ml. This solution was 2 mol l^{-1} in hydroxylamine and 0.1 mol l^{-1} in Ni^{II}.

A solution of Fe^{III} was prepared by dissolving 37.5 g of $NH_4Fe(SO_4)_2 \cdot 12H_2O$ in 250 ml of 0.5 mol l^{-1} sulfuric acid.

Reagents for FI Determination

The following were used: 1 mol l^{-1} hydroxylamine solution, 6.7×10^{-2} mol l^{-1} Ni^{II} solution prepared from nickel chloride, 0.5 mol l^{-1} sulfuric acid and 0.27 mol l^{-1} Fe^{III} solution prepared from $NH_4Fe(SO_4)_2 \cdot 12H_2O$ in 0.5 mol l^{-1} sulfuric acid.

Manual Determination

An aliquot of the sample is placed in a calibrated flask such that the final concentration of aztreonam, after dilution to volume, will lie between 2.0×10^{-5} and 6.0×10^{-4} mol l^{-1} and 2 ml of the hydroxylamine–nickel reagent are added. After waiting for 20 min, 5 ml of the Fe^{III} solution are added and the resulting mixture is shaken and diluted to volume with distilled water. The absorbance is measured at 496 nm against the corresponding blank.

Flow Injection

Using the flow system shown in Fig. 1, different volumes of the aztreonam solution are inserted through the injection port. In

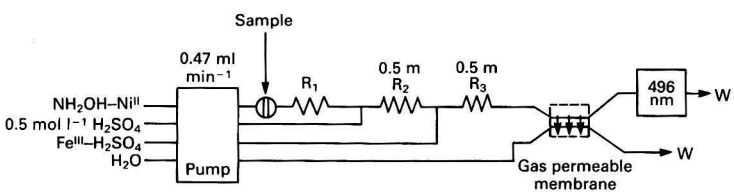

Fig. 1 Diagram of the FI system for the determination of aztreonam

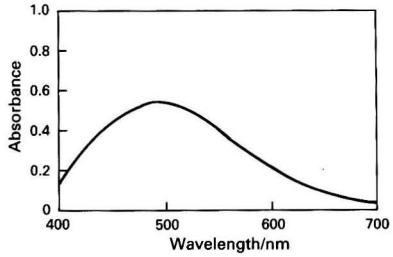

Fig. 2 UV spectrum of the Fe^{III}–hydroxamic acid complex. Aztreonam, 6.0×10^{-4} mol l^{-1}; Ni^{II}, 8.0×10^{-3} mol l^{-1}; NH_2OH, 0.16 mol l^{-1}; and Fe^{III}, 6.2×10^{-2} mol l^{-1}

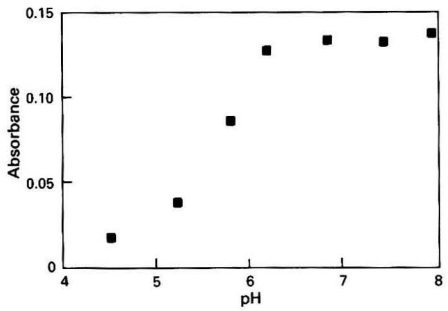

Fig. 3 Manual spectrophotometric determination of aztreonam. Effect of pH on the absorbance of the aztreonam–hydroxylamine complex. Aztreonam, 2.0×10^{-4} mol l^{-1}; Ni^{II}, 1.6×10^{-2} mol l^{-1}; NH_2OH, 0.16 mol l^{-1}; and Fe^{III}, 3.0×10^{-2} mol l^{-1}

this way, a calibration graph is prepared of peak height *versus* concentration. The concentration of the sample is calculated from the calibration graph.

Results and Discussion

Manual Determination

Absorption spectrum of the Fe^{III}–hydroxamic acid complex. Stability

The Fe^{III}–hydroxamic acid complex formed in the reaction displays an absorption spectrum with a maximum around 496 nm (Fig. 2). The absorbance of the complex decreases slowly with time. Although this decrease is not very pronounced, it was decided to carry out the measurements 5 min after adding the Fe^{III} solution.

Aztreonam–hydroxylamine reaction

Presence of Ni^{II} as catalyst. The reaction between aztreonam and hydroxylamine occurs slowly. When the concentration of aztreonam is 2.0×10^{-5} mol l^{-1}, at least 6 h are required for it to be completed. However, considering that Ni^{II} has been used to catalyse the formation of hydroxamic acid from cephalosporin drugs,[10] assays were carried out in the presence of this element, with the observation that in the presence of Ni^{II} maximum values of absorbance are reached 20 min after the reaction has begun. The concentration of Ni^{II} considered optimum is approximately 8.0×10^{-3} mol l^{-1}.

Effect of pH. This part of the study was conducted by applying the general procedure to a series of samples containing a constant concentration of aztreonam (2.0×10^{-4} mol l^{-1}) in the pH range 4–8. The absorbance was found to increase with increase in pH, reaching almost constant values at pH 6.2 (Fig. 3). However, at higher pH (6.7) the solution becomes turbid, with the appearance of a white precipitate. Accordingly, the optimum pH was considered to lie between 6.2 and 6.7.

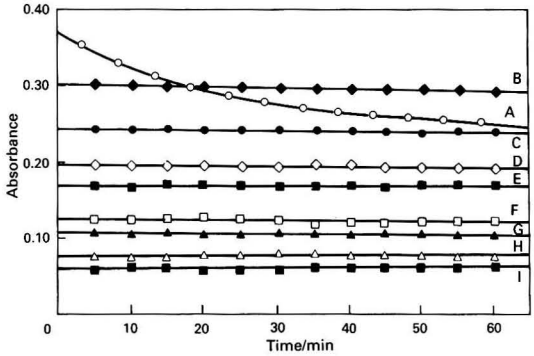

Fig. 4 Manual spectrophotometric determination of aztreonam. Influence of medium on stability. H^+ concentration: A, 0.10; B, 0.15; C, 0.20; D, 0.30; E, 0.41; F, 0.51; G, 0.61; H, 0.91; and I, 1.12 mol l^{-1}. Aztreonam, 4.0×10^{-4} mol l^{-1}; Ni^{II}, 8.0×10^{-3} mol l^{-1}; NH_2OH, 0.16 mol l^{-1}; and Fe^{III}, 1.5×10^{-2} mol l^{-1}

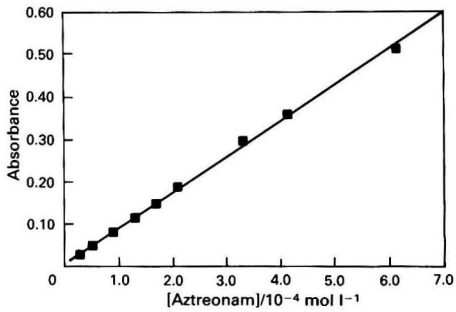

Fig. 5 Manual spectrophotometric determination of aztreonam. Effect of concentration of aztreonam. Ni^{II}, 8.0×10^{-3} mol l^{-1}; NH_2OH, 0.16 mol l^{-1}; and Fe^{III}, 6.2×10^{-2} mol l^{-1}

Effect of hydroxylamine concentration. It was observed that the absorbance increased as the concentration of hydroxylamine increased, attaining an almost constant value at concentrations between 0.2 and 0.4 mol l^{-1}. However, as the concentration of hydroxylamine increased, the stability of the Fe^{III}–hydroxamic acid complex decreased considerably; it is the absorbance of this complex that is measured finally. This decrease in stability is possibly due to the reduction of Fe^{III} by the excess of hydroxylamine. Hence it was considered appropriate to use a 0.16 mol l^{-1} concentration of hydroxylamine as under these conditions sufficiently stable absorbance values can be achieved.

Fe^{III}–hydroxamic acid reaction

Effect of medium. The medium should be sufficiently acidic to avoid the precipitation of Fe^{III}. The results obtained (Fig. 4) show that as the acidity increases, the absorbance signal decreases. Additionally, for the lowest concentration of H^+ studied, the stability is appreciably reduced. In the light of these findings, it was considered appropriate to adopt a compromise solution and operate at an H^+ concentration of 0.15 mol l^{-1}.

Effect of concentration of Fe^{III}. The absorbance signal increases with increase in Fe^{III} concentration, reaching almost constant values for Fe^{III} concentrations $>4.9 \times 10^{-2}$ mol l^{-1}. A study was also carried out into the stability of the Fe^{III}–hydroxamic acid complex for different concentrations of Fe^{III}. The results indicated that high concentrations of Fe^{III} ($>6.0 \times 10^{-2}$ mol l^{-1}) should be used.

Table 1 Determination of aztreonam in pharmaceutical products. Label specification: 1000 mg per vial

	Amount found/mg per vial		
		FI method	
Product	Manual method	20 °C	45 °C
Azactam	1006	997	963
	962	983	
	986	968	
Urobactam	974	1012	1009
	1021	997	
	988	997	

Table 2 Study and optimization of variables for the determination of aztreonam by FI

Variable	Parameter	Range	Optimum value
Chemical	Hydroxylamine/mol l^{-1}	0.40–1.60	>1
	Ni^{II}/mol l^{-1}	1.70×10^{-2}–1.60×10^{-1}	$>6.7 \times 10^{-2}$
	H_2SO_4/mol l^{-1}	0.2–1.3	0.5
	Fe^{III}/mol l^{-1}	0.05–0.45	>0.27
Physical	Reactor R_1 length/m	0.5–13	11
	Pump speed/ml min^{-1}	0.40–1.82	0.47
	Temperature/°C	5–60	45
	Injection volume/ml	80–240	126

Analytical Applications

The relationship between absorbance and concentration of aztreonam is linear: $A = 0.0061 + 845[c\ (\text{mol}\ l^{-1})]$, $r = 0.9995$, for concentrations ranging from 2.0×10^{-5} to 6.0×10^{-4} mol l^{-1} (Fig. 5). The limit of detection found ($3\sigma/m$, where σ = standard deviation of the blank and m = slope of the calibration graph) was 7.9×10^{-6} mol l^{-1}. The relative standard deviation for samples containing 6.0×10^{-4} mol l^{-1} aztreonam was 0.14% ($n = 10$).

The proposed procedure was applied to the determination of aztreonam by the standard additions method in the pharmaceutical products Azactam (Squibb) and Urobactam (Esteve). In both instances the aztreonam is present in combination with L-arginine. From the results obtained (Table 1), values close to those stated by the manufacturers were obtained, with a difference of 1.5% with Azactam and 0.6% with Urobactam.

Flow injection

The optimization of the variables is shown in Table 2, with the range studied and the optimum values for an aztreonam concentration of 2.0×10^{-3} mol l^{-1}. Below the most significant details are summarized.

Chemical variables. As the concentration of hydroxylamine increases so does the signal until a value is reached that remains almost constant above 1 mol l^{-1}.

In the variation of the signal with the concentration of the catalyst, Ni^{II}, maximum and virtually constant values are obtained above 6.7×10^{-2} mol l^{-1}.

The pH range for the Fe^{III}–hydroxamic acid reaction was studied conducted with H_2SO_4. Sulfuric acid was introduced through one channel to avoid precipitation of the iron. If the medium is not very acidic (<0.2 mol l^{-1}), the baseline is seen to become unstable. At high H^+ concentrations the signal decreases.

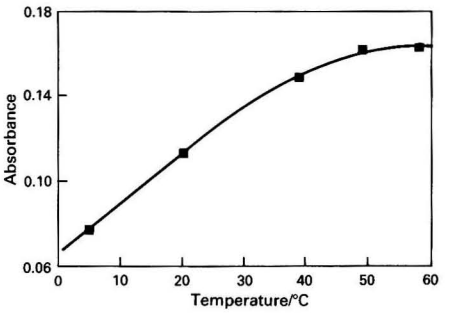

Fig. 6 Manual FI determination of aztreonam. Influence of temperature. Aztreonam, 2.0×10^{-3} mol l^{-1}; Ni^{II}, 6.7×10^{-2} mol l^{-1}; NH_2OH, 1 mol l^{-1}; and Fe^{III}, 0.27 mol l^{-1}

Regarding the concentration of Fe^{III}, maximum and virtually constant signal values are obtained above 0.27 mol l^{-1}.

Physical variables. As the length of the reactor is increased, the signal also increases because the reaction time is longer. This leads to an increase in the time of appearance and of the dispersion. A compromise situation is reached between dispersion and the reaction time. An optimum length of 11 m was chosen for reactor R_1. At low flow rates, higher absorbance values are obtained, but the sampling speed is slow.

Reactor I was thermostated at different temperatures. The signal increases with increase in temperature (Fig. 6); above 45 °C an increase in bubbling occurs. Also, aztreonam in solution seems to be unstable at temperatures above room temperature.[11] The volume injected was studied in the range from 80 to 240 µl. The optimum value is close to 126 µl. With larger injection volumes, double peaks are obtained.

Determination of aztreonam in pharmaceutical products

The relationship between peak height and the concentration of aztreonam is linear for concentrations ranging from 8.0×10^{-5} to 2.0×10^{-3} mol l^{-1}. Calibration was effected at 20 and 45 °C with the equations $A = 1.357 \times 10^{-2} + 49.76\ [c\ (\text{mol}\ l^{-1})]$, $r = 0.09997$, at 20 °C and $A = 1.870 \times 10^{-2} + 64.377\ [c\ (\text{mol}\ l^{-1})]$, $r = 0.9997$ at 45 °C. The relative standard deviation for samples containing 1.2×10^{-3} mol l^{-1} aztreonam was 0.20% ($n = 10$).

Having applied the procedure to the analysis of Azactam and Urobactam by FI, values coinciding with those stated by the manufacturers were obtained with differences of 1.7% for the former drug and 0.2% for the latter (Table 1).

The authors thank Squibb Laboratories for supplying the materials.

References

1 Pilkiewicz, F. G., Remsburg, B. J., Fisher, S. M., and Sikes, R. B., *Antimicrob. Agents Chemother.*, 1983, **23**, 852.
2 Meulemans, A., Mohler, J., Vittecoq, D., Haroche, G., Rosset, M. A., Vulpillat, M., and Modai, J., *J. Chromatogr.*, 1986, **377**, 466.
3 Wahbi, A. A. M., Abounassif, M. A., Gad-Karien, E. A., Mahmoud, E., and Aboul-Enein, H. Y., *J. Assoc. Off. Anal. Chem.*, 1988, **71**, 31.
4 Ehret, W., Probst, H., and Ruckdeschel, G., *J. Antimicrob. Chemother.*, 1987, **19**, 541.
5 Mohamed, M. E., Abdel-Moety, E. M., Abounassif, M. A., and Al-Khamees, H. A., *Anal. Lett.*, 1988, **21**, 1579.
6 Morelli, B., *J. Pharm. Sci.*, 1990, **79**, 261.
7 Uri, J. V., and Jain, T. C., in *Recent Advances in Chemotherapy, Proceedings of 14th International Congress on Chemotherapy (Antimicrobial Sect. 1)*, ed. Joji, I., University of Tokyo Press, Tokyo, 1985, p. 245; *Chem. Abstr.*, 1988, **105**, 21457s.

8 Uri, J. V., and Jain, T. C., *J. Antibiot*, 1986, **39**, 669.
9 Mohamed, M. E., Abounassif, M. A., Al-Khamees, H. A., Kandil, H., and Aboul-Enein, H. Y., *J. Pharm. Belg*, 1988, **43**, 429.
10 Mays, D. L., Banger, F. K., Cantrell, W. C., and Evans, W. G., *Anal. Chem.*, 1975, **47**, 2229.
11 Riley, C. M., and James, M. J., *Am. J. Hosp. Pharm.*, 1986, **43**, 925.

Paper 2/02289C
Received May 5, 1992
Accepted July 9, 1992

COMMUNICATION

Quantitative Analysis of Minor Proteins, Free Amino Acids and Other Components Containing Nitrogen in Crude Tallow

Shi Rong Xu and Takeshi Matsuo
Oil & Fats Research Laboratory, Nippon Oil & Fats Co., 1–56 Ohamacho, Amagasaki, Hyogo, Japan 660

A simple procedure has been developed for the quantification of nitrogen compounds including proteins, free amino acids and other minor components containing nitrogen in crude tallow by modification of the dye-binding method. In addition, novel instrumentation for measuring the total nitrogen content is described.

Keywords: *Dye binding; free amino acid; protein; phospholipid; crude tallow*

Crude lipids always contain small amounts of non-fatty material other than water or insolubles. These include gums, sterols, colour pigments, phospholipids, free amino acids and proteins.[1] In fatty acid and soap manufacturing processes, minor phospholipids, free amino acids and proteins influence the activity of nickel catalysts during hydrogenation and the thermal stability of glycerol.[2–5] Therefore, their contents in crude material must be quantified.

Methods for the quantitative analysis of protein include the micro-Kjeldahl and Sloane-Stanley[6] methods for total nitrogen, and the Lowry method,[7] ultraviolet absorption[8] and the Biuret reaction[9] for soluble protein. Lea and Rhodes[10] reported that the analysis of lipid amino nitrogen can be carried out on intact lipids and is applicable to phospholipids containing free amino groups and to long-chain bases. However, these methods require large amounts of purified and soluble samples. Dye binding[11–13] has become very popular because it is very sensitive, fast and at least as accurate as the Lowry method. Moreover, Felipe *et al.*[14] reported that the simultaneous determination of lipid and protein could be performed using hexane–propan-2-ol (3 + 2 v/v) for precipitating protein instead of trichloroacetic acid. These methods can only be used for quantifying total nitrogen contents or protein concentrations. In this paper, an improved dye-binding method is described for the quantification of free amino acids, proteins and other components containing nitrogen in crude tallow. In addition, novel instrumentation (a chemical luminescence method) was used for measuring the total nitrogen content in samples.

Experimental

Reagents

Coomassie Brilliant Blue G-250, trichloroacetic acid and bovine serum albumin were purchased from Katayama Chemicals. Hexane, pyridine and other reagents used were of analytical-reagent grade.

Instrumentation

Part of the work described was performed using a total nitrogen analytical instrument (Mitsubishikasei Co., TN-05). The determination of nitrogen was carried out by the chemical luminescence method. Two reactions occurred during the determination: (1) the decomposition of nitrogen compounds in the samples to nitrogen oxides (NO, NO_2), nitrogen gas, carbon dioxide and water; and (2) the reaction between nitrogen oxide (NO) and ozone to form nitrogen dioxide, oxygen and luminescence (590–2500 nm) which was detected quantitatively.

Procedure

A mixture of 1 g of crude tallow in 5 ml of hexane and 5 ml of 7.5% trichloroacetic acid was shaken at room temperature for 30 min and filtered through a No. 42 (Whatman) filter-paper. The precipitate on the filter-paper was rinsed with hexane and stained for 30 min by the addition of 10 ml of dye solution[11] (100 mg of Coomassie Brilliant Blue G-250 was dissolved in 10 ml of 7% acetic acid solution and filtered to remove undissolved dye). The dye solution was then discarded and the excess of dye solution that remained on the filter-paper was washed out by the addition of 10 ml of 7% acetic acid solution. After drying the filter-paper, 4 ml of de-staining solution (a mixture of 66 ml of methanol, 34 ml of distilled water and 1 ml of 28% ammonia solution) were added to wash out the dye bound to the proteins. The absorption of the dye released from the filter-paper was measured at 610 nm. The protein concentration was calculated from the absorption at 610 nm with a bovine serum albumin standard.

The nitrogen content of the hexane phase in the above filtrate was determined using the total nitrogen analytical instrument with the pyridine calibration line. In order to determine the contents of amino acids in the 7.5% trichloroacetic acid phase, 1 g of crude tallow was dissolved in 10 ml of hexane and the total nitrogen content in the original crude tallow was also determined using the same instrument. Hence, the content of amino acid in crude tallow (N_{aa}) can be calculated from the following equation:

$$N_{aa} = N_t - (N_{hp} + P/6.25)$$

where N_t = total nitrogen content in crude tallow, N_{hp} = nitrogen content in hexane phase and P = protein content in crude tallow.

Results and Discussion

In order to evaluate the quality of various lipids, and remove effectively their minor components containing nitrogen, it is necessary to quantify rapidly and accurately the content of nitrogen as proteins, free amino acids and other components containing nitrogen such as phospholipids. Fig. 1 shows the nitrogen content of each minor component in crude tallow. The total nitrogen content in crude tallow was 295 ± 1.0 ppm (n = 4). The nitrogen component soluble in hexane, mainly phospholipids, contained 60 ± 0.8 ppm (n = 4) of nitrogen. However, nitrogen contents as proteins and free amino acids were 20 ± 0.5 ppm (n = 4) and 215 ± 2.3 ppm (n = 4), respectively. The dye binding described by Bramhall *et al.*[13] cannot be directly applied to crude tallow because of the very low protein and high triglyceride contents. Moreover, the proteins in crude tallow are always denatured. The procedure

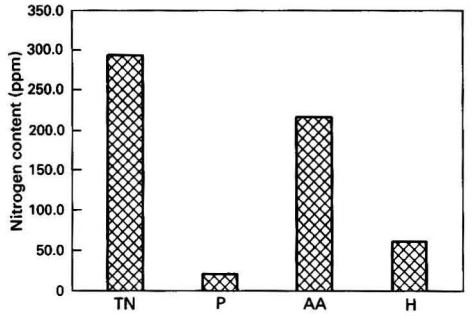

Fig. 1 Nitrogen contents of minor proteins (P), free amino acids (AA) and other components soluble in hexane containing nitrogen (H) in crude tallow. TN = Total nitrogen

reported in this paper simplifies the quantification of free amino acids and proteins in crude tallow. Additionally, the determination of free amino acid, protein and other minor components containing nitrogen in other lipids can also be carried out conveniently using this improved procedure.

We are grateful to Hiroshi Takeo and Chika Ito for their technical assistance.

References

1 George, R. W., *HAPPI Household Pers. Prod. Ind.*, 1991, August, p. 64.
2 Klimmek, H., *J. Am. Oil Chem. Soc.*, 1984, **61**, 200.
3 Drozdowski, B., and Zajac, M., *J. Am. Oil Chem. Soc.*, 1977, **54**, 595.
4 Man, J. M., Pogorzelska, E., and Man, L., *J. Am. Oil Chem. Soc.*, 1983, **60**, 558.
5 Filip, V., Capova, O., and Zajac, J., *Fat Sci. Technol.*, 1988, **90**, 210.
6 Sloane-Stanley, G. H., *Biochem. J.*, 1967, **104**, 293.
7 Lowry, O. H., Rosebrough, N. J., Farr, A. L., and Randall, R. J., *J. Biol. Chem.*, 1951, **193**, 265.
8 Goldfarb, A. R., Saidel, L. J., and Mosovich, E., *J. Biol. Chem.*, 1951, **193**, 397.
9 Itzhaki, R. F., and Gill, D. M., *Anal. Biochem.*, 1964, **9**, 401.
10 Lea, C. H., and Rhodes, D. N., *Biochim. Biophys. Acta*, 1955, **17**, 416.
11 Bradford, M. M., *Anal. Biochem.*, 1976, **72**, 248.
12 Spector, T., *Anal. Biochem.*, 1978, **86**, 142.
13 Bramhall, S., Noack, N., Wu, M., and Loewenberg, J. R., *Anal. Biochem.*, 1969, **31**, 146.
14 Felipe, R. V., Marina, M. C., Flor Zatra, M., Eduardo, G. P., and Ramirez, H., *Lipids*, 1991, **26**, 77.

Paper 2/01565J
Received July 22, 1992

BOOK REVIEWS

The Periodic Table for Chromatographers
By Michael Lederer. Pp. v + 129. Wiley. 1991. Price £60.00. ISBN 0-471-93149-7.

This book is a collection of data for both heterogeneous and homogeneous systems and was stated to be based on an idea of the author's, who is an eminent chromatographer, when contemplating and using a recent wall chart of the Periodic Table, which presented various chemical and physical properties of the elements in smaller tabulations around the main one. Because of the arrangement, it was often impossible to read the smaller tables, and hence the notion arose of supplying the data in a loose-leaf folder.

One wonders why a thing so simple has not been done before, but like other simple and practical ideas it will be of considerable help to analytical chemists in the field.

The tabulations cover: solvent extraction and general properties; data for ion-exchange resins; inorganic ion-exchange; paper chromatography; partition and ion-exchange; paper and thin-layer chromatography information for liquid ion exchangers; thin-layer chromatography partition and ion exchange; and electrophoresis.

The book opens with discussion of the limitations of the Periodic Tables of chemical properties, explanation of symbols used in the tabulations, and a few references. These are followed by the tables (the greater part), and the work ends with a brief index.

In general, the data provided are equilibrium constants; because of the loose-leaf format interactions under different conditions can be compared very conveniently.

This should prove a very useful compilation. Indeed, if as useful as I anticipate it may be that the method of fixing and binding seen in the review copy could prove inadequate. It was noticed at the time of receipt of this copy that some tearing had begun already near the punched holes that take the fixing mechanism, and with considerable handling this damage might get worse. (If a junior is available you could keep him or her busy for a while on your new copy with stick-on reinforcements.)

I would recommend the book not only to libraries of industrial and academic establishments but also in general to all practical chromatographers.

D. Simpson

Practical Fluorescence
Edited by George Guilbault. *Modern Monographs in Analytical Chemistry 3.* Second Edition. Pp. x + 812. Marcel Dekker. 1991. Price US $185.00 (US and Canada); US $222.00 (All other countries). ISBN 0-8247-8350-6.

The first edition of this book, which was received enthusiastically, was used for years as a textbook to introduce students to luminescence techniques on account of its marked didactic character. It was also employed as a reference book, as the wealth of data it included was an appropriate starting point for gathering information on specific topics. However, the fast development of luminescence techniques in the last few years has aroused great interest from teachers and researchers for a second edition.

This new version also fulfils the two aforementioned goals as it contains comprehensive information on the state-of-the-art in luminescence techniques, which are described in a straightforward way that makes them accessible to students, and provides a thoroughly updated bibliography for luminescence methods. Thus, Chapters 5 and 6 include a comprehensive review (nearly 1000 references) of the luminescence methods reported for inorganic and organic compounds, respectively. Didactically, Chapter 2, which is devoted to practical aspects of fluorescence instrumentation, perhaps lacks some illustrative schemes of the instruments concerned.

Some topics such as electrogenerated luminescence, fluorescent indicators and chlorophyll fluorescence, which were included in the first edition, have been very aptly excluded from this second on account of their obsolescence. On the other hand, such other topics as ambient-temperature phosphorimetry, photobiosensors, time-resolved techniques and low-temperature techniques have been revised and updated. A notable point, however, is that such a topical technique as fluoroimmunoassay is missing from the book.

The greatest weakness of this book is probably a somewhat poor organization of its contents that is worsened by the lack of a detailed index allowing readers to locate readily topics of their interest. Thus, synchronous and time-resolved techniques are dealt with in Chapter 7, which is devoted to environmental analysis, whereas the fluorescence polarization technique is described in Chapter 11, which is concerned with proteins and peptides. Placement of these techniques in the aforementioned chapters may confuse readers inasmuch as they are also of use in other fields. Nevertheless, once acquainted with the contents of each chapter, readers are bound to appreciate the valuable contribution of this book to spreading the achievements of luminescence techniques and their current high potential and promising prospects in any field of Science.

Finally, while in Chapter 2 of the book the author states that 'the common scientific parlance fluorescence is used to include phenomena such as phosphorescence, bioluminescence, and other emissive phenomena', IUPAC recommends that all these should be included under the broad term 'luminescence', hence the title of the book may not be too accurate. In any case, this is a purely anecdotal matter taking into account the internationally acknowledged prestige of the author and the high quality of the book.

A. Gómez-Hens

Wilson and Wilson's Comprehensive Analytical Chemistry. Volume XXIX. Chemiluminescence Immunoassay.
By Ian Weeks. Series Editor, G. Svehla. Pp. xvi + 293. Elsevier. 1992. Price US $151.50; Dfl 295.00; Subscription price US $136.00; Dfl 265.00. ISBN 0-444-89035-1.

This, the latest volume in this series, covers chemiluminescence immunoassay. The author is well known for his research and development activity in this area of analysis, particularly chemiluminescent immunoassays based on acridinium ester labels. The application of luminescent techniques (*e.g.*, chemiluminescence, bioluminescence and electroluminescence) in immunoassay and nucleic acid hybridization assays has become a very active area of research and development. The first chemiluminescent label for a ligand–binder assay was described in 1976. Since that time, the range and diversity of chemiluminescent and bioluminescent labels and detection reactions has grown tremendously.

Dr. Weeks' book is divided into eight chapters. Following a brief Introduction, Chapter 2 reviews chemiluminescence and the different types of chemiluminescent and bioluminescent reactions (chemiluminescence *in vivo*). The remaining chapters are devoted to aspects of immunoassay including homogeneous, immunochemical/photochemical interface, early work, state-of-the-art and future prospects. Chapter 3 presents a thorough account of immunoassay technology,

including antibodies, antibody production, separation systems, assay design and assay protocols. In the Immunochemical/Photochemical Interface (Chapter 4), the author discusses in great detail, chemiluminescent labelling and gives experimental protocols for the preparation of 'preactivated labels' (*e.g.*, ABEI isothiocyanate). This chapter also considers the chemiluminescent measurement of different enzyme labels and bioluminescent systems. It could have been enlarged to give a fuller account of these areas, for example details of the non-separation assays possible with glucose 6-phosphate dehydrogenase labels, the use of other bioluminescent labels, such as *Renilla* luciferase and apoaequorin. Developers of immunoassays should find Chapter 7 helpful. It describes the key steps in the development of chemiluminescent immunoassays using phthalhydrazide and acridinium ester labels. Two topics not covered, or only mentioned briefly in this book, are acridinium ester analogues (*e.g.*, the sulfonyl carboxamides and thioesters) and automation of chemiluminescent immunoassays. Perhaps Appendix II, which contains photographs of luminometers, could have been expanded to deal with the issue of automation. The final chapter offers the reader Dr. Weeks' view of the future of chemiluminescence immunoassay. He singles out improved monoclonal and single-domain antibodies, anti-idiotype antibodies, and recombinant labels (*e.g.*, firefly luciferase), and discusses the impact of chemiluminescent immunoassay on the clinical laboratory and other areas of analysis. The index to this book is brief and general, and some readers may have difficulty in locating particular topics within the 289 pages of text. A final word about the cost of this book (a perennial gripe of book reviewers) is that this is a very expensive book and this will detract from its potential use in the laboratory as a source of practical information on the development of chemiluminescent immunoassays.

Larry J. Kricka

Advances in Biosensors. Volume 1
Edited by Anthony P. F. Turner. Pp. xii + 299. JAI Press. 1991. Price £54.00; US$92.50. ISBN 1-55938-240-6.

Analytical systems or techniques that survive a decade or two of preliminary struggle, tend to spawn a series of dedicated texts. This is the case for biosensors, which despite occupying the no-man's land between chemistry and biology, have proved a magnet for researchers with both types of backgrounds. Publication of this first volume of 'Advances' is timely in providing an update, and is also an affirmation of faith in the future. The aim has been to condense descriptions of research contributions made by specific groups. As such, the various reviews are not so much overviews, as less digested compilations of methods and results closer to the 'coal face'.

The first chapter deals with microelectronic devices and microbial layer-sensitized biosensors. It skims through a large variety of transducer–biolayer combinations with a description of an amperometric CO_2 biosensor, through to exploitation of amorphous silicon. Enzyme electrodes have been the most successful of the devices created to date and several chapters are devoted to these. The first presents a series of metabolite sensors where integration with flow systems provides for continuous monitoring; there are good illustrations of the kind of continuous data to be obtained. A limit to sensitivity can be a drawback for some electrode enzyme applications, and the next chapter provides a detailed rundown of how coupled enzyme reactions can be driven in parallel and sequentially to achieve amplification. Illustration of these with calibration data should encourage those whose endeavours have been constrained by inadequate device sensitivity. The next chapter draws attention to the inner enzyme working electrode interface, with a rather more theoretical treatment than previous chapters. Certainly, chemically-modified electrodes are in vogue, and descriptions of low molecular mass electron mediators, electrode surfaces for direct electron transfer and redox surface modifiers, respectively, are worthwhile. However, the mathematical treatment presented warrants a more extensive description than has been possible in this short chapter. For many, an enzyme electrode with an immobilized mediator is virtually synonymous with a biosensor; the next chapter highlights a variety of these, and gives clear descriptions of what is now possible commercially and practically.

After the enzyme, the antibody is probably the most talked about bio-component to have been used. However, immunoassays with electrochemical sensors are often just that: standard immunoassay with electrochemical detection. It has been extraordinarily difficult to integrate antibody with an electrochemical transducer to achieve reliable antigen detection. The chapter on electrochemical immunoassay rightly points this out, but also presents a clear, authoritative account of the many strategies to achieving electrochemical end points. Reviewed here, are organic, metal and enzymic labels in a variety of heterogeneous, homogeneous, competitive and non-competitive immunoassay formats. A good illustration of results is provided throughout, and particularly welcome is the attention given to the elimination of the high background signal when biological fluids are assayed. Much of the presented work has relied on liquid chromatographic sample separation, and flow injection analysis; any future clinical acceptance is going to depend upon how simple these can be made. Optical systems can conform more readily to the rigorous definition of a biosensor with antibody directly over a transducer device. A chapter on optical immunosensors accordingly adds further valuable insights, and the descriptions of basic principles as well as of the experience of different researchers, is of value to specialist and non-specialist alike. The final chapter furnishes a mosaic of electrochemical sensors, piezoelectric crystals and fibreoptic probes for enzyme, antigen and substrate measurement.

This first volume of 'Advances' is a laudable effort, putting on show past achievements of key groups working on biosensors. A fair amount of information is packed into a small volume, and if the descriptions are occasionally not easy to follow, or expect too much background from the reader, fairly up-to-date references at the end of each chapter should provide a good starting point for detailed reading.

P. Vadgama

CUMULATIVE AUTHOR INDEX

JANUARY–NOVEMBER 1992

1993 European Winter Conference on Plasma Spectrochemistry

Palacio de Congresos, Granada, Spain

10–15 January, 1993

The Grupo Espectroquimico and Grupo Español de Espectroscopia of the Spanish Royal Societies of Chemistry and Physics cordially invite your participation in the 1993 European Winter Conference on Plasma Spectrochemistry

SCIENTIFIC PROGRAMME

The scientific programme will include six plenary, ten invited keynote lectures, and oral and poster sessions. Three Special Discussion Sessions on today's 'hot' topics, a varied Short Course Programme and an Instrument Exhibition are also planned.

Plenary—

Paul Boumans, *Eindhoven*	Plasma Spectrochemistry: in Search of Innovation or Confirmation
Gary Horlick, *Alberta*	ICP-MS Perspectives
Les Ebdon, *Plymouth*	Hybrid Techniques with Plasma Detection
Sergio Caroli, *Rome*	Low Pressure Discharges as Atom and Ion Sources
Miguel Valcárcel, *Córdoba*	FIA and Plasma Spectroscopy
Gary Hieftje, *Indiana*	New Perspectives in Atomic/Ionic Sources

Keynote—

Daniel Batistoni, *Buenos Aires*	Plasma Spectrometry in Latin America
Ramon Barnes, *Massachusetts*	Isotopic Analysis in Biomedical Research With Analytical Plasma Source MS
Joe Caruso, *Cincinnati*	Potential of LC–ICP-MS for Trace Metal Speciation
Ignacio García Alonso, *Karlsruhe*	ICP-MS for the Analysis of Nuclear Materials
Sam Houk, *Iowa*	Latest Developments in ICP-MS Instrumentation
Francisco Krug, *São Paulo*	FIA On-line Treatments for ICP-AES
Ken Marcus, *Clemson*	Glow Discharge Mass Spectrometry
Akbar Montaser, *Washington*	Plasmas Other Than Ar-ICP for Atomic Spectroscopy
Niccolo Omenetto, *Ispra*	Laser Atomic Spectroscopy
Carlo Vandecasteele, *Leuven*	ICP-MS for Biological Materials

For further information contact—

Professor Alfredo Sanz-Medel

Department of Physical and Analytical Chemistry, Faculty of Chemistry

University of Oviedo, C/Julian Claveria, 8, 33006 Oviedo, Spain

Telephone: 348510 3480/3474, Telefax: 348523 7850

FIRST FOLD HERE

THE ANALYST READER ENQUIRY SERVICE
For further information about any of the products featured in the advertisements in this issue, write the appropriate number on the postcard, detach and post.

FOLD HERE

THE ANALYST READER ENQUIRY SERVICE

NOV'92

For further information about any of the products featured in the advertisements in this issue, please write the appropriate number in one of the boxes below.
Postage paid if posted in the British Isles but overseas readers must affix a stamp.

PLEASE USE BLOCK CAPITALS LEAVING A SPACE BETWEEN WORDS *Valid 12 months*

1 NAME

2 COMPANY

PLEASE GIVE YOUR BUSINESS ADDRESS IF POSSIBLE. IF NOT, PLEASE TICK HERE ☐

3 STREET

4 TOWN

5 COUNTY
POST CODE

6 COUNTRY

7 DEPARTMENT
DIVISION

8 YOUR JOB TITLE
POSITION

9 TELEPHONE NO

OFFICE USE ONLY REC'D PROC'D

FOLD HERE

Postage will be paid by Licensee

Do not affix Postage Stamps if posted in Gt. Britain, Channel Islands, N. Ireland or the Isle of Man

BUSINESS REPLY SERVICE
Licence No. WD 106

Reader Enquiry Service
The Analyst
The Royal Society of Chemistry
Burlington House, Piccadilly
LONDON
W1E 6WF
England

NEW EDITION

OVER 81,000 SPECTRA

EIGHT PEAK INDEX OF MASS SPECTRA

4th Edition

The essential tool for mass spectrometrists

NOW AVAILABLE – the **new 4th Edition** of the highly regarded ***Eight Peak Index of Mass Spectra.***

This quality compilation is recognised by many mass spectrometrists as the most useful index of mass spectra in print today.

THE *EIGHT PEAK INDEX* EMPOWERS YOU TO:

- ★ identify unknowns rapidly and easily
- ★ locate spectra of compounds quickly by formula or molecular weight
- ★ match spectra simply through direct peak intensity comparison
- ★ find spectra relevant to your area of interest – a wide variety of compound types are included
- ★ access the data at any time with no machine-time restrictions
- ★ use the data with confidence – extensive checks on all records have been performed

Probably the best printed index of mass spectra in the world!

For more information about the ***NEW*** edition, simply contact us at the address below for a copy of our detailed leaflet:

ROYAL SOCIETY OF CHEMISTRY

Information Services

Sales and Promotion Department
Royal Society of Chemistry
Thomas Graham House
Science Park, Milton Road
Cambridge CB4 4WF, United Kingdom
Tel: +44 (0) 223 420066.
Fax: +44 (0) 223 423623.
Telex: 818293 ROYAL

Circle 006 for further information

ANALAO 117(11) 1657–1800 (1992) November 1992

The Analyst

The Analytical Journal of The Royal Society of Chemistry

CONTENTS

Typeset and printed by Black Bear Press Limited, Cambridge, England

0003-2654(1992)11-W